Evaluation of antioxidant and neuroprotective therapies in a mouse model of amyotrophic lateral sclerosis

Katherine Elizabeth Amy Lewis (BBiotech Hons)

School of Medicine

Submitted in fulfilment of the requirements for the

Doctor of Philosophy

University of Tasmania, October 2014

Declaration of originality

This thesis contains no material which has been accepted for a degree or diploma by the University or any other institution, except by way of background information and duly acknowledged in the thesis, and to the best of the my knowledge and belief no material previously published or written by another person except where due acknowledgement is made in the text of the thesis, nor does the thesis contain any material that infringes copyright.

Katherine Lewis ……. October 2014

Authority of access

This thesis may be made available for loan and limited copying and communication in accordance with the Copyright Act 1968.

Katherine Lewis ……. October 2014

Statement of ethical conduct

The research associated with this thesis abides by the international and Australian codes on human and animal experimentation, the guidelines by the Australian Government's Office of the Gene Technology Regulator and the rulings of the Safety, Ethics and Institutional Biosafety Committees of the University.

Katherine Lewis ……. October 2014

Statement regarding published work contained in thesis

Data in this thesis has given rise to one publication in Journal of Neuroinflammation. The authors retain copyright for that article, and grant any third party, in advance and in perpetuity, the right to use, reproduce or disseminate the article, according to the BioMed Central copyright and license agreement. The remaining non-published content of the thesis may be made available for loan and limited copying and communication in accordance with the Copyright Act 1968.

Katherine Lewis ……. October 2014

Statement of co-authorship

The following people and institutions contributed to the publication of work undertaken as part of this thesis:

Katherine E Lewis, School of Medicine, University of Tasmania
Roger Chung, Australian School of Advanced Medicine, Macquarie University
Meng Inn Chuah, School of Medicine, University of Tasmania

Paper 1:

Microglia and motor neurons during disease progression in the SOD1^{G93A} mouse model of amyotrophic lateral sclerosis: Changes in arginase1 and inducible nitric oxide synthase

Katherine E Lewis, Anna L Rasmussen, William Bennett, Anna King, Adrian K West, Roger S Chung, Meng Inn Chuah

Journal of Neuroinflammation, accepted for publication 7 March 2014

Data used for publication is located within Chapter 2 of this thesis.

Katherine Lewis (Candidate) conducted most of the experiments (about 60%) and all analyses; she was also the primary author. In this publication, Anna Rasmussen contributed to some of the data presented in Figures 1, 2, 3 and 6 while Anna King contributed to Figure 7. Authors West, Chung and Chuah contributed to the idea, design and development of the project. Author Bennett collected tissue samples and offered general laboratory assistance.

We the undersigned agree with the above stated "proportion of work undertaken" for each of the above published (or submitted) peer-reviewed manuscripts contributing to this thesis:

Signed: _____ _____

A/Prof MI Chuah	*Prof J Walls*
Supervisor	*Head of School*
School Of Medicine	*School of Medicine*
University of Tasmania	University of Tasmania

Date: _____

Abstract

Amyotrophic lateral sclerosis (ALS) is a fatal neurodegenerative disease, characterised by dysfunction and degeneration of motor neurons innervating skeletal muscle. ALS patients experience progressive muscle weakness and atrophy, leading to paralysis and death within 3-5 years of diagnosis. The mechanisms underlying neurodegeneration in ALS are unknown; studies of patient tissue and of transgenic mouse models of ALS have implicated oxidative stress, neuroinflammation, aberrant RNA metabolism, excitotoxicity, protein misfolding, autophagy and proteasome dysfunction, and intracellular transport deficits in disease processes.

Current ALS therapeutics can only extend lifespan by a matter of months, so it is vital that novel therapeutic targets and therapeutic molecules are identified. The many putative "triggers" of ALS are predicted to converge upon common mechanisms of degeneration, with oxidative stress being identified as one of the major pathological hallmarks of ALS. Therapeutics capable of modulating oxidative stress and preventing neuronal death may be of value in treating human ALS.

In this thesis, the temporal correlations between microglial activation, development of pathological alterations in the spinal cord, and functional decline, were explored in the transgenic SOD1 mouse model of ALS (carrying the ALS-linked mutant human Cu,Zn-superoxide dismutase gene $SOD1^{G93A}$), with non-transgenic (WT) mice used as controls. The ability of three putative therapeutic compounds for ALS – Gemals, metallothionein-2 protein, and Emtin peptides – to increase survival time in SOD1 mice was also examined.

Pathological alterations in motor neurons preceded an increase in microglial numbers, suggesting microglial activation occurs as a reactive response to neuronal degeneration or dysfunction. Microglial activation occurred concurrently with disease onset at 14 weeks of age, but preceded the development of overt functional deficits around 18 weeks of age. Interestingly, microglial activation was associated with an increase in the number of microglia expressing the M2-like, putative neuroprotective, marker arginase1 (Arg1), and to a lesser extent with an increase in the number of microglia expressing the M1-like, putative neurotoxic, marker inducible nitric oxide synthase (iNOS). These data suggest the concurrent presence of ongoing neuroprotective and neuroinflammatory processes in the spinal cord of SOD1 mice; microglial activation may not be a primary

cause of neurodegeneration, but may drive disease progression after onset. Additionally, the expression of the antioxidant protein metallothionein-1/2 (MT-1/2) increased from 18 weeks of age, possibly in response to oxidative stress or neuronal degeneration.

Gemals, an antioxidant and anti-inflammatory combination therapy, has been previously shown to extend the lifespan of an ALS rat model, but has not been tested in ALS mice. Here, Gemals was administered subcutaneously to SOD1 mice from the age of symptom onset through to disease endpoint. No significant changes in survival time were identified in Gemals-treated SOD1 mice compared to controls, indicating that Gemals treatment may be less effective when administered after symptom onset.

MT-1/2 protein has previously shown both antioxidant and neuroprotective properties, and its ablation in SOD1 mice has been shown to accelerate disease progression. In this study, SOD1 mice were treated with MT2 injections, and/or with treadmill running exercise to upregulate endogenous MT-1/2. MT2 treatment slightly but significantly delayed disease onset, and tended to increase survival time, in SOD1 mice, whereas treadmill running exercise had little effect. However, the mechanism of action for MT2 is as yet unknown – preliminary data suggest that MT2 treatment did not substantially prevent spinal cord motor neuron degeneration or muscle endplate denervation.

Peptide derivatives of MT-1/2, termed Emtins, have previously displayed similar neuroprotective properties to their parent MT-1/2 protein *in vitro* and *in vivo*, and additionally can readily cross the blood-brain barrier. Emtins were administered subcutaneously to SOD1 mice from the onset of disease symptoms, resulting in increased survival time compared to control mice, although this result was not significant due to a smaller number of animals used during this trial. These data indicate that both MT2 and Emtins have pro-survival effects in the SOD1 mice. Emtin peptides are thought to have limited metal-binding and antioxidant properties; however, both MT-1/2 and Emtins are known to interact with low-density lipoprotein receptor-related proteins (LRPs) and activate the Akt pathway, leading to increased cellular survival. It is possible that the pro-survival effects of MT2 and Emtins seen in these studies were mediated through LRP binding and activation of downstream pathways. MT2 and Emtins show potential as therapeutic molecules for ALS, but more work is required to elucidate the mechanism of action.

Acknowledgements

First and foremost, I would like to thank my supervisors Associate Professor Meng Inn Chuah, School of Medicine, University of Tasmania, and Professor Roger Chung, Australian School of Advanced Medicine, Macquarie University, for the endless support, advice, and guidance they have given me throughout my candidature.

The work described in this thesis has been supported by funding from the Motor Neuron Disease Research Institute of Australia (MNDRIA) and the National Health and Medical Research Council (NHMRC).

I would like to acknowledge past student Ms Anna Rasmussen for her contribution to the microglial protein expression data in Chapter 2, Dr Bill Bennett for his preparation of the spinal cord tissue library in Chapter 2 and his assistance in the pre-clinical trial in Chapter 3, Ms Emma Eaton for preparing biotinylated Emtin in Chapter 5, and Associate Professor Leigh Blizzard for his patient explanations of statistical procedures involved in constructing linear mixed models.

Thanks also to past and present animal services staff – Murray Plaister, Angela Maher, Keri Playford, and Peta Lawrie – and to animal welfare officer Barrie Wells, for their expert and diligent care of animals, and advice in all aspects of animal trials. I would also like to thank Professor Peep Palumaa and his laboratory, especially Dr Julia Smirnova, Dr Kairit Zovo, Andra Noormägi, and Merlin Friedemann, for their support and assistance during my visit to the Tallinn University of Technology in 2012.

I would like to thank my fellow MT lab students for being the best bunch of people to work with – to Emma Eaton, Ros Herbert, Dr Jackie Leung, and Lila Landowski, thank you for all of your friendship, advice, problem-solving, support, and cake. A huge thankyou goes to Dr Bill Bennett, for being an infinite source of knowledge and support. I would also like to thank Professor Adrian West, and all past members of the MT and MBU groups, for sharing their considerable collective wisdom and insight with me across the years.

To my dear friends and fellow students who have shared this PhD journey with me – thank you so much for the friendship, camaraderie, laughs, commiserations, cups of tea, Friday drinks, and epic ASMR dinners we have shared over the past four years.

Thanks also go to my family – my father David, mother Krystyna, and brothers Andrew and Alex, for always being supportive and interested in what I was doing.

Finally, to my incredible partner Anthony, who has endured the worst of my late nights in the lab and my bad moods when experiments failed; I simply could not have finished my PhD without your unwavering love and support.

Table of contents

List of figures

List of tables

Abbreviations

AF	AlexaFluor
ALS	amyotrophic lateral sclerosis
ALSAQ-40	ALS assessment questionnaire
ALSFRS	ALS functional rating score
ALSTDI	ALS Therapy Development Institute
ALS2	alsin
AMPA	α-amino-3-hydroxyl-5-methyl-4-isoxazoleproprionic acid
ANOVA	analysis of variance
ARE	antioxidant-responsive element
Arg1	arginase1
ATP	adenosine triphosphate
B6	C57Bl/6 strain; genetic background for SOD1 mice
B6SJL	hybrid C57Bl/6 x SJL strain
°C	degrees Celsius
CHMP2B	charged multivesicular body protein 2B
CI	confidence interval
cm	centimetres
CPH	Cox proportional hazards; regression analysis for survival
COX	cyclooxygenase
CNS	central nervous system
CREB	cAMP response element-binding protein
CSF	cerebrospinal fluid
C9orf72	open reading frame 72 on chromosome 9
ΔCT	delta-CT; difference in curve take-off cycle in multiplex qPCR
DAB	3,3’-diaminobenzidine
DDR	DNA damage response
DNA	deoxyribonucleic acid
EAAT2	excitatory amino acid transporter 2
EDTA	ethylenediaminetetraacetic acid
eNOS	endothelial nitric oxide synthase
ER	endoplasmic reticulum
ETC	electron transport chain
FALS	familial amyotrophic lateral sclerosis
FIG4	Fig4 homologue
FTD	frontotemporal dementia
FUS	fused in sarcoma
g	grams; for body weight
g	relative centrifugal force, for centrifuge protocols
GFAP	glial fibrillary acidic protein
HR	hazard ratio

HRP	horseradish peroxidase
hSOD1	protein from the human $SOD1^{G93A}$ transgene
Iba1	ionised calcium-binding adaptor molecule 1
IGF1	insulin-like growth factor 1
IL-6	interleukin 6
iNOS	inducible nitric oxide synthase
L	litres
LRP	low density lipoprotein receptor-related protein
M	molar; moles per litre
MAP	microtubule-associated protein
MAPK/ERK	mitogen-activated protein kinase / extracellular signal-regulated kinase pathway
mApoB	murine apolipoprotein B gene
mg	milligrams
mIL-2	murine interleukin 2 gene
mL	millilitres
MM	mitochondrial membrane
MOM	Mouse on Mouse immunohistochemistry kit
MN	motor neuron
MND	motor neuron disease
mRNA	messenger ribonucleic acid
MS	multiple sclerosis
MT	metallothionein
MT-1/2	metallothionein isoforms 1 and 2; i.e., MT1 and MT2
MT2	Zn_7-metallothionein-2A protein, purified from rabbit liver
MWU	Mann Whitney U test
M1	Macrophage-M1-like, putative neurotoxic, microglial phenotype
M2	Macrophage-M2-like, putative neuroprotective, microglial phenotype
NGS	normal goat serum
nlcom	non-linear combination of estimators
NO	nitric oxide
NOS	nitric oxide synthase
NMDA	N-methyl-D-aspartate
nNOS	neuronal nitric oxide synthase
Nrf1	nuclear factor erythroid 2-related factor 1
Nrf2	nuclear factor erythroid 2-related factor 2
NS	neurological score
NSC34	Motor neuron-like cell line; neuroblastoma/mouse MN hybrid
NY	Nuclear Yellow
OPTN	optineurin

O/N	overnight
PCR	polymerase chain reaction
PBS	phosphate-buffered saline
PBS-T	phosphate-buffered saline containing 0.05% Tween-20
PFA	paraformaldehyde
PLL	poly-L-lysine
PLS	primary lateral sclerosis
PI3K/Akt	Phosphoinositide 3-kinase / serine-threonine kinase Akt pathway
PMA	progressive muscular atrophy
p62	sequestome1
qPCR	quantitative real-time PCR
ROS	reactive oxygen species
RNA	ribonucleic acid
rpm	revolutions per minute
RT	room temperature
SALS	sporadic amyotrophic lateral sclerosis
SETX	senataxin
SIGMAR1	Sigma non-opioid intracellular receptor 1
SMI32	antibody against dephosphorylated neurofilament medium chain
SMN	survival of motor neuron protein
SOD1	Cu,Zn-superoxide dismutase
SOD2	Mn-superoxide dismutase
TAE	tris-acetate-EDTA buffer
TDP43	TAR-DNA binding protein 43
TL	tomato lectin
TNFα	tumour necrosis factor alpha
UBQLN2	ubiquilin2
µL	microlitres
µm	micrometres
VAPB	vesicle-associated membrane protein (synaptobrevin)-associated protein B
VCP	valosin-containing protein
VH	ventral horn
WT	wild type; non-transgenic
-2LL	-2 x log likelihood from maximum likelihood estimation
-2RLL	-2 x restricted log likelihood from restricted maximum likelihood estimation

Chapter 1 Literature Review

Molecular pathology leading to motor neuron degeneration in amyotrophic lateral sclerosis

1.1 Motor neuron disease

1.1.1 An overview of the motor system

Motor neurons are the nerve cells that transmit electrical impulses from motor control areas of the brain to skeletal muscles in order to effect voluntary movement. An upper motor neuron has its cell body located within Layer V of the primary motor cortex and extends its axon to the brainstem via the corticobulbar tract, or to the spinal cord via the corticospinal tract, where a glutaminergic synapse is made with a lower motor neuron cell body (Figure 1.1). Lower motor neurons, located within either the brainstem motor nuclei or Rexed lamina IX of the spinal cord ventral horn, project their axon out of the central nervous system and effect target skeletal muscle contraction via the release of acetylcholine at the neuromuscular junction (Ravits *et al.* 2013) (Figure 1.1).

For voluntary movement of skeletal muscles, the entire pathway from motor cortex to muscle must be intact. Motor neuron disease is characterised by the progressive dysfunction and death of upper or lower motor neurons, and the resulting progressive loss of voluntary movement of skeletal muscles (Ravits *et al.* 2013).

1.1.2 Types of motor neuron disease

Motor neuron diseases comprise a variety of syndromes and diseases caused by degeneration in either the upper or lower, or both upper and lower, motor neurons. The most common form of adult-onset motor neuron disease is amyotrophic lateral sclerosis (ALS) which involves degeneration of both upper and lower motor neurons, and was first described by the French neurologist Charcot in the 19th century (Siddique & Ajroud-Driss 2011). Other motor neuron diseases may involve only the upper or lower motor neurons, such as primary lateral sclerosis (PLS) and progressive muscular atrophy (PMA) respectively. Although PLS and PMA are associated with slower progression rates and longer survival times than ALS, (Visser *et al.* 2007; Talman *et al.* 2009; Wijesekera *et al.* 2009), many patients initially diagnosed with a pure upper or lower motor neuron disease go on to develop signs of involvement of both motor neuron populations (Visser *et al.* 2007; Kim *et al.* 2009), suggesting ALS lies at the centre of a spectrum of motor neuron diseases. As ALS is both the most common form of adult-onset motor neuron disease, and is thought to be at the centre of a continuum of upper and lower motor neuron disorders, this thesis will focus primarily on ALS.

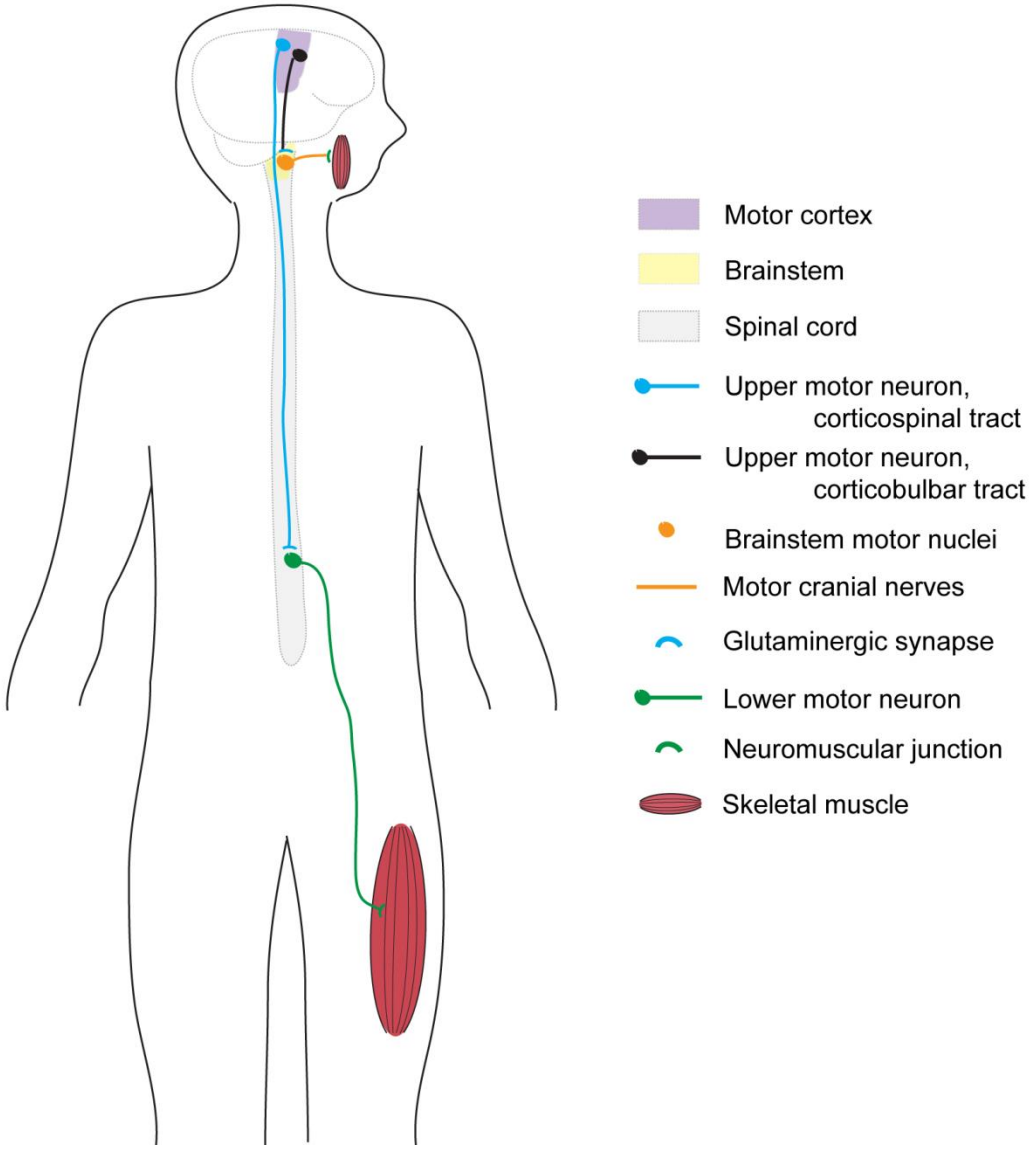

Figure 1.1 Overview of the motor system

Upper motor neurons have a cell body located in the primary motor cortex grey matter, with their axons extending to either the brainstem or the spinal cord via the corticobulbar or corticospinal tracts, respectively. Lower motoe neurons innervating the head and neck have their cell bodies located in brainstem motor nuclei, and their axons travel via the cranial nerves to the bulbar skeletal musculature. Lower motor neurons innervating the trunk and limbs have their cell bodies located in the spinal cord ventral horn, and their axons travel to the axial and limb skeletal musculature via peripheral nerves. Upper motor neurons release glutamate onto lower motor neurons at the synapse, while lower motor neurons release acetylcholine onto nicotinic receptors at the neuromuscular junction.

1.2 Amyotrophic lateral sclerosis

1.2.1 Clinical features and disease course

ALS typically presents as a focal muscle weakness, seen in the limbs in two thirds of patients and in the bulbar region in one third of patients, which worsens with time (Logroscino *et al.* 2010; Kiernan *et al.* 2011; Al-Chalabi *et al.* 2012). Regardless of the site of presentation, the symptoms of motor neuron (MN) degeneration – spasticity, clonic reflexes, and psuedobulbar affect from upper MN loss, and muscle weakness, atrophy, and fasciculations from lower MN loss – spread progressively through the body (Walker 1990; Brooks 1994).

As MNs degenerate, ALS patients lose control over voluntary skeletal muscle movement, resulting in progressive inability to generate limb movement, and also causing difficulties in swallowing, speech, and breathing. In addition to motor impairment, ALS patients may show impaired executive or cognitive function, or behavioural changes; some ALS patients meet the clinical criteria for frontotemporal dementia (Lomen-Hoerth *et al.* 2003; Witgert *et al.* 2010). Sensory neurons are affected to a much lesser extent than motor neurons (Kawamura *et al.* 1981; Gregory *et al.* 1993). ALS ultimately leads to death from failure of the respiratory muscles, with most patients only surviving 3-5 years from diagnosis (Al-Chalabi *et al.* 2012).

1.2.2 Diagnosis

A diagnosis of ALS is made according to the modified El Escorial criteria, and requires signs of both upper and lower motor neuron degeneration upon clinical, electophysiological or neuropathologic examination, with evidence of symptom progression over time (Brooks 1994; Brooks *et al.* 2000; de Carvalho *et al.* 2008). Extensive clinical, neuroimaging and laboratory investigations are required to rule out disorders mimicking ALS, which can include polyneuropathies, endocrine abnormalities, physical injury to the nervous system, malignancies, exposure to exogenous toxins, vasculitis and myelopathies (Kiernan *et al.* 2011). A recent study indicated that average time from symptom onset to diagnosis was over 12 months (Logroscino *et al.* 2010). While less than 10% of patients with diagnoses of ALS are re-diagnosed with an ALS mimic syndrome, some of these mimic syndromes can be effectively treated – making a correct diagnosis extremely important (Ross *et al.* 1998; Traynor *et al.* 2000).

1.2.3 Prevalence and risk factors

ALS affects 2-3 people per 100,000 each year, with a prevalence of 4-8 people per 100,000. Onset is most common between 50-65 years of age, and ALS is slightly more common in males than females (Logroscino *et al.* 2010; Kiernan *et al.* 2011). Environmental and lifestyle risk factors such as pesticide, cyanobacteria, or heavy metal exposure, electric shock, smoking, and high levels of leisure-time physical activity, are associated with increased ALS risk (Das *et al.* 2012; Huisman *et al.* 2013; Trojsi *et al.* 2013). Approximately 5-10% of all ALS cases have a family history (familial ALS, FALS), as opposed to no family history of ALS (sporadic ALS, SALS). Mutations in a number of genes are known to cause familial ALS or inherited ALS-like disorders, and polymorphisms in a number of genes have been shown in genome-wide association studies to increase the risk of developing SALS (Table 1.1); their possible roles in ALS aetiology are discussed in section 1.3. Geographical foci such as Guam and the Japanese Kii peninsula have historically shown high incidence rates of the ALS/parkinsonism/dementia complex (McGeer & Steele 2011; Kaji *et al.* 2012), suggesting that ALS could be caused by a common genetic or environmental factor.

1.2.4 Prognosis and treatment strategies

ALS is currently incurable, and invariably fatal, with the average lifespan only 3-5 years from symptom onset. The only drug currently available for treatment of ALS is the glutamate blocker, Riluzole (Bensimon *et al.* 1994; Georgoulopoulou *et al.* 2013). However, the average patient can expect a survival increase of only 3-6 months from using Riluzole, and the survival-promoting effects of Riluzole are greater for patients with bulbar-onset ALS, and less for those with limb-onset ALS (Bensimon *et al.* 1994). Given that Riluzole does not provide a cure for ALS, treatments are based around the amelioration of symptoms in order to maintain quality of life for the patient, often in the context of a multidisciplinary clinic (Simmons 2005; Mayadev *et al.* 2008). Interventions such as artificial ventilation can increase survival time (Miller *et al.* 2009; Spataro *et al.* 2012), while percutaneous endoscopic gastrostomy can maintain nutrition despite bulbar difficulties (Spataro *et al.* 2011). However, it is clear that novel treatments for ALS are required to halt the disease processes and improve outcomes for patients. However, as the underlying aetiology of ALS is not yet known, more research into the mechanisms of motor neuron degeneration is required. The known pathological features of ALS, and a mouse model mimicking human ALS, are discussed overleaf.

1.2.5 Pathological features of ALS

End-stage CNS pathology in ALS patients reveals four pathological hallmarks of ALS. First, the extensive loss of motor neuron cell bodies in layer V of the motor cortex, in the brainstem motor nuclei, and in the spinal cord anterior horns; motor neuron degeneration is thought to resemble programmed cell death rather than necrosis (Martin 2010). Second, axonal degeneration in CNS white matter tracts such as the corpus callosum, medullary pyramids, and corticospinal tract; and also in ventral roots and peripheral nerves. Third, the presence of ubiquitinated protein aggregates in degenerating motor neurons (Lowe *et al.* 1989) in four neuropathological patterns: (1) SALS and most non-SOD1-linked FALS cases show aggregates containing ubiquitin and TDP43; (2) SOD1-linked FALS aggregates contain SOD1 but not TDP43; (3) FUS-linked ALS aggregates can be basophilic inclusions, or contain FUS but not TDP43; (4) C9orf72-linked ALS aggregates contain ubiquitin and TDP43, and may also contain p62 and ubiquilin2 (Ravits *et al.* 2013). Fourth, widespread activation of glial cells can be seen in the spinal cord and motor cortex (Kamo *et al.* 1987; Schiffer *et al.* 1996). A mouse model of ALS, discussed below, is commonly used to examine mechanisms of motor neuron degeneration.

1.2.6 Mouse models of ALS

1.2.6.1 The SOD1 mouse model of ALS

Sequence alterations in Cu,Zn-superoxide dismutase (SOD1) were the first mutations to be linked with familial ALS (Rosen *et al.* 1993). Transgenic mice, expressing high levels of the mutant human SOD1 protein with a glycine to alanine amino acid substitution at position 93 ($SOD1^{G93A}$ mice; hereafter, the term ‘SOD1 mice’ refers to this mutation unless otherwise specified), mimic the pathological and clinical hallmarks of human ALS (Gurney *et al.* 1994). Clinically, SOD1 mice develop progressive motor deficits characterised by hindlimb weakness, muscle atrophy, and gradual paralysis (Gurney *et al.* 1994). Pathologically, SOD1 mice show extensive degeneration of spinal cord motor neuron cell bodies, axonal degeneration in the lateral motor columns, ventral roots, and peripheral nerves, and denervation at the neuromuscular junction (Gurney *et al.* 1994). Given the similarities of the SOD1 mouse to both familial and sporadic ALS patients, SOD1 mice have been widely used to examine the molecular pathology of motor neuron degeneration, and to perform pre-clinical testing of potential therapeutic

compounds for human ALS. However, it must be noted that no compounds which gave positive effects in the SOD1 mouse model have gone on to perform equally well in clinical trials (Benatar 2007). Putative mechanisms of SOD1-mediated ALS will be discussed in the aetiology section (Chapter 1.3).

1.2.6.2 The TDP43 mouse model of ALS

TDP43 was identified as a major component of ubiquitinated protein aggregates in the central nervous system of sporadic ALS patients, non-SOD1-linked familial ALS patients, and frontotemporal dementia patients (Neumann *et al.* 2006; Sreedharan *et al.* 2008; Ravits *et al.* 2013). As TDP43 may represent a common pathway between the familial and sporadic forms of ALS, the development of a mouse model of TDP43-based pathology may be a big step forward for ALS research. However, development of an ALS mouse model based on TDP43 has encountered some complications. Mouse models expressing prion promoter-driven high levels of human TDP43 with the A315T mutation (Prp-hTDP43-A315T) show a loss of motor function and premature death (Wegorzewska *et al.* 2009). However, the full motor phenotype of the Prp-hTPD43-A315T mouse was thought to be masked by the early development of gastrointestinal problems (Esmaeili *et al.* 2013). A recent study showed intestinal motility problems in Prp-hTDP43-A315T mice leading to premature death, and showed that when these deficits were alleviated by allowing mice to eat a nutrient gel diet, rather than standard laboratory chow, these mice survived for longer and developed pronounced neurodegeneration (Herdewyn *et al.* 2014). The mechanisms by which the overexpressed Prp-hTDP43-A315T exerts its toxic actions are not yet known; the overexpression of TDP43 appears to lead to aberrant mRNA splicing, potentially affecting thousands of downstream gene products, including many genes required for synaptic function (Lagier-Tourenne *et al.* 2012; Xu *et al.* 2013). Interestingly, the TDP43-based ALS mouse model appears to show upper motor neuron pathology more readily than lower motor neuron pathology (Igaz *et al.* 2011; Herdewyn *et al.* 2014). The TDP43 mouse model will provide a complementary model for the current SOD1 mouse model, and the use of both models side by side will help to determine the mechanisms underlying upper and lower motor neuron degeneration.

1.3 Etiology of ALS

The exact causative mechanisms underlying motor neuron degeneration in ALS are not currently known. Combined evidence from ALS patients, SOD1 ALS mouse models, and cell culture models have implicated a wide range of cellular processes in ALS pathology. In this section, the possible contributions of these pathways to the molecular pathogenesis of ALS will be discussed. These cellular events include oxidative stress, glial activation and neuroinflammation, mitochondrial dysfunction, RNA processing, excitotoxicity, protein aggregation and protein degradation dysfunction, and intracellular transport deficits. Possible convergence points between different pathological mechanisms will also be discussed.

1.3.1 Genetic evidence for molecular pathologies in ALS

Although only 10% of ALS cases show a heritable component, both sporadic and familial ALS share similar clinical and pathological characteristics. The identification of mutations causative for familial ALS also contributes to the understanding of pathways potentially involved in sporadic disease (Al-Chalabi *et al.* 2012). Mutations linked to various juvenile-onset or adult-onset familial ALS are present in a range of genes; a list of genes with contributions to various forms of FALS has been compiled in Table 1.1. A full list of genes involved in ALS, as well as ALS-associated risk factors from genome-wide association studies, can be found at www.alsod.iop.kcl.ac.uk.

The genes listed in Table 1.1 have been loosely grouped according to their most well-understood functions. The genes associated with familial ALS, which in some cases have also been associated with sporadic ALS, represent pathways with functions in antioxidant response, intracellular transport (encompassing axonal transport and vesicle trafficking), protein degradation by the proteasome and by autophagy, RNA processing and metabolism, and maintenance of the cytoskeletal protein network (Al-Chalabi *et al.* 2012). The involvement of these genes in familial ALS gives clues to the pathophysiology of ALS. The current hypotheses on ALS aetiology, encompassing the pathways represented by the genetic risk factors listed in Table 1.1, will be discussed in more detail in subsequent sections on disease aetiology.

Table 1.1 Genes associated with familial amyotrophic lateral sclerosis

Gene	Gene product (abbreviation)	Normal function	Mutations are known to cause:	%patients with mutations*	
				FALS	**SALS**
SOD1	Cu,Zn-superoxide dismutase (SOD1)	Antioxidant	FALS	12%	2-7%
DCTN1	Dynactin-1 (DCTN1)	Axonal transport	Familial PMA		
ALS2	Alsin	Vesicle trafficking	Familial juvenile-onset PLS		
OPTN	Optineurin (OPTN)	Vesicle trafficking	Familial juvenile-onset ALS	<1%	<1%
VAPB	Vesicle-associated membrane protein (synaptobrevin)-associated protein B (VAPB)	Vesicle trafficking ER stress	FALS		
FIG4	Fig4 homologue, SAC1 lipid phosphatase domain containing (S. cerevisiae) (FIG4)	Vesicle trafficking	FALS; CMT		
VCP	Valosin-containing protein (VCP)	Protein degradation	FALS; IBMPFD	1%	1%
UBQLN2	Ubiquilin 2 (UBQLN2)	Protein degradation	FALS	<1%	<1%
SQSTM1	Sequestosome 1 (p62)	Protein degradation	FALS	1%	<1%
SIGMAR1	Sigma non-opioid intracellular receptor 1 (SIGMAR1)	ER stress	Familial juvenile-onset ALS		
TARDBP	TAR-DNA binding protein 43 (TDP43)	RNA processing	FALS; FTD	4%	1%
FUS	Fused in sarcoma (FUS)	RNA processing DNA damage response	FALS	4%	1%
TAF15	TAF15 RNA polymerase II, TATA box binding protein-associated factor, 68kDa (TAF15)	RNA processing	FALS		
ELP3	Elongation protein 3 (ELP3)	RNA processing	Increased risk of sporadic ALS		

Table 1.1 (continued)

Gene	Gene product (abbreviation)	Normal function	Mutations are known to cause:	%patients with mutations*	
				FALS	SALS
SETX	Senataxin (SETX)	RNA processing DNA damage response	Familial juvenile-onset ALS; hereditary ataxia		
ANG	Angiogenin (ANG)	Blood vessel formation Neuronal protection RNAse function	FALS; increased risk of SALS		
PFN1	Profilin 1 (PFN1)	Cytoskeletal network	FALS	<1%	<1%
PON	Paraoxonase (PON)	Detoxification of toxins	Increased risk of SALS		
NEFH	Neurofilament heavy chain (NEFH)	Cytoskeletal network	FALS; increased risk of SALS		
DAO	D-amino-acid oxidase (DAO)	Serine metabolism	FALS; increased risk of SALS		
SPG11	Spastic paraplegia 11, spatacsin	Axonal development DNA damage repair	Familial juvenile-onset ALS		
C9orf72	Chromosome 9 open reading frame 72 (C9orf72)	Unknown	FALS; FTD	40%	7%

ALS, amyotrophic lateral sclerosis; CMT, Charcot-Marie-Tooth disease; FALS, familial ALS; FTD, frontotemporal dementia; IBMPFD, inclusion body myopathy and Paget's disease of bone with frontotemporal dementia; PLS, primary lateral sclerosis; PMA, progressive muscular atrophy; SALS, sporadic ALS. *Percentage of ALS cases explained by mutations in the given gene (please note: many genes have been associated with ALS, but these gene alterations occur in few patients, and therefore the occurrence of these genes in sporadic and familial ALS is likely to be infrequent (<1%); the known percentages for well-investigated genes are presented here). Source: Table adapted from information found in the ALSoD database (www.alsod.iop.kcl.ac.uk) and published papers (Schymick *et al.* 2007; Lill *et al.* 2011; Al-Chalabi *et al.* 2012; Renton *et al.* 2014).

1.3.2 Oxidative stress

1.3.2.1 Reactive oxygen species and oxidative damage

The mediators of oxidative damage to macromolecules are reactive oxygen species (ROS) such as hydroxyl and superoxide radicals. Endogenous ROS are formed during normal cellular metabolism; a major source of endogenous superoxide radicals is electron leakage from the mitochondrial respiratory chain during oxidative phosphorylation (Mates *et al.* 1999). Superoxide can react with nitric oxide (NO) to form peroxynitrite (ONOO-), another highly-reactive species. ROS can cause oxidative damage to a variety of cellular macromolecules. Oxidative damage to DNA, left unrepaired, can give rise to mutations in the DNA sequence or block transcription from the affected gene (Cooke *et al.* 2003). Oxidative damage to mRNA leads to reduced protein expression from the affected sequence (Chang *et al.* 2008). Protein oxidation and nitration, through the reaction of peroxynitrite with tyrosine amino acid residues to form nitrotyrosine, can alter protein structure and function (Radi 2013).

Mammalian cells have a complex array of endogenous antioxidants and antioxidant enzymes, to prevent macromolecules from oxidative damage (Mates *et al.* 1999). Antioxidant enzymes include cytosolic Cu,Zn-superoxide dismutase (SOD1) and mitochondrial-localised Mn-superoxide dismutase (SOD2), which catalyse the conversion of superoxide to hydrogen peroxide; cytosolic catalase, glutathione peroxidase, and peroxiredoxin enzymes can then degrade hydrogen peroxide to water and molecular oxygen (Mates *et al.* 1999). A number of endogenous antioxidant compounds, such as vitamins A, C, and E, β-carotene, glutathione, and the metallothionein (MT) protein family, are potent intracellular scavengers of ROS (Mates *et al.* 1999). Oxidative stress occurs when the endogenous protection mechanisms are overwhelmed, resulting in oxidative damage to lipids, nucleic acids and proteins.

1.3.2.2 Oxidative stress in ALS

Increased markers of oxidative damage to macromolecules are present in both ALS patients and ALS rodent models. ALS patient CNS tissue shows marked evidence of carbonyl and nitrotyrosine protein modifications (Bowling *et al.* 1993; Shaw *et al.* 1995; Beal *et al.* 1997; Ferrante *et al.* 1997; Sasaki *et al.* 2000), lipid peroxidation (Ferrante *et al.* 1997; Shibata *et al.* 2001), DNA damage (Ferrante *et al.* 1997) and mRNA damage (Chang *et al.* 2008). Markers of oxidative damage can also be found in

the cerebrospinal fluid (CSF), plasma and urine of ALS patients (Oteiza *et al.* 1997; Smith *et al.* 1998; Bogdanov *et al.* 2000). Markers of oxidative damage are similarly elevated in the central nervous system of SOD1 mice (Andrus *et al.* 1998; Chang *et al.* 2008). In particular, lipid peroxidation occurs very early in disease progression in SOD1 mice (Hall *et al.* 1998a). The occurrence of oxidative stress is a common factor between patients with familial and sporadic ALS, and also in ALS model mice, suggesting an important role of oxidative stress in the pathophysiology of ALS.

1.3.2.3 Oxidative stress mediated by mutant SOD1 protein

The identification of SOD1 as the first ALS-associated protein was a major driver for investigating the role of oxidative stress in ALS (Rosen *et al.* 1993). Over 170 ALS-associated mutations have been identified to date in SOD1, accounting for approximately 20% of familial ALS cases. The normal function of SOD1 is to catalyse the dismutation of superoxide radicals into hydrogen peroxide, and it was initially thought that oxidative stress might result from a loss of SOD1 function upon mutation (Rosen *et al.* 1993). The loss of dismutase function may contribute to oxidative stress in patients with SOD1-linked FALS (Bowling *et al.* 1993; Browne *et al.* 1998). However, many ALS-associated mutant SOD1 proteins show minimal changes in dismutase activity, suggesting that an aberrant gain of function rather than a loss of function may be responsible for SOD1-mediated toxicity (Borchelt *et al.* 1994; Borchelt *et al.* 1995; Bowling *et al.* 1995; Rabizadeh *et al.* 1995). This view is strengthened by the fact that SOD1-deficient mice do not develop the same symptoms of motor neuron disease as transgenic mice expressing mutant SOD1 protein (Reaume *et al.* 1996). Given that oxidative stress is commonly observed both in ALS patients and in mice expressing high levels of mutant SOD1, the question arose as to whether the mutant SOD1 protein itself could catalyse the formation of ROS.

There is some evidence to suggest that the mutant SOD1 protein participates in oxidative damage. Many ALS-associated SOD1 mutations result in structural changes to the protein (Deng *et al.* 1993; Wang *et al.* 2002), with mutant SOD1 showing reduced metal-binding ability compared to wild-type SOD1 (Lyons *et al.* 1996; Hayward *et al.* 2002; Das & Plotkin 2013). Structural changes to the SOD1 protein may expose the bound metal ions to novel substrates, resulting in metal-catalysed formation of reactive oxygen species (Beckman *et al.* 1993; Kitamura *et al.* 2011). Alternatively, it

has been demonstrated that metal-deficient mutant SOD1 species have an increased capacity for nitration of tyrosine residues with peroxynitrite (Ischiropoulos *et al.* 1992; Crow *et al.* 1997). Interestingly, oxidised wild type SOD1 protein also shows increased peroxidase-mediated nitration of tyrosine residues (Crow *et al.* 1997). In SOD1 mice, SOD1 proteins themselves are highly susceptible to oxidation (Andrus *et al.* 1998), indicating that under conditions of oxidative stress, oxidation of mutant or wild type SOD1 may change its function from a ROS scavenger to a mediator of oxidative damage, exacerbating disease processes. The metal status of SOD1 also appears important, with both zinc-deficient mutant SOD1 and zinc-deficient wild type SOD1 protein inducing apoptosis in cultured motor neurons (Estevez *et al.* 1999).

1.3.2.4 Nitric oxide synthesis in ALS

Nitric oxide plays an important role in regulating blood flow and synaptic plasticitiy in the central nervous system (Iadecola *et al.* 1994; Holscher 1997). However, nitric oxide is also involved in oxidative damage through protein tyrosine nitration by peroxynitrite (Drechsel *et al.* 2012); formation of nitrotyrosine can alter protein enzymatic activity and increase the propensity of a protein to aggregate (Reynolds *et al.* 2007).

Nitric oxide is synthesised from L-arginine by one of three nitric oxide synthase (NOS) enzymes: endothelial NOS (eNOS), neuron-specific NOS (nNOS), or inducible NOS (iNOS). eNOS and nNOS are constituitively expressed in endothelial cells and neurons, respectively, whereas iNOS expression is induced in glial cells in response to inflammatory cytokines or tissue damage (Murphy 2000). Upregulation of nNOS and iNOS in neurons and glial cells, respectively, has been observed in the spinal cord of ALS patients (Phul *et al.* 2000; Sasaki *et al.* 2000). iNOS was also observed in degenerating motor neurons, while nNOS expression has been observed in glial cells (Sasaki *et al.* 2000; Anneser *et al.* 2001). The induction of iNOS and nNOS in both neurons and glia indicates scope for increased nitric oxide production in both neuronal and glial cells, potentially increasing peroxynitrite formation and protein nitration.

SOD1 mice show a depletion of nNOS-positive motor neurons (Lee *et al.* 2009). The loss of nNOS-positive motor neurons suggests that lower nNOS expression may confer a survival advantage when mutant SOD1 is expressed, possibly due to a lower rate of peroxynitrite formation and less oxidative damage to proteins in nNOS-negative motor neurons. Additionally, the increased expression of iNOS in glial cells of SOD1 mice

(Almer *et al.* 1999; Lee *et al.* 2009) may lead to increased NO synthesis in the ALS spinal cord. Microglial activation, and the increased production of NO due to alterations in the expression of the L-arginine-metabolising enzymes, iNOS and arginase 1 (Arg1), will be discussed in more detail in section 1.3.3.2.

Thus, in both ALS patients and SOD1 mice, the increased production of nitric oxide may mediate increased oxidative damage to motor neurons. However, the cytotoxicity generated by mutant SOD1 in primary motor neuron cultures and in NSC34 motor neuron-like cells cannot be abrogated by inhibition of nitric oxide synthase, indicating that SOD1-mediated toxicity is not entirely explained by the formation of peroxynitrite species (Doroudchi *et al.* 2001; Cookson *et al.* 2002).

1.3.2.5 The role of mitochondrial dysfunction in oxidative stress

Mitochondria may play multiple roles in the pathogenesis of ALS, via oxidative stress, energy production, apoptosis, and interactions with misfolded SOD1 proteins. In relation to oxidative stress, mitochondria are a major source of cellular superoxide; superoxide is produced by the reaction of oxygen molecules with electrons which have escaped the respiratory electron transport chain (ETC) during oxidative phosphorylation (Mates *et al.* 1999). Inhibition of ETC components can increase the production of superoxide radicals, by causing upstream electron carriers to become fully reduced and unable to accept electrons from subsequent substrates, increasing electron leakage (Pelicano *et al.* 2003; Turrens 2003). Oxidative damage to ETC proteins can inhibit respiration, increasing the amount of superoxide produced and further damaging the respiratory chain proteins in a detrimental feedback cycle (Palacios-Callender *et al.* 2004). Altered function of the mitochondria and of respiratory enzyme complexes has been reported in ALS patients and SOD1 mouse models – the possible role of mitochondria in ALS pathogenesis will be explored further in section 1.3.4.

1.3.2.6 Oxidative stress and exposure to environmental toxins

Exposures to pesticides and heavy metals are thought to be risk factors for developing ALS (Das *et al.* 2012; Trojsi *et al.* 2013). The toxicity of various pesticides has been linked to cholinesterase inhibition, but is increasingly also linked to oxidative stress (Banerjee *et al.* 2001; Turrens 2003). Similarly, the toxicity of heavy metal exposure is partly linked to redox-active and antioxidant-depleting properties of the metal in excess (Ercal *et al.* 2001). Genetic variants in *PON* genes, encoding paraoxonase enzymes

involved in the detoxification of organophosphate pesticides and the prevention of lipid oxidation (Shih *et al.* 1998), are associated with the development of sporadic ALS (Saeed *et al.* 2006; Slowik *et al.* 2006). Polymorphisms in glutathione synthetase, an enzyme which modulates production of the antioxidant glutathione, increased the risk of ALS under conditions of exposure to metals or solvents (Morahan *et al.* 2007). Thus, excessive exposure to environmental toxins, or the failure to appropriately detoxify toxic compounds, could be linked with the development of ALS due to oxidative stress.

1.3.2.7 The Nrf2-ARE antioxidant response pathway in ALS

A key cellular response to oxidative stress is mediated via the translocation of the transcription factor nuclear factor erythroid 2-related factor 2 (Nrf2) to the nucleus, where Nrf2 binds to antioxidant-responsive elements (AREs) in the promoter region of antioxidant genes and promotes their transcription (Joshi & Johnson 2012). Genes under Nrf2-ARE control include enzymes involved in redox regulation such as superoxide dismutase, catalase, peroxiredoxin, thioredoxin, sulfiredoxin, and enzymes for glutathione synthesis (Joshi & Johnson 2012). The antioxidant protein metallothionein (MT), while containing an ARE sequence in its promoter region, is activated more strongly by the related Nrf1 transcription factor than by Nrf2 (Ohtsuji *et al.* 2008).

In ALS patient spinal cord motor neurons, Nrf2 mRNA and protein levels were reduced compared with those of controls (Sarlette *et al.* 2008). Expression of mutant SOD1 in embryonic neurons depleted Nrf2-controlled glutathione synthesis enzymes and increased susceptibility to apoptosis induced by nerve growth factor/p75 signalling (Pehar *et al.* 2007). Interestingly, expression of mutant TDP43 in NSC34 cells prevented Nrf2-ARE-mediated induction of antioxidant genes (Duan *et al.* 2010), indicating that reduced oxidative stress responses may contribute to cell death in ALS.

It is worth noting that the Nrf2-ARE pathways are activated more strongly in astrocytes than in neurons, but induction of Nrf2-ARE-mediated genes in astrocytes confers protection to neurons (Johnson *et al.* 2008). The role of astrocytes in ALS will be discussed further in section 1.3.3 on glia and neuroinflammation.

From the evidence presented above, it appears that oxidative stress is involved in multiple aspects of ALS pathology. The convergence between oxidative stress and other potential pathogenic mechanisms in ALS will be discussed further in section 1.3.9.

1.3.3 Glial activation and neuroinflammation

The mechanisms of neurodegeneration in ALS were originally thought to be cell-autonomous; that is, intrinsic to the motor neurons themselves. However, there is increasing evidence to support the non-cell-autonomous hypothesis, that the involvement of non-neuronal cells is a central driver in disease pathology in ALS. Neuroinflammation, involving activation of both astrocytes and microglia, controls the production of neuroprotective or pro-inflammatory components and may modulate motor neuron degeneration in ALS. ALS patients show indications of neuroinflammation such as increased cytokine levels in the CSF (Sekizawa *et al.* 1998; Ilzecka *et al.* 2002), activation of astrocytes and microglia (Evans *et al.* 2013), and infiltration of immune cells from the systemic circulation (Kawamata *et al.* 1992).

1.3.3.1 Astrocytes

Astrocytes are glial cells which normally provide trophic support and maintain optimum conditions in the CNS for neuronal growth and survival (Vargas & Johnson 2010). Extensive astrogliosis is found in the brain and spinal cord of ALS patients (Kushner *et al.* 1991; Schiffer *et al.* 1996) and SOD1 mouse models of ALS (Wong *et al.* 1995; Bruijn *et al.* 1997b; Hall *et al.* 1998b). Astrogliosis is the abnormal proliferation of astrocytes, usually induced by neuronal damage; these proliferating astrocytes form a glial scar and produce growth-inhibitory extracellular matrix molecules (Fitch & Silver 2008). While astrogliosis in ALS was initially thought to be a reactive response triggered by the presence of degenerating neurons, some SOD1 animal models of ALS have shown astrogliosis preceding motor neuron loss (Wong *et al.* 1995; Bruijn *et al.* 1997b); suggesting that astrocytes may play an active role in neuronal degeneration in SOD1-mediated ALS (Vargas & Johnson 2010).

SOD1-expressing astrocytes can induce motor neuron death in co-cultures (Nagai *et al.* 2007) and when transplanted into WT mouse spinal cord *in vivo* (Papadeas *et al.* 2011). While astrocyte-specific expression of mutant SOD1 protein is not sufficient to induce an ALS phenotype (Gong *et al.* 2000), astrocyte-specific knockdown of mutant SOD1 expression can delay disease onset in $SOD1^{G85R}$ mice (Wang *et al.* 2011a) and affect the rate of disease progression in $SOD1^{G37R}$ mice (Yamanaka *et al.* 2008). The difference between the two SOD1 mouse models may be due to differences in dismutase activity of the $SOD1^{G86R}$ and $SOD1^{G37R}$ mutant proteins (Wang *et al.* 2011a). Interestingly,

cultured astrocytes derived from both sporadic and familial ALS patients can induce motor neuron cell death, indicating a common link between SOD1-FALS and sporadic ALS (Haidet-Phillips *et al.* 2011; Meyer *et al.* 2014).

SOD1-mediated pathology in SOD1 mice is not limited to motor neurons; SOD1-positive inclusions can be observed in both motor neurons and astrocytes (Watanabe *et al.* 2001). The same pathological changes caused by mutant SOD1 expression in motor neurons, such as oxidative stress, mitochondrial dysfunction, dysregulation of protein homeostasis, and inhibition of intracellular transport, could easily be present in SOD1-expressing astrocytes, and may disrupt normal astrocyte function. Activated astrocytes, or astrocytes expressing mutant SOD1 protein, show changes in protein expression which may contribute to motor neuron degeneration, as outlined below.

Astrocytes expressing mutant SOD1 show a decrease in global protein secretion, indicating possible impairment of normal trophic support for motor neurons (Benkler *et al.* 2013). However, SOD1 astrocytes secrete increased amounts of mutant SOD1 protein; this exosome-secreted SOD1 is internalised into motor neurons and causes toxicity, although the toxicity of other additional soluble astrocyte-released factors cannot be ruled out (Nagai *et al.* 2007; Basso *et al.* 2013). Activated astrocytes show decreased expression of glutamate reuptake transporters, which may exacerbate excitotoxicity in ALS (Bruijn *et al.* 1997b; Howland *et al.* 2002). Reactive astrocytes show increased production of neuroinflammatory molecules such as iNOS and nitric oxide (Cassina *et al.* 2002; Barbeito *et al.* 2004), cyclooxygenase and prostaglandins (Yiangou *et al.* 2006), nerve growth factor (Pehar *et al.* 2004), and pro-inflammatory cytokines (Hensley *et al.* 2006; Lee *et al.* 2013a), with detrimental effects on the health of motor neurons (Cassina *et al.* 2002; Barbeito *et al.* 2004; Okuno *et al.* 2004). Reactive astrocytes in ALS also show increased production of Fas ligand and nerve growth factor, which may trigger cell death in Fas-expressing or p75 neurotrophin receptor-expressing motor neurons (Vargas & Johnson 2010). The neuroinflammatory factors produced by astrocytes may play a direct role in motor neuron damage, or may cause activation of microglia and exacerbate neuroinflammation (Wang *et al.* 2011b). Thus, there are multiple possible mechanisms by which astrocytes may contribute to motor neuron degeneration.

1.3.3.2 Microglia

Microglia are the resident immune cells of the central nervous system. Resting microglia constantly sense their environment and are rapidly activated in response to cytokines, chemokines, cellular debris, pathogen motifs such as LPS, and factors released by degenerating neurons (Dewil *et al.* 2007; Kraft & Harry 2011). Activated microglia can produce variable amounts of growth factors, cytokines, and reactive oxygen species, depending on the activating stimulus (Appel *et al.* 2011).

Microglial proliferation and activation is widespread in the spinal cord tissue of ALS patients (Kawamata *et al.* 1992; Appel *et al.* 1993; Henkel *et al.* 2004), and also in SOD1 rat (Graber *et al.* 2010) and mouse (Hall *et al.* 1998b; Almer *et al.* 1999; Alexianu *et al.* 2001) ALS models. Some SOD1 rodent models show microglial activation preceding the onset of disease symptoms, implicating a possible causative role for neuroinflammation in the development of ALS (Alexianu *et al.* 2001; Graber *et al.* 2010). Replacement of $SOD1^{G93A}$ microglia with wild type microglia by bone marrow transfer, or by microglia-specific knockdown of the mutant SOD1 transgene, increases survival time but does not alter disease onset (Boillee *et al.* 2006; Lee *et al.* 2012), indicating that microglial SOD1 expression and microglial activation may accelerate the rate of disease progression after onset. However, ablation of proliferating microglia from SOD1 mice also caused an exacerbation of disease progression, indicating a protective role for microglia in ALS (Audet *et al.* 2012).

These seemingly dual neuroprotective and pro-inflammatory roles for microglia may be explained by different phenotypes of microglial activation (Appel *et al.* 2011). As occurs with macrophages, microglia can adopt either an M1-like neurotoxic phenotype, or an M2-like neuroprotective phenotype, depending on the stimulus inducing microglial activation (Evans *et al.* 2013). The M1 phenotype is characterised by increased production of reactive oxygen species such as NO and pro-inflammatory cytokines such as TNFα and IL-6, and reduced production of growth factors and anti-inflammatory cytokines; conversely, the M2 phenotype is characterised by increased production of BDNF and anti-inflammatory cytokines such as TGFβ and IL-10, and decreased production of pro-inflammatory cytokines (Appel *et al.* 2011). However, these M1 and M2 phenotypes likely exist on a spectrum of possible phenotypes rather than as a ‘pure M1’ or ‘pure M2’ phenotype, with the ultimate pro- or anti-

inflammatory output of individual microglia based on their relative expression of protein markers and cytokines, and their reactive oxygen species production.

In SOD1 mice, recent reports suggest that the M2 microglial phenotype appears to prevail until disease onset, and the M1 microglial phenotype appears predominant throughout the rapidly-progressing phase of disease (Beers *et al.* 2011b; Liao *et al.* 2012). Cultured microglia expressing SOD1 show increased production of superoxide (Ferraiuolo *et al.* 2011) and decreased neuroprotective abilities (Sargsyan *et al.* 2011), indicating that expression of mutant SOD1 may push microglia towards an M1 neurotoxic phenotype. In addition, activation of cultured microglia by extracellular or motor neuron-secreted mutant SOD1 increases microglial TNFα and ROS production; in turn, the factors produced by these SOD1-activated microglia are cytotoxic to motor neurons (Urushitani *et al.* 2006; Roberts *et al.* 2013).

The toxicity of activated microglia to motor neurons may involve the production of NO (Thonhoff *et al.* 2012). Two enzymes involved in the metabolism of L-arginine, Arginase1 (Arg1) and iNOS, control NO production from microglia; increasing expression of Arg1 reduces NO production, while increasing expression of iNOS increases NO production (Andrew & Mayer 1999; Gobert *et al.* 2000; Ash 2004). M1-activated microglia produce more NO than M2-activated microglia (Lewis *et al.* 2012a); the M2 phenotype displays higher levels of Arg1 and lower levels of iNOS, while the M1 phenotype displays lower levels of Arg1 and higher levels of iNOS (Colton 2009). Therefore, Arg1 and iNOS are putative markers of the microglial activation phenotype.

The M1/M2 activation status of spinal cord microglia in SOD1 mice is also influenced by infiltrating T-cells (Beers *et al.* 2008), with T-regulatory cells promoting the neuroprotective M2 microglial phenotype (Beers *et al.* 2011a). The modulation of CNS microglial phenotype by T cells from the systemic circulation indicates that the peripheral immune system may play a role in determining microglial activation in ALS mice. Interestingly, ALS patients show alterations in circulating immune components such as plasma cytokine levels (Houi *et al.* 2002; Cereda *et al.* 2008) and T lymphocyte levels (Banerjee *et al.* 2008), which would suggest alterations of the adaptive immune system in ALS.

Together these data suggest that neuroinflammation, mediated by astrocytes, microglia, and infiltrating immune cells, may prove detrimental to motor neurons in ALS.

1.3.4 Mitochondrial dysfunction

Mitochondria are responsible for oxidative phosphorylation, intracellular calcium buffering, lipid metabolism, and regulation of apoptosis (Karbowski & Neutzner 2012). Damage to the mitochondria or the electron transport chain (ETC) results in a loss of ATP production (Berg *et al.* 2002), increased ROS production (Turrens 2003), loss of intracellular calcium buffering (Ferraiuolo *et al.* 2011), collapse of mitochondrial membrane potential, and ultimately cell death via apoptosis (Beltran *et al.* 2002). In ALS, mitochondrial alterations may be present in both motor neurons and muscle fibres.

1.3.4.1 Mitochondrial alterations in ALS motor neurons

ALS patients show reduced mitochondrial numbers in spinal cord motor neurons, and exhibit axonal clustering of mitochondria compared with controls (Sasaki & Iwata 1996; Wiedemann *et al.* 2002). Spinal cord mitochondria from ALS patients are reported to have reduced levels and activity of electron transport chain protein complexes (Borthwick *et al.* 1999; Wiedemann *et al.* 2002; Ilieva *et al.* 2007); in some ALS patients, this may be explained by alterations in the mitochondrial DNA encoding ETC subunit proteins (Dhaliwal & Grewal 2000; Wiedemann *et al.* 2002).

SOD1 mouse models of ALS show mitochondrial vacuolation and degeneration in spinal cord motor neurons (Wong *et al.* 1995; Kong & Xu 1998), with activation of the mitochondrial permeability transition pore thought to play a role in mitochondrial damage (Martin 2010). Spinal cord mitochondria from SOD1 rodents also show decreased ETC activity and increased ROS production, even preceding disease onset (Browne *et al.* 1998; Jung *et al.* 2002; Panov *et al.* 2011). Decreased ETC activity in symptomatic SOD1 mice is thought to result from decreased respiratory capacity, rather than uncoupling of the ETC from ATP synthesis (De Vos *et al.* 2012). Interestingly, there are reports of increased respiratory activity in the frontal and motor cortices of patients with SOD1-linked familial ALS (Bowling *et al.* 1993; Browne *et al.* 1998), which may indicate that disease processes differ between human and rodent SOD1-linked ALS.

1.3.4.2 Mitochondrial alterations in ALS muscle

Mitochondria from the muscle tissue of ALS patients show impaired respiratory function, with reduced activity of ETC enzymes (Wiedemann *et al.* 1998; Krasnianski *et al.* 2005; Crugnola *et al.* 2010). Deficits in muscle mitochondrial function may be

minor at early stages of disease, but increase as the disease progresses (Echaniz-Laguna *et al.* 2002; Echaniz-Laguna *et al.* 2006). An energy deficit in skeletal muscle may induce denervation of neuromuscular junctions (Dupuis *et al.* 2004; Dupuis *et al.* 2009).

Mitochondrial dysfunction and disorganisation has also been reported in the muscle of several animal model systems expressing ALS-related proteins. ATP production was decreased in isolated muscles from SOD1 mice (Leclerc *et al.* 2001; Derave *et al.* 2003), with a pre-symptomatic upregulation of mRNA for alternative ATP-generating pathways in $SOD1^{G86R}$ mice indicating a possible compensatory response to mitochondrial dysfunction (Gonzalez de Aguilar *et al.* 2008). Additionally, ALS-associated mutations in vesicle-associated membrane protein (synaptobrevin)-associated protein B (VAPB) prevent the secretion of its major sperm protein domain from *Drosophila melanogaster* neurons (Tsuda *et al.* 2008); the loss of this secreted ligand leads to motor impairment in *Caenorhabditis elegans* due to altered mitochondrial positioning and function in the muscle (Han *et al.* 2013); thus, alterations in muscle mitochondrial function may predispose to ALS.

1.3.4.3 Interaction between mutant SOD1 and mitochondria

Two SOD isoforms are normally present in the mitochondria to detoxify superoxide radicals produced by the ETC: SOD1 in the intermembrane space, and SOD2 (Mn-SOD) in the mitochondrial matrix (Turrens 2003). However, ALS-linked mutant SOD1 shows abnormal binding to the cytosolic face of the outer mitochondrial membrane (MM) (Mattiazzi *et al.* 2002; Liu *et al.* 2004; Ferri *et al.* 2006; Vande Velde *et al.* 2008), and to the inner MM in the intermembrane space (Mattiazzi *et al.* 2002; Ahtoniemi *et al.* 2008), with detrimental effects on mitochondrial function. Mutant SOD1 bound to the inner MM may produce ROS which damage ETC components (Ahtoniemi *et al.* 2008), potentially inhibiting respiration. Oligomeric forms of mutant SOD1 are associated with induction of apoptosis when bound to the outer MM are (Rabizadeh *et al.* 1995). Mutant TDP43 also causes mitochondrial injury in NSC34 cells (Duan *et al.* 2010), indicating a possible shared mechanism between SOD1- and TDP43-mediated ALS.

Thus, evidence from both ALS patients and ALS mouse models indicates that pathogenesis of ALS may be due to disruption of mitochondrial function in either motor neurons or skeletal muscle.

1.3.5 RNA processing dysfunction

Sporadic ALS patients show widespread changes in motor neuron gene expression and mRNA splicing (Rabin *et al.* 2010). A number of RNA-processing proteins are associated with ALS and other motor neuron diseases, as discussed below.

1.3.5.1 TDP43 and FUS

TAR-DNA binding protein 43 (TDP43) and fused in sarcoma (FUS) are both DNA/RNA binding proteins which are major components of ubiquitinated protein inclusions in ALS and in frontotemporal dementia (FTD) (Neumann *et al.* 2006; Kwiatkowski *et al.* 2009; Vance *et al.* 2009). Mutations in TDP43 and FUS are associated with both familial and sporadic forms of ALS (Sreedharan *et al.* 2008; Kwiatkowski *et al.* 2009; Vance *et al.* 2009). TDP43 and FUS are usually localised to the nucleus, and have roles in multiple aspects of RNA processing such as transcription, exon splicing, microRNA biogenesis, and mRNA transport and stabilisation (Strong *et al.* 2007; Lagier-Tourenne & Cleveland 2009; Buratti *et al.* 2010). ALS-associated mutations cause mislocalisation of TDP43 and FUS to the cytoplasm, with their subsequent aggregation (Kabashi *et al.* 2008; Winton *et al.* 2008; Igaz *et al.* 2009; Kwiatkowski *et al.* 2009; Vance *et al.* 2009). Cytoplasmic aggregation of ALS-linked mutant TDP43 or FUS implies the development of pathology in ALS by either impairment of normal RNA processing, or sequestration of RNA and RNA-binding components in the cytoplasm (Siddique & Ajroud-Driss 2011; Lagier-Tourenne *et al.* 2012).

TDP43 and FUS are involved in the processing of thousands of pre-mRNA transcripts (Polymenidou *et al.* 2011), and regulate splicing of several genes involved in neuronal differentiation, survival, and synaptic function (Polymenidou *et al.* 2011; Tollervey *et al.* 2011; Lagier-Tourenne *et al.* 2012). TDP43 and FUS also show roles in stabilisation of mRNA for transport down the axon for localised protein translation (Kanai *et al.* 2004; Wang *et al.* 2008; Fallini *et al.* 2012). Additionally, FUS plays a role in DNA damage repair (DDR) by recruiting DDR proteins to the sites of double-stranded breaks (Rulten *et al.* 2013; Wang *et al.* 2013). Aggregated pathological TDP43 proteins, and C-terminal TDP43 fragments, appear hyperphosporylated and insoluble (Neumann *et al.* 2006; Kabashi *et al.* 2008; Winton *et al.* 2008; Igaz *et al.* 2009), supporting the idea that

the loss normal TDP43 RNA-processing function may lead to the development of ALS (Polymenidou *et al.* 2011),

However, aggregated cytoplasmic TDP43 displays aberrant interactions with other cytoplasmic components (Ravits *et al.* 2013), and may sequester essential RNA-processing components such as heterogeneous nuclear ribonuclear proteins, with which TDP43 would normally associate in a spliceosome complex (Buratti *et al.* 2005). TDP43 aggregation may indirectly affect RNA processing by sequestration of other RNA-processing proteins. Thus, the loss of RNA-binding function by TDP43 and FUS, or their sequestration of other RNA-binding components in the cytoplasm, may play a role in ALS pathogenesis.

1.3.5.2 Other RNA-binding proteins associated with motor neuron diseases

Several proteins with various functions in RNA metabolism are associated with the development of motor neuron diseases other than ALS.

Mutations in senataxin (SETX), a DNA/RNA helicase with roles in the initiation and termination of mRNA transcription, the resolution of DNA /RNA hybrids, and mRNA splicing (Suraweera *et al.* 2009; Skourti-Stathaki *et al.* 2011; Bennett *et al.* 2013; Yuce & West 2013), are associated with childhood- and juvenile-onset forms of ALS and hereditary ataxia (Chen *et al.* 2004; Moreira *et al.* 2004). Varying lengths of poly-glutamine repeat expansions in the RNA-binding protein, Ataxin2, lead to spinocerebellar ataxia type 2 and increased risk for sporadic ALS (Imbert *et al.* 1996; Pulst *et al.* 1996; Sanpei *et al.* 1996; Elden *et al.* 2010). Angiogenin, mutations in which are associated with ALS (Greenway *et al.* 2004), requires its RNAse activity to provide neuroprotection in response to stress (Aparicio-Erriu & Prehn 2012). Reduced expression of survival of motor neuron (SMN) protein, required for the formation of small nuclear ribonucleoproteins in the spliceosome complex, causes spinal muscular atrophy (Lefebvre *et al.* 1995; Fischer *et al.* 2011). Variations in the FUS-related RNA-processing protein, TAF15, are linked with ALS risk (Ticozzi *et al.* 2011).

Finally, the ALS/FTD-associated hexanucleotide repeat expansion in C9orf72 produces repeat-containing RNA, which forms nuclear RNA foci (DeJesus-Hernandez *et al.* 2011). These foci sequester RNA-binding proteins and prevent normal RNA processing, causing cellular toxicity (Lee *et al.* 2013b).

Together, these data suggest a role for impaired RNA processing in ALS aetiology.

1.3.6 Excitotoxicity

In the motor system, signals are transmitted from upper to lower motor neurons through the release of the neurotransmitter glutamate from the pre-synaptic membrane. Glutamate activates glutamate receptors on the lower motor neuron, allowing influx of calcium into the cell. Calcium activates many intracellular pathways, so intracellular calcium levels are tightly controlled. Excitotoxicity is the excessive stimulation of ionotropic glutamate receptors, overloading intraneuronal calcium-buffering capacity and leading to cell death through calcium-dependent pathways (Ferraiuolo *et al.* 2011; Bae *et al.* 2013). Excitotoxicity is implicated in ALS pathogenesis, with increased levels of neuronal calcium reported in ALS patients (Siklos *et al.* 1996).

Furthermore, the only effective drug which can mildly slow disease progression in ALS patients is Riluzole (Bensimon *et al.* 1994), a drug which is thought to act by altering multiple aspects of glutamate dynamics around the synapse (Martin *et al.* 1993; Lamanauskas & Nistri 2008; Cheah *et al.* 2010). Together, these data suggest that excitotoxicity plays an aetiological role in ALS. Glutamate excitotoxicity in ALS could be mediated by deficits in glutamate-reuptake proteins, by excessive glutamate release from upper motor neurons, or by intrinsic factors specific to motor neurons.

1.3.6.1 Deficits in glutamate handling

In line with deficits in glutamate handling, the distribution of glutamate appears to be altered in ALS. ALS patients show elevated levels of glutamate in both CSF (Rothstein *et al.* 1990) and plasma (Plaitakis *et al.* 1988), but show decreased glutamate levels within the spinal cord tissue, implicating redistribution of glutamate from the intracellular to the extracellular compartment (Plaitakis *et al.* 1988).

Glutamate is normally cleared from the synaptic cleft by astrocytes expressing the glutamate transporter, excitatory amino acid transporter 2 (EAAT2). The glial expression of EAAT2 was reduced in the spinal cord of ALS patients (Rothstein *et al.* 1995), and the expression level of the mouse EAAT2 homologue was reduced in the SOD1 mouse spinal cord (Bendotti *et al.* 2001). These data indicate that faulty glutamate reuptake from the synaptic cleft in ALS may be responsible for the increased

levels of glutamate in ALS CSF, potentially leading to excitotoxicity in ALS via excessive activation of glutamate receptors on the post-synaptic membrane.

1.3.6.2 Excessive glutamate release and glutamate receptor stimulation

In line with excessive glutamate release from upper motor neurons, cortical motor neurons exhibit hyperexcitability (Bae *et al.* 2013). Excessive firing of upper motor neurons would lead to increased glutamate levels in the synaptic cleft, chronically stimulating glutamate receptors on lower motor neurons and potentially leading to excitotoxicity. The hyperexcitability of motor neurons could be due to loss of inhibitory synaptic inputs from cortical or spinal interneurons (Sunico *et al.* 2011; Turner & Kiernan 2012; Bae *et al.* 2013).

Excitotoxicity may be exacerbated in ALS by elevated levels of the NMDA receptor co-agonist, D-serine, which have been reported in both SOD1 mouse and ALS patient spinal cord (Sasabe *et al.* 2007). Familial ALS in some patients is associated with mutations in D-amino oxidase, which normally degrades D-serine (Mitchell *et al.* 2010), strengthening an association between excitotoxicity and ALS.

Additionally, the diet of the Chamorro people of the Mariana Islands can be high in cyanobacteria-derived glutamate receptor agonist and excitotoxin, β-methylamino-L-alanine, implicating the dietary ingestion of an environmental excitotoxin in the historical high prevalence of ALS in Guam (Papapetropoulos 2007; Chiu *et al.* 2011).

1.3.6.3 Motor neuron-specific vulnerability to excitotoxicity

Motor neurons may be specifically vulnerable to glutamate-mediated excitotoxicity. This may be partly due to low expression of calcium-binding proteins, which might limit ability of motor neurons to handle a large calcium influx (Appel *et al.* 2001). Motor neurons express low levels of the calcium-impermeable GluR2 AMPA receptor subunit (Kawahara *et al.* 2003). Additionally, motor neurons in ALS show deficient editing of the GluR2 AMPA receptor subunit mRNA at the Q/R site, resulting in ALS-affected motor neurons expressing calcium-permeable AMPA receptors (Kawahara *et al.* 2004; Kwak & Kawahara 2005). These motor neuron-specific factors may predispose motor neurons to excitotoxic cell death, and underlie the selective degeneration of motor neurons and the relative sparing of sensory neurons in ALS (Van Den Bosch *et al.* 2000).

Therefore, multiple lines of evidence suggest excitotoxicity as a possible mechanism for motor neuron degeneration in ALS.

1.3.7 Protein misfolding and protein degradation pathways

1.3.7.1 Misfolded proteins in ALS

Ubiquitinated protein aggregates are a pathological hallmark of both sporadic and familial ALS. Polyubiquitin chains target misfolded proteins for degradation through the proteasome or via autophagy. The protein products of many ALS-related genes are found within ubiquitinated aggregates in the cytoplasm of motor neurons in ALS, notably SOD1, TDP43, FUS, p62, OPTN, UBQLN2 and neurofilaments (Ravits *et al.* 2013). ALS-linked mutations in SOD1 and TDP43 proteins increase their propensity for misfolding and aggregation (Bruijn *et al.* 1998; Johnston *et al.* 2000; Wang *et al.* 2002; Furukawa & O'Halloran 2005; Johnson *et al.* 2009). In addition, the ALS-associated C9orf72 repeat expansion (DeJesus-Hernandez *et al.* 2011) produces RNA which undergoes repeat-associated non-ATG translation (Zu *et al.* 2011) to produce dipeptide repeat proteins, which form cytoplasmic aggregates (Mori *et al.* 2013).

Misfolded and aggregated proteins could perturb normal neuronal metabolism in a number of ways. The aggregation of proteins into cytoplasmic inclusions may impair the normal function of the aggregated proteins, sequester other protein or mRNA species which interact with the aggregated proteins, or overwhelm protein degradation mechanisms (Blokhuis *et al.* 2013). Mammalian cells have several mechanisms for dealing with the presence of unfolded proteins. Misfolded proteins in the endoplasmic reticulum (ER) trigger ER stress responses, while ubiquitinated proteins in the cytoplasm are degraded by the proteasome or through autophagy (Xu *et al.* 2005). Some proteins found in ALS aggregates have normal functions in protein degradation pathways, such as p62, OPTN, and UBQLN2 (Fecto & Siddique 2011). The formation of aggregates containing ubiquitinated proteins, including those with roles in protein degradation pathways, links faults in protein degradation pathways with the development of ALS pathology (Fecto & Siddique 2011).

1.3.7.2 ER stress and the unfolded protein response

The ER is an important site for the folding of nascent polypeptides (Schroder 2008). Accumulation of unfolded proteins within the ER (ER stress) triggers a series of events intended to clear the ER of unfolded proteins, the unfolded protein response (UPR) (Xu *et al.* 2005). Initially, the UPR upregulates protein chaperones involved in protein folding, and promotes removal of unfolded proteins from the ER for degradation by the

proteasome; however, prolonged ER stress triggers pro-apoptotic pathways (Xu *et al.* 2005). Induction of the UPR, and of apoptotic mediators, can be observed in the spinal cords of sporadic ALS patients and SOD1 rodents (Ilieva *et al.* 2007; Atkin *et al.* 2008). Mutations in VCP, a protein which mediates removal of misfolded proteins from the ER for degradation (Raasi & Wolf 2007; Yang *et al.* 2013), are associated with familial ALS (Johnson *et al.* 2010). VAPB, whose mutations are also associated with ALS (Nishimura *et al.* 2004), is thought to induce the UPR in response to ER stress (Kanekura *et al.* 2006; Suzuki *et al.* 2009; Chen *et al.* 2010). Mutations in SIGMAR1, another ER-stress-modulating protein, have been implicated in familial ALS (Al-Saif *et al.* 2011; Ha *et al.* 2011), although a recent study suggests that SIGMAR1 mutations segregate closely with c9orf72 expansions (Belzil *et al.* 2013). Impairment of UPR pathways may exacerbate ER stress and induce cell death in ALS.

1.3.7.3 The ubiquitin-proteasome system and the autophagy system

The proteasome complex mediates the unfolding and degradation of polyubiquitinated proteins (Jung & Grune 2013), while autophagy engulfs protein aggregates and organelles in membrane-bound vesicles for degradation through fusion with lysosomes (Chen *et al.* 2012). Autophagy degrades long-lived proteins, but excessively-induced autophagy can lead to autophagic cell death (Nagley *et al.* 2010; Chen *et al.* 2012). Several proteins whose mutations are associated with ALS are involved in protein degradation pathways. VCP is required for the maturation of autophagic vesicles (Ju *et al.* 2009). UBQLN2 binds to polyubiquitin chains and to the proteasome, directing the degradation of ubiquitinated proteins (Deng *et al.* 2011); ubiquilins are also required for the formation of autophagic vesicles (N'Diaye *et al.* 2009). p62 is also involved in the transport of ubiquitinated proteins to the proteasome and to autophagic vesicles (Seibenhener *et al.* 2004; Pankiv *et al.* 2007; Fecto *et al.* 2011). Charged multivesicular body protein 2B (CHMP2B) acts in an endosomal sorting complex in the formation of multivesicular bodies in autophagy (Parkinson *et al.* 2006; Rusten & Simonsen 2008). FIG4 may mediate formation and clearance of autophagic vesicles (Chow *et al.* 2009; Ferguson *et al.* 2009), while OPTN functions as an adaptor molecule facilitating autophagosome-lysosome fusion (Maruyama *et al.* 2010; Tumbarello *et al.* 2013). As multiple genes involved in ER stress and protein degradation pathways show ALS-linked mutations, accumulation of misfolded proteins and protein degradation pathway dysfunction could play a role in ALS pathogenesis.

1.3.8 Intracellular transport deficits

Intracellular transport to deliver cellular components to their required location is a vital function for all living cells; motor neurons, however, have a particularly high demand for intracellular transport in order to sustain the distal portions of their long axons (Collard *et al.* 1995). Deficits in axonal transport may result in insufficient distal delivery of organelles and proteins required for axonal maintenance and synaptic function, insufficient recycling of faulty synaptic components, and blockage of trophic factor signalling pathways (Breuer *et al.* 1987). The delivery of cytoskeletal proteins, and their proper assembly at the distal axon, is essential for axonal maintenance in motor neurons (Lariviere & Julien 2004). At the cell body, transport deficits may interfere with ER-Golgi transport and with autophagy. Trafficking of organelles, vesicles, and proteins around the cell body and along axons is mediated by molecular motor proteins moving along cytoskeletal protein tracks (Hirokawa 1998). Intracellular transport deficits appear to play a role in the pathophysiology of ALS – both anterograde and retrograde axonal transport are decreased in ALS patients (Breuer *et al.* 1987; Sasaki & Iwata 1996), and SOD1 and TDP43 mouse models of ALS also show impairment of axonal transport (Zhang *et al.* 1997; Murakami *et al.* 2001; Magrane *et al.* 2013).

1.3.8.1 Molecular motor proteins in ALS

Dyneins and kinesins are the motor proteins responsible for retrograde and anterograde transport, respectively. The dynein molecular motor is a large complex of proteins including dynein subunits and dynactin, which plays a role in facilitating interaction between the dynein motor, the cargo and the microtubule track (Waterman-Storer *et al.* 1995; Waterman-Storer *et al.* 1997). Both ALS patients and SOD1 mice show decreased levels of dynactin mRNA (Kuzma-Kozakiewicz *et al.* 2013b), and mutations of dynactin subunits cause a slowly-progressive MN disease in humans (Puls *et al.* 2003; Munch *et al.* 2004) and in mice (Hafezparast *et al.* 2003; Laird *et al.* 2008). Additionally, ALS patients show lower expression of kinesin family proteins than controls (Pantelidou *et al.* 2007; Kuzma-Kozakiewicz *et al.* 2013a), showing that ALS may be associated with the disruption of both retrograde and anterograde transport. The mutant SOD1 protein may interact with kinesin-associated proteins or with subunits of the dynein/dynactin complex (Ligon *et al.* 2005; Zhang *et al.* 2007; Tateno *et al.* 2009), disrupting their normal roles in axonal transport.

1.3.8.2 Cytoskeletal protein alterations in ALS

Cytoskeletal elements in motor neurons comprise microtubules, intermediate filaments, and actin microfilaments, and alterations to these proteins are associated with ALS.

1.3.8.2.1 Microtubule alterations

Microtubules provide structural support for the neuron and form the network along which molecular motor proteins move, but may become destabilised in ALS. Microtubule-associated proteins (MAPs), which stabilise microtubules, are downregulated or show production of aberrant isoforms in SALS patients (Binet & Meininger 1988; Jiang *et al.* 2005), while aberrant isoform production and increased phosphorylation of the MAP tau are observed in SOD1 mouse models (Farah *et al.* 2003; Usarek *et al.* 2006). Disruptions of the microtubule cytoskeleton may play a role in ALS, through the loss of cytoskeletal structure or the inhibition of axonal transport.

1.3.8.2.2 Intermediate filament alterations

Intermediate filament proteins – neurofilaments, peripherin, and α-internexin – anchor organelles, maintain cytoarchitecture, and prevent tension on the axon (Szaro & Strong 2010). The correct expression level and phosphorylation status of peripherin and of the neurofilament triplet protein subunits are important for the normal formation of neurofilament networks (Straube-West *et al.* 1996; Beaulieu *et al.* 2000; Robertson *et al.* 2001). Intermediate filaments are normally moved down the axon via anterograde axonal transport, but are frequently observed in motor neuron cell body inclusions and in proximal axonal spheroids in ALS patients (Migheli *et al.* 1993) and SOD1 mice (King *et al.* 2011), suggesting improper intermediate filament trafficking in ALS.

Mutations in neurofilament and peripherin genes are associated with a small number of sporadic ALS patients; these mutations may promote intermediate filament aggregation and impair axonal transport, through aberrant isoform production or through hyperphosphorylation (Figlewicz *et al.* 1994; Al-Chalabi *et al.* 1999; Gros-Louis *et al.* 2004; Leung *et al.* 2004; Xiao *et al.* 2008). Expression of aberrant neurofilament isoforms in mice leads to neurofilament aggregation and motor neuron degeneration (Cote *et al.* 1993; Lee *et al.* 1994; Collard *et al.* 1995). The presence of accumulated neurofilaments in the proximal axon may impair the process of axonal transport as a whole, by sequestering motor proteins or by physically blocking the axon (Zhang *et al.* 1997).

1.3.8.3 Vesicle trafficking deficits in ALS

Several proteins involved in vesicle transport and intracellular protein trafficking are associated with ALS (Ferraiuolo *et al.* 2011; Soo *et al.* 2011). ALS patient motor neurons show fragmentation of the Golgi apparatus, indicating possible disruption of the intracellular protein shuttling pathways (Gonatas *et al.* 1992; Okamoto *et al.* 2010). Many ALS-associated gene mutations are in proteins involved in vesicle trafficking.

Actin filaments and their associated myosin motor proteins, as well as microtubules and their dynein/kinesin motor proteins, facilitate transport of membrane-bound vesicles between intracellular compartments (Chevalier-Larsen & Holzbaur 2006; Laird *et al.* 2008). Mutations in profilin1, a protein required for actin filament formation, are associated with familial ALS (Wu *et al.* 2012). Mutations in alsin, a protein involved in endosomal trafficking and fusion, and actin cytoskeleton rearrangement in growth cones (Topp *et al.* 2004), are linked to juvenile-onset primary lateral sclerosis (Yang *et al.* 2001). FIG4, a phosphoinositide phosphatase which mediates the retrograde trafficking of endosomal vesicles to the Golgi network, shows mutations in sporadic and familial ALS patients (Chow *et al.* 2009). Mutations in OPTN were identified in familial and sporadic ALS patients (Maruyama *et al.* 2010); OPTN is involved in vesicle and lysosome trafficking, and protein secretion from the Golgi apparatus, in conjunction with Rab8 and myosin IV proteins (Sahlender *et al.* 2005).

VAPB is an integral membrane protein which localises to the ER and to ER-Golgi intermediates, and is involved in vesicle transport (Skehel *et al.* 2000; Tran *et al.* 2012). Mutations in VAPB are associated with ALS, and VAPB expression may be reduced in the motor neurons of ALS patients (Nishimura *et al.* 2004; Teuling *et al.* 2007). Mutations in VAPB may perturb its interaction with microtubules, disorder the ER, contribute to the fragmentation of the Golgi apparatus and prevent transport of proteins on the ER-Golgi axis (Mitne-Neto *et al.* 2007; Teuling *et al.* 2007; Gkogkas *et al.* 2008; Fasana *et al.* 2010; Papiani *et al.* 2012). Additionally, expression of mutant SOD1 inhibits the classical ER-Golgi secretory pathway (Atkin *et al.* 2013), and the normal function of C9orf72 may relate to membrane trafficking (Levine *et al.* 2013).

Thus, several proteins involved in ALS have vital functions in both axonal transport and intracellular protein and vesicle trafficking, suggesting transport deficits contribute to the pathophysiology of ALS.

1.3.9 Convergent pathological mechanisms in ALS aetiology

The major pathophysiologies involved in ALS are oxidative stress, neuroinflammation and glial activation, mitochondrial dysfunction, RNA processing, excitotoxicity, protein aggregation and dysfunction of protein degradation, and inhibition of intracellular transport. The presence of multiple molecular mechanisms causing similar phenotypes suggests a downstream convergence of mechanisms (Ravits *et al.* 2013). While each possible cause of ALS has been considered separately in the previous sections, these cellular processes are in reality interwoven, with alterations in a given pathway having downstream effects on other ALS-related pathways. This section will attempt to outline some of the convergence points which may be related to ALS pathophysiology.

1.3.9.1 Oxidative stress as a convergence point

Oxidative stress is intricately linked to a number of other pathways affected in ALS, occurring either upstream of, or as a consequence of, other ALS-associated pathways. First, oxidative stress could contribute to protein aggregation. Protein oxidation and nitration can increase the propensity of proteins such as SOD1 to aggregate and can induce improper neurofilament assembly and aggregation (Chou *et al.* 1996; Crow *et al.* 1997; Sasaki *et al.* 2000; McLean & Robertson 2011). An oxidative environment may also promote the formation of protein aggregates through inter-molecular disulphide bond formation (Banci *et al.* 2008), with protein aggregation placing pressure on the proteasome and autophagy systems. Oxidative stress can cause ER stress (Soo *et al.* 2011); interestingly, mutant proteins undergoing several rounds of oxidative folding in the ER due to their incorrect folding may increase the production of ROS from the ER as well as triggering ER stress (Schroder 2008).

Second, oxidative stress is both an upstream cause of and a downstream effect of mitochondrial dysfunction. Oxidative damage can inhibit the mitochondrial respiratory chain enzymes, causing mitochondrial dysfunction (Poderoso *et al.* 1996; Drechsel *et al.* 2012), and contributing to mitochondrial permeability transition pore opening and apoptosis (Chernyak 1997). In turn, respiratory chain inhibition increases the formation of reactive oxygen species and further contributes to oxidative stress (Turrens 2003).

Third, oxidative stress is linked to excitotoxicity. Oxidative damage to the glutamate reuptake transporter EAAT2 in astrocytes may inactivate the receptor, prevent glutamate clearance from the synaptic cleft, and contribute to excitotoxicity (Trotti *et al.*

1999). Stimulation of NMDA receptors can induce the production of superoxide radicals (Lafon-Cazal *et al.* 1993; Al-Chalabi *et al.* 1995), and elevated calcium concentration can cause isolated mitochondria to produce hydroxyl radicals (Dykens 1994), providing a link between excitotoxicity and oxidative stress.

Fourth, oxidative stress may play a role in glial cell activation. Nitric oxide is a key effector of astrocyte-mediated toxicity to motor neurons (Ferri *et al.* 2004; Vargas & Johnson 2010), while Fas ligand released from activated astrocytes causes ROS-mediated damge in motor neurons through respiratory chain inhibition (Beltran *et al.* 2002). Oxidative stress also acts as a trigger for neuroinflammation (Mates *et al.* 1999).

Fifth, protein and RNA oxidation may contribute to global protein dysregulation and dysfunction. Oxidative or nitrative damage to proteins can alter normal protein structure and function (Reynolds *et al.* 2007); oxidative stress could conceivably impact on any of the other pathways involved in ALS by oxidative damage to the relevant proteins. As mentioned earlier, mRNA oxidation can prevent normal protein expression (Chang *et al.* 2008); uncontrolled oxidative stress therefore has the potential to alter the expression levels of proteins involved in multiple cellular pathways.

Much of the information on ALS-associated pathways comes from research on animal models expressing mutant SOD1 protein, so it is reasonable to question their validity when applied to non-SOD1 ALS. However, the gain of toxic properties by oxidised wild-type SOD1 protein (Deng *et al.* 2006; Furukawa *et al.* 2006; Ezzi *et al.* 2007), and production of oxidative stress associated with mutant TDP43 (Duan *et al.* 2010), suggest that motor neurons in both sporadic ALS and SOD1-mediated familial ALS may experience common degenerative pathways downstream of mutant or oxidatively-damaged SOD1 protein, further implicating oxidative stress in the pathogensis of ALS.

1.3.9.2 Mitochondrial dysfunction as a convergence point

Mitochondrial dysfunction is closely linked to oxidative stress, as outlined above, but is also linked to excitotoxicity and to activation of the autophagy system. Increased calcium levels from excitotoxic stimuli contribute to mitochondrial dysfunction, loss of the electrochemical gradient across the inner mitochondrial membrane, mitochondrial permeability transition pore formation, and apoptosis (Martin 2010). The autophagy system functions in mitochondrial quality control, by degrading damaged mitochondria

to limit their production of ROS (Dodson *et al.* 2013). Widespread dysfunction of mitochondria may overwhelm the normal capacity of the autophagy system, and impair the autophagy-mediated degradation of protein aggregates.

Mitochondrial dysfunction and the associated loss of ATP production can impair energy-dependent cellular processes necessary for normal cellular function; in motor neurons, the energy demands are large due to the large cytoplasmic volume and the requirement to maintain appropriate axonal transport to and from the neuromuscular junction (Ferraiuolo *et al.* 2011; Ludolph *et al.* 2012). The energy deficit created by dysfunction of mitochondria could potentially impact on any of the ATP-dependent cellular processes which are linked with ALS.

1.3.9.3 Excitotoxicity as a convergence point

The role of excitotoxicity and elevated calcium levels have been discussed in the context of oxidative stress and mitochondrial dysfunction; but intracellular calcium levels also modulate other pathways related to ALS. Intracellular calcium levels are a regulator of axonal transport, with elevated calcium dissociating molecular motors from microtubules (Breuer & Atkinson 1988a, 1988b; Morotz *et al.* 2012). Neurofilament phosphorylation and aggregation can also be mediated by glutamate-stimulated activation of calcium-sensitive kinases (Al-Chalabi *et al.* 1995; Takeuchi *et al.* 2005), implicating excitotoxicity as a potential upstream mechanism of impaired intracellular transport. Additionally, excitotoxicity and calcium dysregulation can induce ER stress and autophagy (Tarabal *et al.* 2005; Ilieva *et al.* 2007; Soo *et al.* 2011), possibly due to dysfunction of calcium-sensitive folding proteins within the ER (Prell *et al.* 2013).

1.3.9.4 Glial activation as a convergence point

Astrocytes are intricately linked with excitotoxicity due to their modulation of the expression of glutamate reuptake transporters (Vargas & Johnson 2010). Interactions between glial cells and motor axons may underlie the formation of axonal spheroids (King *et al.* 2011) – microglial activation in culture induces both the accumulation of neurofilaments and the decrease of axonal transport by molecular motors, through the activation of NMDA receptors (Takeuchi *et al.* 2005). TNFα can also disrupt kinesin function, by activation of intracellular kinase pathways (De Vos *et al.* 2000).

1.3.9.5 Intracellular transport as a convergence point

Intracellular transport impairments in ALS may be linked to functional deficits in the axon terminal, excitotoxicity and protein degradation impairment. Impaired intracellular transport of mitochondria and other essential synaptic components to the axon terminal may result in an energy deficit or impaired function at the neuromuscular junction, causing the axon terminal to detach from the muscle in a 'dying-back' mechanism (Cozzolino & Carri 2012). It is possible that altered intracellular trafficking pathways may result in reduced internalisation of glutamate receptors from the post-synaptic membrane, contributing to excitotoxicity (Hirling 2009). Motor proteins contribute to the trafficking of autophagic vesicles, and thus play a role in autophagic clearance of misfolded and aggregated proteins (Soo *et al.* 2011; Ikenaka *et al.* 2013).

1.3.9.6 Protein degradation pathways as convergence points

The argument for protein aggregation and protein degradation pathways as a common downstream pathway is led by the ubiquitous presence of aggregated proteins in ALS, and the presence of ALS-associated mutations in a number of genes encoding protein degradation pathway proteins (Fecto & Siddique 2011). The accumulation of misfolded proteins, and resultant ER stress, could alter ER-mitochondrial calcium dynamics, making motor neurons more susceptible to excitotoxic stress (Ferraiuolo *et al.* 2011).

1.3.9.7 RNA processing as a convergence point

Deficits in RNA processing could impact a wide range of ALS-associated pathways. In particular, TDP43 and FUS appear to regulate splicing of several genes encoding ALS-associated, autophagy-related proteins – CHMP2B, FIG4, OPTN, VAPB, and VCP (Ling *et al.* 2013). Aberrant astrocytic RNA processing may additionally impair the function of the EAAT2 astrocytic glutamate transporter, contributing to glutamate excitotoxicity (Lin *et al.* 1998). In addition, oxidative stress and ER stress may increase the formation of neuronal stress granules, sequestering RNA-binding proteins and their associated RNAs into aggregates (Kedersha *et al.* 1999; Bentmann *et al.* 2013; Walker *et al.* 2013). Pathological events resulting in irreversible protein aggregation in stress granules, or inability to reverse stress granule formation, may result in TDP43- or FUS-containing aggregates in ALS (Ling *et al.* 2013).

1.3.9.8 Summary of convergence points

In summary, many pathways appear to be involved in the disease pathogenesis of ALS, and there is much cross-talk between the various pathways involved. However, as outlined above through the convergence of ALS-linked pathways, oxidative stress does appear to stand out as a highly involved pathway. Oxidative stress is a potential cause of mitochondrial dysfunction, protein aggregation, ER stress, autophagy and glial activation; oxidative stress is also produced downstream of mitochondrial dysfunction, glial activation, and ER stress. The oxidative stress seen in mouse models of ALS and in ALS patients may be a primary initiator of disease processes or a downstream consequence of disease processes. The targeting of oxidative stress may therefore be an efficient way to 1) prevent primary oxidative damage to motor neurons and their organelles, and 2) prevent the downstream oxidative damage caused by upstream aetiological events such as mitochondrial dysfunction. Antioxidant-based therapies may be useful in preventing damage to cells and organelles in ALS.

1.4 Therapeutic strategies to combat ALS

As demonstrated by the multitude of convergence points in ALS (section 1.3.9), there are many pathways that are thought to be involved in ALS aetiology and many possible therapeutic strategies to combat these pathways. Multi-functional therapeutic strategies, involving compound mixtures or compounds known to have multiple functions, may be the best approach in providing a treatment for ALS. Some potential therapeutic options in the treatment of ALS, namely Gemals compound, metallothionein protein, and Emtin peptide derivatives of metallothionein, are discussed briefly below.

1.4.1 Gemals

Gemals is a cocktail of small molecules – fatty acids, amino acids, vitamins, and antioxidants – that has been shown to have beneficial effects on the survival of a SOD1 rats, but has not yet been tested in SOD1 mice (Nicaise *et al.* 2008). Gemals is a kind of 'Endotherapia' therapy, intended to have antioxidant, immunomodulatory, and neuroprotective activity for the amelioration of complex neurodegenerative disease (Geffard *et al.* 2010). The compounds comprising Gemals are listed in Table 3.1, and the chemical composition of the drug mixture is detailed in Table 3.2.

1.4.2 Metallothionein and Emtins

Metallothioneins (MTs) are small, metal-binding proteins rich in cysteine residues (Aschner 1996). MT proteins act as potent antioxidants (Thornalley & Vasak 1985), and the MT-1 and MT-2 isoforms (MT-1/2) are known to have neuroprotective properties: MT-1/2 is upregulated by astrocytes and secreted extracellularly in response to neuronal damage (Chung *et al.* 2008a); extracellularly applied MT-1/2 promotes neurite outgrowth *in vitro* (Chung *et al.* 2003; Kohler *et al.* 2003) and *in vivo* after neuronal injury (Chung *et al.* 2003; Fitzgerald *et al.* 2007). MT-1/2 is known to be protective in the context of ALS: genetic alteration of MT-1/2 levels in SOD1 mice show a positive correlation between MT-1/2 expression and survival time (Nagano *et al.* 2001; Puttaparthi *et al.* 2002; Tokuda *et al.* 2013). Therefore, administration of MT-2 may be able to increase survival time in SOD1 mice. Emtins are peptide derivatives of the human MT2 protein that show similar neuroprotective properties to the parent MT2 molecule (Ambjorn *et al.* 2008; Asmussen *et al.* 2009a; Sonn *et al.* 2010). Emtins have an additional advantage of readily being able to cross the intact blood-brain barrier (Sonn *et al.* 2010), and may also be appropriate therapeutic molecules for ALS.

1.5 Research questions and aims

Given the many pathways involved in the aetiology of ALS, multi-purpose therapeutics which have some component addressing oxidative stress may provide the best defence for motor neurons against the development of ALS pathology. In seeking to understand which therapeutic targets might be important in ALS, the contribution of microglial phenotype to oxidative stress, through the production of nitric oxide, should be further investigated. In addition, given that oxidative stress is a common pathology between sporadic and familial ALS, multi-functional therapies with some antioxidant properties such as Gemals and metallothionein treatment should be trialled in SOD1 mice as potential treatments for ALS.

Research Question 1:

How does the expression of the neuroinflammatory markers, Arg1 and iNOS, change over time in SOD1 mice and what does this tell us about the role of neuroinflammation and oxidative stress in ALS pathogenesis?

Aim 1: To characterise spinal cord microglia changes in Arg1 and iNOS expression over time in SOD1 mice, and to temporally correlate these changes with development of pathology in motor neurons, induction of oxidative stress responses, and functional decline over time. This aim is addressed in Chapter 2.

Aim 2: To establish baseline measures of functional decline in SOD1 mice over time, to determine measures of disease progression for later pre-clinical studies. This aim is addressed in Chapter 2.

Research Question 2:

Will treatment with an antioxidant therapy for ALS, Gemals, extend survival time and prevent the decline of functional ability in SOD1 mice?

Aim 3: To examine the effects of Gemals treatment on SOD1 mice in a pre-clinical study, with treatment starting from the age of disease onset and continuing until disease endpoint, with survival and maintenance of functional ability as outcome measures. This aim is addressed in Chapter 3.

Research Question 3:

Will treatment with the neuroprotective protein MT2, or its peptide derivatives, or increasing spinal cord MT levels through treadmill exercise, extend survival time and prevent the decline of functional ability in SOD1 mice?

Aim 4: To examine the effects of pre-symptomatic MT2 administration, or treadmill exercise, on disease onset and survival time in SOD1 mice. This aim is addressed in Chapter 4.

Aim 5: To examine the effects of post-symptom-onset administration of the MT2 derivatives, Emtin peptides, on survival time in SOD1 mice. This aim is addressed in Chapter 5.

Chapter 2

Characterisation of neuroinflammatory and functional changes over time in SOD1 mice

2.1 Background

2.1.1 Microglial activation status in ALS

Microglial activation is a major pathology in the spinal cord of ALS patients and SOD1 mice, as discussed in Chapter 1. Microglial activation is commonly seen in the spinal cord of SOD1 animal models at disease onset, and increases with disease progression (Hall *et al.* 1998b; Almer *et al.* 1999; Chiu *et al.* 2008; Gowing *et al.* 2008; Beers *et al.* 2011b; Yang *et al.* 2011), although microglial activation has also been demonstrated to precede disease onset in some studies (Alexianu *et al.* 2001; Graber *et al.* 2010; Sanagi *et al.* 2010). Microglial activation may play an active role in disease progression, as replacing SOD1 microglia with WT microglia in SOD1 mice modulated the rate of disease progression (Boillee *et al.* 2006; Lee *et al.* 2012). SOD1 mice are thought to show a biphasic pattern of disease symptoms, with a brief plateau after onset where symptoms progress slowly, followed by a more rapid decline in functional ability (Beers *et al.* 2011a). This switch, from slowly-progressing to rapidly-progressing phases of disease, is thought to correspond to a switch between anti-inflammatory and pro-inflammatory phenotypes of microglial activation (Beers *et al.* 2011b; Liao *et al.* 2012).

Microglia can show two phenotypes of activation, which are best characterised by protein expression and cytokine production. The M1-like, neurotoxic, pro-inflammatory phenotype of microglial activation is characterised by the elevated expression of pro-inflammatory cytokines and production of reactive oxygen species and nitric oxide (NO); whereas the M2-like, neuroprotective, anti-inflammatory phenotype of microglial activation is characterised by increased expression of anti-inflammatory cytokines and reduced production of free radicals (Colton 2009; Appel *et al.* 2011).

The microglial production of NO is a key factor in the toxicity of activated microglia to motor neurons (Zhao *et al.* 2004; Zhao *et al.* 2006; Thonhoff *et al.* 2012). Microglial production of NO is controlled by the inducible nitric oxide synthase enzyme (iNOS), which converts L-arginine to L-citrulline, producing NO in the process (Andrew & Mayer 1999). L-arginine, the iNOS substrate, is also metabolised by another enzyme, arginase-1 (Arg1), which converts L-arginine to L-ornithine and urea but does not produce NO (Ash 2004). The relative expression of these two L-arginine-metabolising enzymes, iNOS and Arg1, determines how much NO will be produced from a given cell (Gobert *et al.* 2000). Accordingly, high levels of Arg1 and low levels of iNOS are

associated with the M2-like, neuroprotective microglial phenotype, while high levels of iNOS and low levels of Arg1 are associated with the M1-like, neurotoxic microglial phenotype (Colton 2009).

The reported switch between M2-like and M1-like microglial phenotypes in mouse models of ALS has mainly been investigated using cytokine mRNA expression levels (Beers *et al.* 2011a). It is therefore of interest to determine whether changes in iNOS and Arg1 protein expression also occur over time in the microglia of SOD1 mice, and how these changes are temporally related to the development of motor neuron pathology and functional deterioration, as any such protein changes may be reflective of a change in microglial phenotype. As oxidative damage from microglial-produced NO is thought to injure motor neurons, the expression of the antioxidant-response protein, metallothionein-1/2 (MT-1/2), should also be examined in the spinal cord of SOD1 mice to examine the evolution of oxidative stress over the disease course. The timing of oxidative stress response induction may relate to the production of NO by microglia, which in turn may be increased by any shift from an M2-type (Arg1-expressing) microglial phenotype to an M1-type (iNOS-expressing) microglial phenotype.

2.1.2 Measuring disease progression in SOD1 mice

As the underlying aetiology of ALS is as yet unknown, current therapeutic strategies involve addressing the known pathologies which occur in ALS patients and SOD1 mouse models, such as oxidative stress and neuroinflammation. Addressing these pathologies may limit disease processes, and slow disease progression. It is therefore necessary to track the functional decline in SOD1 mice over time, in order to evaluate any beneficial effects of therapeutic compounds. The age of onset, rate of symptom progression, and survival times vary in SOD1 mice according to the level of mutant SOD1 protein expression, gender, and genetic background strain (Alexander *et al.* 2004; Heiman-Patterson *et al.* 2005; Acevedo-Arozena *et al.* 2011; Bame *et al.* 2012).

The SOD1 colony maintained at the University of Tasmania expresses the SOD1 transgene on a congenic C57BL/6 background. As this colony was to be used for evaluation of potential disease therapeutics (see Chapters 3, 4 and 5), it was necessary to establish baseline measurements of functional decline over time.

2.1.3 Aims and hypothesis

This study had two aims. First, to characterise the spinal cord microglia changes in Arg1 and iNOS expression over time in SOD1 mice, and to examine these changes in the temporal context of the appearance of pathological changes in motor neurons, induction of oxidative stress responses, and onset of functional deficits in SOD1 mice. Second, to establish baseline measures of functional decline in SOD1 mice compared to their wild-type littermates which could be used in future studies to monitor disease onset and progression.

Hypothesis: Microglia will shift their expression of L-arginine metabolising enzymes with disease onset: prior to disease onset, the expression of Arg1 will be prevalent, while the expression of iNOS will be prevalent after disease onset, indicating a shift in the spectrum of microglial phenotypes from an M2-predominant to an M1-predominant phenotype in the lumbar spinal cord of SOD1 mice.

Two cohorts of SOD1 mice and their WT littermates were examined in this chapter. Spinal cord samples were obtained from the first cohort at various ages between 6 and 25 weeks of age, and these samples were immunostained for the glial markers Iba1, tomato lectin, and GFAP, for the M1/M2 markers Arg1 and iNOS, for the pathological markers ubiquitin, neurofilament, and protein from the human SOD1 transgene, and for the antioxidant protein MT-1/2. The second cohort of SOD1 and WT mice were monitored for body weight, stride pattern, wire hang duration ability, and neurological score between 6 and 25 weeks of age, in order to characterise functional aspects of disease progression.

2.2 Methods

2.2.1 Animal ethics

All procedures and protocols involving animals were approved by the University of Tasmania's Animal Ethics Committee (permit numbers A10995 and A11958) and were carried out in accordance with the Australian Code of Practice for the Care and Use of Animals for Scientific Purposes.

2.2.2 Maintenance and genotyping of SOD1 mice

2.2.2.1 Strain and colony maintenance

High copy-number founder SOD1 mice, expressing the human $SOD1^{G93A}$ transgene on a C57Bl/6J background, were originally obtained from The Jackson Laboratory (B6.Cg-Tg(SOD1*G93A)1Gur/J, Strain #004435, ME, USA) and a breeding colony of heterozygotes was maintained by the University of Tasmania Animal Services. Animals were housed in OptiMICE cages (Animal Care Systems, CO, USA) in a controlled environment with a 12 hour light/dark cycle and a temperature range of 21-23°C. All mice had access to standard laboratory rodent chow and water *ad libitum*. As SOD1 mice experienced progressive paresis with disease progression, food pellets were placed directly on cage bedding at later stages of disease to ensure continued nutrition.

2.2.2.2 Genotyping

Mice carrying the SOD1 transgene, and their non-transgenic wild type (WT) littermates, were identified by polymerase chain reaction (PCR) and gel electrophoresis, and copy number homogeneity was assessed by quantitative real time PCR (qPCR).

2.2.2.2.1 DNA extraction

Tail-tip samples were collected upon weaning by University of Tasmania Animal Services staff. Genomic DNA was extracted using the GenElute Mammalian Genomic DNA Miniprep Kit (Sigma-Aldrich, NSW, Australia) according to the manufacturer's instructions, with the exception that all centrifugation steps were performed in a benchtop microcentrifuge (Heraeus Biofuge Pico) at 10,000*g*.

2.2.2.2.2 PCR and gel electrophoresis for the presence of the SOD1^{G93A} transgene:

PCR reactions (12.75µL) were prepared containing 1x GoTaq Green Master Mix (Promega, WI, USA), 1µL of genomic DNA template, nuclease-free water (Qiagen, VIC, Australia), and 0.39µM forward and reverse primers for either the human SOD1 (hSOD1) or the murine interleukin-2 gene (mIL-2) (GeneWorks, SA, Australia) (Table 2.1).

PCR was performed using a Corbett Research thermocycler (Qiagen). Reactions were held at 95°C for 3 minutes, then cycled through 95°C for 30 seconds, 60°C for 30 seconds and 72°C for 30 seconds (35 cycles), then held at 72°C for 5 minutes, 30°C for 3 minutes and 24°C for 30 seconds. PCR products were transferred to an agarose gel for electrophoresis, containing 1% w/v agarose (Bioline, NSW, Australia) and 0.01% v/v SYBR-Safe (Life Technologies, CA, USA) in tris-acetate-EDTA (TAE) buffer (40mM tris [Sigma-Aldrich], 20mM acetic acid [Merck Millipore, VIC, Australia], 1mM ethylenediaminetetraacetic acid [EDTA] disodium salt [Sigma-Aldrich]). The PCR products were electrophoresed in TAE buffer for 30 minutes at 100V using a Horizon58 electrophoresis rig (Biometra, NI, Germany) and PowerPac power source (BioRad, CA, USA), and band presence/absence was assessed under UV light in a gel doc imager (BioRad). SOD1 mice showed a PCR product from both the mIL-2 and the hSOD1 reactions, while WT mice showed only a PCR product from the mIL-2 reaction (Table 2.1). Positive controls (SOD1), negative controls (WT) and no-template controls were included in each PCR run. SOD1 mice were then assessed for transgene copy number.

2.2.2.2.3 qPCR for SOD1^{G93A} transgene copy number

Homogeneity of transgene copy number in the genomic DNA of SOD1 mice was assessed using multiplex quantitative PCR. qPCR reactions (12.5µL) contained 1x KAPA ProbeFast Universal Master Mix (KAPA Biosystems, MA, USA), 0.15µM forward and reverse primers for human SOD1 (hSOD1), 0.50µM forward and reverse primers for murine apolipoprotein-B (mApoB), 0.16µM labelled oligonucleotide probes for hSOD1 and mApoB (Table 2.1) (GeneWorks), and nuclease-free water (Qiagen). qPCR was performed using a RotorGene Q real-time PCR cycler (Qiagen) – reactions were held at 95°C for 5 minutes, and cycled through 95°C for 15 seconds and 60°C for 15 seconds (45 cycles); a ramped melt curve from 60°C to 99°C was then performed. Positive (SOD1), negative (WT) and no-template controls were included with each run. All SOD1 samples were run in triplicate.

The relative take-off points of the hSOD1 and mApoB fluorescence curves were compared using the comparative quantitation tool in the RotorGene Q Series software v2.0.2 (Qiagen). The delta-CT (ΔCT) value, representing the difference in the take-off points for the hSOD1 and mApoB curves (measured as the number of cycles), was compared to that of SOD1 positive control DNA. Average ΔCT values for all mice were recorded, for inclusion in statistical analyses of survival if necessary; SOD1 mice showing very low ΔCT values were excluded from trials.

Table 2.1 Primers and probes for genotyping and copy number check

Primers for PCR / gel electrophoresis genotyping		
Gene	**Primers**	**PCR product**
hSOD1	F: 5'-caccaagtagacaggctctc-3' R: 5'-cagtaaccttagttccgcag-3'	321bp from last intron[1]
mIL-2	F: 5'-ctaggccacagaattgaaagatct-3' R: 5'-gtaggtggaaattctagcatcatcc-3'	324bp from exon 3[2]
Reagents for qPCR copy number check		
Gene	**Primers**	**PCR product**
hSOD1	F: 5'-gggaagctgttgtcccaag-3' R: 5'-caaggggaggtaaaagagagc-3'	88bp from last intron
mApoB	F: 5'-cacgtgggctccagcatt-3' R: 5'-tcaccagtcatttctgcctttg-3'	74bp from exon 26
Gene	**Labelled oligonucleotide probe**	
hSOD1	6-FAM-ctgcatctggttcttgcaaaacacca-BHQ-1	
mApoB	HEX-ccaatggtcgggcactgctcaa-BHQ-1	

[1](Rosen *et al.* 1993); [2](Schorle *et al.* 1991)

2.2.3 Spinal cord changes between SOD1 and WT mice

Characterisation of spinal cord changes between SOD1 and WT mice was carried out under ethics permit A11958. To examine temporal changes in oxidative and microglial markers in the spinal cord of SOD1 mice, a tissue library of spinal cord samples from SOD1 and WT mice from 6 to 25 weeks of age was created by Dr Bill Bennett.

2.2.3.1 Preparation of a time series of spinal cord tissue

Lumbar spinal cord samples were obtained from SOD1 mice and WT mice at 6, 10, 14, 18 and 22 weeks of age. Three animals per genotype per time point were used, with the exception of 2 WT mice at 6 weeks of age and 4 SOD1 and 4 WT mice at 22 weeks of age. A mixture of male and female mice was used. Spinal cords of three SOD1 mice were obtained at disease endpoint (a 20% reduction of their pre-disease maximum body weight, at 24.8±0.1 weeks of age); three WT mice at 25-26 weeks of age were used as a comparison for endpoint SOD1 mice.

At the appropriate time point, animals were deeply anaesthetised with sodium pentobarbitone (60mg/kg, i.p.). When all reflexes were absent, mice were transcardially perfused with 10mL of 10mM phosphate-buffered saline (PBS; 2mM sodium phosphate monobasic; 8mM sodium phosphate dibasic, 154mM sodium chloride [all Sigma-Aldrich]; pH 7.4) followed by 20mL of 4% w/v paraformaldehyde (PFA, Sigma-Aldrich) in PBS. The T12-L1 vertebrae, containing the L2-L5 lumbar spinal cord segment, were dissected and post-fixed in 4% w/v PFA overnight at 4°C, then stored in PBS with 0.01% w/v sodium azide (Fluka, Sigma-Aldrich). The cervical vertebrae, containing the cervical spinal cord, were collected from a subset of mice (2 WT and 2 SOD1 mice at 10 weeks of age, 3 WT and 2 SOD1 mice at 14 weeks of age, and 3 WT and 3 SOD1 mice at 18 and 22 weeks of age).

The vertebrae surrounding the spinal cord were decalcified by incubation of the sample in fast decalcification solution (5% v/v nitric acid [Fluka, Sigma-Aldrich] with 0.05% w/v urea [Sigma-Aldrich] in distilled water) for 2 hours at room temperature; decalcified samples were washed thoroughly with distilled water, then stored in 50-70% ethanol until being dehydrated and embedded in paraffin wax using an automated tissue processor (Leica Biosystems ASP200-S, NSW, Australia). Wax sections (5µm) were cut on a microtome (Microm HM325, BW, Germany), mounted on Flex slides (Dako, CA, USA), dried at 37°C overnight and then stored at room temperature. Prior to immunohistochemistry, paraffin-embedded sections were dewaxed in two changes of xylene, and rehydrated through a series of graded ethanols to distilled water.

2.2.3.2 Immunostaining of SOD1 and WT spinal cord tissue

Normal goat serum (NGS), Mouse on Mouse immunolabelling (MOM) kit, 3,3'-diaminobenzidine substrate (DAB), biotin/streptaviding blocking kit, and biotinylated

Lycopersicon esculentum (tomato) lectin were all obtained from Vector Laboratories (CA, USA). Primary antibodies were obtained from various sources (Table 2.2). AlexaFluor (AF)-conjugated secondary antibodies, AF-conjugated streptavidins and Nuclear Yellow (NY) dye were obtained from Molecular Probes (Life Technologies). Unless otherwise specified, all steps were carried out at room temperature in a humidified light-safe chamber; buffer solutions for antibodies and washing were either PBS or PBS containing 0.05% v/v Tween-20 (Sigma-Aldrich) (PBS-T) unless otherwise specified; slides were washed in buffer solution between each immunolabelling step.

2.2.3.2.1 Microglia and inflammatory markers

Microglia were labelled with an antibody against ionised calcium binding adaptor molecule 1 (Iba1) (Imai *et al.* 1996), or with tomato lectin (TL) (Herbert *et al.* 2012) (Table 2.2). Tomato lectin binds (*N*-acetylglucosamine)$_{2\text{-}4}$ residues, and in addition to microglia also appeared to label endothelial cells and motor neurons, which could be identified as such by their different morphology.

To detect Iba1, citrate buffer antigen retrieval was employed. Slides were immersed in a 10mM citrate buffer (2mM citric acid, 8mM sodium citrate [both from Sigma-Aldrich], pH 6) and heated in a pressure cooker (Russell Hobbs, VIC, Australia) at 100% power for 6 minutes followed by 60% power for 14 minutes, then allowed to cool. Sections were then blocked in 10% v/v NGS for 1 hour, incubated with rabbit anti-Iba1 (1:500) for 2 hours, biotinylated goat-anti-rabbit (1:500) for 1 hour, and streptavidin-AF488 (1:500) for 1 hour; nuclei were stained with NY (1:10000) for 15 minutes.

Tomato lectin labelling was carried out in conjunction with immunolabelling for putative markers of microglial status, Arg1 (M2-like microglia) and iNOS (M1-like microglia) (Colton 2009). Citrate buffer antigen retrieval, as above, was required for Arg1 immunoreactivity but not that of iNOS. The MOM kit was used according to the manufacturer's instructions for Arg1 or iNOS detection. Slides were blocked with MOM blocking reagent for 1 hour, then rinsed in PBS and incubated with MOM diluent for 5 minutes. The diluent was removed but the section was not washed in buffer; primary antibody was applied in fresh MOM diluent and incubated either overnight at 4°C (Arg1, 1:100) or for 2 hours at room temperature (iNOS, 1:100). Primary antibody was detected by incubation with MOM biotinylated anti-mouse secondary antibody (1:250) for 20 minutes and streptavidin-AF488 (1:500) for 1 hour. Any free

streptavidin-binding sites were then blocked with either the biotin/streptavidin blocking kit as per the manufacturer's recommendations, or with avidin and biotin solutions as follows: sections were incubated in diluted, filtered egg white solution (1 egg white in 80-100mL distilled water) for 20 minutes, washed in water, incubated with 0.001% w/v biotin (Sigma-Aldrich) solution for 20 minutes, and washed in water again. Sections were then incubated with biotinylated tomato lectin (1:500) for 1 hour and with streptavidin-AF594 (1:500) for 2 hours; nuclei were stained with NY (1:10000) for 15 minutes, and slides were coverslipped with fluorescence mounting medium (Dako).

2.2.3.2.2 Pathological, astroglial, and oxidative stress markers

For qualitative analysis, pathological alterations in motor neurons were detected using antibodies against ubiquitin (Ubi, 1:1000), dephosphorylated neurofilaments (SMI32, 1:500), and human SOD1 protein (hSOD1, 1:500); astrocytes were detected using an antibody against glial fibrillary acidic protein (GFAP, 1:1000) (Table 2.2). Sections were blocked with 5% v/v NGS for 1 hour, incubated with the appropriate primary antibody for 1 hour, then with goat anti-mouse-AF or goat anti-rabbit-AF secondary antibody (1:500) for 1 hour and with NY (1:10000) for 15 minutes, then coverslipped with fluorescence mounting medium (Dako).

For quantitative analysis, the antioxidant protein MT-1/2 was detected using DAB immunohistochemistry. The MT-1 and MT-2 isoforms are structurally and functionally similar (West *et al.* 2008); an antibody recognizing both isoforms (MT-1/2, Table 2.2) was used. Endogenous peroxidases were quenched with 3% hydrogen peroxide (Sigma-Aldrich) in PBS for 20 minutes. Sections were blocked with MOM kit blocking reagent for 1 hour, incubated with MOM diluent for 5 minutes followed by mouse anti-MT-1/2 (MT, 1:300, Table 2.2) in MOM diluent for 1 hour. Primary antibody was detected with biotinylated MOM anti-mouse-IgGs (1:250) in MOM diluent for 10 minutes and HRP-conjugated streptavidin (1:1000) for 1 hour. The sections were exposed to DAB for 1 minute, then counterstained with nuclear fast red for 3 minutes, dehydrated with graded alcohols, cleared in xylene and coverslipped with Pertex mounting medium.

Double immunolabelling was performed sequentially using the above procedures where appropriate; for double immunolabelling of GFAP and MT-1/2, the quenching step was omitted from the MT-1/2 procedure, and the biotinylated MOM anti-mouse secondary was detected with AF-conjugated streptavidin instead of HRP-conjugated streptavidin.

2.2.3.2.3 Image analysis and cell counts

Fluorescence images were captured on an Olympus BX50 microscope (Olympus, VIC, Australia) and CoolSNAP-HQ2 camera (Photometrics, AZ, USA) using NIS-Elements software (Nikon Instruments, NY, USA). Bright field images were captured using a Leica DM2500 microscope and DFC495 camera (Leica Biosystems, NSW, Australia).

To quantify the microglial markers Iba1, TL, Arg1 and iNOS, immunostaining was performed on 3 sections from each lumbar spinal cord, separated by a minimum distance of 45µm. The spinal cord ventral horn (VH) was defined as the region of grey matter on the ventral side of a horizontal line crossing through the central canal, bounded by a vertical line through the sagittal plane. VH images for cell counts were taken at 400x magnification and cells were counted using ImageJ software (National Institutes of Health, MD, USA) and Adobe CS6 (Adobe Systems Incorporated, CA, USA). Counts from the right and left ventral horns of each section were averaged and divided by the area in square millimetres. To avoid pseudoreplication, the average count from three sections was used as a single measurement per animal for statistical analysis.

Semi-quantitative analysis of the expression level of Arg1 and iNOS was performed in a subset of SOD1 microglia. For both Arg1 and iNOS, one section was randomly selected from each animal at 6 weeks (n=3) and 22 weeks of age (n=4). The cell bodies of eight microglia, showing the strongest Arg1 or iNOS staining in these sections, were outlined in ImageJ, and the percentage area occupied by positive Arg1 or iNOS labelling was calculated. To account for variations in intensity and background between sections, positive labelling in 8-bit black and white images was defined as any pixels having a grey value greater than 3.5 standard deviations above the mean grey value of the image.

To quantify the number of MT-1/2 positive cells, immunostaining was performed on one section from the lumbar spinal cord of each animal. MT-1/2-positive cell bodies were counted in each spinal cord region outlined in the diagram shown in Figure 2.7A.

At each time point, SOD1 and WT counts were compared using an independent samples t-test. A Welch t-test correction was applied if Levene's test showed that the variance in WT and SOD1 measurements was substantially different. Data are presented as mean ± standard error of the mean, and the statistical test used for the comparison is indicated (t-test = independent samples t-test for equal variances; Welch t-test = independent samples t-test for unequal variances), with $p<0.05$ considered significant.

Table 2.2 Antibodies used for immunostaining of mouse spinal cord

Antibody target	**Cell type**	**Species and type (clone)**	**Company (catalogue number)**
Dephosphorylated neurofilaments (SMI32)	Motor neurons	Mouse monoclonal IgG1 (SMI32)	Covance, NJ, USA (SMI-32R)
Ubiquitin (Ubi1)	-	Rabbit polyclonal	Dako, CA, USA (Z0458)
Human Cu,Zn-superoxide dismutase (hSOD1)	-	Rabbit polyclonal	Abcam, MA, USA (ab52590)
Glial fibrillary acid protein (GFAP)	Astrocytes	Rabbit polyclonal	Dako, CA, USA (Z0334)
(*N*-acetylglucosamine)$_{2-4}$ residues (TL)	Microglia; endothelium	Biotinylated lectin from *Lycopersicum esculentum*; tomato lectin	Vector Laboratories, CA, USA (B1175)
Ionised calcium-binding adaptor molecule1 (Iba1)	Microglia	Rabbit polyclonal	Wako, Osaka, Japan (019-19741)
Arginase1 (Arg1)	-	Mouse monoclonal IgG1 (E-2)	Santa Cruz Biotechnology, CA, USA (sc-271430)
Inducible nitric oxide synthase (iNOS)	-	Mouse monoclonal IgG1 (C-11)	Santa Cruz Biotechnology, CA, USA (sc-7271)
Metallothionein-1/2 (MT-1/2)	-	Mouse monoclonal IgG1 (E9)	Dako, CA, USA (M0639)

2.2.4 Functional characterisation of SOD1 and WT mice

The functional characterisation of SOD1 and WT mice was carried out under ethics permit A10995. A cohort of female SOD1 mice (n=17) and their female WT littermates (n=13) was assessed for changes in body weight, stride pattern, wire hang duration and neurological score rating over time. Mice in this cohort ranged from 5-13 weeks of age when measurements were commenced, and all mice were followed through to disease endpoint in SOD1 mice (23-25 weeks of age) and up to 28 weeks of age in WT mice.

2.2.4.1 Survival time and humane endpoint

As SOD1 mice are known to display progressive paralysis with disease progression (Gurney *et al.* 1994), a humane endpoint was employed in order to prevent a slow death by starvation due to inability to feed. Disease endpoint was considered to have been reached when mice displayed the earliest of either 1) a drop in body weight to 80% of pre-disease maximum body weight, or 2) inability to right themselves within 30 seconds of being placed on their back (Solomon *et al.* 2011). Having reached disease endpoint, mice were euthanised with carbon dioxide (2 litres/minute; 10 minutes).

2.2.4.2 Body weight measurements

Body weight, measured in grams, was recorded at least twice each week for each mouse, and more frequently in SOD1 mice approaching disease endpoint.

2.2.4.3 Stride pattern testing

Stride pattern testing was performed weekly. Nontoxic BodyArt face paint (Global Colours, NSW, Australia), diluted to a thin consistency with water, was placed on the front (red) and hind (blue) paws of a gently-restrained mouse. The mouse was then allowed to walk along a 7cm x 60cm strip of white paper bounded on each side by 10cm-high plastic barriers, leaving a trail of paw prints from which various measures could be recorded. The mouse's feet were rinsed in water and dried in a tissue-lined cage; the mouse was then returned to its home cage. A detailed diagram of stride pattern testing setup is included in the Appendix. If the initial walk did not yield a clear set of prints, the procedure was repeated once more, and the most consistent pattern from the two attempts was used for measurement.

Parameters measured from the stride pattern test were stride length (distance between consecutive rear paw prints on the same side), hind-base width (distance between right

and left hind paws), front-base width (distance between right and left front paws) and uniformity measurement (difference in placement of the hind paw compared with that of the front paw from the previous step) (Figure 2.11A,B). From each stride pattern test strip, stride length and uniformity were measured for 1-3 steps on the right and the left sides, and hind-base width and front-base width were measured for 1-3 steps.

2.2.4.4 Wire hang duration testing

The wire hang duration test was assessed weekly as an indicator of muscle strength. Mice were placed on the wire bars (1mm diameter) of a large transport cage lid, which was gently inverted and suspended approximately 20cm over a foam pad (Appendix 1). Mice were able to move about freely on the inverted bars in a 250cm^2 area for the duration of the test. The wire hang duration was recorded as the time the mouse could remain suspended from the bars while inverted, before releasing the bars and dropping onto the foam pad below. The longest wire hang duration of three attempts was recorded for analysis, with a maximum possible value of 60 seconds.

2.2.4.5 Neurological scoring

Visible signs of neurological deficit in SOD1 mice were assessed at least twice weekly according to neurological score criteria (Table 2.3) developed by the ALS Therapy Development Institute (ALSTDI, MA, USA) (Scott *et al.* 2008).

Table 2.3 Neurological score criteria

Score	Score Criteria
NS=0	Full extension of hind legs away from lateral midline when mouse is suspended by its tail, and mouse can hold this for 2 seconds.
NS=1	Collapse or partial collapse of leg extension towards lateral midline, or trembling of hind legs, during tail suspension.
NS=2	Toes curl under at least twice during walking of 12 inches, or any part of foot is dragging along cage bottom/table.
NS=3	Rigid paralysis or minimal joint movement, foot not being used for forward motion.
NS=4	Mouse cannot right itself within 30 seconds from either side.

NS, neurological score.

2.2.4.6 Statistical methods for analysis of functional data

All statistical analyses were carried out in either IBM SPSS Statistics, version 20 (IBM Corporation, NY, USA) or Stata IC, version 12.1 (StataCorp LP, TX, USA). All data are presented as mean ± standard error of the mean unless otherwise specified, with $p<0.05$ considered significant.

Mean and median survival times were evaluated using Kaplan-Meier survival analysis. The influence of transgene copy number (ΔCT value from genotyping) on survival time was examined using Cox proportional hazards (CPH) regression, and was reported as the hazard ratio for reaching endpoint (HR, equal to e^{β}) and 95% confidence interval for the hazard ratio (95% CI).

To avoid pseudoreplication, stride pattern parameters (stride length, uniformity, front-base width and hind-base width) were averaged to give a single measurement per mouse per week for each parameter; values for WT and SOD1 mice were then compared using the Mann-Whitney U test (MWU) for non-parametric data. Similarly, average body weight and the maximum wire hang duration times for WT and SOD1 mice were compared using the MWU. Maximum body weight and the age at which the maximum body weight was reached could be calculated.

Additionally, an exploration of body weight analysis using linear mixed modelling was conducted. A linear mixed model contains both 'fixed' effects and 'random' effects: fixed effects alter the value of the mean, whereas random effects alter the amount of variation around the mean. Mixed models can be particularly useful in longitudinal experiments where repeated measurements are made on the same experimental subjects over time. For example, genotype is expected to affect the value of the body weight measurement, so genotype would be included as a fixed effect. In contrast, giving identifiers to each individual mouse in the dataset, and including these identifiers in random effects, allows variation around the overall body weight mean to be partly explained due to unique changes over time for individual mice. This allocation of variance results in a better model fit to the data, and allows differences between genotypes or treatment groups to be identified, despite differences in starting body weight and rate of change over time between individual mice in each group.

The steps taken for model fitting are included in Supplementary Data 1 and Supplementary Data 2, with the final model demonstrated in the results.

In modelling SOD1 and WT body weight, a random slope and random intercept were included, allowing for unique starting body weights and unique rates of weight gain and loss over time for individual mice. Age in days was used as a fixed effect, allowing inclusion of all daily body weight measurements, rather than using a weekly average for each mouse. Age^2 and Age^3 fixed effects were sequentially added to the model, to examine whether their inclusion resulted in a better model fit to the observed data than a linear trajectory alone. Model fit was evaluated by examining log-likelihood (as -2LL, in smaller-is-better format) values between models with and without the covariate being tested; the covariate was considered to give a significantly better model fit if a significant result ($p<0.05$) was obtained from the right-tailed chi-squared test of the difference in log-likelihood between models (i.e., if $\chi^2(LR, df) <0.05$, where LR (likelihood ratio) = $-2LL_{\text{model without covariate}} - -2LL_{\text{model with covariate}}$; $df = df_{\text{model with covariate}} - df_{\text{model without covariate}}$).

To examine at what age the body weight trajectories for SOD1 and WT mice became significantly different, the final model was centred at a range of Age values, and the intercept parameter p-value was recorded. The intercept parameter p-value gives a direct test of whether the two curves differ in body weight value as they cross the intercept (where 'Age'=0); this is normally of no use then looking at body weight because weight at birth was outside the range of recorded raw data. However, when the model was centred by substituting, for example, Age for (Age-50), the intercept parameter p-value gives a direct test of whether the SOD1 and WT body weights are different at 50 days of age. By centring at a range of Age values (between 80 and 110 days), the age at which SOD1 and WT body weight estimates were significantly different could be obtained.

The non-linear combination of estimators (nlcom) procedure (Stata IC, StataCorp LP) was used to provide point estimates for maximum body weight of SOD1 mice and age at which the maximum body weight was reached. The estimates from the linear mixed model / non-linear combination of estimators could then be compared with those generated from the averaged data alone.

2.3 Results

2.3.1 Cellular changes over time in SOD1 mouse spinal cord

2.3.1.1 Total microglial numbers

The microglial markers Iba1 and TL both indicated an increase in the number of microglia over time in SOD1 mice, but not in WT mice (Figure 2.1A-E). In the lumbar spinal cord VH, SOD1 mice had more Iba1-positive microglia than WT mice from 18 weeks of age (SOD1 178±7 vs. WT 85±26 microglia/mm^2, t-test p=0.025) and thereafter (Figure 2.1D). TL labelling proved more sensitive, indicating differences between the SOD1 and WT VH microglia from 14 weeks of age (SOD1 208±9 vs. WT 169±8 microglia/mm^2, t-test p=0.034), although these differences were more substantial from 18 weeks of age onwards (Figure 2.1E).

2.3.1.2 Changes in inflammatory marker expression over time

The number of TL-positive microglia expressing the M2 marker Arg1 or the M1 marker iNOS were counted in the lumbar and cervical spinal cord regions.

2.3.1.2.1 Expression of Arg1 and iNOS in lumbar ventral horn microglia

Within the lumbar spinal cord VH, a subset of TL-positive microglial cells expressed Arg1 (Figure 2.2). The proportion of Arg1-positive and Arg1-negative microglia stayed relatively constant in WT mice over time, with more Arg1-negative than Arg1-positive microglia present at all time points (Welch t-test p=0.079 at 6 weeks; t-test p<0.05 at 10-25 weeks) (Figure 2.2A-C, G). Few Arg1-positive microglia were observed at 6 and 10 weeks of age in the SOD1 VH; however, the number of Arg1-positive microglia (arrows in Figure 2.2B,E,F) increased from 14 weeks of age, while the number of Arg1-negative microglia did not change substantially with time (Figure 2.2D-F, H). By 22 and 25 weeks of age, many more Arg1-positive than Arg1-negative microglia were present in the SOD1 VH (22 weeks, 286±29 Arg1-positive vs. 157±22 Arg1-negative microglia/mm^2, t-test p=0.006; 25 weeks, 377±24 Arg1-positive vs. 180±27 Arg1-negative microglia/mm^2, t-test p=0.005) (Figure 2.2H). These changes represent an 18-fold increase in Arg1-expressing microglia between 10 weeks of age (21±3 Arg1-positive microglia/mm^2) and 25 weeks of age (377±24 Arg1-positive microglia/mm^2) in the lumbar spinal cord VH. Additionally, the percentage of total microglia expressing Arg1 increased from 14% at 10 weeks of age to 65% at 22 weeks of age (Figure 2.5F).

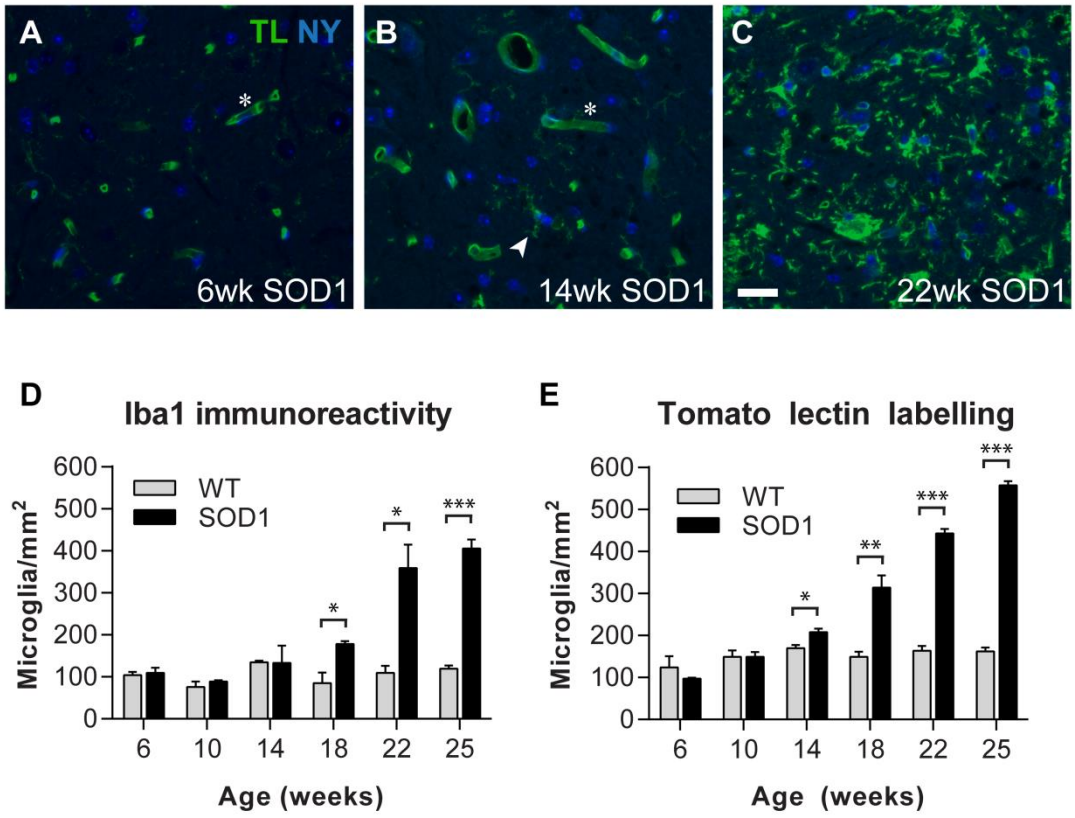

Figure 2.1 Microglia in the lumbar spinal cord of SOD1 mice over time

Tomato lectin binds to both endothelial cells (asterisks, A,B) and microglial cells (arrowhead, B). The number of microglia increased over time in the lumbar spinal cord of SOD1 mice, as measured by both Iba1 immunoreactivity (D) and tomato lectin labelling (A-C, E). SOD1 mice showed greater numbers of Iba1-positive microglia than WT mice from 18 weeks of age (D), and greater numbers of tomato lectin-positive microglia than WT mice from 14 weeks of age (E). Scale bar 20µm. *p<0.05, **p<0.01, ***p<0.001. Iba1, ionised calcium-binding adaptor molecule 1; TL, tomato lectin; NY, Nuclear Yellow. Error bars represent standard error of the mean.

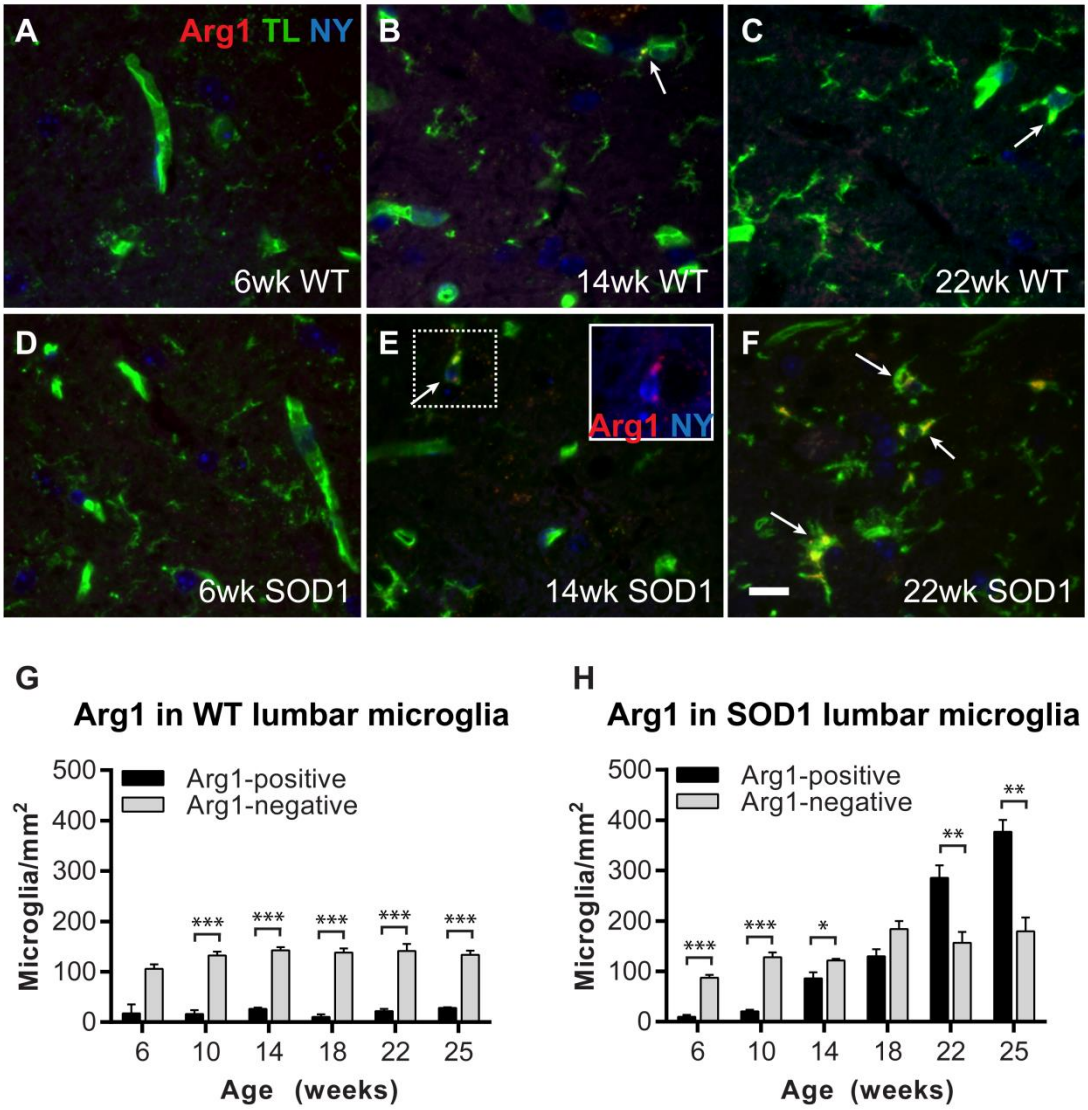

Figure 2.2 Arg1-positive microglia in the lumbar spinal cord ventral horn

Arg1 immunolabelling in tomato lectin-positive microglia is shown in the WT (A-C, G) and SOD1 (D-F, H) lumbar spinal cord ventral horn at 6 weeks (A,D), 14 weeks (B,E), and 22 weeks (C,F) of age. WT mice show few Arg1-positive microglia (arrows, B,C) throughout the time series (G), while SOD1 mice show an increasing number of Arg1-positive microglia (arrows, E,F; inset in E shows Arg1 labelling) from 14-18 weeks of age (H). Scale bar 10µm for A-F, 6.7µm for inset in E. *p<0.05, **p<0.01, ***p<0.001. Arg1, arginase1; TL, tomato lectin; NY, Nuclear Yellow. Error bars represent standard error of the mean.

A subset of microglia within the lumbar ventral horn showed iNOS expression (Figure 2.3). More iNOS-negative than iNOS-positive microglia were present in the WT lumbar VH at all time points (Welch t-test $p=0.126$ at 6 weeks; t-test $p<0.05$ at 10-25 weeks) (Figure 2.3A-C, G). The number of iNOS-positive microglia increased from 14 weeks of age in the SOD1 lumbar VH (Figure 2.3D-F, H; arrow in Figure 2.3F). Additionally in SOD1 mice, the number of iNOS-negative microglia increased from 18 weeks of age onwards (Figure 2.3H; arrowheads in Figure 2.3E,F). Due to the concomitant increase in both iNOS-positive and iNOS-negative microglia, the SOD1 VH contained more iNOS-negative than iNOS-positive microglia at all time points (t-test $p<0.05$ from 6 to 22 weeks; t-test $p=0.069$ at 25 weeks) (Figure 2.3H).

The number of iNOS-positive microglia increased approximately 8-fold between 10 weeks of age (15±8 iNOS-positive microglia/mm^2) and 22 weeks of age (116±18 iNOS-positive microglia/mm^2) (Figure 2.3H). The percentage of microglia expressing iNOS increased from 8% at 10 weeks of age to 33% at 22 weeks of age (Figure 2.5F).

When the numbers of Arg1-positive microglia (Figure 2.2H) and iNOS-positive microglia (Figure 2.3H) in the SOD1 lumbar spinal cord ventral horn are compared, the numbers of Arg1-positive microglia were greater than those of iNOS-positive microglia as the disease progressed over time.

2.3.1.2.2 Expression level of Arg1 and iNOS in SOD1 lumbar VH microglia

Ventral horn microglia from randomly-selected lumbar spinal cord sections (see methods) showed an increase in the percentage area occupied by Arg1 or iNOS immunoreactivity between 6 weeks and 22 weeks of age (Figure 2.4A-E). Arg1 immunoreactivity occupied approximately 6% of microglial cell body area at 6 weeks of age, which increased five-fold to approximately 30% of the cell body area at 22 weeks of age (Figure 2.4A,B,E). iNOS immunoreactivity was present in less than 1% of the cell body area at 6 weeks of age, which increased 25-fold to around 5% at 22 weeks of age (Figure 2.4C-E). These data indicate that in addition to the increase in the number of Arg1-expressing and iNOS-expressing microglial cells (Figure 2.2, Figure 2.3), the expression level of Arg1 and iNOS protein also increases over time in SOD1 lumbar spinal cord VH microglia.

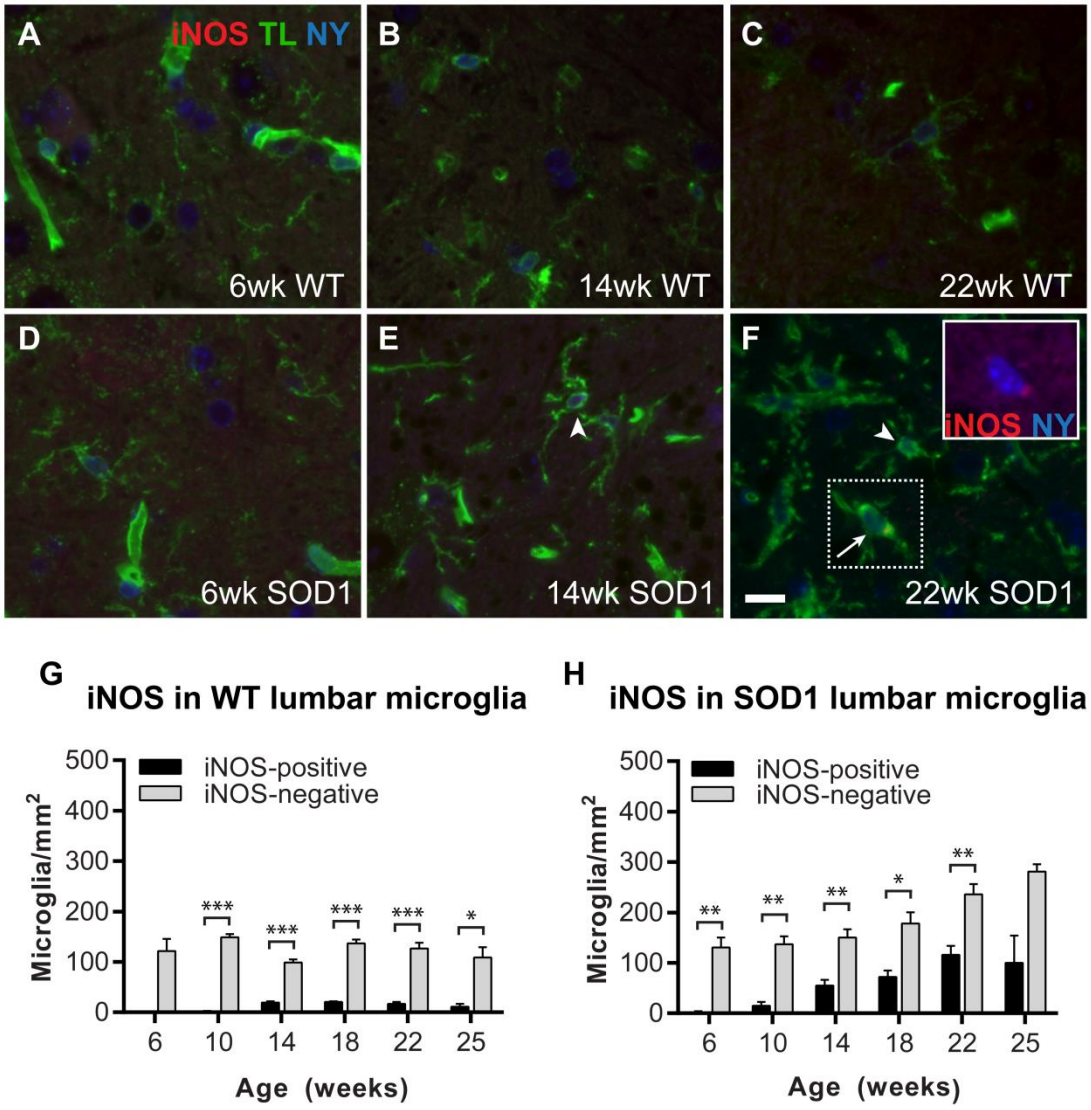

Figure 2.3 iNOS-positive microglia in the lumbar spinal cord ventral horn

iNOS immunolabelling in tomato lectin-positive microglia is shown in WT (A-C, G) and SOD1 (D-F, H) lumbar spinal cord at 6 (A,D), 14 (B,E), and 22 (C,F) weeks of age. WT mice show few iNOS-positive microglia at any time point (G), while SOD1 mice show an increase in both iNOS-positive (arrow, F; inset in F shows iNOS labelling) and iNOS-negative (arrowheads, E,F) microglia over time (H). Scale bar 10µm for A-F, 6.7µm for inset in F. *p<0.05, **p<0.01, ***p<0.001. iNOS, inducible nitric oxide synthase; TL, tomato lectin; NY, Nuclear Yellow. Error bars represent standard error of the mean.

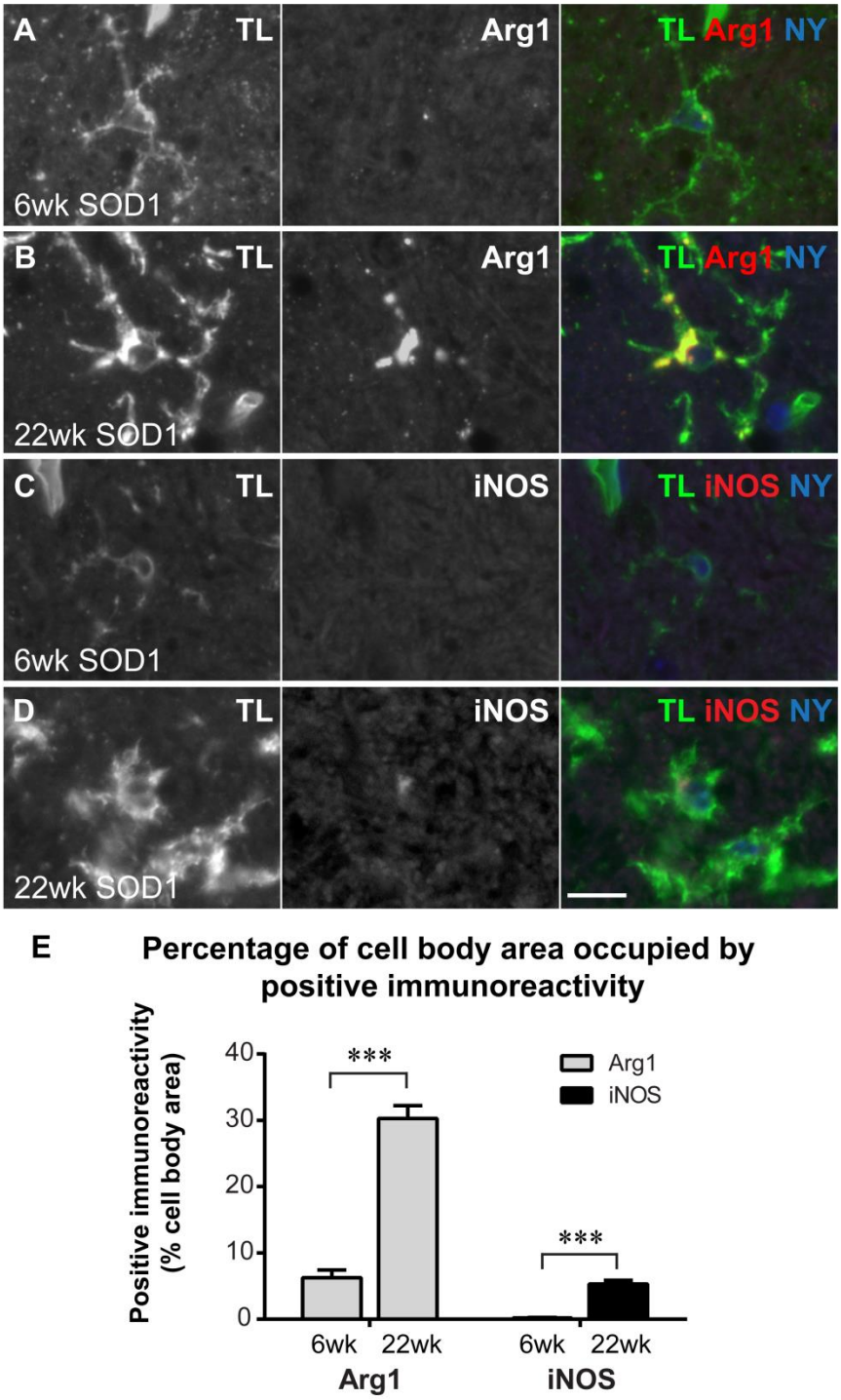

Figure 2.4 Percentage area occupied by Arg1 or iNOS immunoreactivity in SOD1 lumbar spinal cord microglia

The percentage area of the microglial cell body occupied by Arg1 (A,B) or iNOS (C,D) immunoreactivity was examined at 6 (A,C) and 22 weeks (B,D) of age in a subset of microglia displaying the strongest immunoreactivity. The percentage of cell body area occupied by Arg1 was higher at 22 weeks than at 6 weeks; the percentage of cell body area occupied by iNOS was also higher at 22 weeks than at 6 weeks (E). Scale bar 10µm in A-D. *** $p<0.001$. TL, tomato lectin; Arg1, arginase1; iNOS, inducible nitric oxide synthase; NY, Nuclear Yellow. Error bars represent standard error of the mean.

2.3.1.2.3 Expression of Arg1 and iNOS in cervical ventral horn microglia

Motor weakness in the SOD1 mice is first detectable in the hindlimbs, with later involvement of the forelimbs (Kuntz *et al.* 2000); thus, the lumbar spinal cord was the primary focus in this study. However, a brief comparison of microglial Arg1 and iNOS expression was made in the cervical spinal cord of WT and SOD1 mice from 10 to 22 weeks of age, to examine any temporal differences in expression of these inflammatory markers between the lumbar and cervical spinal cord which may correlate with later involvement of the forelimb muscles.

Similar to the lumbar spinal cord, there were more Arg1-negative microglia than Arg1-positive microglia at all time points in the WT cervical spinal cord VH (Welch t-test $p=0.120$ at 10 weeks; t-test $p<0.05$ at 14-22 weeks) (Figure 2.5A). In the SOD1 cervical VH, there were equal numbers of Arg1-positive and Arg1-negative microglia from 10-18 weeks of age (Figure 2.5B). At 22 weeks of age, there were more Arg1-positive than Arg1-negative microglia (265±39 Arg1-positive microglia/mm^2 vs. 71±22 Arg1-negative microglia/mm^2, t-test $p=0.012$). In contrast, the number of Arg1-negative microglia remained constant in the SOD1 cervical VH from 10 to 22 weeks of age (Figure 2.5B). The SOD1 cervical VH also showed an increase in the percentage of microglia expressing Arg1 over time, from 45% at 10 weeks of age to 79% at 22 weeks of age (Figure 2.5E).

Microglial iNOS expression in the cervical spinal cord remained fairly constant over time in the WT VH, with more iNOS-negative than iNOS-positive microglia at all time points (Welch t-test $p<0.05$ at 10 weeks; t-test $p<0.05$ from 14 to 22 weeks), despite a slight increase in iNOS-positive microglia over time (Figure 2.5C). In the SOD1 ventral horn, both the number of iNOS-positive and iNOS-negative microglia increased over time (Figure 2.5D). There were more iNOS-negative than iNOS-positive microglia in the SOD1 mice at each time point (Figure 2.5D), however these differences did not reach statistical significance (Welch t-test $p=0.051$-0.076 from 10 to 22 weeks). The percentage of SOD1 cervical VH microglia expressing iNOS increased from 11% at 10 weeks of age to 24% at 18 weeks of age, then slightly decreased to 20% at 22 weeks of age (Figure 2.5E). Similar to the lumbar spinal cord, more cervical microglia were Arg1-positive than iNOS-positive (Figure 2.5E).

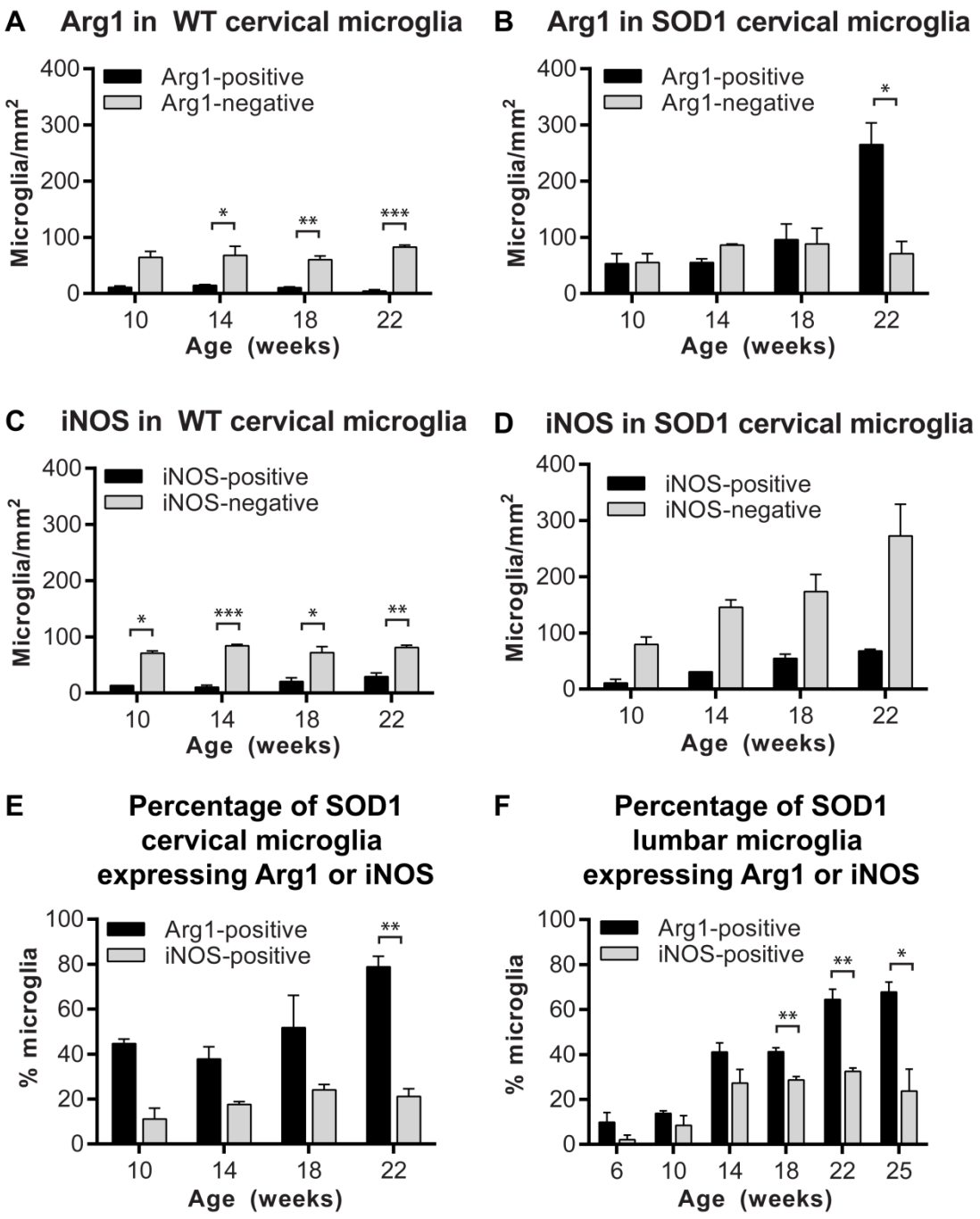

Figure 2.5 Arg1 and iNOS expression in cervical spinal cord ventral horn microglia

In WT mice the majority of tomato lectin-positive microglia are negative for Arg1 (A) and for iNOS (C). In the SOD1 cervical ventral horn, there are equivalent numbers of Arg1-positive and Arg1-negative microglia until 22 weeks of age, when Arg1-positive microglia are more prevalent (B). In SOD1 mice, the numbers of both iNOS-positive and iNOS-negative microglia increase over time (D). A higher percentage of microglia in both the cervical (E) and lumbar (F) spinal cord express Arg1 than iNOS at later time points. *p<0.05, **p<0.01, ***p<0.001. Error bars represent standard error of the mean.

2.3.1.3 Neurofilament, ubiquitin and hSOD1 labelling over time

To examine timing of degenerative changes in SOD1 motor neurons, immunolabelling for dephosphorylated neurofilaments (SMI32), ubiquitinated inclusions (Ubi), and protein produced from the human SOD1 transgene (hSOD1) was performed in the lumbar spinal cord VH of SOD1 and WT mice. Changes over time in SOD1 spinal cord were not present in WT spinal cord, unless otherwise specified below.

Diffuse ubiquitin immunolabelling was present in motor neuron nuclei in both SOD1 and WT lumbar VH at all time points examined (Figure 2.6A-C, I). The SOD1 lumbar VH showed ubiquitin-positive inclusions (arrows, Figure 2.6A-C) in the cell bodies of SMI32-positive motor neurons as early as 6 weeks of age (Figure 2.6A), and in both motor neuron somas and in the neuropil from 10 weeks of age (Figure 2.6B). The number of ubiquitinated inclusions in the lumbar spinal cord increased over time; at 25 weeks of age, the SOD1 VH showed many large ubiquitin-positive inclusions which were not located within SMI32-positive cell bodies (arrow, Figure 2.6C). These ubiquitinated inclusions may be present within neuritic processes, glial cells, or the remnants of degenerating neurons. No inclusions were found in WT VH (Figure 2.6I).

SMI32 labelled motor neuron somas and processes within the neuropil (Figure 2.6A-F, I). SMI32-encircled vacuoles developed in the cytoplasm of SOD1 motor neurons from 10 weeks of age (asterisks, Figure 2.6B); at 14 weeks of age, some of these cytoplasmic vacuoles contained hSOD1 protein (asterisk, Figure 2.6E). SMI32 formed ring-like, annular structures in the neuropil from 10 weeks of age (arrowheads, Figure 2.6B,C). Interestingly, while some hSOD1 was present in a diffuse cytoplasmic pattern in motor neurons at 6 weeks of age (Figure 2.6D), hSOD1 also formed ring-like, annular structures in the neuropil from 6 weeks of age onwards (chevrons, Figure 2.6D-F). At 14 weeks of age, some hSOD1-positive annular structures partially colocalised with SMI32-positive annular structures (inset, Figure 2.6E; magnified in Figure 2.6G). The size and complexity of both SMI32-positive and hSOD1-positive annular structures increased with time; at 22 weeks of age, large, complex annular structures positive for SMI32, hSOD1, or both, were present in the SOD1 lumbar spinal cord ventral horn (inset, Figure 2.6F; magnified in Figure 2.6H). The presence of annular structures, particularly in a grouped arrangement (as seen in Figure 2.6F,H) may indicate internal partitioning or vacuolisation of motor neuron axons or somas. No neurofilament alterations were present in the motor neurons of the WT lumbar VH (Figure 2.6I).

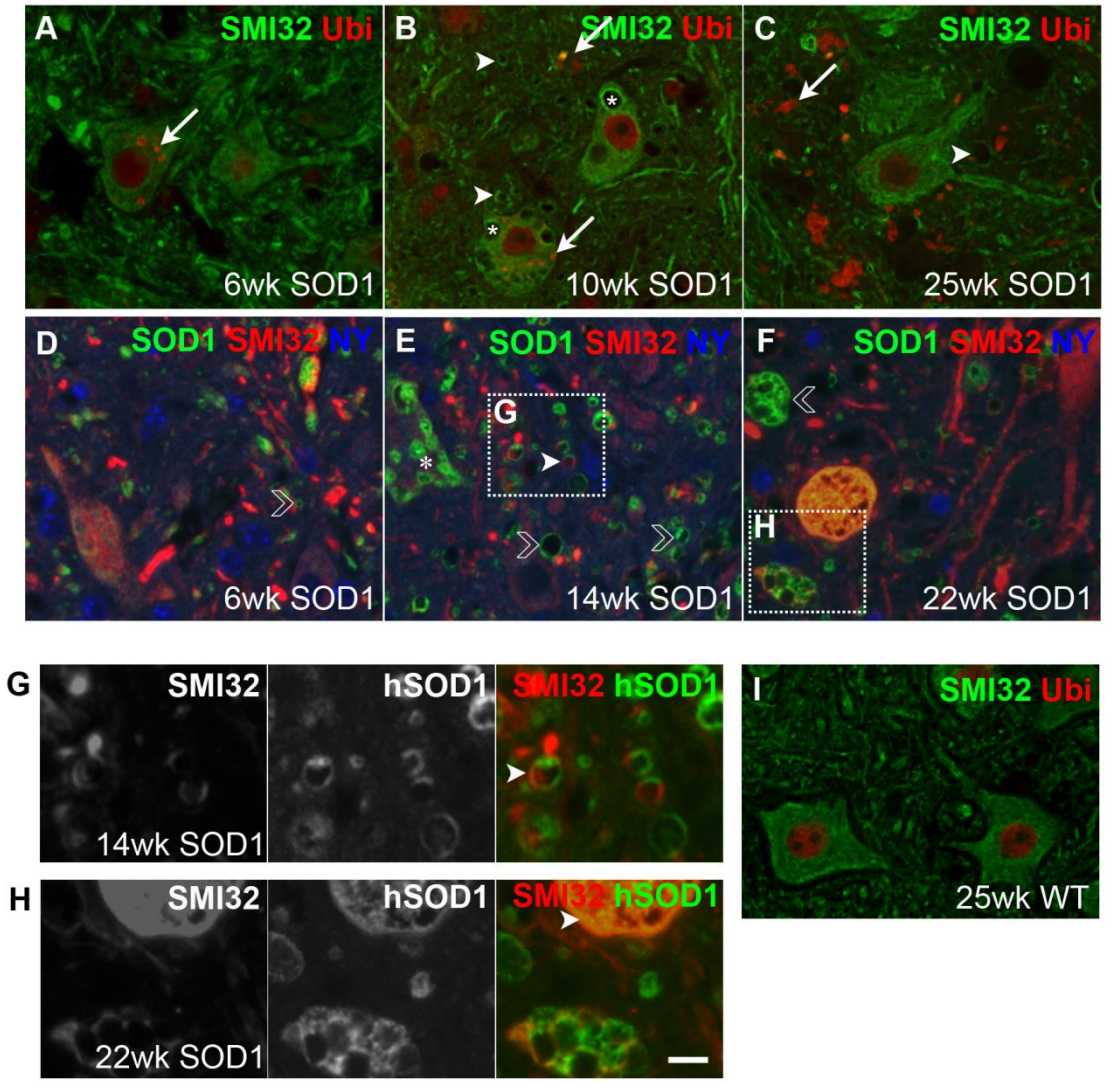

Figure 2.6 Ubiquitin, SMI32, and hSOD1 labelling in the SOD1 lumbar spinal cord

Motor neurons showed cytoplasmic ubiquitinated inclusions from 6 weeks of age (arrow, A), and ubiquitin aggregates in the neuropil from 10 weeks of age (arrows, B,C). SMI32-edged vacuoles were present in the cytoplasm from 10 weeks of age (asterisks, B), some of which contained hSOD1 protein from 14 weeks of age (asterisk, E). SMI32-positive annular structures were also present in the neuropil from 10 weeks of age (arrowheads, B). hSOD1 protein formed annular structures in the neuropil from 6 weeks of age (chevrons, D-F); these were closely associated or colocalised with SMI32-positive annular structures from 14 weeks of age (arrowhead, G). Annular structures in the neuropil, consisting of hSOD1 and/or SMI32, increased in size and complexity with disease progression, and at 22 weeks of age some annular structures showed colocalisation between SMI32 and hSOD1 (arrowhead, H). Wild type (WT) mice showed no ubiquitinated aggregates or neurofilament abnormalities at 25 weeks of age. Scale bar 10µm for A-F, I; 5µm for G,H. hSOD1, protein produced from the SOD1G93A transgene; NY, Nuclear Yellow; SMI32, dephosphorylated neurofilament medium chain; Ubi, ubiquitin.

2.3.1.4 Changes in MT-1/2 over time

2.3.1.4.1 Metallothionein-1/2 immunoreactivity

Immunostaining for metallothionein-1/2 isoforms (MT-1/2) revealed that expression of MT-1/2 was quite varied between individual mice. Despite this variation, WT and SOD1 mice showed differences in MT-1/2 expression over time (Figure 2.7A-J).The density of MT-1/2-positive cells was evaluated in the ventral horn and dorsal horn grey matter, and in the dorsal and the ventral/lateral white matter, as outlined in Figure 2.7A.

MT-1/2 expression in the ventral horn grey matter of WT mice was generally quite low, with the exception of 14 weeks of age when many MT-1/2-positive cells were counted in the VH (Figure 2.7B,C,G). In SOD1 mice, few MT-1/2-positive cells were observed in the VH at 6, 10, and 14 weeks of age (Figure 2.7D). However, there was a marked increase in the density of MT-1/2-positive cells in the VH of SOD1 mice compared to WT mice at 18, 22, and 25 weeks of age (18wks, WT 3±2 vs. SOD1 141±35 MT-1/2-positive cells/mm^2, Welch T-test p=0.059; 22wks, WT 17±1 vs. SOD1 253±16 MT-1/2-positive cells/mm^2, T-test p=0.001; 25wks, WT 22±21 vs. SOD1 156±11 MT-1/2-positive cells/mm^2, T-test p=0.005) (Figure 2.7G). In addition to the increase in MT-1/2-positive cells in the SOD1 VH, some diffuse staining with no apparent cellular localisation was also seen in the VH parenchyma; this diffuse immunoreactivity was absent in WT mice (Figure 2.7B-F).

In the dorsal horn of WT mice, MT-1/2-positive cells and diffuse MT-1/2 immunoreactivity were predominantly present in lamina II-III near the most dorsal portion of the dorsal horn, although the intensity of immunolabelling in this region varied amongst WT mice (Figure 2.7B,C). In SOD1 mice, MT-1/2 immunoreactivity at the top of the dorsal horn appeared either absent or present to a lesser extent than in age-matched WT mice; however, from approximately 18 weeks of age onwards, the number of MT-1/2-positive cells in the lower half of the dorsal horn increased in SOD1 mice but not in WT mice (Figure 2.7B-F). Diffuse MT-1/2 immunoreactivity in the lower half of the ventral horn was also noted from 18 weeks of age in SOD1 mice but not in WT mice. Overall quantitation of MT-1/2-positive cells in the dorsal horn revealed more MT-1/2-positive cells in the WT dorsal horn than SOD1 dorsal horn at 6 weeks of age (WT 107±18 vs. SOD1 6±4 MT-1/2-positive cells/mm^2, T-test p=0.006), but no significant differences at other time points.

MT-1/2 immunoreactivity in the white matter showed no significant differences between WT and SOD1 mice at any time point (Figure 2.7B-E, I,J), due to variable staining between individual mice. Qualitatively, WT mice showed slightly more MT-1/2-positive cells in the white matter tracts than SOD1 mice at 6-14 weeks of age (Figure 2.7I,J). This was not the case at 18-25 weeks of age, when the numbers of MT-1/2-positive cells in the white matter tracts appeared either equivalent between WT and SOD1 mice, or were higher in SOD1 than WT mice (Figure 2.7I,J). However, the high variation in white matter MT-1/2 immunolabelling in both WT and SOD1 mice means few conclusions about the dynamics of MT-1/2 change in white matter can be drawn from this data, and indicates that the changes observed in grey matter MT-1/2 expression may be more important than changes in white matter MT-1/2 expression.

2.3.1.4.2 Astrocytic localisation of MT

Noting that the number of MT-positive cells increased over time, the localisation of MT-1/2 in astrocytes was examined. Qualitative examination of GFAP immunolabelling indicated that the number of reactive astrocytes appeared to increase with disease progression. At 6 weeks of age, astrocyte cell bodies and some processes were noted in the grey matter (Figure 2.8A), while extensive staining of astrocyte processes was seen within the white matter. The number of astrocytes in the ventral horn grey matter appeared to increase progressively between 6 and 22 weeks of age (Figure 2.8A-C). The increase in astrocyte numbers was also accompanied by a slight change in morphology, with astrocytes at 22 weeks of age showing slightly larger cell bodies and thicker processes than those at earlier time points (Figure 2.8C).

At 18 weeks of age, when the numbers of MT-1/2-positive cells were increased (Figure 2.7), MT-1/2 was predominantly expressed in GFAP-positive astrocytes (Figure 2.8D, shown here in the lumbar spinal cord white matter). Some MT-1/2 immunoreactivity in the ventral horn did not colocalise with GFAP (data not shown), indicating that MT-1/2 may be expressed in other glial cells such as microglia.

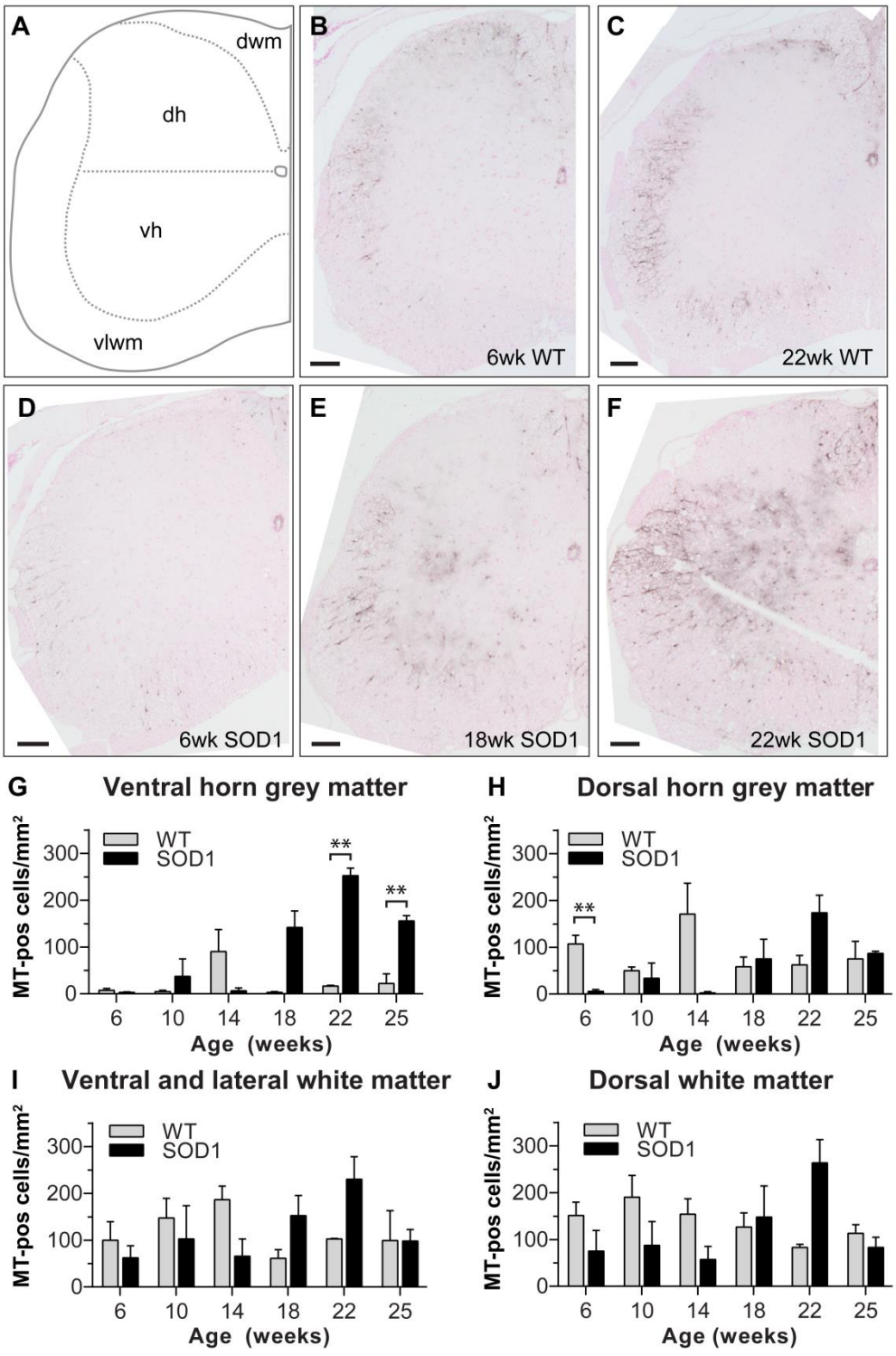

Figure 2.7 MT-1/2 immunoreactivity in the SOD1 and WT spinal cord

Line drawing of spinal cord regions (A; not to scale; dh, dorsal horn; vh, ventral horn; dwm, dorsal white matter; vlwm, ventral and lateral white matter). The density of MT-1/2 -positive (MT-pos) cells did not change substantially in WT mice between 6 (B) and 22 (C) weeks of age, but increased in SOD1 mice between 6 and 22 weeks of age (D-F). MT-1/2 increased in the SOD1 ventral horn from 18 weeks of age (G), and in the dorsal horn at 22 weeks of age (H), but did not change substantially in the white matter (I, J). Scale bars 100µm for B-F. **p<0.01. Error bars represent standard error of the mean.

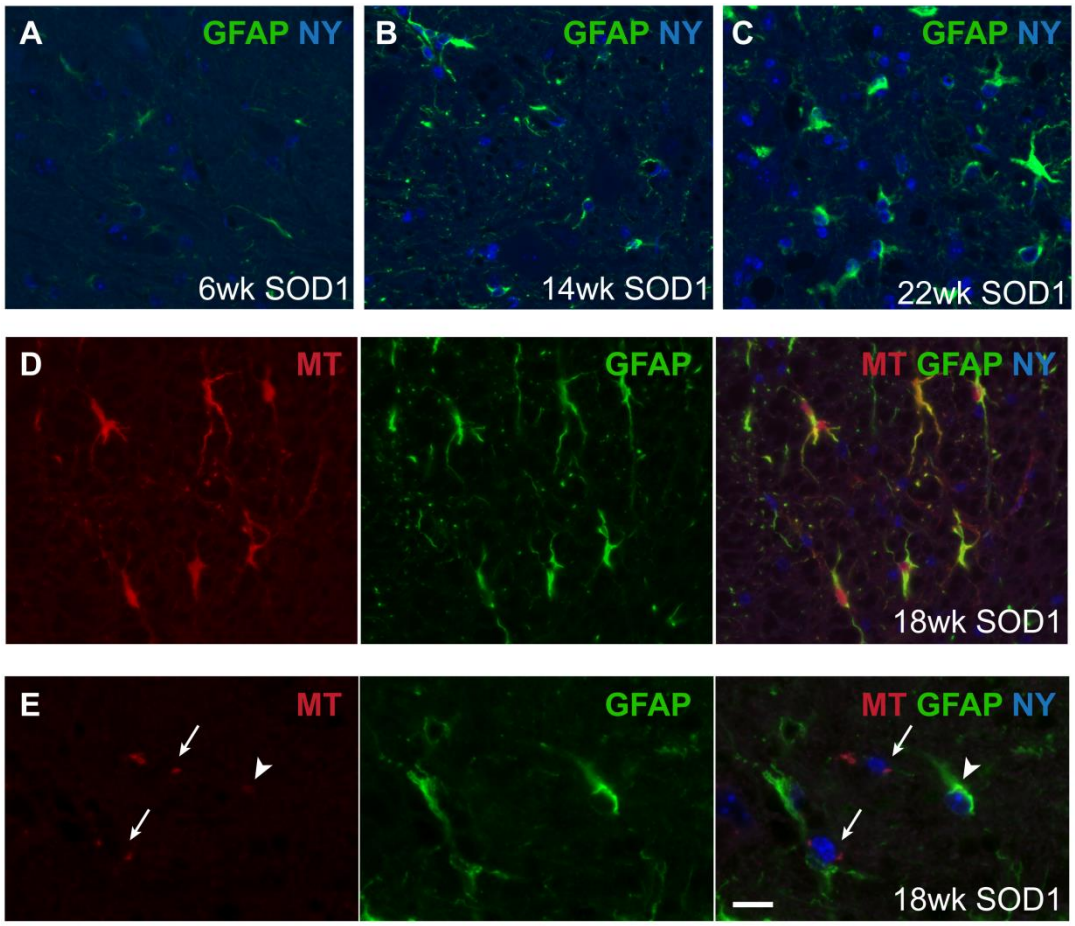

Figure 2.8 Astrocytic expression of MT-1/2 in the lumbar spinal cord of SOD1 mice

The number of astrocytes appeared to increase over time in the lumbar spinal cord ventral horn of SOD1 mice (A-C). MT-1/2 expression (D, left panel) was predominantly seen in GFAP-positive astrocytes (D, middle panel; merged image shown in D, right panel), pictured above at 18 weeks of age in the SOD1 lumbar spinal cord white matter. In the ventral horn of 18-week-old SOD1 mouse lumbar spinal cord, MT-1/2 expression was seen in GFAP-positive astrocytes (E, arrowhead in left and right panels), yet some MT-1/2 expression was observed in cells which did not label with GFAP (E, arrows in left and right panels). Scale bar 20µm for A-D, 10µm for E. GFAP, glial fibrillary acidic protein; MT, metallothionein-1/2; NY, Nuclear Yellow.

2.3.2 Functional changes over time in SOD1 mice

2.3.2.1 Survival

In this cohort, the ethics-approved disease endpoint was measured as either the loss of 20% from maximum body weight, or the inability of the mouse to right itself within 30 seconds of being placed on its side, whichever occurred earlier. All SOD1 mice in this cohort reached the body weight endpoint before a loss of their righting reflex, and therefore the body weight endpoint was used for survival analysis. As determined by Kaplan-Meier analysis, average survival time for SOD1 mice was 163.8±2.1 days; median survival time was 166.0±1.5 days (Figure 2.9). All WT mice remained healthy past the endpoint ages of their SOD1 littermates.

CPH regression was used to assess the effect of $SOD1^{G93A}$ transgene copy number (using the ΔCT value) on survival times. Survival time was not significantly associated with the ΔCT value (HR 2.452, 95% CI 0.071-84.488, p=0.609); perhaps due to the small range of ΔCT values recorded for the functional cohort (range 4.62-5.26), which would indicate relatively small variations in transgene copy number within this cohort. However, copy number could be included in future survival analyses to minimise the effect of any copy number variations.

2.3.2.2 Body weight

2.3.2.2.1 Body weight averages

Body weight rose continuously for WT mice throughout the duration of the study (Figure 2.10A). In contrast, the SOD1 mice displayed a characteristic curved body weight trajectory, achieving average maximal weight (21.0±0.3g) at the average age of 114.1±3.1 days (approximately 16.3 weeks) (Figure 2.10A). The curved body weight trajectory in SOD1 mice likely represents growth during the pre-symptomatic phase of disease, with a subsequent reduction in body weight after disease onset due to loss of muscle mass as part of the disease processes. The average body weight of SOD1 mice was significantly lower than that of WT mice at 14 weeks of age (SOD1 20.0±0.2g vs. WT 21.0±0.5g, MWU p=0.035) and remained lower than that of WT mice until disease endpoint (Figure 2.10A).

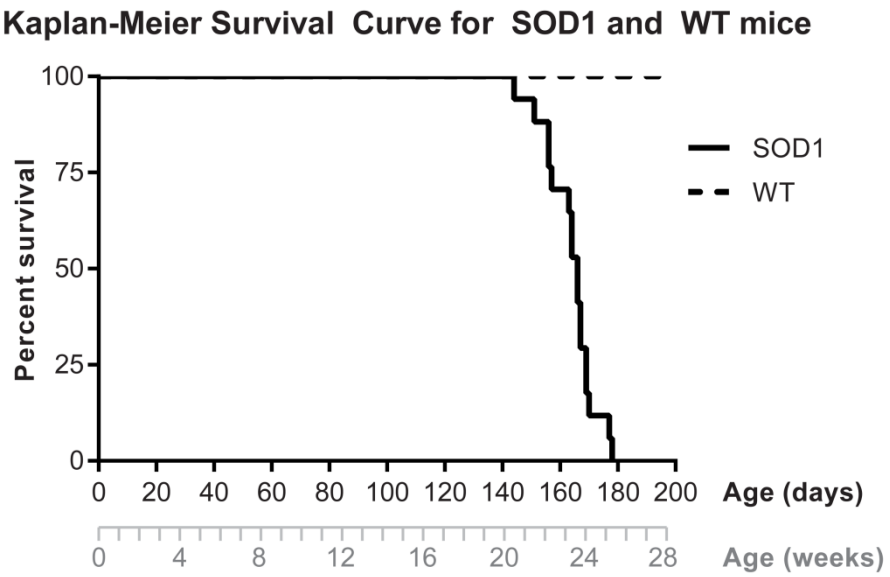

Figure 2.9 Kaplan-Meier survival curve for SOD1 and WT mice

Disease endpoint was measured as a loss of 20% from pre-disease maximum body weight. Survival times for SOD1 mice ranged from 144-177 days, while WT mice remained healthy throughout the study period.

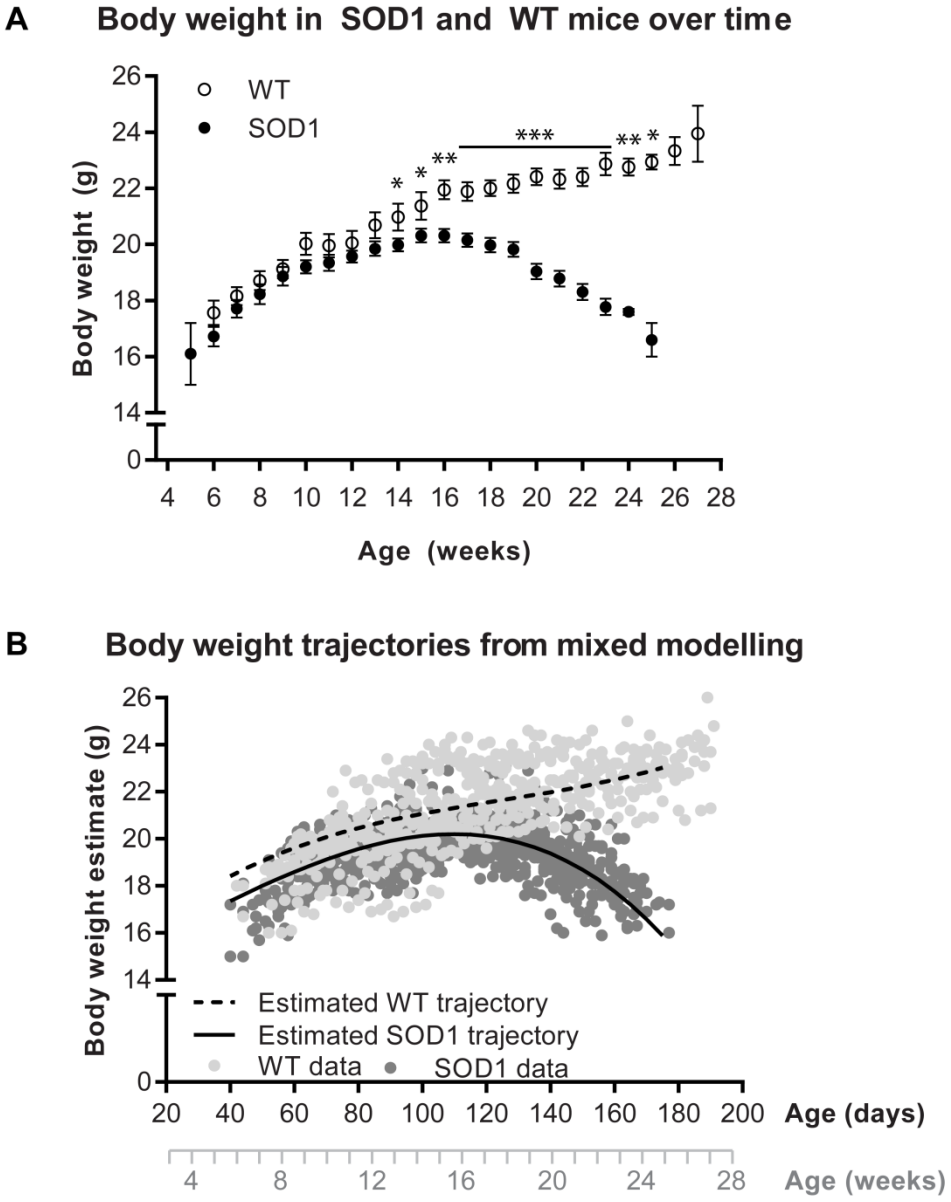

Figure 2.10 Body weights of SOD1 and WT mice over time

Body weight averages (A) were lower for SOD1 mice than WT mice from 14 weeks of age onwards, with SOD1 mice reaching maximum body weight at approximately 16 weeks of age. Body weight trajectory estimates from linear mixed modelling (B, lines, from parameters in Table 2.4) appeared a good fit to the raw data (B, data points). *p<0.05, **p<0.01, ***p<0.001. Error bars represent standard error of the mean.

2.3.2.2.2 Body weight trajectories with linear mixed modelling

Linear mixed modelling was explored as a way to model the curved body weight trajectory of SOD1 mice. Stepwise addition of fixed effects (Age in days, Age^2, Age^3) and random effects (intercept and slope, accounting for different starting body weights and different rates of change over time for different mice), assessment of model fit at each step, and variance-covariance matrix estimates for random effects, are detailed in Supplementary Data 2. The body weight trajectory of SOD1 mice fits more closely to a cubic curve than a quadratic curve (see Supplementary Data 2). The final linear mixed model has fixed effects of the form $\boldsymbol{Body\ weight = \beta_0 + \beta_1 * Age + \beta_2 * Age^2 + \beta_3 * Age^3}$, where each $\boldsymbol{\beta}$ coefficient has a unique value for WT and SOD1 groups (Table 2.4), confirming that body weight trajectory in SOD1 mice is altered from that of WT mice. When the body weight estimates calculated using these coefficient values are graphed, the model confirms the increase in WT body weight over time, and the curved body weight trajectory of SOD1 mice (Table 2.4, Figure 2.10B).

Table 2.4 Parameter estimates from linear mixed model of body weight trajectory

Fixed effects parameter	Parameter estimates (β)		p-value*
	WT	SOD1	
Intercept (β_0)	14.50	14.69	0.868
Age (β_1)	0.128	0.062	0.012
Age^2 (β_2)	-8.53×10^{-4}	2.43×10^{-4}	<0.001
Age^3 (β_3)	2.28×10^{-6}	-3.19×10^{-6}	<0.001

*p-value for whether the parameter estimates were significantly different between WT and SOD1 mice.
Coefficient estimates correspond to the equation $\boldsymbol{Body\ weight = \beta_0 + \beta_1 * Age + \beta_2 * Age^2 + \beta_3 * Age^3}$

The age at which the two trajectory curves diverged was investigated by centring the model at various values of Age; SOD1 body weights became significantly lower than WT body weights from 99 days (14 weeks) of age onwards (p=0.045). Using the $\boldsymbol{\beta}$ estimates in the nlcom procedure (Stata IC), the point estimate for maximum body weight in SOD1 mice was calculated to be 20.0±1.1g, occurring at 110±2 days of age (around 15.7 weeks). These estimates are close to those calculated manually from the raw body weight data (21.0±0.3g, at 114±3 days of age, approximately 16.3 weeks).

2.3.2.3 Stride pattern testing

2.3.2.3.1 Stride Length

The stride length of WT mice stayed constant over time, with only a small decrease around 22-24 weeks of age (Figure 2.11A,B,E). From around 17 weeks of age onwards, the stride length of SOD1 mice declined markedly (Figure 2.11C-E). SOD1 stride length was significantly lower than WT stride length from 18 weeks of age onwards (SOD1 18wk 5.2±1.0cm vs. WT 18wk 5.9±0.8cm, MWU p=0.021) (Figure 2.11E).

2.3.2.3.2 Uniformity

The uniformity measurement, indicating any disparity between placement of the hind paw compared to where the front paw was placed on the previous step (Figure 2.11A), differed between WT and SOD1 mice over time. WT mice maintained a consistent uniformity measurement of less than 0.5cm over time; whereas uniformity measurement increased in SOD1 mice over time (Figure 2.11A-D, F). SOD1 mice showed a larger uniformity measurement than WT mice from 18 weeks of age (SOD1 0.7±0.1cm vs. WT 0.3±0.1cm, MWU p=0.002) onwards (Figure 2.11F). These data indicate that when walking forwards, WT mice were consistently able to bring the hind paw forwards to place it within 0.5cm of where the front paw had been on the previous step; however, SOD1 mice were increasingly unable to bring the hind paw forwards. The increasing uniformity measurement and decreasing stride length over time in the SOD1 mice likely reflect diminishing muscle strength in SOD1 mice as the disease progressed.

2.3.2.3.3 Front-base width and hind-base width

Front-base width was significantly greater in WT mice than in SOD1 mice at 17 weeks and 24 weeks of age (p=0.037 and p=0.034, respectively), however there was no consistent difference between WT and SOD1 mice over time (Figure 2.11B,G).

Measurements of hind-base width appeared variable, with no consistent pattern of change between WT and SOD1 mice over time (Figure 2.11B,H). Hind-base width was greater for WT mice than SOD1 mice at 10, 11, 14, and 15 weeks of age ($p<0.05$), but between these time points there was no significant difference between WT and SOD1 hind-base width (Figure 2.11H). Although measurements of hind-base width in SOD1 mice remained within the range of measurements obtained at earlier time points, they showed a gradual decline from 21-24 weeks of age, such that at these time points the hind-base width was greater for WT mice than SOD1 mice ($p<0.05$) (Figure 2.11H).

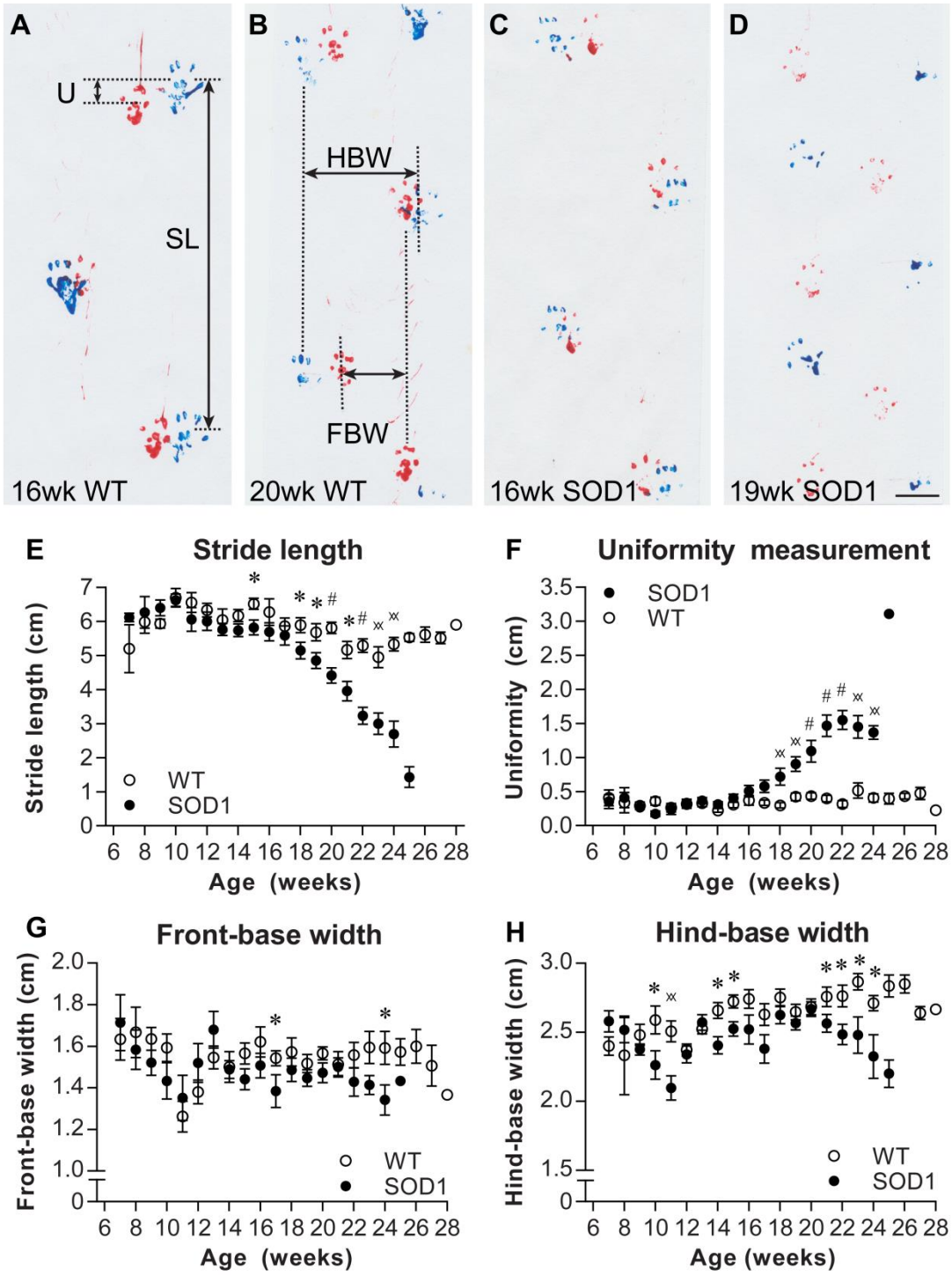

Figure 2.11 Stride pattern testing in SOD1 and WT mice

Representative stride patterns from WT mice at 16 (A) and 20 (B) weeks of age, and from SOD1 mice at 16 (C) and 19 (D) weeks of age, with hind paws in blue and front paws in red. SL, stride length; U, uniformity; FBW, front-base width; HBW, hind-base width (A,B). SOD1 mice showed decreasing stride length (E) and increasing uniformity measurement (F) with age compared to WT mice; front-base width (G) and hind-base width (H) did not differ substantially between WT and SOD1 mice over time. Scale bar 1cm for A-D. *p<0.05, ⁜p<0.01, #p<0.001. Error bars show standard error of the mean.

2.3.2.4 Wire hang duration

Wire hang duration, up to a maximum of 60 seconds, was maintained throughout the study in WT mice but declined over time in SOD1 mice (Figure 2.12).

Out of the 13 WT mice, 4/13 (31%) attained the 60-second maximum on every attempt, while 9/13 WT mice (69%) showed durations of less than 60 seconds on at least one occasion. These sub-maximal results for WT mice can be attributed to either a training effect, where wire hang duration increased up to 60 seconds with experience (see Appendix 1); or to single-week lapses in hang duration, where WT mice would attain less than 60 seconds in a particular week but would return to consistently attaining 60 seconds in the following weeks. In contrast to WT mice, only 12/17 SOD1 mice (71%) ever attained the maximum wire hang duration of 60 seconds; 5/17 SOD1 mice (29%) were unable to maintain hang duration for 60 seconds at any time point measured.

All SOD1 mice displayed reduced wire hang duration as the disease progressed over time (Figure 2.12). In the 12 SOD1 mice attaining 60-second wire hang durations, the average age at which they were no longer able to maintain the maximum hang duration was 114.5±2.4 days of age (approximately 16 weeks of age). SOD1 mice attained a significantly lower average wire hang duration than WT mice at 15 weeks of age (42±5 seconds vs. 58±2 seconds respectively, MWU p=0.012) and thereafter. The average age at which SOD1 mice could only hold on for 30 seconds, half of the maximum time, was 126.3±2.4 days (approximately 18 weeks of age). By 20 weeks of age, SOD1 mice could only hang onto the wire bars for less than 10 seconds, representing a clear decrease in muscle strength between 15 and 20 weeks of age (Figure 2.12).

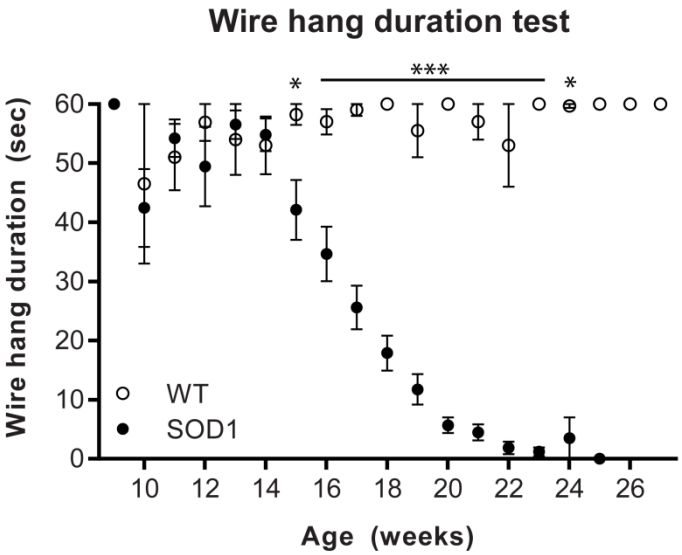

Figure 2.12 Wire hang duration in SOD1 and WT mice

After an initial training period, WT mice were able to maintain the maximum wire hang duration of 60 seconds throughout the study; SOD1 mice showed a marked decrease in wire hang duration from 15 weeks of age onwards. *$p<0.05$, ***$p<0.001$. Error bars represent standard error of the mean.

2.3.2.5 Neurological scoring

The neurological scoring system employed for this analysis ranged from a neurological score (NS) of NS=0 (no symptoms) through to NS=4 (inability to right within 30 seconds of being placed on side) (Table 2.3). SOD1 mice showed an increase in neurological score rating with time, from NS=0 to NS=3 (Figure 2.13). As previously mentioned, all SOD1 mice reached their body weight endpoint before reaching the righting endpoint. Upon reaching the body weight endpoint, 1/17 SOD1 mice (6%) were scored as NS=1, 10/17 SOD1 mice (59%) were scored as NS=2, and 4/17 SOD1 mice (24%) were scored as NS=3; endpoint data on neurological score were not recorded for 2/17 SOD1 mice. Thus, no SOD1 mice were ever rated as NS=4.

WT mice were generally rated as NS=0; however, some WT mice were rated as NS=1 at some time points (Figure 2.13). This may be attributable to the author's strict interpretation of the neurological scoring criteria at NS=1, where the criteria are 'Collapse or partial collapse of leg extension towards lateral midline, or trembling of hind legs, during tail suspension' (Table 2.3). Gradual movement of the hind limbs during tail suspension might have been interpreted as partial collapse, perhaps caused by muscle relaxation in WT mice rather than lack of muscular strength. To ensure that NS=1 was assessed in the SOD1 mice as a true indicator of disease onset, disease onset was considered to be the point at which the mouse was consistently rated as NS=1, or higher, upon every examination. The average age at which SOD1 mice consistently displayed symptoms (NS=1) was 110.5±3.3 days, or approximately 15.8 weeks of age.

There appeared to be a substantial interval between the ages at which SOD1 mice reached NS=1 and NS=2; the average age at which SOD1 mice reached NS=2 was 160.7±2.6 days, or approximately 22.9 weeks of age. Within this interval, observation of the mice identified some features of disease which were not described within the neurological system used here. As disease progressed, the SOD1 mice appeared to display an altered gait pattern in which the legs tended to splay outwards while walking, with the hindquarters being lower than those of WT mice – perhaps due to decreased muscle strength in the hind limbs. In the ALSTDI criteria (Table 2.3), altered gait as required for NS=2 is quite a severe change, with mice dragging their feet and toes along the bench only when within a few weeks of disease endpoint (Figure 2.13).

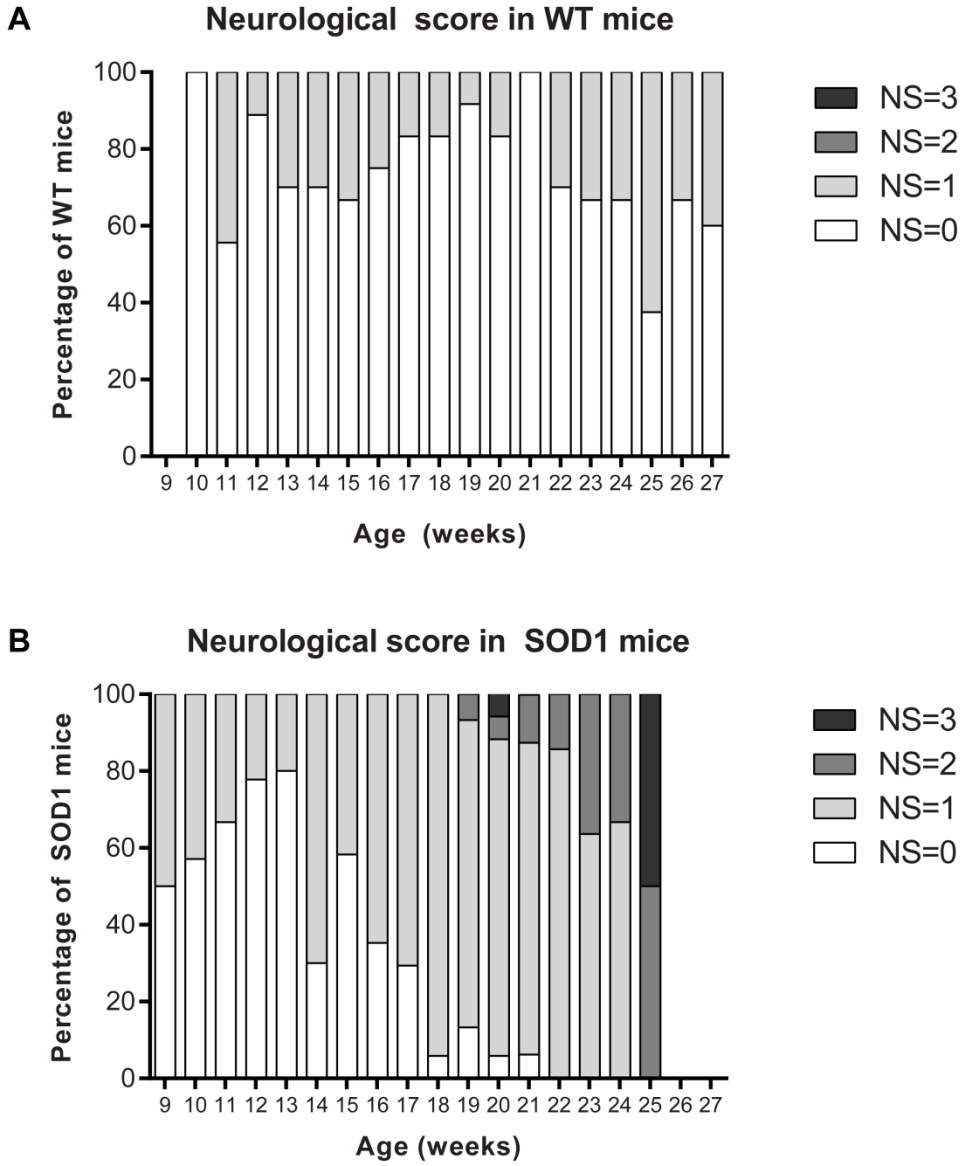

Figure 2.13 Neurological scoring in SOD1 and WT mice

At each week of age, the percentage of mice rated as a particular neurological score (NS=0 through NS=3) is indicated. WT mice were rated as either NS=0 or NS=1 throughout the study (A), whereas SOD1 mice showed a progression from NS=0 (no symptoms) through to NS=3 (hindlimb paralysis), indicating increasing neurological motor deficits over time in SOD1 mice.

2.4 Discussion

The findings in this chapter show that the number of Arg1-positive microglia and iNOS-positive microglia increased in the SOD1 lumbar spinal cord from 14 weeks of age (Figure 2.1 to Figure 2.5), while ubiquitinated inclusions were present in SOD1 motor neurons from as early as 6 weeks of age (Figure 2.6). Functional deficits in SOD1 mice developed from 14 weeks of age onwards (Figure 2.9 to Figure 2.13). The number of MT-1/2-positive cells increased from 18-22 weeks of age (Figure 2.7). Thus, motor neuron pathology precedes microglial activation and functional decline, while microglial activation becomes apparent around the time of symptom onset.

2.4.1 The relationship between microglial activation and disease progression

The results of the present study demonstrated a substantial increase in the number of microglia in the lumbar spinal cord of SOD1 mice, starting from 14 weeks of age and continuing to increase with time (Figure 2.1) The increase in microglial numbers starts from 14 weeks of age, concurrent with the onset of disease symptoms, as measured by decreased body weight in SOD1 mice compared to their WT littermates. This study confirms previous observations that activated microglia are increased in the SOD1 spinal cord at disease onset, and increase in number throughout disease progression (Almer *et al.* 1999; Chiu *et al.* 2008; Gowing *et al.* 2008; Beers *et al.* 2011b; Yang *et al.* 2011). However, a few previous studies have identified a pre-symptomatic increase in microglial number in SOD1 mice (Alexianu *et al.* 2001), $SOD1^{G93A}$ rats (Graber *et al.* 2010), and $SOD1^{H46R}$ rats (Sanagi *et al.* 2010). Earlier apparent activation of microglia in these three studies may be due to the use of a different, perhaps more sensitive, microglial marker CD11b (Alexianu *et al.* 2001); or alternatively the disease course in SOD1 rodent models may show subtle differences depending on species, transgene copy number, or activity level of the mutant SOD1 protein (Pan *et al.* 2012).

Pathological changes in motor neurons, including the presence of ubiquitinated aggregates and the formation of SOD1-positive annular structures, were observed from 6 weeks of age onwards, well before the increase in microglia was first detected at 14 weeks of age (Figure 2.6). The timing of these changes suggests that the increase in spinal cord microglia is a reactive response to neuronal dysfunction or degeneration, rather than a primary initiator of neuronal damage. However, microglial activation may play a key role in modulating disease progression after disease onset (Boillee *et al.*

2006; Beers *et al.* 2011a; Beers *et al.* 2011b; Audet *et al.* 2012). Indeed, we observed that SOD1 mice developed overt functional changes in stride pattern from 18 weeks of age, four weeks after the initial increase in lumbar spinal cord microglia (Figure 2.1, Figure 2.11). Thus, the increase in microglial number preceded the transition into a rapidly-progressing phase of disease, where functional ability rapidly declined.

2.4.2 Microglial phenotype in SOD1 mice

In spinal cord tissue from ALS patients and SOD1 rodents, activated microglia can form aggregates in close proximity to motor neurons (Alexianu *et al.* 2001; Henkel *et al.* 2004; Sanagi *et al.* 2010), suggesting that any microglial activation will directly affect motor neurons. As M1-like and M2-like microglial phenotypes appear to be an important determinant of disease progression in SOD1 mice (Beers *et al.* 2011b), SOD1 lumbar spinal cord ventral horn microglia were characterised through their expression of putative M1/M2 markers iNOS and Arg1, respectively (Colton 2009).

2.4.2.1 Lumbar spinal cord Arg1 and iNOS expression

In this study it was expected that the lumbar spinal cord microglia in SOD1 mice would show a shift in the spectrum of their activation phenotype, from Arg1-predominant to iNOS-predominant, in line with other studies which have suggested an M2-to-M1 shift over time (Beers *et al.* 2011a; Beers *et al.* 2011b; Liao *et al.* 2012). However, the current study found that both Arg1-positive and iNOS-positive microglia increased in number with disease progression (Figure 2.2, Figure 2.3). The number of Arg1-positive lumbar spinal cord microglia increased at disease onset, and continued to increase with disease progression, such that the number of Arg1-expressing microglia increased 18-fold between the pre-symptomatic stage and disease endpoint (Figure 2.2). Less than 20% of microglia expressed Arg1 at the pre-symptomatic stage, but this figure rose to over 60% at disease endpoint (Figure 2.5F). The increase in Arg1-expressing microglia may suggest an increase in the number of microglia displaying an M2-like neuroprotective phenotype.

However, the number of iNOS-positive lumbar spinal cord microglia also increased from disease onset, with a 7-fold increase in microglia expressing iNOS between the pre-symptomatic stage and disease endpoint (Figure 2.3). Less than 10% of microglia

expressed iNOS at pre-symptomatic stages, with this figure rising to over 30% at 22 weeks of age (Figure 2.5F). It was noted that the increase in iNOS-positive microglia was also accompanied by an increase in the number of iNOS-negative microglia (Figure 2.3); in the absence of double-immunostaining for Arg1 and iNOS together, one may speculate that these iNOS-negative microglia showed an M2-like, possibly Arg1-positive, phenotype. Despite the reported M2-to-M1 shift in microglial phenotype in SOD1 spinal cord (Liao *et al.* 2012), two studies have shown the maintenance of M2 markers and M2-like characteristics in SOD1 microglia at disease endpoint (Chiu *et al.* 2008; Tada *et al.* 2011); consequently, the concept of microglia retaining some of their neuroprotective function throughout disease progression is not unprecedented.

A semi-quantitative analysis of Arg1 and iNOS immunoreactivity in individual microglia indicated that both Arg1 and iNOS expression levels were increased during disease progression (Figure 2.4). The percentage area occupied by Arg1 immunoreactivity increased approximately 5-fold between 6 and 22 weeks of age, yet the percentage area occupied by iNOS immunoreactivity increased approximately 25-fold between 6 and 22 weeks of age due to the small amount expressed at 6 weeks of age (Figure 2.4). Although these data would hint that the percentage area occupied by Arg1 appears greater than that occupied by iNOS (Figure 2.4), the absolute levels of Arg1 and iNOS protein cannot be reliably compared by immunohistochemistry intensity due to different antibody-antigen binding strengths. These data do suggest that iNOS shows a greater fold increase than Arg1 between 6 and 22 weeks of age.

The increasing number of iNOS-positive microglia seen in the present study, along with the large fold increase in iNOS immunoreactivity, may represent an increase in M1 neurotoxic microglia, which could increase the production of toxic factors such as nitric oxide within the spinal cord (Appel *et al.* 2011). In contrast, the continuing increase in Arg1-positive microglia may represent an ongoing attempt by M2 neuroprotective microglia to limit tissue damage and neuronal degeneration (Colton 2009; Henkel *et al.* 2009). The increase in iNOS-positive microglia, while lesser in magnitude than the increase in Arg1-positive microglia, may result in a higher net production of nitric oxide in the lumbar spinal cord ventral horn, with deleterious effects on the surrounding motor neurons. Thus, the results of this study show evidence of concomitant neurotoxic and neuroprotective processes in SOD1 spinal cord microglia.

2.4.2.2 Cervical spinal cord Arg1 and iNOS expression

The expression of Arg1 and iNOS was examined in the cervical spinal cord of SOD1 mice aged 10 to 22 weeks, to determine whether differences in microglial phenotype between the lumbar and cervical regions may explain the later involvement of the forelimbs in SOD1 mice (Kuntz *et al.* 2000).

In the cervical spinal cord ventral horn of SOD1 mice, the number of Arg1-positive microglia was increased at 22 weeks of age, while the number of microglia expressing iNOS also increased slightly over time (Figure 2.5). Although these trends were similar to those seen in the lumbar spinal cord, three pieces of data indicate that the cervical spinal cord may present a slightly M2-skewed microglial environment compared with the lumbar spinal cord. First, at 10 weeks of age, there were equivalent numbers of Arg1-positive and Arg1-negative microglia in the cervical spinal cord, whereas in the lumbar spinal cord the majority of microglia did not express Arg1. Second, at 22 weeks of age, the cervical spinal cord shows a higher percentage of microglia expressing Arg1 (79%) than the lumbar spinal cord (64%). Third, at 22 weeks of age, the cervical spinal cord shows a lower percentage of microglia expressing iNOS (24%) than the lumbar spinal cord (32%). These slight differences indicate that neuroprotective M2-phenotype microglia may be more prevalent in the cervical spinal cord than the lumbar spinal cord at pre-symptomatic stages of disease, and that the activation state of cervical microglia at 22 weeks of age involves greater numbers of microglia expressing of the M2 marker Arg1, and lower numbers of microglia expressing the M1 marker iNOS.

These results are in line with a previous study showing early upregulation of M2 markers in the cervical spinal cord of SOD1 mice (Beers *et al.* 2011b). From the current study, it is difficult to elucidate whether the apparently less-inflammatory microglial environment in the spinal cord is due to a reduced reactive response from decreased or delayed neuronal degeneration, or whether the relative prevalence of M2-phenotype microglia directly provides a protective environment, delaying neuronal dysfunction and degeneration. However, comparing ubiquitin pathology at 10 weeks of age in the lumbar spinal cord (aggregates in the motor neuron somas and in the neuropil; Figure 2.6) and the cervical spinal cord (aggregates in the motor neuron somas, and mostly absent from the neuropil) (Lewis *et al.* 2014) indicates that the microglial expression of inflammatory markers may be influenced by the prevalence of ubiquitinated aggregates.

2.4.2.3 Technical limitations to discussion of microglial phenotype

The results from the present study do not show a shift from Arg1-predominant, M2-like phenotype to an iNOS-predominant, M1-like phenotype over time, and as such differ slightly from previously reported studies. M2 markers such as Ym1 and MCP-1 have previously been reported as upregulated in the SOD1 spinal cord during the early, slow-progressing phase of disease (Beers *et al.* 2011a; Beers *et al.* 2011b), with a subsequent downregulation of M2 markers, and upregulation of M1 markers such as TNFα, IL-6 and NOX2 during the rapidly-progressive disease phase (Almer *et al.* 1999; Yoshihara *et al.* 2002; Gowing *et al.* 2009; Beers *et al.* 2011a; Beers *et al.* 2011b; Liao *et al.* 2012). The differences between the current study and these previous studies may be due to the use of protein markers rather than mRNA markers of M1/M2 microglial phenotype.

There are both positive and negative aspects to the use of protein markers rather than mRNA analysis. While analysis of spinal cord mRNA can provide an excellent overview of the proteins cells are capable of producing, not all mRNAs may be effectively translated into protein. Furthermore, analysis of mRNA from homogenised spinal cord cannot determine the subcellular localisation of specific mRNAs. While microglia are likely to be the primary cell type for cytokine production within the spinal cord, other cell types including astrocytes, infiltrating immune cells, and even motor neurons may also produce cytokines and inflammatory markers; the use of mRNA from homogenised spinal cord alone may limit interpretation of protein expression in microglia. Indeed, Arg1 expression in motor neurons was observed in the current study (data not shown). Immunolabelling allows cell-specific localisation of inflammatory markers, ensuring that the results are specific to microglia.

Conversely, while the use of immunostaining allows identification of cell-specific protein expression, persistent antibody cross-reactivity when attempting double-labelling for Arg1 and iNOS (both mouse monoclonals) meant that the relative expression of Arg1 and iNOS within specific cells could not be compared. As Arg1 and iNOS are inversely regulated in CNS glia (Bonaparte *et al.* 2006), it could be assumed that cells expressing Arg1 expressed low levels of iNOS, and vice versa – however, it is likely that some, but not all, Arg1-positive microglia also express iNOS. Thus, not all Arg1-positive microglia may show a neuroprotective phenotype. While the presence of

a higher percentage of microglia expressing Arg1 than iNOS does suggest an M2-predominant, anti-inflammatory environment in the SOD1 spinal cord, this interpretation is over-simplistic without the consideration of additional M1 and M2 markers. It is also possible that the expression of Arg1 and iNOS may not correlate directly with M2 and M1 phenotypes. The ideal analysis of microglial phenotypes would combine mRNA data, protein immunohistochemistry, and cytokine profiles of the SOD1 spinal cord.

2.4.3 Pathological changes in SOD1 motor neurons

The timing of motor neuron pathology in the SOD1 lumbar spinal cord was examined with immunostaining for neurofilaments, ubiquitin and hSOD1. Pathological alterations in lumbar motor neurons were seen from as early as 6 weeks of age (Figure 2.6), well before the development of microgliosis in the lumbar spinal cord (Figure 2.1). The current study confirms previous results showing pre-symptomatic presence of ubiquitianted aggregates and vacuolar neurofilament pathology in the SOD1 spinal cord (Bruijn *et al.* 1997a; Vinsant *et al.* 2013), indicating that the initial increase in microglia is likely a neuroprotective response to neuronal degeneration.

From 6 weeks of age onwards, vacuolar pathology involving both hSOD1 and neurofilaments develops in spinal cord motor neurons (Figure 2.6). The source of these 'empty' vacuoles may be due to the breakdown of the Golgi apparatus or the swelling of mitochondria (Vinsant *et al.* 2013), or due to direct effects of mutant SOD1 on neurofilament proteins. The formation of ring-like structures in the neuropil, which are positive for either hSOD1 or dephosphorylated neurofilament medium chain (SMI32), and sometimes both, suggests a direct role for the mutant SOD1 in vacuole formation by neurofilament modification. SOD1-mediated protein nitration by nitric oxide may be one such detrimental way for SOD1 to disrupt neurofilament formation (Bruijn *et al.* 1997a). As neurofilament content normally regulates axonal calibre (Hoffman *et al.* 1984; Perrot *et al.* 2007), it is possible that aberrant accumulations of neurofilament protein are misinterpreted as a local stimulus for expansion of axon, creating a vacuole.

Additionally, the appearance of neuronal pathology precedes the onset of functional deficits by several weeks in this study. This is consistent with previous studies showing pre-symptomatic degenerative changes at the neuronal cell body well before loss of

function, due to compensatory re-innervation of muscle fibres by surviving motor neurons (Frey *et al.* 2000; Nandedkar *et al.* 2010; Vinsant *et al.* 2013).

2.4.4 Increasing expression of the antioxidant response protein, MT-1/2

Increasing iNOS expression in microglia may contribute to the production of nitric oxide, and in turn the production of peroxynitrite, in the spinal cord of SOD1 mice. The expression of the protein metallothionein-1/2 was examined as a measure of the antioxidant response taking place in spinal cord glia. In the lumbar spinal cord, an increase in MT-1/2-expressing glial cells was seen in the ventral horn from 18 weeks of age (Figure 2.7). The amount of diffuse MT-1/2 immunostaining also qualitatively increased from 18 weeks of age in SOD1 mice (Figure 2.7), indicating a possible increase in both MT-1/2 expression and MT-1/2 secretion into the extracellular space.

The increase in MT-1/2 expression with disease progression confirms previous studies showing increased MT-1/2 production in the SOD1 spinal cord over time (Gong & Elliott 2000; Nagano *et al.* 2001; Tokuda *et al.* 2007; Tokuda *et al.* 2013). However, the current study was only able to detect increased MT-1/2 in the ventral horn from 18 weeks of age onwards, while previous studies have all demonstrated pre-symptomatic MT-1/2 increases (Gong & Elliott 2000; Nagano *et al.* 2001; Tokuda *et al.* 2007; Tokuda *et al.* 2013). The earlier increase in MT-1/2 seen in previous studies may be due to differences in genetic background strain of SOD1 mice – a congenic B6 background was used in the current study, compared to a hybrid B6SJL background used in previous studies (Gong & Elliott 2000; Nagano *et al.* 2001; Tokuda *et al.* 2007; Tokuda *et al.* 2013). Alternatively, the earlier detection of MT-1/2 in previous studies may be due to the use of more sensitive detection techniques such as radioimmunoassay (Nagano *et al.* 2001). The increased production of MT-1/2 during only the symptomatic stage of disease in the current study (Figure 2.7) does not negate the presence of oxidative stress in pre-symptomatic SOD1 mice, as MT-1/2 is only one of many antioxidant response proteins (Mates *et al.* 1999; Ahsan *et al.* 2009). The post-symptomatic increase in MT-1/2 may indicate the presence of detrimental oxidative stresses at later phases of disease.

The upregulation of MT-1/2 from 18 weeks of age (Figure 2.7) does correlate with the increase in microglial activation in the lumbar spinal cord, and occurs around the time that overt functional deficits in SOD1 stride pattern were detected (Figure 2.11).

Together, these data suggest that the increasing number of iNOS-expressing ventral horn microglia increases total NO synthesis; the increased NO- or peroxynitrite-mediated oxidative stress may damage motor neurons, causing overt functional deficits, and inducing expression of MT-1/2 in astrocytes.

Alternatively, the role of MT-1/2 in SOD1 mice may be more complex than purely providing an antioxidant response. MT-1/2 show neuroprotective properties, which will be further discussed in Chapter 4, as well as antioxidant properties. Astrocytes increase MT-1/2 production upon cortical neuronal injury, and MT-1/2 is secreted from astrocytes onto surrounding neurons to elicit pro-survival and pro-outgrowth effects (Chung *et al.* 2008b). In SOD1 mice, the increase in MT-1/2 expression could be in response to widespread neuronal degeneration in the later stages of disease from 18 to 25 weeks of age, as a possible attempt to protect motor neurons from degeneration.

While MT-1/2 immunoreactivity was mainly colocalised with the astrocyte marker GFAP (Figure 2.8), some glial MT-1/2 labelling was not colocalised with GFAP (data not shown). In the SOD1 spinal cord, MT-1/2 was originally thought to be expressed only in astrocytes (Gong & Elliott 2000); however, a recent publication demonstrated MT-1/2 in SOD1 microglia as well as astrocytes (Tokuda *et al.* 2013). The small amount of non-GFAP-associated MT-1/2 immunostaining in the present study (data not shown) could be present in microglia. Future studies could examine whether microglial MT-1/2 expression may attenuate microglial ROS production, and consequently correlate with neuroprotective rather than neurotoxic microglial phenotypes.

There are some limitations to the interpretation of MT-1/2 induction as an antioxidant or neuroprotective response. As mentioned above, MT-1/2 is induced in response to neuronal injury; MT-1/2 induction is additionally controlled by the presence of metal ions, cytokines, and corticosteroids (Richards *et al.* 1984; Cousins & Leinart 1988). The increased astrocytic MT-1/2 in the SOD1 spinal cord could reflect metal dyshomeostasis, which has been proposed as a possible mechanism of ALS (Roos *et al.* 2006), or the presence of inflammatory cytokines due to increasing microglial activation and T-cell infiltration (Beers *et al.* 2011a). Alternatively, as the number of astrocytes appeared to increase over time in the SOD1 lumbar spinal cord in the present study (Figure 2.8), and as astrogliosis has been reported previously in SOD1 mice (Vargas & Johnson 2010), the increased amount of MT-1/2 in the spinal cord may purely reflect

the increasing number of astrocytes. Regardless of the multiple possible mediators of MT-1/2 upregulation, the presence of diffuse MT-1/2 immunoreactivity indicates that MT-1/2 is released into the extracellular space of the SOD1 lumbar spinal cord and may comprise an attempt at astrocyte-mediated neuroprotection. The protective effects of MT-1/2 in SOD1 mice will be further explored in Chapter 4.

2.4.5 Functional decline

As expected, the present study confirmed the decline in functional ability over time in SOD1 mice (Gurney *et al.* 1994). SOD1 mice showed lower body weights than wild-type mice from 14 weeks of age (Figure 2.10), deficits in wire hang duration from 15 weeks of age (Figure 2.12), observable neurological deficits from 16 weeks of age (Figure 2.13), and altered stride pattern from 18 weeks of age (Figure 2.11). Thus, disease onset was detected around 14 to 15 weeks of age in this study. The timing of disease onset is considered a conservative estimate compared to other studies using the SOD1 mouse on a congenic B6 background, which found the earliest appearance of disease symptoms at around 11 weeks of age (Beers *et al.* 2011a; Beers *et al.* 2011b).

2.4.5.1 The use of mixed modelling to assess body weight peak

In this study a slightly novel approach to measuring disease onset was used – mixed modelling was used to generate a curve to model the body weight trajectory of SOD1 mice, and the age at which maximum body weight was reached was estimated using calculus. This method was compared with the calculation of weekly averages. Both the average body weight, and the trajectory estimated with mixed modelling, showed differences between SOD1 and WT mice from 14 weeks of age (Figure 2.10). The model-derived estimated maximum body weight, and the model-derived age at which the maximum body weight occurs, were similar to those calculated from the raw data.

The mixed model has both advantages and disadvantages over weekly body weight averages. The advantages are that: the mixed model allows all recorded body weight measurements, even taken on a daily basis, to be used instead of creating a weekly average for each mouse; and that the mixed model is able to assign some of the variance in the data to variations over time for individual mice, reducing the residual variance and increasing statistical power to detect differences between treatment or genotype

groups (Murnane & Willett 2011). The disadvantage of a mixed model is that if the model is not fitted correctly, the estimates generated by the model will not be an accurate reflection of the true data. However, the body weight trajectories of SOD1 mice appear to be well modelled by a cubic function (Figure 2.10), with a cubic function showing superior model fit over a quadratic function (Supplementary Data 1). Thus, mixed modelling may be a novel method of increasing statistical power in studies which examine body weight measurements in the same mice over time.

2.4.5.2 Comparison of tests for functional deficits

Functional decline in SOD1 mice was evident in wire hang duration times prior to becoming evident in stride pattern (Figure 2.11, Figure 2.12). This earlier detection using the wire hang test may be due to the nature of each task – maintaining grip on suspended wire bars requires constant muscle activation, whereas walking along a strip of paper likely requires less muscle strength, and has the advantage that each limb gets a transient rest period while it is in the stationary phase of walking.

The wire hang duration, or paw grip endurance, test has been used previously to assess functional ability and muscle strength in SOD1 mice, with deficits in wire hang duration ability found as early as 12 weeks of age (Weydt *et al.* 2003). In the present study, wire hang duration was tested to a maximum of 60 seconds, compared with a maximum of 90 seconds in previous studies (Weydt *et al.* 2003). The use of a longer test time may pick up earlier changes in muscle strength, as increasing the hang time requires an increased amount of strength and endurance.

Computerised treadmill analysis of SOD1 gait pattern indicates that changes between SOD1 and WT mice occur as early as 8 weeks of age (Wooley *et al.* 2005); however, in the current study differences between SOD1 and WT mice only became apparent from 18 weeks of age onwards (Figure 2.11). The late change in stride lengths observed here are consistent with those observed in other studies using non-treadmill-based footprint analysis (Gurney *et al.* 1994; Knippenberg *et al.* 2010). These data indicate that measurements of stance and stride times during treadmill running (Wooley *et al.* 2005) provide a much more sensitive measure of dysfunction than measurement of stride length on paper. However, the late decline in stride length may correspond to the rapidly-progressing phase of disease, where motor units are lost without compensatory

re-innervation in the muscle; stride length may be useful in monitoring disease progression during this phase.

In this study we report increasing uniformity measure in SOD1 mice; that is, reduced ability of hindlimb musculature to move the leg in a forward motion during stepping, such that the hindlimb placement falls short of front limb placement on the previous step (Figure 2.11). To our knowledge, this measure has not been previously reported in SOD1 mice and, like the late change in stride length, may be an appropriate measure of measuring the effect of therapeutic interventions on the late phase of disease.

2.4.5.3 Neurological scoring system

The neurological scoring system employed in this study, designed by the ALSTDI, was used to assess neurological deficits present in SOD1 mice through observation. The ALSTDI scoring system allows only five possible neurological scores: no symptoms (NS=0), mild symptoms at disease onset (NS=1), dragging of feet due to loss of muscle strength (NS=2), rigid paralysis or minimal movement (NS=3), and inability to right (NS=4) (Scott *et al.* 2008). SOD1 mice showed a progressive increase in the neurological score rating throughout disease progression (Figure 2.13); however, of the four neurological scores observed in this study (NS=0-3), there was a substantial time gap between a rating of NS=1 and a rating of NS=2 (see text, Chapter 2.3.2.5). During the period when a given mouse was rated NS=1, alterations in gait could be observed which did not meet the criteria for a rating of NS=2. Additionally, some WT mice were also rated as NS=1 – possibly due to mis-interpretation of the neurological score criteria to include any inwards collapse of the legs upon tail suspension, as sometimes occurred in WT mice – but no WT mice showed gait abnormalities as seen in SOD1 mice. A neurological scoring system with more specific detail around gait abnormalities, such as the Beers/Appel/Simpson/Henkel (BASH) scoring system (Beers *et al.* 2011b), may be more appropriate for detailed comparison of neurological symptoms present after disease onset in SOD1 mice.

Although the NS=2 rating was reached rather late in disease progression, a rating of NS=2 with dragging feet, or toes curling under while walking, was easily identified and may be a useful tool for measuring the age at which mice develop overt difficulties maintaining normal hindlimb function.

2.4.5.4 Functional measures of disease progression for evaluating therapeutics

Peak body weight, and the inability to maintain wire hang duration for 60 seconds, may be used to evaluate disease onset in future cohorts of SOD1 mice. Changes in stride length, uniformity measure, wire hang duration, body weight, and neurological score rating (foot dragging), may be useful for monitoring disease progression over time in SOD1 mice.

2.4.6 Summary and conclusions

There are four main findings of this study:

First, the increase in microglial numbers does not precede onset of disease symptoms but does precede the development of overt functional deficits;

Second, the number of Arg1-positive microglia and the number of iNOS-positive microglia both increase in the SOD1 lumbar spinal cord over time, suggesting ongoing conflicting actions of neuroprotective and neurotoxic microglia;

Third, cervical spinal cord microglia show more common expression of Arg1 and less common expression of iNOS than the lumbar spinal cord, indicating that a more M2-like inflammatory environment may be responsible for the later involvement of the forelimbs;

Fourth, the antioxidant protein MT-1/2 is increased after disease onset, possibly induced by neuronal damage, or by the release of free radical species or inflammatory cytokines from activated microglia.

These findings implicate microglial activation and microglial phenotype as contributors to the degeneration of motor neurons after disease onset. It is likely that microglial activation occurs as a result of early changes in dysfunctional or degenerating motor neurons, with microglial activation then affecting disease progression (Beers *et al.* 2006; Liao *et al.* 2012). Microglial activation in the spinal cord involved increased numbers of cells expressing the M2 marker Arg1, and increased numbers of cells expressing the M1 marker iNOS, showing that both neurotoxic and neuroprotective processes are ongoing within the spinal cord of SOD1 mice.

The results presented here highlight the need to use a panel of inflammatory markers to determine microglial phenotype. Although this study showed a predominance of Arg1-expressing microglia, the phenotype of each individual cell will depend on the balance of Arg1/iNOS expression and on cytokine expression. The ideal study of microglial phenotype would combine mRNA, protein, and cytokine expression profiles.

The modulation of microglial activation remains a key target for ameliorating disease in ALS patients (Beers *et al.* 2008; Chiu *et al.* 2008; Pollari *et al.* 2011; Lee *et al.* 2012). Pro-inflammatory microglial activation, as seen by the increasing number of iNOS-positive microglia, likely causes neuronal damage regardless of an increase in anti-inflammatory microglial activation as seen by Arg1 expression in this study. It is likely that the detrimental effects of an M2-to-M1 microglial phenotype switch come primarily from the gain of toxic properties in M1 microglia, but may also involve the loss of protective properties in M2 microglia. As such, potential ALS therapies designed to modulate microglial activation should concentrate on the reduction of the pro-inflammatory phenotype and the promotion of the anti-inflammatory phenotype. Modulation of microglial immune responses remains an important target for ameliorating disease symptoms and slowing the rate of disease progression in ALS.

Chapter 3

The effects of Gemals compound in SOD1 mice

3.1 Background

3.1.1 The need for multi-action therapies in ALS

Clinical trials of single-drug interventions in ALS patients have shown little efficacy (Gordon & Meininger 2011). In addition, single-drug studies which were successful in SOD1 mice have not translated into successful clinical trials in ALS patients (Benatar 2007). As mentioned in Chapter 1, the etiology of ALS is thought to be highly complex, with evidence of multiple pathological changes present. These changes include oxidative stress and marked activation of glial cells, in both ALS patients and SOD1 mice. The multifactorial aetiology of ALS indicates that a single therapeutic compound may not be sufficient to successfully address the multiple aspects of ALS pathology. Therefore, multifactorial or multi-action therapies may have more success as effective therapeutics for preventing neuronal death in ALS.

3.1.2 Endotherapia – a drug cocktail of small molecules

One such drug cocktail under consideration for an ALS treatment is known as Endotherapia, a mixture of small molecules each conjugated to poly-L-lysine (PLL) (Geffard *et al.* 2010). The mixture of small molecules consists of fatty acids, amino acids, antioxidant compounds, and vitamins, thought to have neuroprotective, antioxidant, and immunomodulatory activity (Geffard *et al.* 2010). Additionally, while the role of chronic infection in neurodegeneration is controversial (Nicolson 2008), the fatty acids in Endotherapia may prevent bacterial adhesion to reduce chronic infections (Geffard *et al.* 2010). The multiple potential actions of Endotherapia could affect several pathways at once, and thus would have more chance of ameliorating complex neurodegenerative diseases. Endotherapia complexes have been tested in the neurodegenerative diseases multiple sclerosis (MS) and ALS, using an MS-tailored Endotherapia mixture of 19 compounds, named ‘GEMSP’ (Mangas *et al.* 2006), and an ALS-tailored Endotherapia mixture containing 25 compounds, named ‘Gemals’ (Nicaise *et al.* 2008); 12 compounds are common to both GEMSP and Gemals. The base components of Gemals, along with information on their functions, are listed in Table 3.1. The composition of formulated Gemals, where the components are linked to PLL in various combinations, is listed in Table 3.2.

Table 3.1 Functional categories of Gemals components

Constituent	Molecule type; function
Oleic acid	Unsaturated fatty acid; antioxidant, anti-inflammatory
Thioctic acid	Dithiol; antioxidant
Myristic acid	Saturated fatty acid
Palmitic acid	Saturated fatty acid
Lauric acid	Saturated fatty acid; anti-inflammatory
Linoleic acid	Unsaturated fatty acid; antioxidant, anti-inflammatory
Palmitoleic acid	Unsaturated fatty acid; anti-inflammatory
Caprylic acid	Saturated fatty acid
T-T-Farnesyl-L.Cysteine	Amino acid derivative;
Cholesterol	Sterol; anti-inflammatory
L. Cysteine	Amino acid; antioxidant
Taurine	Amino acid derivative; antioxidant, neuroprotective
L. Methionine	Amino acid; antioxidant, anti-inflammatory
L. Glutathione	Tripeptide; antioxidant
Alpha-tocopherol-succinate	Vitamin E; antioxidant
Ascorbic acid	Vitamin C; antioxidant
Coenzyme Q10	Respiratory chain component; antioxidant, anti-inflammatory, neuroprotective
Retinoic acid	Vitamin A derivative; antioxidant, anti-inflammatory, neuroprotection
Pantothenic acid	Vitamin B5; antioxidant, anti-inflammatory, neuroprotection
Biotin	Vitamin B7; essential coenzyme for carboxylases
Uric acid	Organic acid; antioxidant
Agmatine	Amino acid derivative; antioxidant, anti-inflammatory, neuroprotective
Glucosamine	Monosaccharide; antioxidant, anti-inflammatory, neuroprotective

Table 3.2 Gemals components and their concentration in the current study

Constituent	Concentration
Oleic acid – PLL – Thioctic acid	66µM
Oleic acid – PLL – Myristic acid	66µM
Oleic acid – PLL – Palmitic acid	66µM
Oleic acid – PLL – Lauric acid	66µM
Oleic acid – PLL – Linoleic acid	66µM
Oleic acid – PLL – Palmitoleic acid	66µM
Lauric acid – PLL – Caprylic acid	66µM
T-T-Farnesyl-L.Cysteine – PLL – Palmitic acid	66µM
Cholesterol – PLL – Oleic acid	66µM
L. Cysteine – RG – PLL	66µM
L. Cysteine – GA – PLL	66µM
Taurine – RG – PLL	66µM
Taurine – GA – PLL	66µM
L. Methionine – RG – PLL	66µM
L. Methionine – GA – PLL	66µM
L. Glutathione – RG – PLL	66µM
Alpha-tocopherol-succinate – PLL	20µM
Ascorbic acid – PLL	20µM
Oleic acid – PLL – Coenzyme Q10	20µM
Oleic acid – PLL – Retinoic acid	20µM
Pantothenic acid – PLL	20µM
Biotin – PLL	20µM
Uric acid – F – PLL	66µM
Agmatine – RG – PLL	66µM
Glucosamine – GA – PLL	66µM

PLL, conjugated to poly-L-lysine; RG, reduced glutaraldehyde linkage; GA, glutaric anhydride linkage; F, formaldehyde linkage.

3.1.2.1 Endotherapia as a treatment for multiple sclerosis

The therapeutic effects of Endotherapia have been examined in a rat model of MS and in MS patients. The Endotherapia mixture, GEMSP, was able to reduce brain leukocyte infiltration across the blood-brain barrier (BBB) after induction of acute experimental autoimmune encephalomyelitis (EAE) in rats, but did not diminish the short-term neurological symptoms of acute EAE (Mangas *et al.* 2006). However, in a chronic EAE rat model, GEMSP treatment abolished clinical symptoms of nerve damage (Mangas *et al.* 2008), indicating that GEMSP is capable of modulating clinical outcomes in rats in a chronic EAE model of multiple sclerosis.

The use of GEMSP has also been extended beyond rat models of MS, with two open clinical trials conducted using Endotherapia compounds. In the first, small, open clinical trial, most MS patients treated with GEMSP for 6 months experienced a stabilisation (55% of patients) or an amelioration (18% of patients) of disease symptoms (Geffard *et al.* 2010). In the second, larger, open clinical trial, over two thirds of MS patients receiving an Endotherapia mixture of PLL-conjugated compounds (exact composition unknown, patent pending as of Geffard *et al.* 2010) showed positive outcomes, with 35% showing ameliorated disability scores, 17% showing stabilisation of disease, and 20% showing a lower rate of disease progression than the expanded disability status score (EDSS) worldwide reference rate (Geffard *et al.* 2010). Thus, Endotherapia compounds appear to show beneficial effects in slowing disease progression in MS patients, with the caveat that these studies did not use an untreated control group. As GEMSP and Endotherapia contain multiple compounds, it is unclear whether Endotherapia acts through immunomodulatory or direct neuroprotective mechanisms.

3.1.2.2 Endotherapia as a treatment for ALS

Endotherapia compounds have also been tested in a rat model of ALS and in ALS patients. An Endotherapia mixture of PLL-conjugated compounds known as Gemals (Table 3.2) delayed disease onset, delayed body weight decline, delayed the onset of limb paralysis and increased survival time when administered pre-symptomatically in a SOD1 rat model of ALS (Nicaise *et al.* 2008). Gemals-treated SOD1 rats also tended to maintain motor performance, maintain compound muscle action potentials, and showed lower spontaneous muscle activity than vehicle-treated SOD1 rats (Nicaise *et al.* 2008). However, the effect of Gemals when administration was started from the onset of disease symptoms has not been investigated.

In addition, a Gemals-like Endotherapia compound (exact composition unknown, patent pending as of Geffard *et al*. 2010) was tested in a small, open clinical trial of 12 ALS patients (Geffard *et al.* 2010). Endotherapia-treated ALS patients showed a decreased loss of functional capacity on the ALS assessment questionnaire (ALSAQ-40) compared with the worldwide ALSAQ-40 reference score (Geffard *et al.* 2010). Thus, preliminary studies of Endotherapia suggest that the drug mixture is not detrimental in ALS patients and may even have beneficial effects – however, the absence of a control group from the study relies on the assumption that the worldwide ALSAQ-40 reference score has not changed over time. Given that these preliminary studies hint that Endotherapia may have some positive effects, a randomised, controlled trial would provide stronger evidence for a protective effect in ALS patients. Despite its evaluation in SOD1 rat models and in ALS patients, the Endotherpia mixture 'Gemals' is yet to be tested in the commonly-used SOD1 mouse model of ALS.

3.1.3 Aims and hypothesis

The aim of this chapter was to examine the ability of Gemals compound (Nicaise et al. 2008) to extend the survival of SOD1 mice when administered after symptom onset, compared against untreated control mice.

Hypothesis: Administration of Gemals to SOD1 mice after disease onset would slow disease progression and increase survival time.

A cohort of SOD1 mice were treated from 100 days of age with Gemals or a vehicle control, and were compared in terms of survival, body weight, rotarod performance and grip strength over time.

3.2 Methods

3.2.1 Animals

All procedures and protocols involving animals were approved by the University of Tasmania's Animal Ethics Committee (permit number A12234). Transgenic SOD1 mice were genotyped and copy number was determined by qPCR at weaning, according to the procedure in Chapter 2. Upon genotyping at weaning, gender-paired SOD1 littermates were identified, with a total of 14 female pairs and 16 male pairs (a total of 60 mice, born over a 51-day period) used in the current study. All mice were housed in standard housing conditions as described in Chapter 2; mice were co-housed with their paired littermate, with the only exception when male mice fought with each other and were subsequently singly housed. As each littermate pair sequentially reached 95-100 days of age, each mouse was weighed, and allocated to receive either Gemals or vehicle; allocation of littermate pairs between treatment groups was performed on the basis of keeping the average body weight each treatment group as close as possible (Scott *et al.* 2008). Copy number, body weight at start of treatment, and age at start of treatment were not different in Gemals and vehicle treatment groups, although starting body weight was higher in male mice than female mice (Table 3.3). From 20 weeks of age onwards, mice were given bacon-flavoured NutraGel cubes in their home cages to ensure adequate nutrition and hydration as mice continued through disease progression.

Table 3.3 Cohort demographics at start of treatment

	Female SOD1 mice		**Male SOD1 mice**	
Factor	**Gemals**	**Vehicle**	**Gemals**	**Vehicle**
Number (n)	14	14	15*	16
Copy number (ΔCT)	5.41 ± 0.09	5.53 ± 0.04	5.35 ± 0.05	5.44 ± 0.07
Body weight	19.6 ± 0.1	19.6 ± 0.1	26.3 ± 0.1	26.3 ± 0.1
Age (days)	101.1 ± 0.4	101.1 ± 0.4	100.9 ± 0.3	100.9 ± 0.3

No significant difference in cohort parameters at the start of treatment (copy number, body weight at start of treatment). *One of pair was WT; hence 16 male pairs started but the data from the WT was discarded.

3.2.2 Drug and dosage schedule

Lyophilised Gemals was obtained from Gemacbio S.A. (Cenon, France) and was resuspended in filter-sterilised PBS at 2.5mg/mL. Gemals-treated mice were injected subcutaneously with 100µL resuspended Gemals per mouse (250µg/mouse, equivalent to between 10mg/kg and 12.5mg/kg for a 20-25g mouse), 5 days per week, from approximately 100 days of age through to disease endpoint. Vehicle control mice received an equivalent volume of filter-sterilised PBS. The final concentrations of individual components within the 2.5mg/mL Gemals suspension are listed in Table 3.2. Injections were carried out under light isoflurane (Attane, Bayer AG, NRW, Germany) anaesthesia (The Stinger Anaesthesia Machine, Advanced Anaesthesia Specialists, NSW, Australia; 3.5% isoflurane in 2L/min oxygen). The injection site was varied over the dorsal back surface and flanks, to minimise any irritation due to repeated injections.

3.2.3 Outcome measures

3.2.3.1 Survival time

Survival time was initially measured as the age at which mice had lost 20% of their peak body weight. However, in line with the growing preference in the ALS field for the use of a function endpoint rather than a body weight endpoint, ethics approval was sought and obtained to use loss of the righting reflex (the animal's normal ability to right itself within 30 seconds of being placed on its back) as the disease endpoint. Thus, part way through the trial the endpoint measure was changed. A breakdown of the survival outcomes for the 60 mice in this trial is given in Table 3.4. For the first 10 mice to reach endpoint in the study, only weights endpoint data was collected.

In order to use all available data, separate survival analyses were carried out using the age at the loss of the righting reflex, and the age at loss of 20% from peak body weight. For animals with only one endpoint measure recorded (e.g. weight loss endpoint), the data was censored at the time of this endpoint for the purposes of analysis of the alternative endpoint measure (e.g. righting reflex endpoint analysis).

Survival curves and average survival time (mean ± standard error of the mean) were compared using Kaplan-Meier analysis with the Log Rank test. Factors (categorical independent variables) and covariates (continuous independent variables) influencing

survival time were examined using Cox proportional hazards regression, and were reported as hazard ratios (HR) with 95% confidence interval (CI).

Table 3.4 Numbers of SOD1 mice through trial

	Female mice		Male mice	
Number of mice (n)	**Gemals**	**Vehicle**	**Gemals**	**Vehicle**
Allocated to trial	14	14	16	16
Removed from trial				
Incorrect genotype	0	0	1	0
Survival data censored				
Died under anaesthesia	0	0	0	2
Culled due to lesion	1	1*	1	1*
Found dead in cage			2	1*
Endpoint conditions				
Earliest of righting or weights	2	1	3	4
Righting only	11	12	9	7

*culled due to littermate partner affected

3.2.3.2 Body weight

Body weight was recorded at least twice weekly; after the age of 18 weeks, body weight was recorded daily. Body weights were analysed separately for each gender, with Gemals-treated and saline-treated mice compared using T-tests at each week of age, with a Welch T-test correction applied if Levene's test showed that variances were substantially different between groups.

3.2.3.3 Rotarod performance

Motor performance was assessed weekly from 100 days of age, using a 5-lane mouse rotarod (Rotarod Advanced for 5 mice, TSE Systems, Hesse, Germany). From approximately 85-90 days of age, mice were acclimatised to the Rotarod (three once-daily sessions of 5 minutes, with the drum rotating at 3 revolutions per minute [rpm]); and subsequently trained to stay on the accelerating drum (at least two once-daily sessions where the drum accelerated from 3rpm to 16rpm over 3 minutes).

On the day preceding the weekly Rotarod test, mice were given a practice session where the drum rotated at 3rpm for 1 minute, then accelerated from 3rpm to 16rpm over 3 minutes. On the day of the test, mice were given a 5-minute warm up session on the Rotarod at 3rpm, then had a 10-minute break, then went through the acceleration protocol where the speed was increased from 3rpm to 16rpm over 3 minutes. The speed at which mice could not stay on the rotating drum was recorded. Mice which could not stay on the Rotarod due to advancing disease were given the minimum score of falling at 3rpm. Average speeds at which falls occurred were compared separately for female and male mice, with Gemals-treated and vehicle-treated mice compared by T-tests at each week of age, with appropriate corrections for unequal variances where necessary.

3.2.3.4 Grip strength

Hindlimb grip strength was measured using a grip strength (force) meter (Columbus Instruments, OH, USA). A single grip strength meter, with a triangular bar for mice, was mounted above bench level on a spacer arm and platform. Mice were scruffed and were allowed to grab the bar with their hind paws, then moved away from the grip strength apparatus until they let go of the bar, with the maximum force of three attempts recorded in newtons (N). Grip strengths were analysed separately for male and female mice, and experimental groups were compared by T-tests with appropriate correction for unequal variances where necessary.

3.3 Results

3.3.1 Adverse effects

3.3.1.1 Reaction to drug

Most mice injected with the Gemals compound showed an adverse reaction within 5-10 minutes of injection. Affected mice showed reduced mobility within the cage, tending to stay in one corner and sometimes adopting a hunched position. The drug appears to cause irritation, with mice sometimes scratching at the injury site and in the worst cases giving continuous shudders / shrugs of the shoulders while maintaining the hunched position. None of these symptoms were seen in vehicle-treated mice. Some particulate matter remained following resuspension of Gemals in PBS. A batch of Gemals was therefore centrifuged to remove particulates which might cause irritation after injection; however, the particulate-free Gemals elicited the same reaction as seen with resuspended Gemals, indicating a soluble component was causing the adverse reaction.

Topical application of lignocaine and bupivacaine, either with Gemals injection or at 90 minutes prior to Gemals injection, was not effective at reducing the adverse reaction, nor was injection of meloxicam together with Gemals effective at reducing the reaction; however, injecting meloxicam 60-90 minutes prior to Gemals injection suppressed most of the adverse response (Data from Dr Bill Bennett). Subcutaneous injection of meloxicam (5mg/kg, 40-60µL of 1:1 meloxicam:saline) was therefore performed approximately 60 minutes prior to injection with either Gemals or vehicle.

3.3.1.2 Development of skin lesions

In some Gemals-treated mice, the skin around the injection site appeared to become tough and fibrotic. A number of mice also developed isolated open wounds or lesions, which were initially observed on male mice and were attributed to fighting, but also appeared in female mice. Lesions occurred almost exclusively in Gemals-treated mice (6/14 female and 6/15 male Gemals-treated mice); lesions were rarely seen in vehicle-treated mice (1/14 female and 0/16 male vehicle-treated mice). Lesions occurred on the skin of the flanks, back, or shoulders/neck, although one female mouse showed a lesion on the forelimb, and one male mouse showed a lesion at the base of the tail, both located far from any sites of drug injection. To treat these lesions, mice were placed under light isoflurane anaesthesia; the lesion was swabbed with sterile saline and had

betadine (Sanofi-Aventis, povidone-iodine antiseptic ointment) applied. If the skin surrounding the lesion site appeared irritated, imflamol (Apex Laboratories, broad spectrum anti-bacterial, anti-inflammatory, anti-fungal ointment) was applied. Treatment was applied daily while the lesion was present. Most lesions healed within 4±1 days of appearance; two mice developed a lesion at 2-3 days before disease endpoint, which did not resolve by disease endpoint. Three mice developed a lesion on two separate occasions; in these mice, the first lesion was small and healed quickly, while on the second occasion the lesion was larger. The lesion appeared severe in two of these mice developing a second lesion, and these two mice were culled, along with their respective paired littermates (Table 3.4).

The aetiology of these lesions is unclear. While some lesions may be possibly attributable to fighting between mice, lesions developed primarily in Gemals-treated mice, and were most common on the flanks, back and shoulders where Gemals injections took place. It is possible that the meloxicam injection did not completely relieve the irritant effect of Gemals injections, so the lesion may have been caused by excessive grooming or scratching of the injection site. Even more so, the analgesic effects of the meloxicam may have removed painful stimuli from excessive scratching, leading to more scratching and exacerbation of the lesion.

3.3.2 Survival

3.3.2.1 Kaplan-Meier analysis

Kaplan-Meier was used to assess the effect of a single variable, such as Gemals treatment vs. vehicle treatment, or male vs. female gender, on survival outcomes.

3.3.2.1.1 Kaplan-Meier analysis: Loss of righting reflex

The average age at which righting reflex was lost was not different between Gemals-treated and vehicle-treated mice (Gemals 171.2±2.9 days vs. vehicle 172.8±2.9 days, p=0.762) (Figure 3.1A), nor between female and male mice (female 172.4±2.8 days vs. male 171.1±3.0 days, p=0.706) (Figure 3.1B). Gemals treatment did not affect survival time in either female or male mice when each gender was considered separately (males: Gemals 167.7±1.6 days vs. vehicle 175.6±5.5 days, p=0.156; females: Gemals 173.1±4.9 days vs. vehicle 171.8±3.0 days, p=0.307) (Figure 3.1C,D).

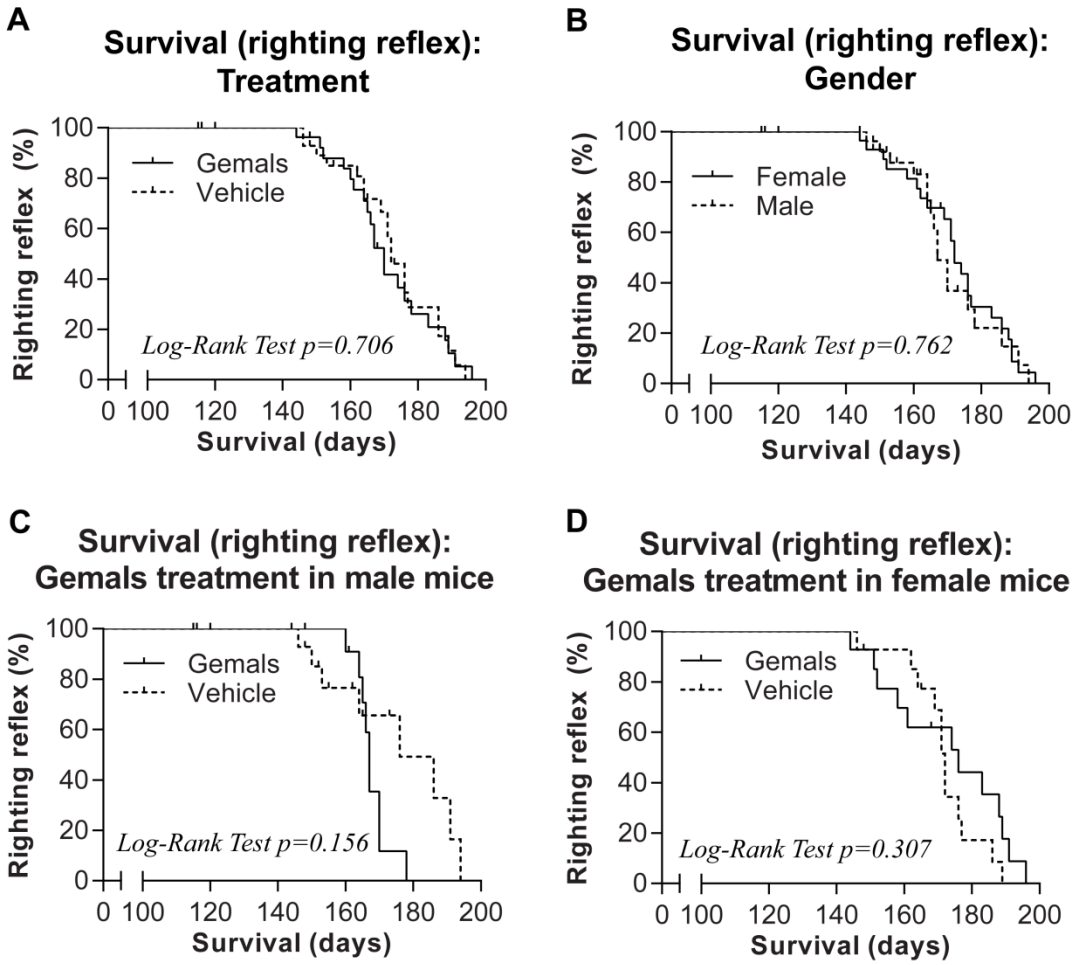

Figure 3.1 Kaplan-Meier survival curves for loss of the righting reflex

The loss of the righting reflex reflects the age at which mice were no longer able to right within 30 seconds of being placed on their side. Kaplan-Meier survival curves were not significantly different between Gemals-treated mice and vehicle-treated mice (A), nor between female mice and male mice (B). Gemals treatment did not substantially alter retention of the righting reflex in male (C) or female (D) mice. Vertical dashes represent censored data points.

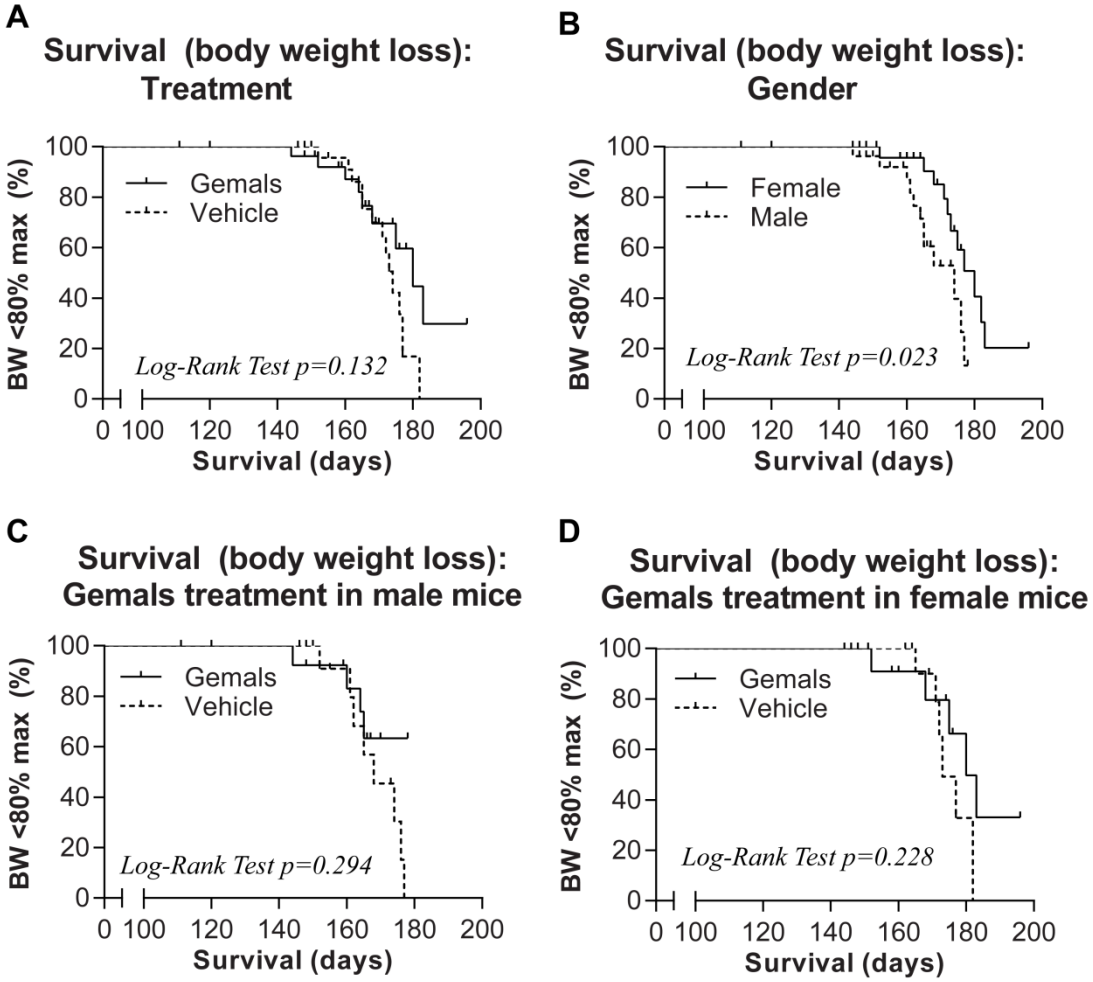

Figure 3.2 Kaplan-Meier survival curves for loss of 20% from peak body weight

The survival curves for the age at which SOD1 mice had lost 20% from their pre-disease maximum body weight were not significantly different between Gemals-treated mice and vehicle-treated mice (A). Female mice showed significantly longer times to loss of 20% body weight than male mice (B). No significant effect of Gemals treatment was seen in either male (C) or female (D) mice. Vertical dashes represent censored data points. BW, body weight.

3.3.2.1.2 Kaplan-Meier analysis: Loss of 20% body weight

The age at which mice had lost 20% of their body weight was not different between Gemals-treated mice and vehicle-treated mice (Gemals 178.7±3.8 days vs. 172.2±1.8 days, p=0.132) (Figure 3.2A). However, female mice displayed a delayed loss of 20% body weight compared to male mice (females 179.0±2.8 days vs. males 169.2±1.9 days, p=0.023) (Figure 3.2B). Considering male and female mice separately, Gemals showed no effect on the loss of 20% body weight compared to the vehicle control (females: Gemals 181.2±4.5 days vs. vehicle 175.5±2.1 days, p=0.228; males: Gemals 171.1±3.0 days vs. vehicle 168.2±2.7 days, p=0.294) (Figure 3.2C,D).

3.3.2.2 Cox proportional hazards regression analysis

CPH regression was used to assess the effects of gender, Gemals treatment and possible covariates (copy number ΔCT, starting body weight, maximum body weight, and access to Nutragel cubes) on survival.

3.3.2.2.1 Cox proportional hazards regression: Loss of righting reflex

In univariable analyses, none of the factors and covariates tested (gender, Gemals treatment, copy number, starting and maximum body weights, and access to Nutragel cubes) showed any significant effect on the loss of the righting reflex (Table 3.5). Multivariable analysis including both gender and Gemals treatment also revealed no significant effects on loss of the righting reflex (Table 3.5). However, inclusion of an interaction term between gender and Gemals treatment revealed a significant interaction term (p=0.048, Table 3.5), indicating that the effect of Gemals on the loss of the righting reflex was different between male and female mice. Survival curves showing effects of Gemals treatment in male mice reveal a higher percentage of Gemals-treated male mice than vehicle-treated male mice surviving between 150-170 days of age, and a higher percentage of vehicle-treated than Gemals-treated male mice surviving between 170-190 days of age (Figure 3.1C). This pattern is indeed reversed for female mice (Figure 3.1D), with a higher percentage of Gemals-treated female mice than vehicle-treated female mice surviving between 150-170 days of age, and fewer Gemals-treated than vehicle-treated female mice surviving between 170-190 days of age. Thus, while Gemals did not show an increase in survival in either gender, Gemals treatment exerted different effects on the survival curves of female and male mice. However, this interaction drifted out of statistical significance when adjusted for other covariates which may influence survival (p=0.056, Table 3.5).

Table 3.5 Cox proportional hazards regression model for reaching disease endpoint: Righting reflex endpoint

Factor(s) in the CPH model	Loss of Righting Reflex HR (95% CI), p-value
Univariable analyses[1]	
Gender (female)	0.888 (0.471, 1.675), p=0.714
Treatment (Gemals)	1.097 (0.589, 2.043), p=0.769
Copy number (ΔCT)	1.066 (0.278, 4.093), p=0.926
Starting body weight	1.010 (0.919, 1.110), p=0.832
Maximum body weight	1.004 (0.915, 1.102), p=0.927
Access to Nutragel	1.141 (0.259, 5.018), p=0.861
Multivariable analysis[2]	
Gender (female)	0.860 (0.447, 1.657), p=0.653
Treatment (Gemals)	1.137 (0.599, 2.159), p=0.695
Multivariable analysis, including interaction[3]	
Gender (female)	1.659 (0.653, 4.216), p=0.288
Treatment (Gemals)	2.603 (0.927, 7.310), p=0.069
Gender*Treatment	**0.243 (0.060, 0.990), p=0.048**
Multivariable analysis, including interaction, adjusted[4]	
Gender (female)	0.255 (0.017, 3.884), p=0.325
Treatment (Gemals)	2.406 (0.833, 6.955), p=0.105
Gender*Treatment	0.239 (0.055, 1.035), p=0.056

[1]Univariable analyses were carried out with models containing only one of the following factors: Gender (male/female), Treatment (Gemals/vehicle), or access to Nutragel (yes/no); or with one of the following covariates: copy number (ΔCT), starting body weight, or maximum body weight. [2]Multivariable analysis includes both Gender and Treatment as factors. [3]Multivariable analysis includes Gender, Treatment, and a Gender*Treatment interaction term as factors. [4]Adjusted multivariable analysis contains Gender, Treatment, Gender*Treatment, copy number, starting body weight, maximum body weight, and access to Nutragel; HRs for Gender, Treatment, and Gender*Treatment are therefore adjusted for copy number, starting body weight, maximum body weight, and access to Nutragel.

3.3.2.2.2 Cox proportional hazards regression: Loss of 20% body weight

In contrast to the loss of the righting reflex, univariable analysis found that gender (p=0.030), starting body weight (p=0.037), maximum body weight (p=0.021), and access to Nutragel (p<0.001) influenced the loss of 20% from peak body weight (Table 3.6). In multivariable analysis, the survival-promoting effect of female gender persisted upon adjustment for Gemals treatment (HR_{female}=0.383, 95% CI 0.154-0.951, p=0.039) (Table 3.6). When a gender*treatment interaction was included in the multivariable analysis for body weight endpoints, the interaction term was not significant (p=0.777, Table 3.6), indicating that Gemals affected survival time no differently in female mice than in male mice. When the multivariable analysis (excluding the non-significant gender*treatment interaction term) was adjusted for other covariates, the only factor independently associated with increased survival times was access to Nutragel cubes ($HR_{Nutragel}$=0.060, 95% CI 0.013-0.268, p<0.001) (Table 3.6).

These data indicate that mice with access to Nutragel cubes showed a slower loss of body weight than mice without access to Nutragel cubes. Interestingly, access to Nutragel cubes had no effect on the loss of righting reflex (Table 3.5) – perhaps indicating that access to continued easy nutrition maintained body weight but did not maintain muscle function, and suggesting that a major component in body weight survival analysis is hydration status which is maintained by the use of Nutragel cubes. Alternatively, the correlation may be due to changes in trial design at the early stages – the mice enrolled earliest in the trial did not have access to Nutragel cubes, and also had their survival times measured solely under the weight loss endpoint.

Overall, survival data indicate that Gemals-treated mice showed no significant increase in survival time compared to that of vehicle-treated mice, as measured by either the loss of 20% body weight or the loss of the righting reflex.

Table 3.6 Cox proportional hazards regression model for reaching disease endpoint: Body weight endpoint

Factor(s) in CPH model	Loss of 20% Body Weight HR (95% CI), p-value
Univariable analyses[1]	
Gender (female)	**0.365 (0.146, 0.909), p=0.030**
Treatment (Gemals)	0.516 (0.213, 1.252), p=0.143
Copy number (ΔCT)	1.229 (0.222, 6.083), p=0.813
Starting body weight	**1.152 (1.008, 1.317), p=0.037**
Maximum body weight	**1.168 (1.023, 1.334), p=0.021**
Access to Nutragel	**0.064 (0.018, 0.221), p<0.001**
Multivariable analysis[2]	
Gender (female)	**0.383 (0.154, 0.951), p=0.039**
Treatment (Gemals)	0.548 (0.224, 1.335), p=0.185
Multivariable analysis[3]	
Gender (female)	0.417 (0.141, 1.235), p=0.115
Treatment (Gemals)	0.619 (0.183, 2.099), p=0.442
Gender*Treatment	0.771 (0.128, 4.311), p=0.777
Multivariable analysis, adjusted[4]	
Gender (female)	0.601 (0.010, 36.438), p=0.808
Treatment (Gemals)	0.538 (0.214, 1.353), p=0.188
Access to Nutragel	**0.066 (0.016, 0.280), p<0.001**

[1]Univariable analyses were carried out with models containing only one of the following factors: Gender (male/female), Treatment (Gemals/vehicle), or access to Nutragel (yes/no); or with one of the following covariates: copy number (ΔCT), starting body weight, or maximum body weight. [2]Multivariable analysis includes both Gender and Treatment as factors. [3]Multivariable analysis includes Gender, Treatment, and a Gender*Treatment interaction term as factors. [4]Adjusted multivariable analysis contains Gender, Treatment, copy number, starting body weight, maximum body weight, and access to Nutragel; HRs for Gender, Treatment, and Access to Nutragel are therefore adjusted for copy number, starting body weight, and maximum body weight.

3.3.3 Body weights

Weekly body weight averages were calculated for all mice. As expected, male mice showed higher body weights than female mice at all ages (Figure 3.3). Average body weights were not different between Gemals-treated mice and vehicle-treated mice at any age, for either male or female mice (Figure 3.3A,B). When body weights were expressed as a percentage of maximum attained by each mouse, there was a slight trend for higher percentage body weights in Gemals-treated female mice than vehicle-treated female mice between 23-27 weeks of age (Figure 3.4A). Body weight percentages did not differ between Gemals-treated and vehicle-treated male SOD1 mice (Figure 3.4B).

As an aside, a transient stabilisation of body weight was seen in all mice at 20-21 weeks of age (Figure 3.3, Figure 3.4), corresponding to the age at which mice first had access to bacon-flavoured Nutragel cubes in addition to their normal *ad libitum* food; this temporary attenuation of body weight loss may be due to increased overall food intake.

3.3.4 Rotarod performance

Mice were trained on the Rotarod one to two weeks prior to testing; most mice never attained the maximum possible rotarod performance of 16rpm, so future studies should commence Rotarod training well before the onset of disease symptoms.

Rotarod performance was similar between Gemals-treated and vehicle-treated mice at most time points. Female Gemals-treated mice showed better Rotarod performance than vehicle-treated female mice at 23 weeks of age (speed at fall: Gemals 8.9±1.2 rpm vs. vehicle 5.4±0.9 rpm, $p=0.033$) and showed a trend towards better Rotarod performance at 24 weeks of age (speed at fall: Gemals 8.1±1.5 rpm vs. vehicle 4.7±0.9 rpm, $p=0.086$) (Figure 3.5A). Male Gemals-treated mice showed a slightly better Rotarod performance at 16-18 weeks of age; this tended towards significance at 17 weeks of age (speed at fall: Gemals 10.5±0.7 rpm vs. vehicle 8.6±0.6 rpm, $p=0.050$) (Figure 3.5B).

Gemals treatment produced some transient improvements in Rotarod performance for both male and female mice at certain time points mentioned above. Gemals treatment may help to maintain Rotarod performance and therefore retain motor function in female mice at 23 and 24 weeks of age; however, these effects were not continued out past 24 weeks of age and additionally were not observed in male mice.

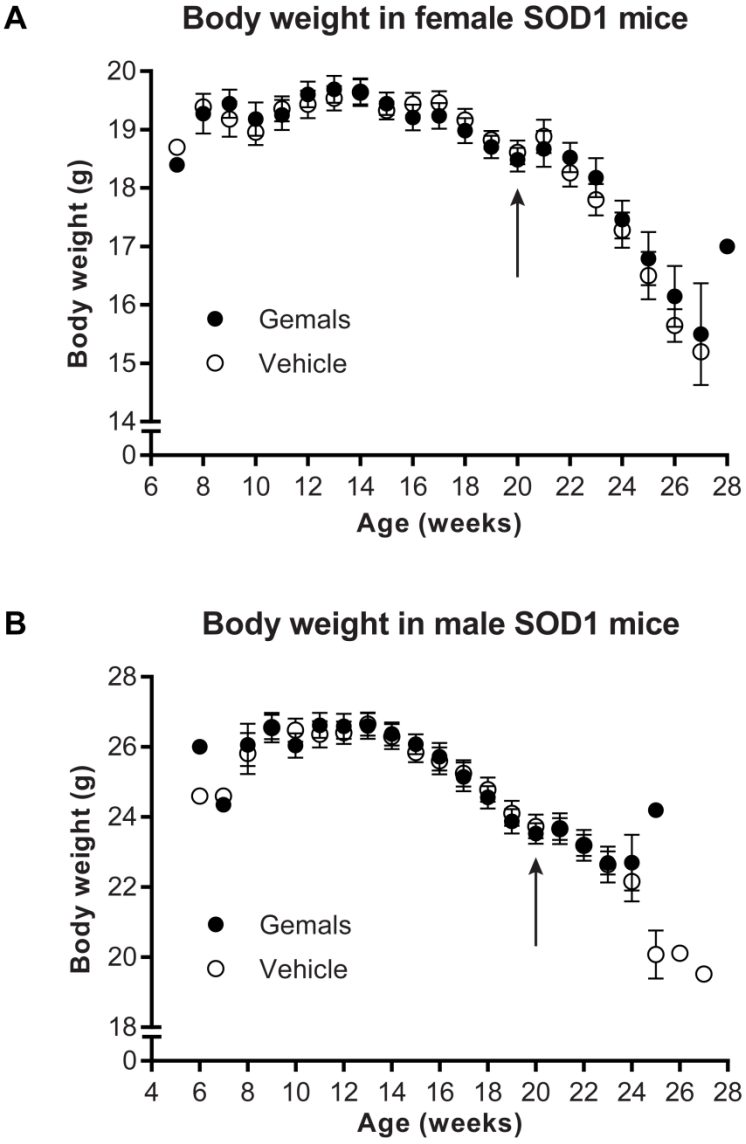

Figure 3.3 Average body weights for Gemals-treated and control mice over time

Body weight declined with disease progression over time in all SOD1 mice. No significant changes were observed in the body weights of female mice (A) or male mice (B) when treated with Gemals compared to vehicle alone. Bacon-flavoured Nutragel cubes were placed in cages from 20 weeks of age (arrow, A,B), leading to a slight increase or temporary stabilisation in body weight at 21 weeks of age, likely due to increased food intake. Error bars represent standard error of the mean.

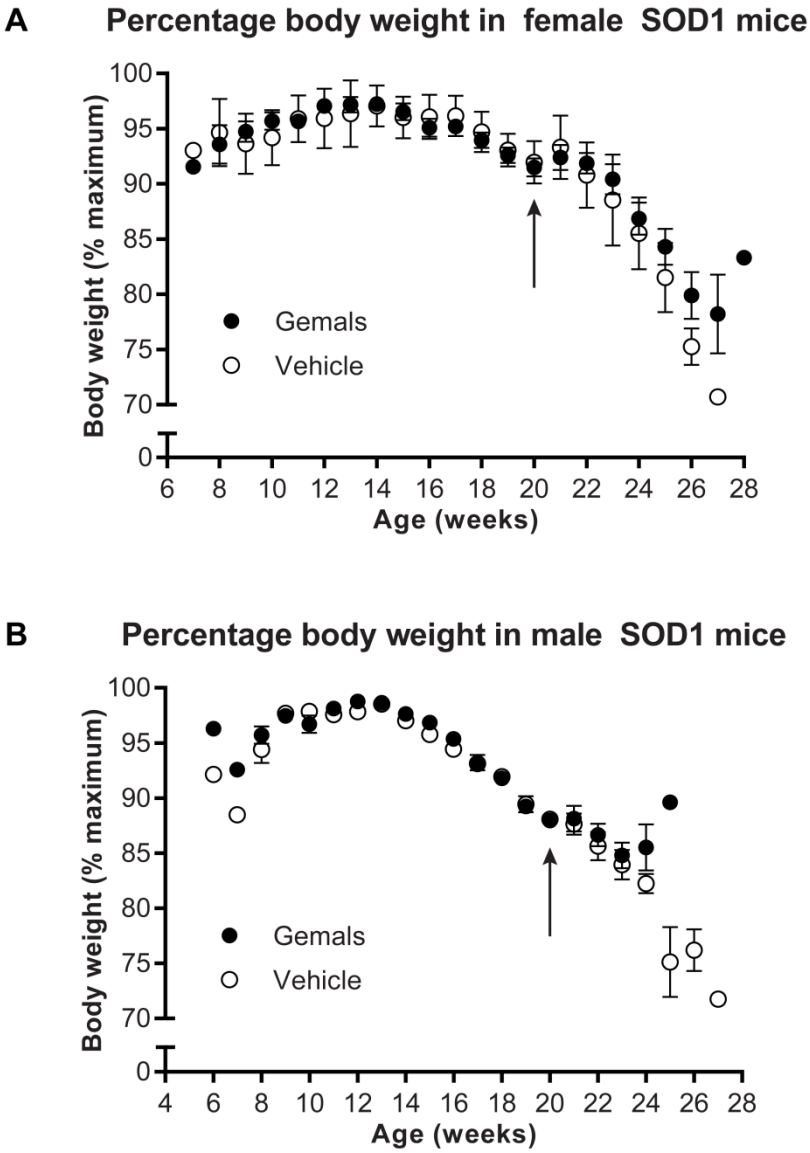

Figure 3.4 Percentage body weights in Gemals-treated and vehicle mice

Percentage of maximum body weight was calculated for both female (A) and male (B) mice. Percentage body weight was not significantly different between Gemals-treated and vehicle-treated female mice, although Gemals-treated female mice appeared to have slightly higher body weights than vehicle-treated female mice at 25-26 weeks of age (A). Body weight percentages were not different between Gemals-treated and vehicle-treated male mice (B). A temporary stabilisation of body weight percentage was noted at 21 weeks of age, following the introduction of Nutragel cubes to the home cages at 20 weeks of age (arrow, A,B). Error bars represent standard error of the mean.

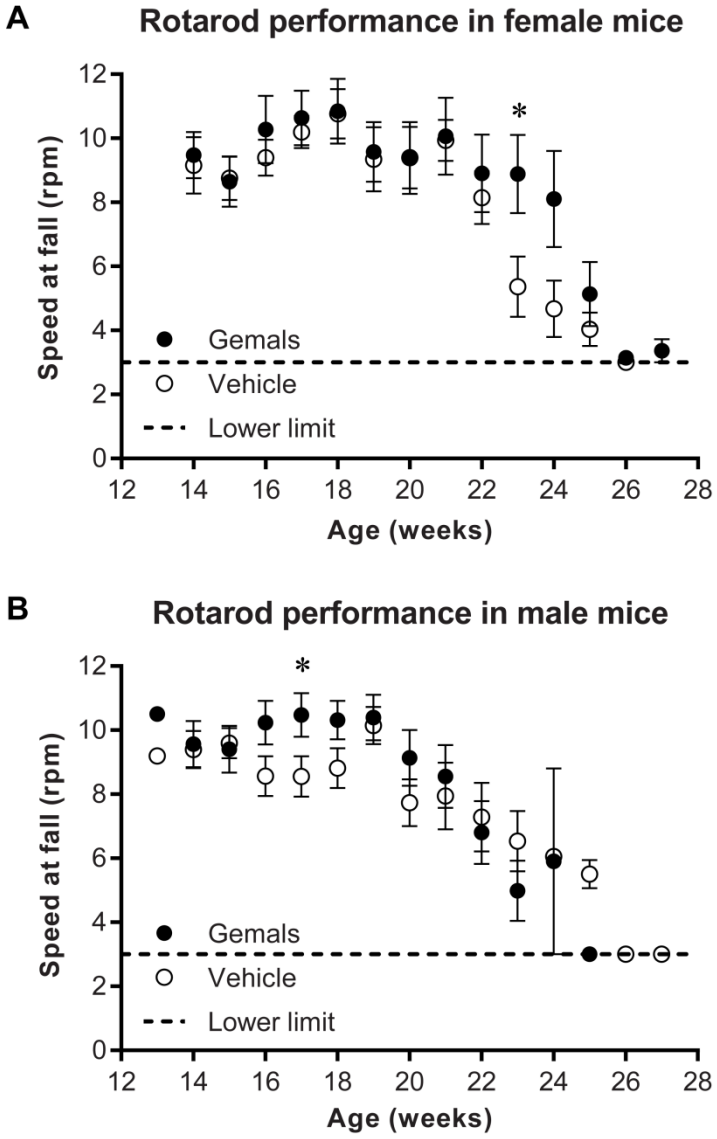

Figure 3.5 Rotarod performance in Gemals-treated and control mice

Rotarod performance, measured as the speed at which mice could not stay on the Rotarod drum during acceleration from 3rpm to 16rpm, declined with time in all SOD1 mice. Gemals-treated female mice showed better Rotarod performance than vehicle-treated female mice at 23-24 weeks of age (A), while Gemals-treated male mice showed better Rotarod performance than vehicle-treated mice at 16-18 weeks of age (B). However, these improvements were not continued throughout the disease course in either female or male Gemals-treated mice. *$p<0.05$, t-test. Error bars represent standard error of the mean.

3.3.5 Grip strength

Hindlimb grip strength showed high variability in both male and female mice (Figure 3.6A,B), and did not demonstrate a clear decrease over time as the disease progressed. In female SOD1 mice, vehicle-treated mice had a stronger grip strength than Gemals-treated mice at 21 weeks of age (Gemals 0.022±0.007N vs. vehicle 0.036±0.007N, T-test p=0.010), while Gemals-treated mice had a stronger grip strength than vehicle-treated mice at 22 weeks of age (Gemals 0.034±0.010N vs. vehicle 0.021±0.008N, T-test p=0.045) (Figure 3.6A). In male SOD1 mice, Gemals treatment did not significantly affect grip strength (Figure 3.6B).

Grip strength was measured sporadically throughout the study, at constant dates rather than constant ages in the SOD1 mice; therefore, not all mice were measured at each weekly time point. In order to reduce the amount of variability in the data set, grip strength data were collected into age bins (13-15 weeks, 16-18 weeks, 19-21 weeks, 22-24 weeks, 25-27 weeks; Figure 3.6C,D) for analysis, averaging data from the same animal where necessary to avoid pseudoreplication. However, similar to the weekly age data (Figure 3.6A,B), binned grip strength data showed no substantial decrease over time for either male or female Gemals-treated or vehicle-treated SOD1 mice (Figure 3.6C,D).

The lack of a substantial change over time, in any group of SOD1 mice, indicates that grip strength as measured here may not be a reliable indicator of decreasing muscle strength due to disease progression. Mice were not pre-trained in this muscle strength test, as it was thought to be a natural response of mice to grip the bar. However, it is possible that the mice habituated to the testing procedure over the course of the disease, and that increased technique and ability to grip the bar compensated for a lack of muscle strength. This may explain the lack of decline in grip strength over time. As with the Rotarod, earlier habituation to this grip strength test may allow more accurate recording of change in muscle strength over time in SOD1 mice.

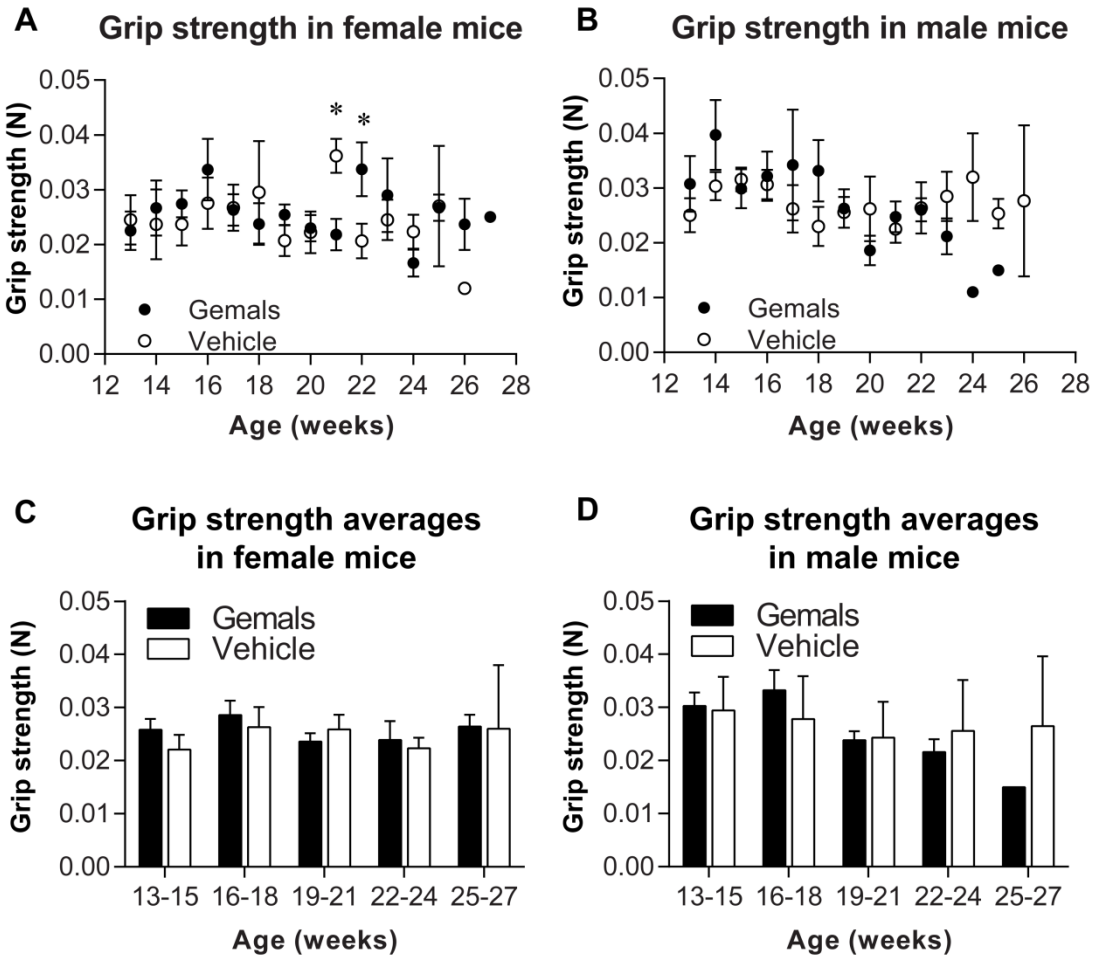

Figure 3.6 Grip strength in Gemals-treated and control mice over time

Grip strength measurements (in newtons, N) varied over time and showed no clear pattern for either female (A) or male (B) mice. The only differences between Gemals-treated and vehicle-treated SOD1 mice occurred in female mice; vehicle-treated mice showed a higher grip strength at 21 weeks of age, while Gemals-treated mice showed a higher grip strength at 22 weeks of age (A). Grouping of data into categories each spanning three weeks (C,D) did not reveal any differences in grip strength between Gemals-treated and vehicle-treated female (C) or male (D) mice. *$p<0.05$. Error bars represent standard error of the mean.

3.4 Discussion

3.4.1 Summary of results

Male and female SOD1 mice were treated with Gemals compound or a control vehicle, with treatment commencing at 100 days of age, after the onset of disease symptoms. Gemals treatment did not significantly affect survival time for either male or female SOD1 mice (Figure 3.1, Figure 3.2); nor did Gemals treatment show substantial effects on the decline of body weight and rotarod performance over time (Figure 3.3, Figure 3.4, Figure 3.5). However, the Gemals treatment was not well tolerated, with irritation after administration and the gradual development of skin lesions (see section 3.3.1), and these issues may have confounded any beneficial effects of the drug.

3.4.2 Comparison of the present study with previous Endotherapia studies

A previous study of Gemals in ALS rodent models tested the pre-symptomatic effects of Gemals in the $SOD1^{G93A}$ rat model (Nicaise *et al.* 2008). Three experimental groups were used – a control group, a low-dose Gemals group, and a high-dose Gemals group, each containing 8-11 animals. Nicaise and colleagues found that pre-symptomatic Gemals treatment significantly delayed onset of disease symptoms (hindlimb paresis) and increased survival time in a dose-dependent manner, with survival time extended by up to 18% by the higher dosage (Nicaise *et al.* 2008). Additionally, a Gemals-like compound has been tested in a small open clinical trial of ALS patients – this small trial reported positive outcomes in the ALS functional rating score (ALSFRS) of treated patients compared against a worldwide reference ALSFRS score (Geffard *et al.* 2010). In contrast, the present study found no significant effect on survival time when Gemals was administered after disease onset in SOD1 mice (Figure 3.1, Figure 3.2).

There are two main possibilities as to why Gemals showed no survival effects in the present study. The first possibility is that the administration of an antioxidant therapy after the onset of disease is ineffective at halting disease processes. The second possibility is that the presence of several confounding factors in this study, such as the irritation following injection and the need to administer an analgesic, may have obscured any beneficial effect of Gemals treatment on survival.

3.4.3 Antioxidants as a therapeutic strategy for ALS

Oxidative stress appears to be a convergence point for several ALS-related pathologies, as discussed in Chapter 1. The components of Gemals are designed to limit oxidative stress and neuroinflammation (Nicaise *et al.* 2008; Geffard *et al.* 2010). The administration of Gemals to pre-symptomatic SOD1 rats increased survival time (Nicaise *et al.* 2008), but Gemals treatment after the onset of disease symptoms did not increase survival time in the current study. This discrepancy could indicate that the timing of antioxidant therapy is important in the treatment of SOD1-mediated ALS.

Disease processes in SOD1 motor neurons are generally accepted to start long before the onset of disease symptoms (Vinsant *et al.* 2013); indeed, the results of Chapter 2 showed that ubiquitinated inclusions were present 8 weeks prior to the earliest disease symptoms. Oxidative stress may be a key disease process in ALS, and signs of oxidative stress are present in SOD1 mice before the development of disease symptoms (Hall *et al.* 1998a). Oxidative stress is linked into several other pathologies, such as protein aggregation, mitochondrial dysfunction, excitotoxicity, and glial activation (Barber & Shaw 2010); see section on convergent pathology (section 1.3.9). It may be the case that the downstream effects of oxidative stress, such as the formation of protein aggregates and the dysfunction of mitochondria, cannot be remedied by the amelioration of the oxidative stress itself. In line with this theory, antioxidant compounds such as vitamin E and N-acetyl-L-cysteine have shown benefits when administered before symptom onset in SOD1 mice, but showed no effects on survival in ALS patients (Gibson & Bromberg 2012). It is possible that Gemals reduced oxidative stress but did not protect motor neurons from degeneration.

The amelioration of oxidative stress early in the disease course may have beneficial effects for the survival of motor neurons; however, in the absence of biochemical markers for pre-symptomatic testing for ALS, therapies which can be used after the onset of disease symptoms in ALS patients are required. Treatment of oxidative stress should be incorporated as part of a multi-action therapy targeting multiple cellular pathways, with the aims of simultaneously reducing oxidative stress, increasing clearance of aggregated proteins, attenuating glial activation, and increasing motor neuron survival. The data generated from this study may not be a true reflection of the potential of Gemals to ameliorate disease due to the presence of confounding factors, as explained in the following section.

3.4.4 Confounding effects in the current study

3.4.4.1 Lesions and irritation

Gemals did not appear to be well tolerated in this study, with mice showing irritation at the injection site and adopting a hunched demeanour, usually indicative of pain or illness, within minutes of the Gemals injection. These symptoms were not observed in mice injected with vehicle alone. Some Gemals-treated mice also developed skin lesions. The positioning of the skin lesions, mostly seen on the flank or shoulders but in some instances occurring at the base of the tail or on the forelimb, indicates that the lesions may have been a result of scratching at the lesion site, or possibly a result of excessive grooming due to stress in these animals. Both restraint stress and elevated corticosterone levels are associated with accelerated disease progression and shortened survival times in SOD1 mice (Fidler *et al.* 2011), and thus, any stressful effects of irritation and/or lesion development in Gemals-treated mice may have masked neuroprotective effects of Gemals.

The source of irritation in the Gemals mixture has not been determined. The study by Nicaise and colleagues in 2008 reported no such irritation or adverse response to subcutaneous injection of Gemals in SOD1 rats, and sublingual Endotherapia compounds are reported to have few side effects in humans (Geffard *et al.* 2010). The concentration of injected Gemals compound in the present study was 2.5mg/mL, while the highest concentration injected in the Nicaise study was 3.75mg/mL, which was reported to be well tolerated (Nicaise *et al.* 2008).

Mice and rats may show different tolerance doses for specific Gemals components, which may help to explain the irritation seen in mice in the current study but not reported in the Nicaise (2008) study. Additionally, it is possible that the dosage of Gemals may have been slightly higher in the present study than in the Nicaise (2008) study of Gemals in SOD1 rats. Nicaise and colleagues used a dose of 1.87mg/rat/day, equivalent to 9.4mg/kg for a 200g rat, and 7.5mg/kg for a 250g rat. If the body weight of SOD1 rats was generally greater than these estimates, the 10mg/kg dosage for mice in the current study may result in a greater dose compared to the Nicaise (2008) study.

A difference between the Nicaise (2008) study and the present study was the choice of vehicle – saline in the study by Nicaise and colleagues, and phosphate-buffered saline in the present study. However, as the same irritation was observed when saline was used

as a vehicle in the present study (data not shown), it is unlikely that the choice of vehicle contributes to the irritation. The Gemals compound is mostly soluble, with a few suspended particles. However, centrifugation to remove these insoluble particles did not remove the irritation caused by Gemals treatment, indicating that the responsible component was soluble (data from Dr Bill Bennett). It is unclear whether the irritation seen in this study is a phenomenon specific to mice, or whether some kind of contamination had occurred in the preparation of the Gemals compound for injection. Future work with the Gemals compound in mice should carefully monitor mice for symptoms of irritation, and examine whether the dosage or concentration of specific components in the Gemals mixture requires adjustments for use in mice.

3.4.4.2 Administration of meloxicam

Administration of meloxicam at 60-90 minutes prior to administration of Gemals was effective at ameliorating Gemals-induced irritation. Meloxicam preferentially inhibits cyclooxygenase2 (COX2), resulting in decreased COX2-mediated synthesis of the inflammatory mediators prostaglandins (Engelhardt *et al.* 1996), and relief from inflammatory pain (Hilario *et al.* 2006). Importantly in the context of this study, COX2 may play a role in neuroinflammation in ALS. COX2 is upregulated in the spinal cord of both ALS patients (Yasojima *et al.* 2001; Kiaei *et al.* 2005) and SOD1 mice (Almer *et al.* 1999; McGeer & McGeer 2002; Okuno *et al.* 2004). Pre-symptomatic treatment with COX2 inhibitors delays disease onset and extends survival in SOD1 mice (Drachman *et al.* 2002; Pompl *et al.* 2003; Klivenyi *et al.* 2004); it is therefore possible that inhibition of COX2 activity by meloxicam in this study affected disease progression in our cohort of mice. Drachman (2002), Pompl (2003), and Klivenyi (2004) all studied the effects of diet-based COX2 inhibition in SOD1 mice. Drachman used the COX2-selective inhibitor celecoxib at 1500ppm (1500mg/kg) in feed, "equivalent to 400-800mg/day in humans" (Drachman *et al.* 2002) (approximately 5-10mg/kg/day for a 75kg adult) and saw a reduction in prostaglandin E2 (PGE2) production (a marker of COX2 activity) in the SOD1 spinal cord down to the levels of the WT spinal cord (Drachman *et al.* 2002). Similarly, Pompl used nimesulide at 1500ppm in feed and reduced SOD1 spinal PGE2 production down to WT levels (Pompl *et al.* 2003). Klivenyi used 0.012% (120ppm) celecoxib or 0.005% (50ppm) rofecoxib in feed, and saw reduced PGE2 production in the SOD1 spinal cord, although the levels were still slightly higer than those of WT mice (Klivenyi *et al.* 2004). SOD1

mice in the present study were administered meloxicam, a COX2-selective inhibitor, subcutaneously at 5mg/kg body weight. This would be at least equivalent to, if not greater than, the same milligram dosage given for celecoxib in the study by Drachman (2002), with the meloxicam likely more bioavailable given its subcutaneous rather than oral delivery in the present study. If Gemals were to act through a COX2-dependent pathway, any Gemals-mediated protective effects may have been masked by the use of meloxicam in both Gemals-treated and vehicle-treated SOD1 mice. In this situation, the dose of meloxicam used in the present study would be sufficient to reduce COX2 activity levels in the SOD1 spinal cord back down to those of WT mice. Therefore, there may be no scope for the components of Gemals to further reduce COX2 activity beyond the reduction carried out by meloxicam. This may explain why no survival effects were observed with Gemals treatment in the current study.

In line with this theory, several Gemals components are saturated or unsaturated fatty acids (Table 3.1), which have the capacity to modulate COX2 activity (Lee *et al.* 2001; Ringbom *et al.* 2001). Saturated fatty acids increase COX2 activity, whereas unsaturated fatty acids inhibit COX2 activity (Lee *et al.* 2001; Ringbom *et al.* 2001). Although COX2 inhibition appears beneficial for SOD1 mice as described above, downstream prostaglandin products of COX2 activity can also show neuroprotective effects (Bilak *et al.* 2004; Consilvio *et al.* 2004). As Gemals contains both kinds of fatty acids, it is unclear whether Gemals would inhibit COX2 activity via unsaturated fatty acids, reducing the production of inflammatory prostaglandins; or instead promote COX2 activity via saturated fatty acids, potentially increasing the production of neuroprotective prostaglandins (Bilak *et al.* 2004); the former is the more likely option. Regardless of the direction of the effects of Gemals on COX2 activity, COX2 inhibition by meloxicam administration could have masked any neuroprotective effects of Gemals from being detected in the current study.

3.4.4.3 Nutritional supplementation

Bacon-flavoured Nutragel cubes were given to SOD1 mice from 18 weeks of age, to ensure easy access to nutrition and hydration as disease progressed and functional ability declined. As the Nutragel only became available after the trial had started, some mice did not have access to Nutragel during the trial period. Access to Nutragel influenced the time at which mice reached their body weight endpoint (20% loss from peak body weight), but had no effect on the ability of SOD1 mice to right themselves

(Table 3.5). While this effect can be accounted for in statistical analyses, any dietary supplementation needs to be kept constant between all mice in future studies.

3.4.5 Species differences

The absence of a Gemals-mediated survival increase in this study is likely due to the post-onset treatment and confounding factors discussed above, and less likely due to differences between mouse models of ALS, rat models of ALS, and human ALS patients. Both SOD1 mice and SOD1 rats over-express $SOD1^{G93A}$ protein, such that SOD1 activity increases four-fold in SOD1 mice (Gurney *et al.* 1994) and three-fold in SOD1 rats (Nagai *et al.* 2001), and the pathogenic processes and disease course are similar between rat and mouse models. It therefore seems unlikely that Endotherapia compounds should show robust increased survival when used pre-symptomatically in SOD1 rats, and appear to show positive effects in an open clinical trial of ALS patients, but not influence survival in SOD1 mice as observed in the present study. It is possible that the higher SOD1 expression and activity (Gurney *et al.* 1994; Nagai *et al.* 2001) results in a more aggressive disease process in SOD1 mice than SOD1 rats, and may indicate that the pathogenic processes in SOD1 rats are a closer echo of those seen in ALS patients.

It is possible that Endotherapia, a multi-action mixture, has different effects in the ALS patients and in rodent models. While the evidence for chronic bacterial infection as a causative factor in ALS is not comprehensive (Nicolson 2008), the fatty acid components of Endotherapia are intended to sequester bacterial cell wall moieties which would normally be used for attachment to cell membranes (Geffard *et al.* 2010). If such chronic infections were present in some, or all, of the small ALS patient cohort used for the open clinical trial, the putative anti-infection, antioxidant, and anti-inflammatory properties of Endotherapia may contribute to the positive outcome observed (Geffard *et al.* 2010). It seems unlikely that such environmentally-acquired infections would occur in SOD1 animal models, considering that most laboratory animals are kept in sterile environments, and therefore the effects of Gemals compounds in SOD1 animals are limited to its antioxidant and anti-inflammatory properties. Once again, the differing effects of Gemals in rats and mice may come down to the differences in disease severity and timing of administration in relation to the dynamics of oxidative stress.

3.4.6 Summary and conclusions

In conclusion, this study found no survival effect of Gemals in SOD1 mice when administered after symptom onset. This may be due to oxidative stress in the pre-symptomatic phase setting up pathogenic pathways such as protein aggregation which cannot be ameliorated by treating oxidative stress alone; or may be due to the presence of confounding factors such as the administration of meloxicam to alleviate irritation caused by Gemals injection.

The fact that we also administered meloxicam and in this study saw no change in disease outcome measures that could be attributed to Gemals treatment, hints that the beneficial effect of Gemals seen in the previous study (Nicaise *et al.* 2008) may involve a COX2-dependent mechanism of action. Future work on this compound should include identification of the component causing irritation to mice, and further investigation of the mechanism of action in the SOD1 rat spinal cord.

Endotherapia has previously shown promise in an open clinical trial of ALS patients; yet without a control group, the results of the open trial cannot be distinguished from any drift in the ALSAQ-40 reference rate over time (Geffard *et al.* 2010). For its further development as a potential therapeutic for ALS, Endotherapia should be trialled using a traditional clinical trial design series: first, a safety trial to ensure no adverse events occur in human ALS patients; and second, a double-blind, randomised clinical trial to look at drug efficacy.

Chapter 4

The effects of metallothionein-2 treatment and treadmill exercise in SOD1 mice

4.1 Background

Multiple pathologies are present in ALS, and thus multi-action drugs are needed to address multiple aspects of the disease process. Oxidative stress has already been addressed as a key pathology (see Chapter 1, section 1.3.9). The protein metallothionein-1/2 (MT-1/2), which is upregulated in SOD1 mice (see Chapter 2), plays multiple roles in neuronal protection and response to oxidative stress, and may be an appropriate multi-action therapeutic compound for the treatment of ALS.

4.1.1 Metallothioneins

4.1.1.1 Structure and function of metallothioneins

Metallothioneins (MTs) are a highly conserved family of small, metal-binding proteins (Hamer 1986; Aschner 1996). There are four mammalian MT isoforms, MT-1 to MT-4, which share a similar structure comprising two metal-binding domains and a central linker region (Figure 4.1) (Hamer 1986). MT proteins are rich in cysteine residues, used for the coordination of zinc, copper, and cadmium *in vivo*, as well as iron, lead, silver, gold, platinum, arsenic, and bismuth *in vitro* (Kagi & Valee 1960; Good & Vasak 1986; Ngu & Stillman 2006). The cysteine residues can also bind reactive oxygen species in preference to metal ions under conditions of oxidative stress, conferring potent antioxidant properties on MT proteins (Thornalley & Vasak 1985).

The MT-1 and MT-2 isoforms, considered to be functionally similar and sometimes referred to as a single 'MT-1/2' isoform, are expressed at low levels in most body tissues but are absent from neurons (Chung *et al.* 2003). MT-3 is expressed only in the central nervous system (Palmiter *et al.* 1992), while MT-4 is expressed only in stratified squamous epithelia (Quaife *et al.* 1994). MT-1/2 is the most well-characterised isoform of the MT family, and shows neuroprotective properties in a range of contexts as will be discussed below. Expression of MT-1/2 is increased in response to high levels of metal ions such as zinc and copper (Richards *et al.* 1984; Suzuki & Koizumi 2000), oxidative stress (Campagne *et al.* 2000), glucocorticoids (Richards *et al.* 1984), and the presence of inflammatory cytokines such as IL-1 (Cousins & Leinart 1988). Astrocytes are the major source of MT-1/2 within the central nervous system, and can rapidly induce MT-1/2 expression in response to neuronal damage, and secrete MT-1/2 to act

extracellularly on surrounding neurons (Chung *et al.* 2004; Chung *et al.* 2008b). The expression of MT-1/2 in response to these cellular stresses implicates MT-1/2 in metal homeostasis, cellular defenses against oxidative stress, and neuroprotection (Michalska & Choo 1993; Aschner 1996; West *et al.* 2008; Blindauer & Leszczyszyn 2010).

4.1.1.2 Growth-promoting and neuroprotective roles of MT-1/2

MT-1/2 shows growth-promoting and neuroprotective roles in both *in vitro* and *in vivo* paradigms. MT-1/2 promotes neurite outgrowth when applied to cultured cortical, dopaminergic, hippocampal, and cerebellar granule neurons; and promotes reactive sprouting in response to axon bundle transection (Chung *et al.* 2003; Kohler *et al.* 2003; Asmussen *et al.* 2009b). *In vivo*, MT-1/2 promotes regenerative axonal sprouting after a focal brain injury (Chung *et al.* 2003), and optic nerve regeneration following axonal transection (Fitzgerald *et al.* 2007). In terms of neuroprotection, MT-1/2 promotes survival of dopaminergic and hippocampal neurons from 6-hydroxydopamine and β-amyloid toxicity, respectively (Kohler *et al.* 2003). MT-1/2 promotes neuronal survival in mice following ischaemia/reperfusion injury (van Lookeren Campagne *et al.* 1999; Trendelenburg *et al.* 2002) and focal brain injury, as well as reduction of the glial scar and increased wound healing in the latter injury (Chung *et al.* 2003). MT-1/2 also promotes neuronal survival in mouse models of Parkinson's disease (Ebadi *et al.* 2005) and Alzheimer's disease (Manso *et al.* 2011).

4.1.1.3 Mechanisms of MT-1/2-mediated neuroprotection

Extracellular MT-1/2 interacts with neurons via the low-density lipoprotein receptor-related proteins, LRP1 and LRP2, on neuronal cell bodies (Fitzgerald *et al.* 2007; Ambjorn *et al.* 2008; Chung *et al.* 2008b). The interactions between MT-1/2 and LRPs promote neurite outgrowth and neuronal survival via activation of the intracellular growth-promoting and pro-survival PI3K, MAPK, Akt, and CREB pathways (Fitzgerald *et al.* 2007; Ambjorn *et al.* 2008; Asmussen *et al.* 2009b). MT-1/2 may also be internalised into neurons by its interaction with LRPs (Chung *et al.* 2008b), and if able to avoid lysosomal degradation, could play an intracellular role in ROS scavenging and intracellular metal homeostasis. Internalised MT-1/2 may additionally protect against apoptosis via an interaction of the apo-MT protein with the tumour suppressor protein p53 (Ostrakhovitch *et al.* 2006; Ruttkay-Nedecky *et al.* 2013). MT-1/2 also shows a role in modulating glial cell activation and neuroinflammation, by suppressing astrogliosis and microglial reactivity following cortical needlestick injury (Chung *et al.* 2003).

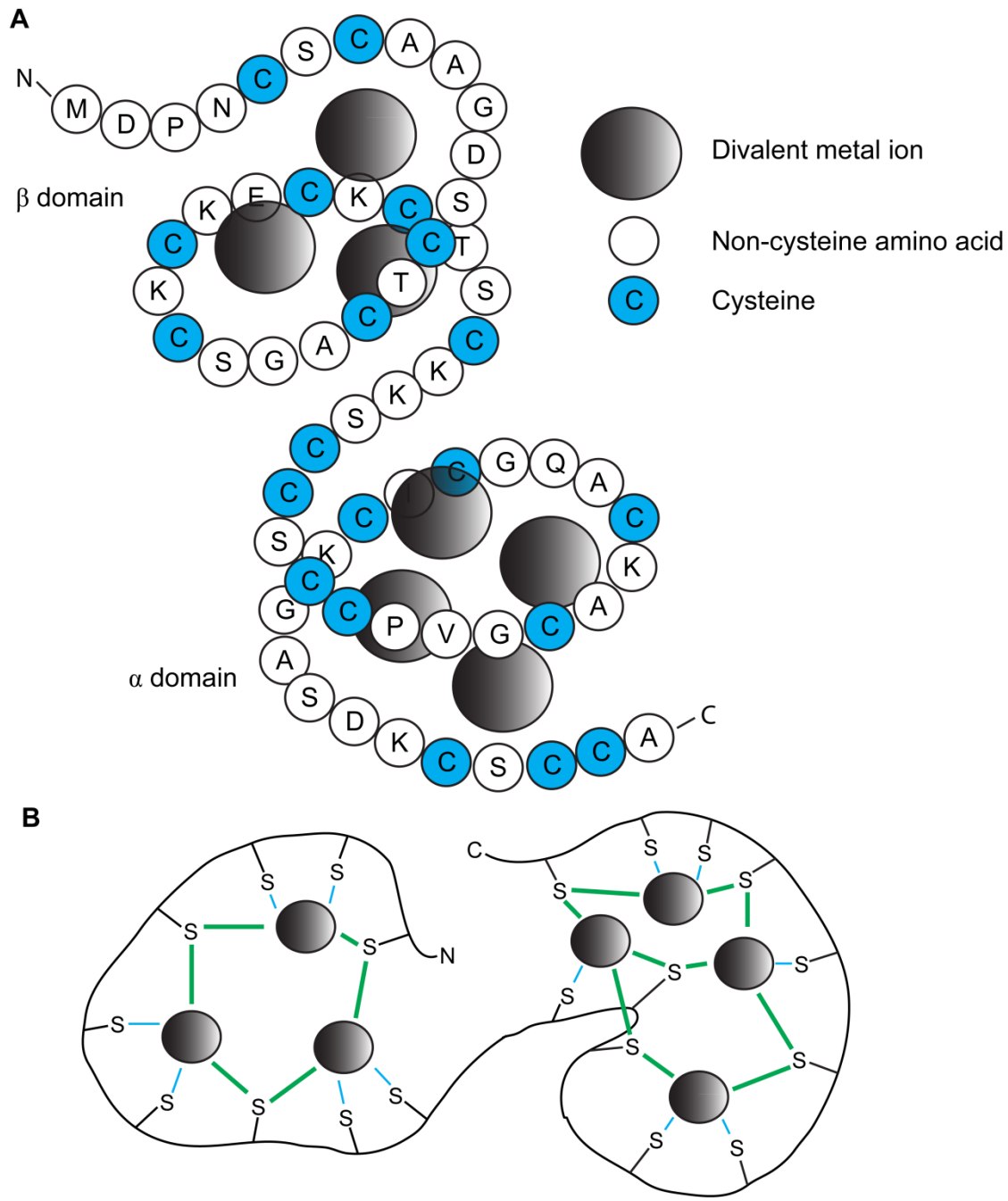

Figure 4.1 The structure and sequence of MT2

(A) A stylised diagram of MT2 protein, binding seven divalent metal ions in two clusters, is shown here. All MT proteins share the same basic structure: a C-terminal metal-binding domain (α domain) and an N-terminal metal-binding domain (β domain), joined by a short linker region (Hamer 1986). The abundant cysteine residues in MT, shown as blue circles, coordinate metal-binding in thiolate clusters. One MT molecule may bind up to seven divalent metal ions (as shown above) or twelve monovalent metal ions. Amino acids are labelled with standard single-letter notation. (B) A schematic diagram (adapted from Fischer and Davie 1998) showing the coordination of divalent metal ions in two thiolate clusters through bonds from direct (blue) and bridging (green) cysteine sulfur (S) ligands.

4.1.1.4 MT-1/2 in ALS

Alterations in CNS levels of MT-1/2 in ALS patients are unclear. An early study indicated increased MT-1/2 immunoreactivity in ALS patient spinal cord (Sillevis Smitt *et al.* 1994), while a subsequent study indicated no consistent change in mRNA levels for several MT-1/2 genes in ALS patients (Blaauwgeers *et al.* 1996). A more recent study indicated that MT-1/2 protein levels were reduced in ALS spinal cord at end-stage (Hozumi *et al.* 2008). However, MT-1/2 protein levels are consistently reported as increased in the spinal cord of SOD1 mouse models of ALS compared with controls (Gong & Elliott 2000; Tokuda *et al.* 2007; Tokuda *et al.* 2013), and this is consistent with the results from Chapter 2 of this thesis. Upregulation of MT-1/2 with disease progression may be in response to oxidative stress in ALS tissue, but also may play a role in protecting motor neurons from toxicity. Genetic ablation of MT-1/2 in SOD1 mice shortened survival times and hastened disease progression (Nagano *et al.* 2001; Puttaparthi *et al.* 2002), while SOD1 mice over-expressing MT-1/2 showed delayed disease onset and lengthened survival times (Tokuda *et al.* 2013). Thus, MT-1/2 appears to play a protective role in ALS and is a suitable candidiate therapeutic for testing in SOD1 mice. Although our laboratory previously showed minimal CNS entry of injected MT2 through the intact BBB (Lewis *et al.* 2012b), the SOD1 mouse BBB is known to be compromised from early in the disease course (Garbuzova-Davis *et al.* 2007), increasing the likelihood of successful CNS delivery of injected therapeutic compounds.

4.1.2 Exercise in ALS

The relationship between exercise and ALS is complex, with exercise having been implicated as both a cause and a potential therapy for ALS. Some epidemiological studies have indicated that increased vocational and leisure-time or sport-related physical activity has been linked with an increased ALS risk (Beghi *et al.* 2010; Huisman *et al.* 2013), and clusters of ALS have been observed amongst those with high occupational levels of physical activity, such as athletes (Chio *et al.* 2009; Lehman *et al.* 2012) and military personnel (Weisskopf *et al.* 2005). However, it is unclear whether these increased risks are due to physical activity itself, genetic factors predisposing to fitness, or shared environmental exposures (Cox *et al.* 2009; Chio & Mora 2012). Conversely, a number of small studies indicate a therapeutic benefit of exercise in ALS patients (Drory *et al.* 2001; Dal Bello-Haas *et al.* 2007; Sanjak *et al.* 2010), although any positive effects of exercise on slowing disease progression are yet to be confirmed

by a large, randomised controlled trial (Dal Bello-Haas *et al.* 2008). The potential for exercise to modulate survival of SOD1 mice has been explored with wheel running, treadmill running and swimming paradigms, but consensus on the effects of exercise is still lacking within the literature. Daily wheel running showed a non-significant increase in survival times of SOD1 mice (Liebetanz *et al.* 2004), while most studies on moderate-intensity treadmill exercise showed increased survival times (Kirkinezos *et al.* 2003; Kaspar *et al.* 2005; Carreras *et al.* 2010). However, an alternate study found increased survival in SOD1 mice undergoing swimming exercise, but no benefit from treadmill running (Deforges *et al.* 2009). In addition, high-intensity treadmill running showed a detrimental effect on SOD1 mouse survival times (Mahoney *et al.* 2004). Thus, the duration, intensity, and type of exercise appeared to affect how exercise modulates survival in SOD1 mouse models of ALS.

4.1.3 Aims and hypothesis

As described in section 4.1.1.3, MT-1/2 appears neuroprotective via a range of mechanisms which could include ROS scavenging, preventing apoptosis, modulating glial reactivity, and activating neuronal signalling pathways; MT-1/2 protein is therefore a suitable candidate therapeutic for ALS. Interestingly, moderate-intensity treadmill running exercise has been shown to upregulate MT-1/2 in the spinal cord of non-transgenic mice (Hashimoto *et al.* 2009). It is possible that the protective effects of treadmill exercise in SOD1 mice may be due to increased production of the neuroprotective MT-1/2 protein in the spinal cord. This study aims to test the protective effects of MT-1/2 in SOD1 mice, via administration of exogenous MT-2A protein (the most common MT-1/2 isoform), or via upregulation of endogenous MT-1/2 by exercise.

Hypothesis: Pre-symptomatic administration of exogenous MT-2A protein, and/or treadmill running exercise, will improve functional and survival outcomes in SOD1 mice compared with untreated controls.

This longitudinal study was designed to monitor disease onset, disease progression, and survival time in a cohort of female SOD1 mice. The cohort was split into 4 treatment groups in a 2x2 design, with mice receiving either: treadmill exercise alone; MT-2A treatment alone; treadmill exercise and MT2 treatment; or no treatment (vehicle/sedentary control). A factorial approach was used in order to identify any synergistic effects of concurrent MT-2A treatment and treadmill running.

4.2 Methods

4.2.1 Animals

All procedures and protocols involving animals were approved by the University of Tasmania's Animal Ethics Committee (permit number A10995). SOD1 mice were housed and genotyped according to the protocols in Chapter 2.

4.2.2 Treatments

Female SOD1 mice were assigned to one of four treatment groups in a 2x2 design (n=13-16/group). Mice received two simultaneous treatments: 1) administration of MT2 protein, or saline control; and 2) treadmill exercise, or sedentary control. The treatment groups were MT2+Exercise, Saline+Exercise, MT2+Sedentary, and Saline+Sedentary. All treatments started at 6 weeks of age, during the pre-symptomatic stage of disease, and stopped after 16 weeks of age (Figure 4.2). Copy number, age at start of treatment, and starting body weight did not differ between treatment groups (Table 4.1).

Table 4.1 Characteristics of SOD1 mice at start of treatment

Treatment Group	n	Copy number (ΔCT)	Age at start (days)	Starting weight (g)
MT2/Exercise	14	5.33 ± 0.07	46.7 ± 1.2	17.7 ± 0.4
MT2/Sedentary	14	5.33 ± 0.08	46.9 ± 1.2	17.6 ± 0.3
Saline/Exercise	14	5.31 ± 0.05	47.7 ± 1.1	17.4 ± 0.2
Saline/Sedentary	16	5.31 ± 0.05	48.6 ± 1.2	17.3 ± 0.3

Omnibus one-way ANOVA: Copy number, p=0.994; Age at start, p=0.665; Starting weight, p=0.790.

4.2.2.1 MT2 administration

Lyohilised, purified rabbit-liver Zn_7-metallothionein-2A (MT2; >98% purity by HPLC, Bestenbalt LLC, Tallinn, Harjumaa, Estonia), was dissolved in 0.9% sterile saline solution for injection. MT2 treatment consisted of twice-weekly intramuscular injections of 10mg MT2/kg body weight, giving a weekly total dose of 20mg MT2/kg. MT2 solution, or sterile saline for control mice, was injected into the caudal thigh musculature via a 31-gauge needle, with a maximum volume of 30µL per injection, under light isoflurane (Attane) anaesthesia (3.5% isoflurane in 2L/min oxygen flow).

4.2.2.2 Treadmill running exercise

Exercised mice were exercised five days per week on a mouse treadmill (Exer 3/6, Columbus Instruments, OH, USA). Daily sessions consisted of a warm-up (5min, 0m/min to 10m/min) followed by constant speed exercise (25min, 10m/min), and a cool-down (1min, 10m/min to 0m/min), performed between 9am and 12noon as much as practicable. Sedentary controls spent 25 minutes on the stationary treadmill, to try to control any effects of environmental enrichment due to a novel treadmill environment.

4.2.3 Outcome measures

4.2.3.1 Functional assessments

Stride pattern testing and wire hang duration (Chapter 2) were tested weekly, and body weight at least twice weekly, in all mice throughout the treatment period, and in those mice followed through to disease endpoint (Figure 4.2). Weekly average stride length, uniformity, body weight, percentage body weight, and wire hang duration ability were compared using two-way ANOVA, with MT2/saline and exercise/sedentary as factors. All data are reported as mean ± standard error of the mean; F tests of fixed effects in the two-way ANOVA are also reported. Linear mixed modelling was also used to model body weight trajectories over time (see Chapter 2), and the non-linear combination of estimators (nlcom) procedure in StataIC was used to estimate age at which maximum body weight was attained (mean ± standard error for each group). Point estimates of age at maximum body weight were compared between treatment groups using Z scores. $p<0.05$ was considered significant in all analyses.

4.2.3.2 Histological and immunostaining analyses

At 17 weeks of age, 3-4 mice per group were sacrificed for histological analysis (MT2/Exercise n=3, MT2/Sedentary n=3, Saline/Exercise n=4, Saline/Sedentary n=4) (Figure 4.2), and perfused with 4% PFA (see Chapter 2). The lumbar spinal cord was decalcified, embedded in paraffin, and microtome-sectioned at 5µm; the hindlimb calf musculature was post-fixed in 4% w/v PFA in PBS at 4°C, cryoprotected in 10% and 30% w/v sucrose (Sigma-Aldrich) in PBS, embedded in OCT cryomatrix (Sakura Finetek, Tokyo, Japan) and cryostat-sectioned (Leica) at 80µm onto slides; excess cryomatrix was removed with PBS prior to immunolabelling. Spinal cord sections were dewaxed in xylene and rehydrated through graded alcohols prior to labelling, and also quenched with 3% H_2O_2 in PBS (20 minutes) prior to DAB immunohistochemistry.

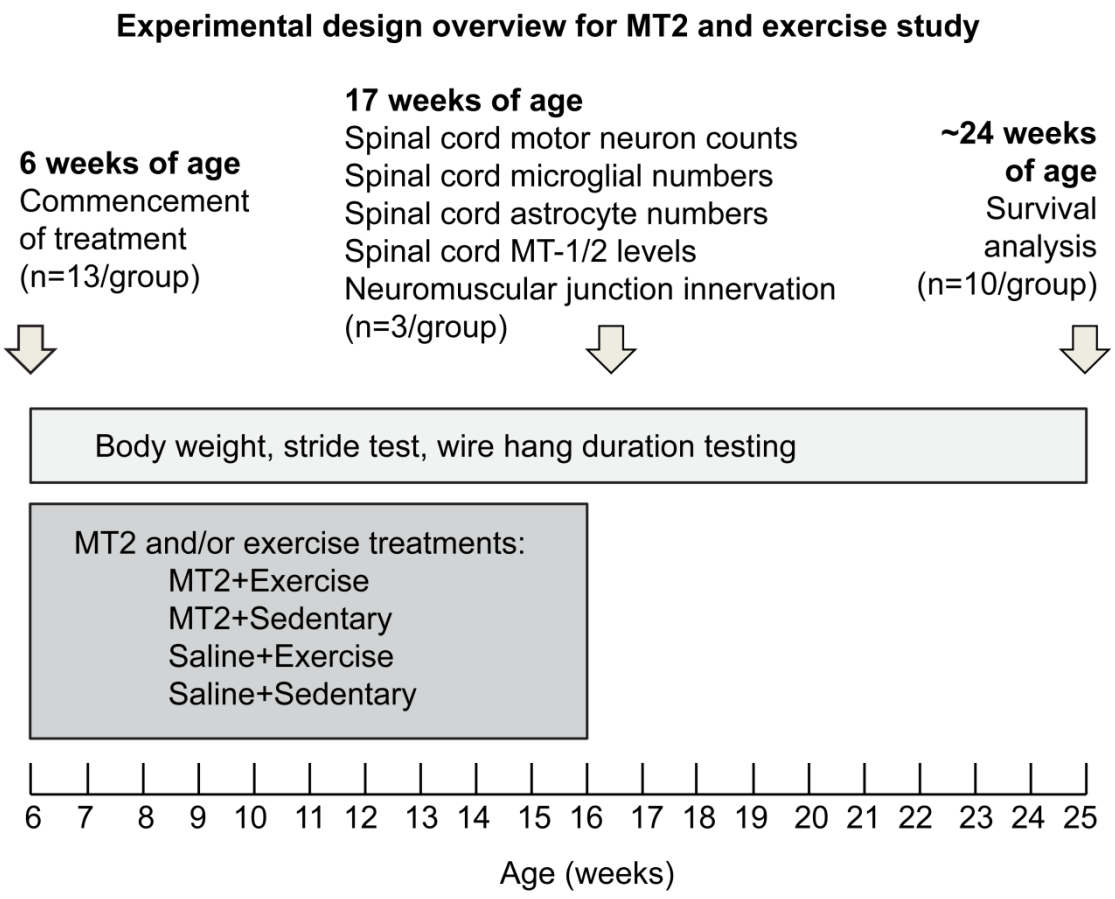

Figure 4.2 Experimental design for the MT2 and/or exercise trial

Female SOD1 mice were divided into 4 treatment groups at 6 weeks of age. Treatment with MT2 (MT-2A 10mg/kg i.m., twice per week) or treadmill running exercise (10m/min, 30min, 5 days per week), or both, was carried out from 6 to 16 weeks of age (n=13-16 per group). Body weight, stride pattern testing, and wire hang duration were measured at least weekly from 6 weeks of age through to disease endpoint. At 17 weeks of age, at least 3 mice in each treatment group were sacrificed for histological analysis of spinal cord motor neuron, microglia, and astrocyte numbers, spinal cord MT-1/2 levels, and neuromuscular junction innervation. Ten mice in each treatment group were followed for survival analysis, with disease endpoint measured as a loss of 20% from peak body weight.

4.2.3.2.1 Nissl stain

Eight to ten sections per spinal cord, each separated by a minimum distance of 40µm, were incubated with cresyl violet solution (1% w/v cresyl fast violet, acidified with 0.25% v/v acetic acid [both Sigma-Aldrich]) for 30 minutes, then washed in slowly-running water until dye no long leached from the sections. Slides were then passed through 95% ethanol for 4 minutes, 100% ethanol for 2 minutes, incubated in xylene, passed through 100% ethanol and incubated with cajeput oil for 3 minutes, then rinsed twice in xylene and coverslipped using Pertex mounting medium (Leica).

4.2.3.2.2 MT-1/2 immunohistochemistry

Immunolabelling for MT-1/2 was performed as described in Chapter 2, with the exception that the primary mouse anti-MT-1/2 antibody was used at 1:750. MT-1/2-positive cells were counted in the lumbar spinal cord ventral horn, dorsal horn, dorsal white matter, corticospinal tract, and ventral/lateral white matter (see Figure 4.10A).

4.2.3.2.3 Tomato lectin labelling

Tomato lectin (TL) labelling was performed to label microglial cells. Three lumbar spinal cord sections from each mouse, each separated by a minimum distance of 80µm, were blocked and incubated with biotinylated TL as described in Chapter 2. TL was detected with stretapvidin-HRP (Life Technologies, 1:1000 for 1 hour in PBS) and DAB substrate (Vector Laboratories, 1 minute); sections were counterstained with nuclear fast red, dehydrated and coverslipped using Pertex.

4.2.3.2.4 GFAP immunohistochemistry

Three lumbar spinal cord sections from each mouse, each separated by a minimum distance of 80µm, were blocked and incubated with anti-GFAP antibody as described in Chapter 2. The primary antibody was detected with HRP-conjugated goat anti-rabbit antibody (1:1000 for 1 hour, Dako) and DAB substrate (Vector Laboratories) for 1 minute. All sections were counterstained and coverslipped as above.

4.2.3.2.5 Neuromuscular junction counts

To examine neuromuscular junction (NMJ) innervation, colocalisation between nicotinic acetylcholine receptors and neuronal markers was examined. Cryosections of calf and gastrocnemius musculature (80µm) were incubated with α-bungarotoxin-AF594 (αBTx [Life Technologies], 1:200 for 45 minutes), washed with PBS, then fixed with ice-cold methanol for 5 minutes. After 2 PBS washes, the tissue was permeabilised

by a 2-hour incubation with 0.3% TritonX-100 in PBS, then washed twice in PBS. A cocktail of primary antibodies against neuronal markers (mouse anti-dephosphorylated neurofilament SMI32 1:500, mouse anti-phosphorylated neurofilament SMI312 1:750 [Covance], mouse anti-synaptophysin 1:500 [Santa Cruz Biotechnology] and mouse anti-tau 1:500 [Santa Cruz Biotechnology]) was applied O/N at RT. Primary antibodies were detected with goat anti-mouse-AF488 (1:500 for 2 hours); nuclei were stained with Nuclear Yellow (1:10000 for 15 minutes). Muscle sections were coverslipped in aqueous mounting medium and examined under a fluorescence microscope (Olympus) for colocalisation between αBTx and neuronal markers. An innervated NMJ was scored as having any colocalisation between neuronal markers and αBTx labelling. For each animal, the innervation status of at least 100 NMJs was scored.

4.2.3.2.6 Counts and statistical analysis

DAB-stained slides were imaged under bright field microscopy (Leica Biosystems). Cell counts for motor neurons, MT-1/2-positive cells, and TL-positive cells were carried out in ImageJ (NIH). GFAP labelling was thresholded in the HSB colour space (hue, stop 83-84; saturation, pass 0-112; brightness, pass 170-255) in ImageJ, and quantified as a percentage area showing positive immunoreactivity in each region (see Figure 4.12F). Statistical analysis of all histological markers was carried out in SPSS, using one-way and two-way ANOVA to check for differences between treatment groups.

4.2.3.3 Survival

Survival time, measured as the earliest of either a loss of 20% from maximum recorded body weight or inability of a mouse to right within 30 seconds of being placed on its side, was analysed in SPSS using Kaplan-Meier analysis and Cox proportional hazards regression. Of 58 treated mice (Table 4.1), four mice died prior to disease endpoint – two Saline+Sedentary mice died under anaesthesia, and one MT2+Exercise mouse and one MT2+Sedentary mouse were found deceased in their cages unexpectedly. Examination by the animal welfare officer was unable to isolate a cause of death, but it is possible that these two mice died due to complications from intramuscular injections. These four unexpected deaths in the cohort represent a rate of 7%, a rate slightly lower than the 10% observed in previous SOD1 studies (Scott *et al.* 2008). After removing mice for histological analyses, and accounting for unexpected deaths, ten mice per treatment group (40 of the original 58) provided data for survival analysis.

4.3 Results

4.3.1 Survival

Survival time was recorded as the earliest of either the mouse losing 20% from its pre-disease maximum body weight, or the inability to right within 30 seconds. Four SOD1 mice (10%) reached their righting endpoint prior to their weight endpoint; 34 SOD1 mice (85%) displayed a 20% loss of peak body weight while still able to right within 30 seconds. Two SOD1 mice (5%) were culled just prior to disease endpoint due to 1) a mistake with ear ID clips and 2) an eye infection; data from these mice were censored appropriately in the survival analyses. Kaplan-Meier survival curves were plotted, and interactions between MT2 treatment and exercise were analysed using CPH analysis.

4.3.1.1 Kaplan-Meier survival analysis

Kaplan-Meier survival curves, with each treatment group plotted separately, indicate that MT2-treated mice (red lines) showed a more right-shifted survival curve with longer survival times than saline-treated mice (blue lines) (Figure 4.3A). Survival curves for exercised mice (solid lines) and sedentary mice (dashed lines) were approximately equal, although a very slight right-shift for exercised mice could be observed (Figure 4.3A). Average survival time estimates from Kaplan-Meier analysis were Saline+Sedentary 165.6±2.7 days, Saline+Exercise 168.0±2.3 days, MT2+Sedentary 170.5±1.8 days, and MT2+Exercise 172.7±1.8 days. Differences between the four individual treatment groups did not reach statistical significance (Log Rank test, p=0.146). Kaplan-Meier analysis was also used to split the mice on the basis of MT2 treatment or exercise treatment; MT2-treated mice showed longer survival times than saline-treated mice (Log-Rank test p=0.070; Figure 4.3B), whereas exercised and sedentary mice showed similar survival times (Log-rank test p=0.147; Figure 4.3C).

4.3.1.2 Cox proportional hazards regression

Cox proportional hazards regression (CPH) was used to examine the effects of exercise and MT2 treatment separately. Univariable CPH modelling showed that the hazard rate for MT2-treated mice was reduced compared to saline-treated mice, and the hazard rate for exercised mice was slightly reduced compared to sedentary mice (Table 4.2). Copy number, age at start of treatment, starting body weight, maximum body weight, and age at maximum body weight had negligible effects on survival (Table 4.2).

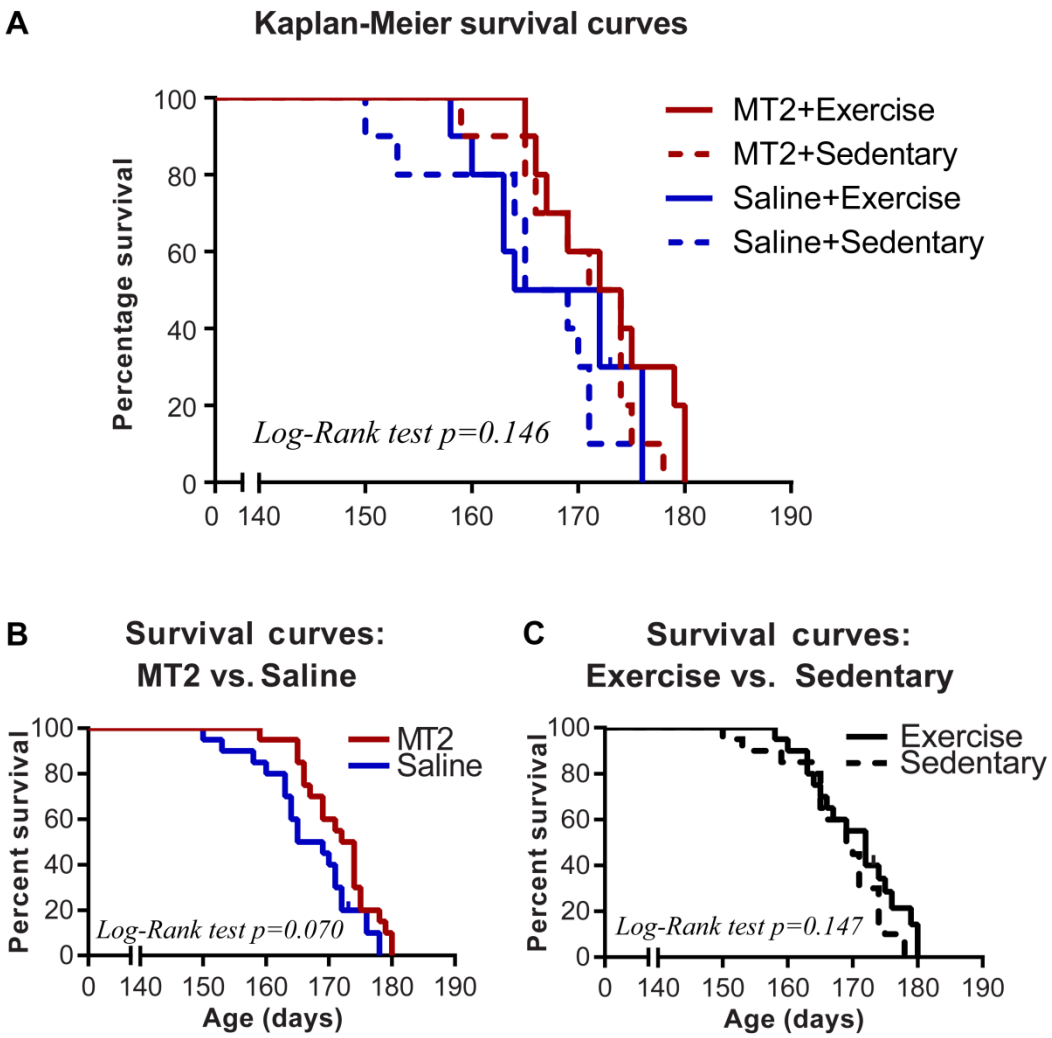

Figure 4.3 Kaplan-Meier survival curves for MT2-treated and exercised SOD1 mice

Comparing all four treatment groups (A) revealed that MT2-treated mice (red lines) showed right-shifted survival curves compared to saline-treated mice (blue lines), while exercised mice (solid lines) showed slightly right-shifted survival curves compared to sedentary mice (dashed lines); there were no significant differences between the four treatment groups. When MT2 treatment was compared with saline, regardless of exercise status (B), MT2-treated mice showed longer survival times than saline-treated mice. When exercise was compared with remaining sedentary, regardless of MT2 status (C), the survival curves showed few differences between exercised and sedentary mice. Vertical dashes represent censored data points.

Multivariable CPH regression, including both MT2 and exercise treatment, indicated that the hazard rate for MT2-treated mice was reduced by approximately 45% compared to saline-treated mice, and this effect approached statistical significance (HR_{MT2}=0.556, 95% CI 0.284-1.091, p=0.088). The hazard rate for exercise-treated mice was reduced by approximately 35% compared to sedentary mice, although this was not significant ($HR_{exercise}$=0.626, 95% CI 0.318-1.230, p=0.174) (Table 4.2). The associations between MT2 treatment and reduced hazard ratio, and exercise and reduced hazard ratio, became stronger when the multivariable model was adjusted for possible confounders copy number, age at start of treatment, starting body weight, maximum body weight, and age at maximum body weight (Table 4.2). The results of survival analyses show that MT2 treatment increases survival time by approximately 5 days (around 3% of SOD1 mouse lifespan), and that these effects approach statistical significance.

Table 4.2 Cox proportional hazards regression model for disease endpoint

Factor(s) in CPH model	HR (95% CI)	p-value
Univariable analysis[1]		
MT2	0.555 (0.283, 1.089)	0.087
Exercise	0.624 (0.318, 1.226)	0.171
Copy number (ΔCT)	0.911 (0.271, 3.065)	0.880
Age at start	1.009 (0.933, 1.092)	0.817
Starting weight	1.096 (0.836, 1.436)	0.506
Maximum body weight	1.067 (0.825, 1.380)	0.624
Age at maximum body weight[#]	0.992 (0.975, 1.009)	0.342
Multivariable analysis[2]		
MT2	0.556 (0.284, 1.091)	0.088
Exercise	0.626 (0.318, 1.230)	0.174
Multivariable analysis, adjusted[3]		
MT2	0.351 (0.149, 0.828)	**0.017**
Exercise	0.531 (0.259, 1.088)	0.084

[1]Univariable analysis contains the listed factor/covariate. [2]Multivariable analysis contains both exercise and MT2. [3]Multivariable analysis contains exercise, MT2, and possible confounders copy number, age at start of treatment, starting body weight, maximum body weight and age at maximum body weight. [#]If maximum body weight was achieved on more than one occasion, the largest age was used in the analysis.

4.3.2 Body weight

4.3.2.1 Average body weight per week

The body weight trajectories of SOD1 mice were curved, with all SOD1 mice showing weight gain from 6 to approximately 18 weeks of age, and weight loss therafter (Figure 4.4A). MT2-treated mice appeared to have higher average body weight than saline-treated mice at 17-22 weeks of age (Figure 4.4A); however, body weights differences between treatment groups were not significant by one or two-way ANOVA.

4.3.2.2 Linear mixed modelling of body weight

The MT2/saline treatment and the exercise/sedentary status of SOD1 mice both contributed to the fit of the model, such that the model fit the raw data better when these factors were included rather than excluded (Supplementary Data 3). The model fit was not improved by including interaction terms (MT2*exercise) (Supplementary Data 3); thus, the final model, with parameters outlined in Table 4.3, contained no interaction term (for full model specification, see Model 3, Supplementary Data 3).

The results of the linear mixed model give a set of parameters for the equation $\boldsymbol{Body\ weight = \beta_0 + \beta_1 * Age + \beta_2 * Age^2 + \beta_3 * Age^3}$, where each $\boldsymbol{\beta}$ coefficient has a unique value for each SOD1 treatment group (listed in Table 4.3). The $\boldsymbol{\beta}$ coefficients for MT2-treated mice were significantly different from those of saline-treated mice, whereas the $\boldsymbol{\beta}$ coefficients for exercised mice were not significantly different from those of sedentary mice (Supplementary Data 3). When graphed, the body weight trajectory curves indicated that MT2-treated mice (red lines) showed slightly higher body weights than saline-treated control mice (blue lines) at 120-140 days of age (Figure 4.4B).

Table 4.3 Parameter estimates from linear mixed modelling of body weight

Fixed effects parameter[1]	Saline + Sedentary	Saline + Exercise	MT2 + Sedentary	MT2 + Exercise
Intercept (β_0)	17.36	17.39	17.78	17.81
Age (β_1)	2.10×10^{-2}	1.89×10^{-2}	-4.33×10^{-3}	-6.40×10^{-3}
Age^2 (β_2)	4.78×10^{-4}	4.30×10^{-4}	9.88×10^{-4}	9.39×10^{-4}
Age^3 (β_3)	-5.55×10^{-6}	-4.74×10^{-6}	-8.13×10^{-6}	-7.32×10^{-6}

[1]For equation: $\boldsymbol{Body\ weight = \beta_0 + \beta_1 * Age + \beta_2 * Age2 + \beta_3 * Age3}$, where Age = Age, centered at 42 days.

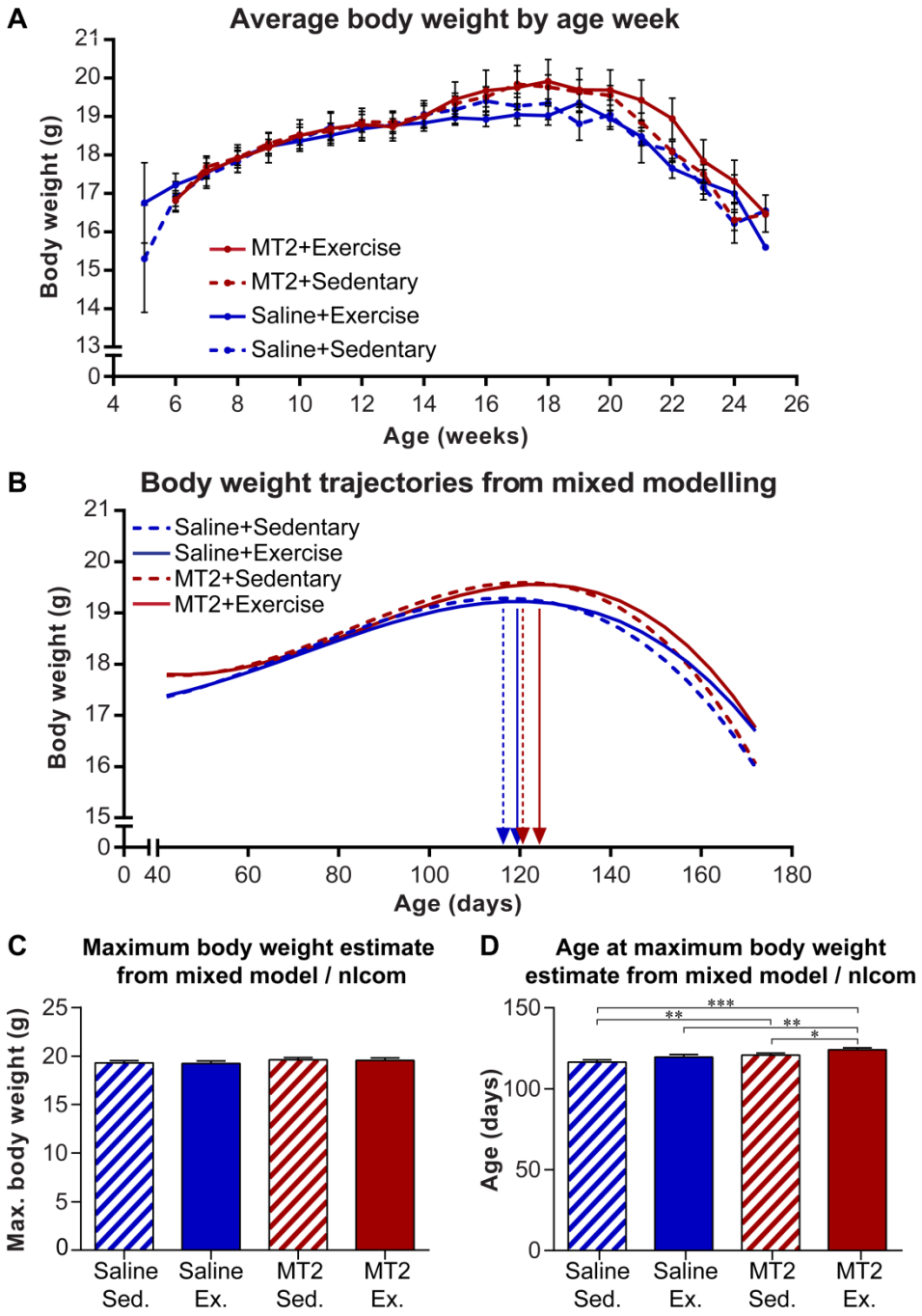

Figure 4.4 Body weight averages and modelled body weight trajectories in MT2-treated and exercised SOD1 mice over time

Average body weight at each age week (A) was not significantly different between treatment groups. Linear mixed model body weight trajectories (B) for MT2-treated (red lines), saline-treated (blue lines), exercised (solid lines), and sedentary (dashed lines) SOD1 mice are shown, corresponding to parameter estimates from Table 4.3. Model-based nlcom estimates of maximum body weight did not differ between treatment groups (C). Model-based nlcom estimates of the age at maximum body weight (D; arrows in B) showed later age at maximum body weight in MT2-treated mice than in saline-treated mice. *p<0.05 **p<0.01 ***p<0.001. Sed., sedentary; Ex., exercise. Error bars represent standard error of the mean (A) or of the nlcom point estimate (C,D).

4.3.2.3 Estimation of maximum body weight, and age at maximum body weight, from mixed model parameters using nlcom

From the mixed model parameters for each group, point estimates of the maximum body weight and the age at maximum body weight were calculated. MT2-treated mice had a slightly higher peak body weight than saline-treated mice, although this was not significant (Figure 4.4C). The age at which mice reached maximum body weight (point estimate ± standard error) was 116.4±1.4 days in Saline+Sedentary mice, 119.6±1.5 days in Saline+Exercise mice, 120.8±1.1 days in MT2+Sedentary mice, and 124.0±1.2 days in MT2+Exercise mice (Figure 4.4D; arrows in Figure 4.4B).

MT2+Exercise and MT2+Sedentary mice reached maximum body weight at a later age than Saline+Sedentary mice ($p<0.05$). MT2+Exercise mice also reached maximum body weight at a later age than Saline+Exercise and MT2+Sedentary mice ($p<0.05$) (Figure 4.4D). This indicated that MT2-treated mice reached their maximum body weight, a proxy of disease onset, slightly later than saline-treated mice. This was not due to differences in maximum body weight attained (Figure 4.4), nor due to differences in the amount of weight gained between starting treatment and reaching maximum body weight (weight gains: Saline+Sedentary 2.5±0.3g, Saline+Exercise 2.6±0.3g, MT2+Sedentary 2.7±0.3g, MT2+Exercise 2.4±0.2g; $p>0.4$ by one-way and two-way ANOVA). Thus, it would appear that MT2 treatment slightly delays disease onset.

4.3.2.4 Percentages body weight by week.

Interestingly, the body weight trajectories for exercised mice (solid lines) appeared to decline less steeply than those of sedentary mice (dashed lines) (Figure 4.4B). To determine whether any treatment had an effect on body weight decline over time, the ages at which mice reached 95, 90, and 85% of their maximum body weight were examined. Body weights were converted to a percentage of each mouse's maximum body weight, and percentage body weights were compared at each week using two-way ANOVA, including an MT2*exercise interaction term. At 22 weeks of age, exercise and MT2 treatment appeared to act together to produce the highest percentage of maximum body weight remaining (MT2+Exercise 92±1%, MT2+Sedentary 88±1%, Saline+Exercise 89±1%, Saline+Sedentary 90±1%; while main effects were not significant, $F_{MT2*exercise}(1,34)=5.065$, $p=0.031$). At 24 weeks of age, exercised mice showed higher percentage body weights than sedentary mice (MT2+Exercise 83±1%,

MT2+Sedentary 82±1%, Saline+Exercise 85±1%, Saline+Sedentary 81±2%; $F_{exercise}(1,20)=5.655$, p=0.027) (Figure 4.5A). However, these changes were not consistent throughout the disease course (Figure 4.5A).

The ages at which mice reached 95%, 90% and 85% of their maximum body weight were also examined using survival analysis; Kaplan-Meier survival curves are provided in Figure 4.5B, while CPH regression was used for statistical analysis. Exercised mice had a reduced hazard ratio for reaching 95% body weight compared to sedentary mice ($HR(95\%BW)_{Exercise}=0.468$, 95% CI 0.238-0.918, p=0.027, adjusted for MT2 treatment), indicating that exercised mice stayed above 95% of their maximum body weight for longer than sedentary mice (Figure 4.5B, left panel). MT2-treated mice tended towards a reduced hazard ratio for reaching 90% of peak body weight compared to saline-treated mice ($HR(90\%BW)_{MT2}=0.511$, 95% CI 0.255-1.021, p=0.057, adjusted for exercise), indicating that MT2-treated mice stayed above 90% of their maximum body weight for slightly longer than saline-treated mice. Examination of the Kaplan-Meier survival curves indicates this effect is driven mainly by maintenance of >90% body weight in MT2+Exercise mice (Figure 4.5B, middle panel). There were no differences between treatment groups for the age at reaching 85% body weight (Figure 4.5B, right panel).

In summary, MT2 treatment appears to affect the body weight of SOD1 mice, with a slightly later age at disease onset compared to saline-treated mice.

4.3.3 Stride pattern

The stride pattern parameters, stride length and uniformity measurement (see Figure 2.11A,B), were measured weekly in all treatment groups.

4.3.3.1 Stride length

Stride length decreased over time in all SOD1 mice (Figure 4.6A). Stride lengths were similar between treatment groups at most weekly time points, although Saline+Sedentary mice tended to have shorter stride lengths than other treatment groups at 16, 18, 19 and 20 weeks of age (Figure 4.6A). At 12 and 14 weeks of age, exercised mice showed longer stride lengths than sedentary mice (12 weeks: $F_{exercise}(1,50)=6.153$, p=0.017); 14 weeks: $F_{exercise}(1,48)=6.356$, p=0.014).

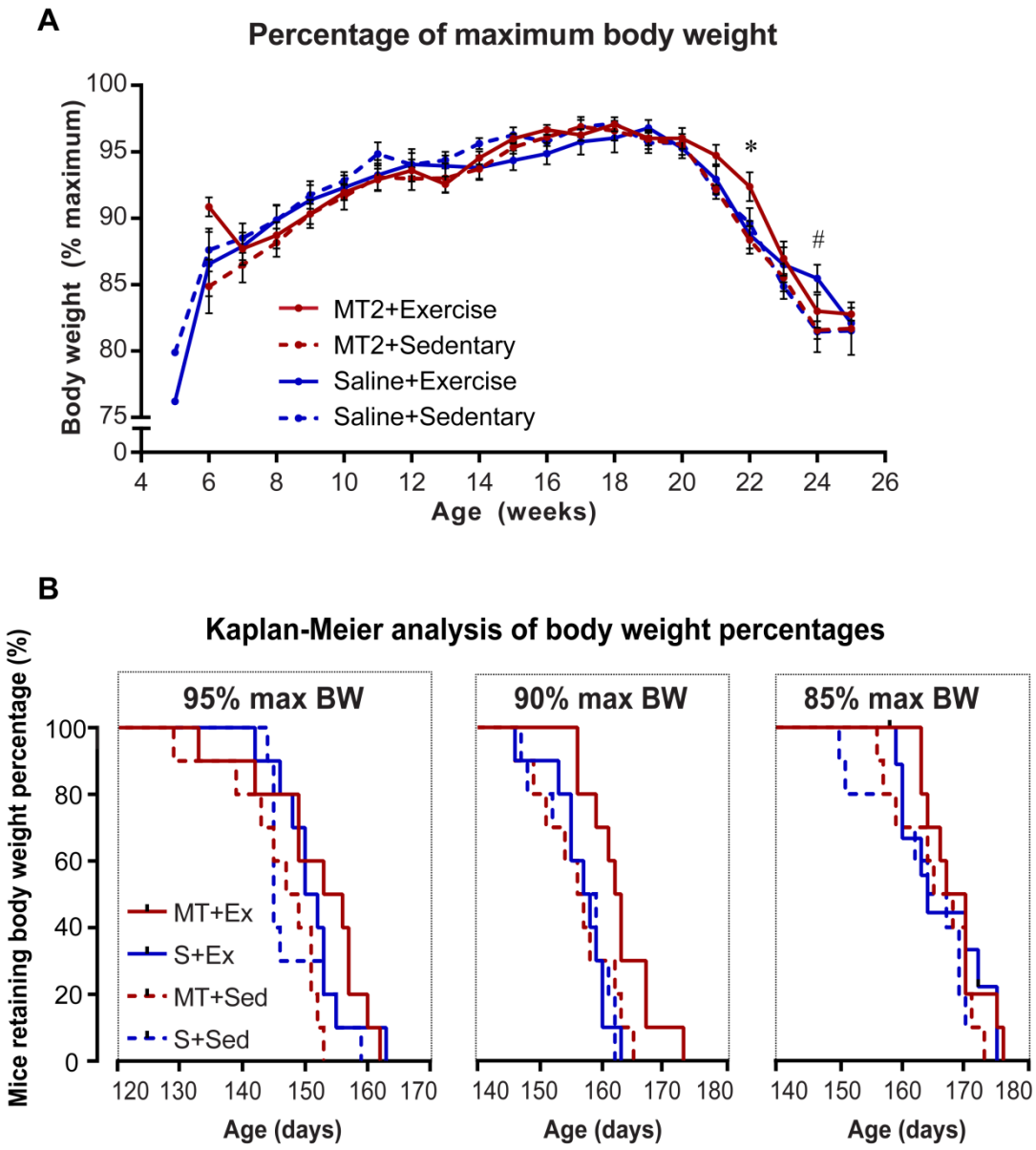

Figure 4.5 Percentage body weights of MT2-treated and exercised SOD1 mice

MT2+Exercise mice showed slightly higher retention of percentage body weight at 22 weeks of age, while exercised mice displayed higher body weight percentages than sedentary mice at 24 weeks of age (A). Kaplan-Meier curves for falling below 95%, 90%, and 85% percent of maximum body weight (B) show that exercised mice appeared to drop below 95% of maximum body weight later than sedentary mice (B, left panel), and MT2+Exercise mice appeared the last to drop below 90% of maximum body weight (B, middle panel). *$p<0.05$ MT2+Exercise mice vs. all other groups, #$p<0.05$ exercised mice vs. sedentary mice. BW, body weight; MT+Ex, MT2+Exercise; MT+Sed, MT2+Sedentary; S+Ex, Saline+Exercise; S+Sed, Sedentary+Saline. Vertical dashes in B represent censored data. Error bars represent standard error of the mean.

At 16 weeks of age, exercised mice had a slightly longer stride length than sedentary mice ($F_{exercise}(1,39)=3.951$, p=0.054); although the main effect for MT2 was not significant ($F_{MT2}(1,39)=0.486$, p=0.490), there was a significant interaction between MT2 and exercise ($F_{MT2*exercise}(1,39)=4.179$, p=0.048), indicating that the effect of exercise was not the same for mice receiving MT2 and mice receiving saline. Examining stride length averages confirmed that at 16 weeks of age, Saline+Exercise mice had a longer stride length than Saline+Sedentary mice, but there was no difference in stride length between MT2+Exercise mice and MT2+Sedentary mice. However, this effect was not maintained at 17 or 18 weeks of age. At 19 weeks of age, exercised mice again showed longer stride lengths than sedentary mice ($F_{exercise}(1,36)=7.864$, p=0.008).

At 20 weeks of age, MT2-treated mice showed longer stride lengths than saline-treated mice ($F_{MT2}(1,32)=5.833$, p=0.022), and exercised mice showed longer stride lengths than sedentary mice ($F_{exercise}$ (1,32)=6.453, p=0.016). However, the interaction term was also significant ($F_{exercise*MT2}(1,32)=5.175$, p=0.030), with average values indicating that MT2+Exercise mice had no further increase in stride length above that seen by either treatment applied individually, i.e. MT2+Exercise stride length was no different to either Saline+Exercise or MT2+Sedentary stride length. At 23 weeks of age, exercised mice showed longer stride lengths than sedentary mice ($F_{exercise}$ (1,24)=8.060, p=0.009)

4.3.3.2 Uniformity:

Uniformity measurements increased over time in SOD1 mice (Figure 4.6B). Uniformity measurements were relatively constant between treatment groups (Figure 4.6B), although slight differences were noted at 19 and 20 weeks of age where MT2-treated mice (red lines) appeared to have smaller uniformity measures than saline-treated mice (blue lines). At 9 weeks of age, exercised mice showed increased uniformity measures compared to sedentary mice ($F_{exercise}(1,51)=11.971$, p=0.001), although uniformity measures between all mice subsequently remained similar until 19 weeks of age. At 19 weeks of age, MT2-treated mice showed lower uniformity measures than saline-treated mice ($F_{MT2}(1,36)=4.675$, p=0.037). A similar trend for decreased uniformity in MT2-treated mice was present at 20 weeks of age, but this did not reach statistical significance (p=0.077). Thus, both exercise and MT2 treatment appear to have slight effects on stride pattern – at select time points, exercise and MT2 both appeared to maintain stride length, while MT2 treatment appeared to promote lower uniformity values, although these effects were not consistent throughout disease progression.

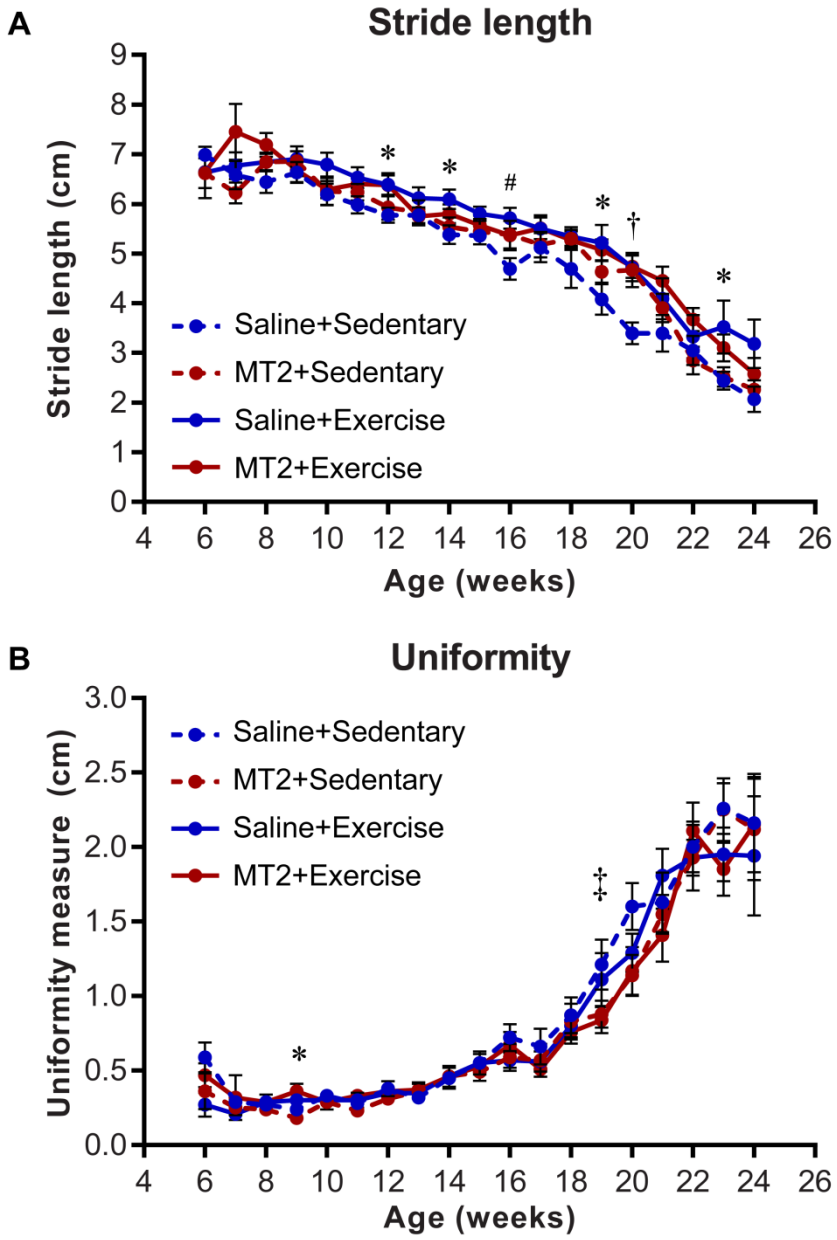

Figure 4.6 Stride pattern in MT2-treated and exercised SOD1 mice

Stride length, the distance between consecutive hind paw prints (A), and uniformity measure, the distance between placement of the front paw and subsequent hind paw placement when passing over the same spot (B), were similar between treatment groups. Stride length appears shortest in Saline+Sedentary mice at 18-20 weeks, while uniformity appears longer in saline-treated mice than MT2-treated mice at 19-20 weeks of age. *p<0.05 exercised mice vs. sedentary mice; #p<0.05 Saline+Exercise mice vs. Saline+Sedentary mice;†p<0.05 Saline+Sedentary vs. all other groups; ‡p<0.05 MT2-treated mice vs. saline-treated mice. Error bars represent standard error of the mean.

4.3.4 Wire hang duration

The wire hang duration testing revealed a large amount of variation within treatment groups (Figure 4.7A). Two-way ANOVA revealed only a significant interaction between exercise and MT2 at 17 weeks of age ($F_{exercise*MT2}(1,35)=6.502$, $p=0.015$), indicating that the effect of MT2 treatment on wire hang duration varied depending on whether the mice were exercised or not. Specifically, the average wire hang values indicated that MT2+Exercise mice had a slightly longer wire hang duration than Saline+Exercise mice at 17 weeks of age, but MT2+Sedentary mice in fact had a shorter wire hang duration than Saline+Sedentary mice at 17 weeks of age (Figure 4.7A).

From the 40 mice which were measured from 6 weeks of age until endpoint, 32 recorded the maximum wire hang duration of 60 seconds on at least one time point. Eight of the 40 mice (20%) were unable to hang on for 60 seconds at any time point; by group, these were 1 x MT2+Exercise, 2 x Saline+Exercise, 4 x MT2+Sedentary, and 1 x Saline+Sedentary. Amongst the 32 mice which attained a wire hang duration of 60 seconds, there were no differences between treatment groups for 1) the age at mice were no longer able to consistently hold on for 60 seconds (Figure 4.7B), 2) the age at which mice were no longer able to consistently hold on for 30 seconds (Figure 4.7C), and 3) the age at which mice were unable to grip the bars, i.e. wire hang duration = 0 seconds (Figure 4.7D). Amongst all 40 mice, even those which did not attain a wire hang duration of 60 seconds at any time point, there was no difference between treatment groups in the age at which mice were able to hold on for less than 50% of their maximum attained hang duration (Figure 4.7E).

4.3.5 Nissl staining

The number of Nissl-stained motor neurons present in the lumbar spinal cord ventral horn at 17 weeks of age, after the 10 weeks of MT2 and/or exercise treatment, was counted and compared between treatment groups. The number of motor neurons remaining at 17 weeks of age was not different between the four treatment groups (Figure 4.8). The number of large, vacuolated, degenerating motor neurons present in the ventral horn was likewise not different between treatment groups (data not shown). These data indicate that neither exercise nor MT2 treatment were particularly effective at preventing motor neuron degeneration in the pre-symptomatic period.

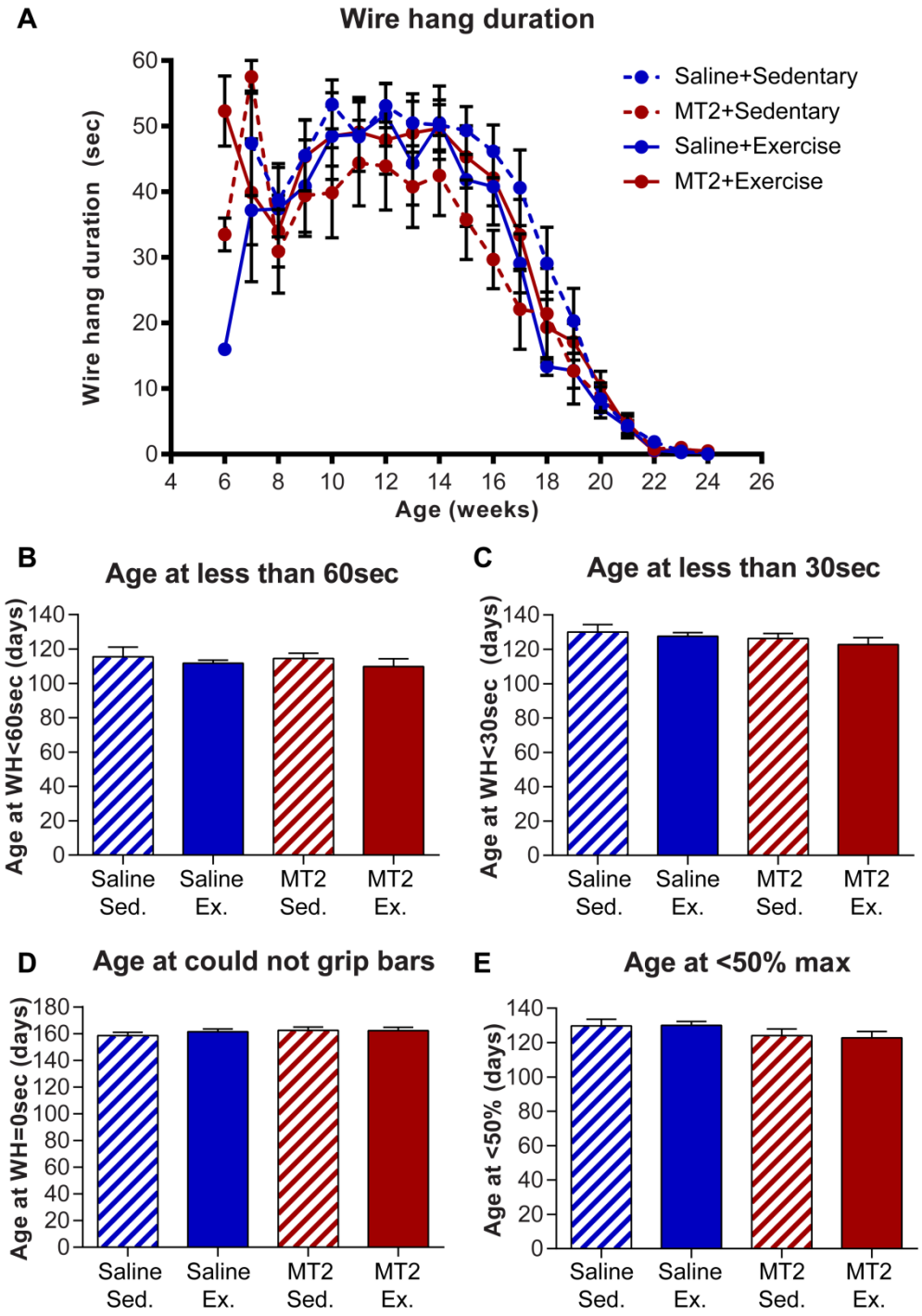

Figure 4.7 Wire hang duration in MT2-treated and exercised SOD1 mice

Average wire hang durations were similar between experimental groups at all time points (A). In mice which recorded the maximum of 60 seconds' hang duration at any time point, no between-group differences were seen in the age at which mice were subsequently unable to hang on for 60 seconds (B), unable to hang on for 30 seconds (C), or unable to grip bars at all (D). Amongst all mice, including those which did not record 60 seconds' grip duration at any time point, there was no difference in the age at which mice were unable to hang on for 50% of their maximum time (E). WH, wire hang duration. Error bars represent standard error of the mean.

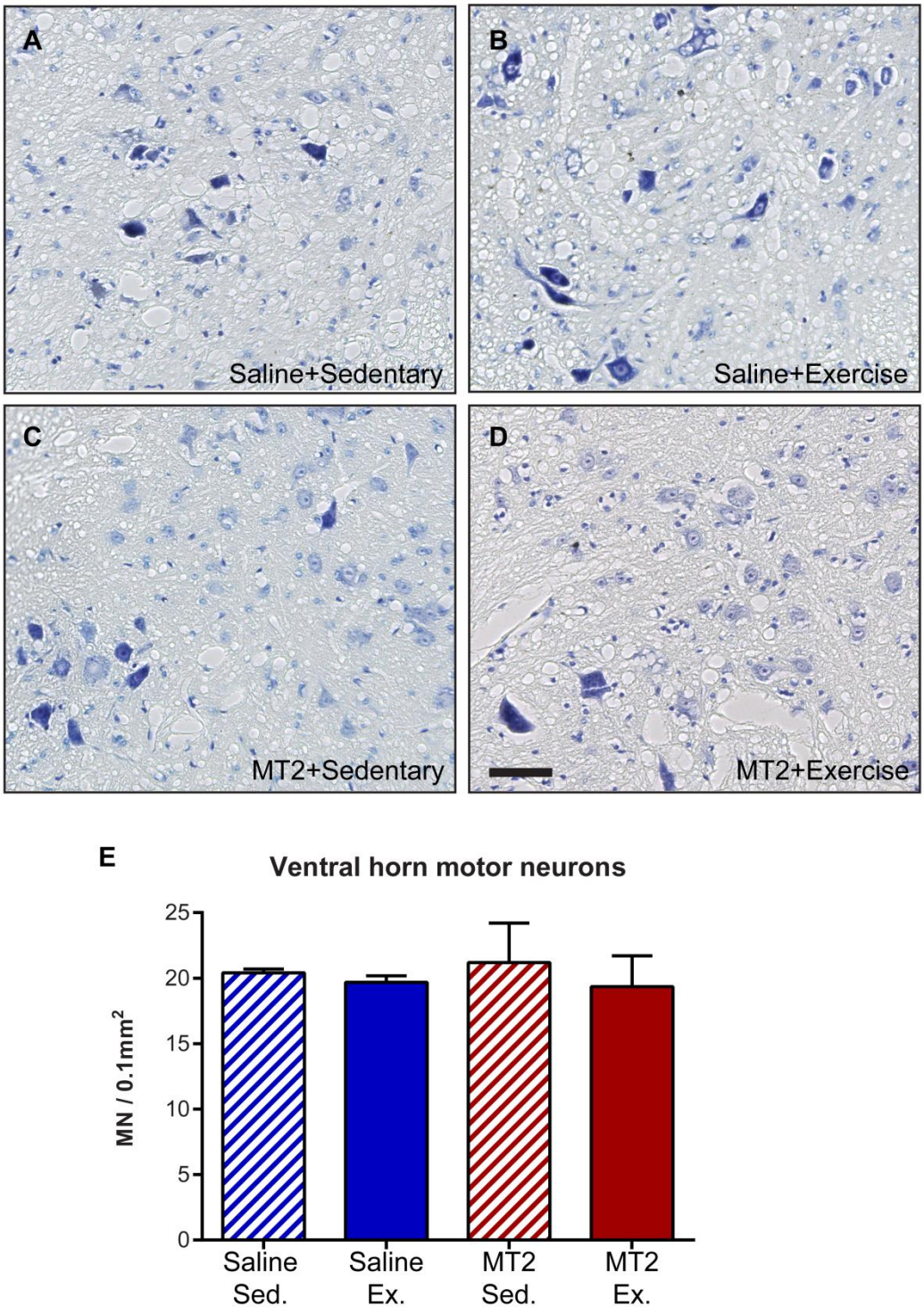

Figure 4.8 Nissl-stained motor neurons in the ventral horn of MT2-treated and exercised SOD1 mice

The number of motor neurons (MNs) remaining in the spinal cord ventral horn of Saline+Sedentary (A), Saline+Exercise (B), MT2+Sedentary (C), and MT2+Exercise (D) mice was not different at 17 weeks of age (E). Scale bar 50µm for A-D. Error bars in E represent standard error of the mean.

4.3.6 MT-1/2 immunostaining

MT-1/2 was observed within glial cells in both the white and grey matter of all SOD1 mice (Figure 4.9A-D). The number of MT-1/2-positive cells in the different spinal cord regions (Figure 4.10A) was compared between treatment groups. The numbers of MT-1/2-positive cell bodies in both the dorsal and ventral/lateral white matter columns appeared to increase slightly with exercise but not with MT2 treatment (Figure 4.10B,C). In the ventral horn grey matter, Saline+Exercise mice showed the largest number of MT-1/2-positive cells, although MT2+Exercise mice showed no increase in MT-1/2-positive cells compared to MT2+Sedentary mice (Figure 4.10D). However, there were no significant changes as assessed by two-way ANOVA. Few MT-1/2-positive cells were observed in the corticospinal tract white matter and in the dorsal horn grey matter (Figure 4.10E,F).

4.3.7 GFAP immunostaining

Quantification of GFAP immunolabelling in different spinal cord regions (Figure 4.11A-D, Figure 4.12F) revealed that that percentage area of the ventral horn grey matter, dorsal horn grey matter, corticospinal tract white matter, and dorsal column white matter occupied by GFAP immunoreactivity appeared to be increased by exercise (Figure 4.12A-E). The exercise-mediated increase in percentage area occupied by GFAP immunoreactivity was only significant in the dorsal column ($F_{exercise}(1,9)=5.881$, $p=0.038$) (Figure 4.12D). In contrast, MT2 treatment did not affect GFAP immunoreactivity in any region.

4.3.8 Tomato lectin labelling

Quantification of ventral horn microglial cells revealed a slight, but not significant, increase in Saline+Exercise mice compared to Saline+Sedentary mice (Figure 4.13). Neither MT2 nor exercise treatment appeared able to attenuate microglial activation.

4.3.9 Neuromuscular junction innervation

The percentage of innervated neuromuscular junctions in skeletal muscle from each treatment group was compared. No treatment appeared to significantly change the percentage of neuromuscular junctions innervated by motor axons (Figure 4.14). Neither MT2 treatment nor exercise was able to prevent muscle denervation in SOD1 mice (Figure 4.14).

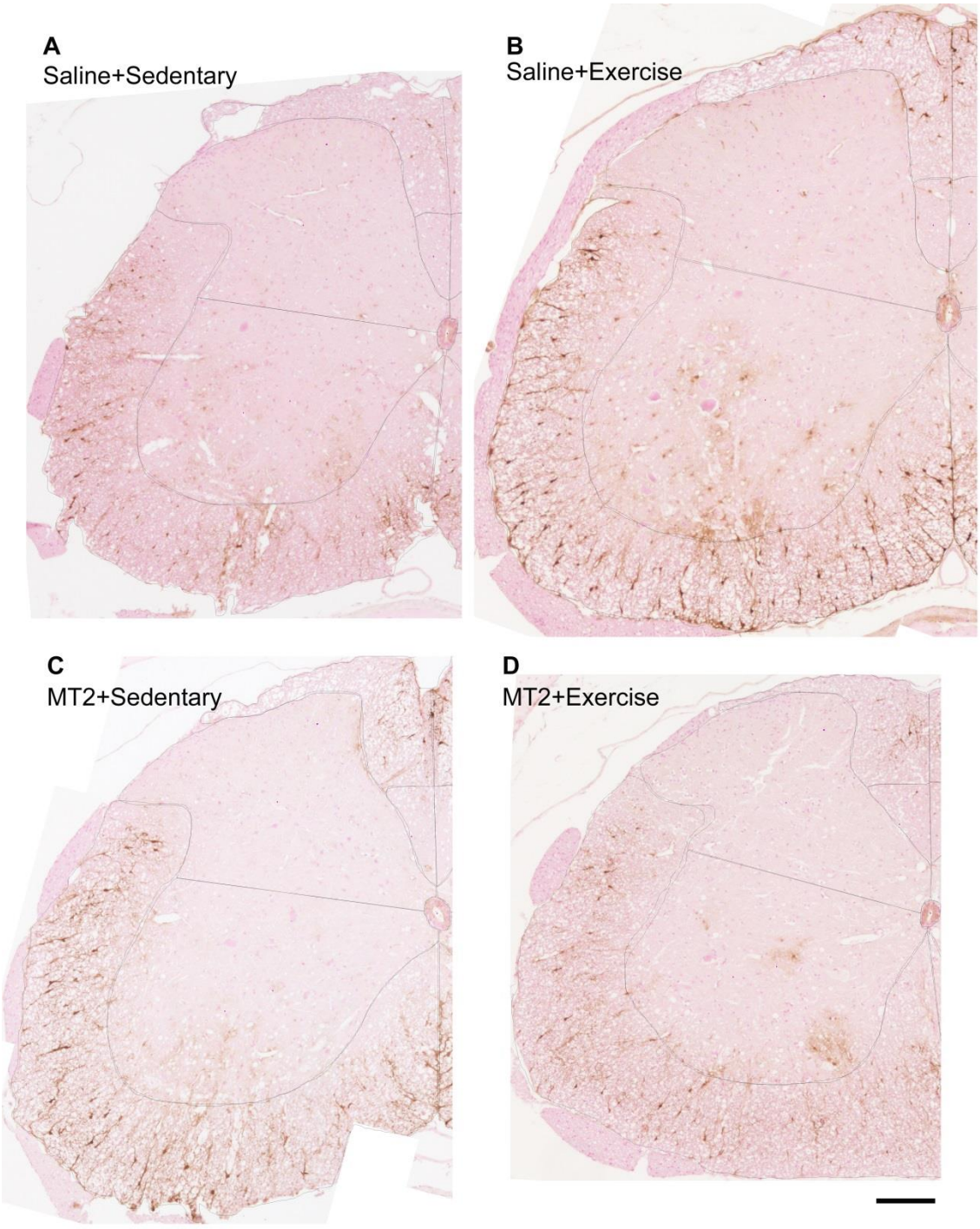

Figure 4.9 Representative images of MT-1/2 immunoreactivity in the spinal cord of MT2-treated and exercised SOD1 mice.

Representative images of the MT-1/2 immunoreactivity (DAB chromogen, positive immunoreactivity gives a brown precipitate). Representative images are shown from the spinal cord of Saline+Sedentary (A), Saline+Exercise (B), MT2+Sedentary (C) and MT2+Exercise (D) mice. Black lines denote region dividers (see Figure 4.10A). Scale bar is 150µm in A-D. Quantitation of MT-1/2-positive cells is presented in Figure 4.10.

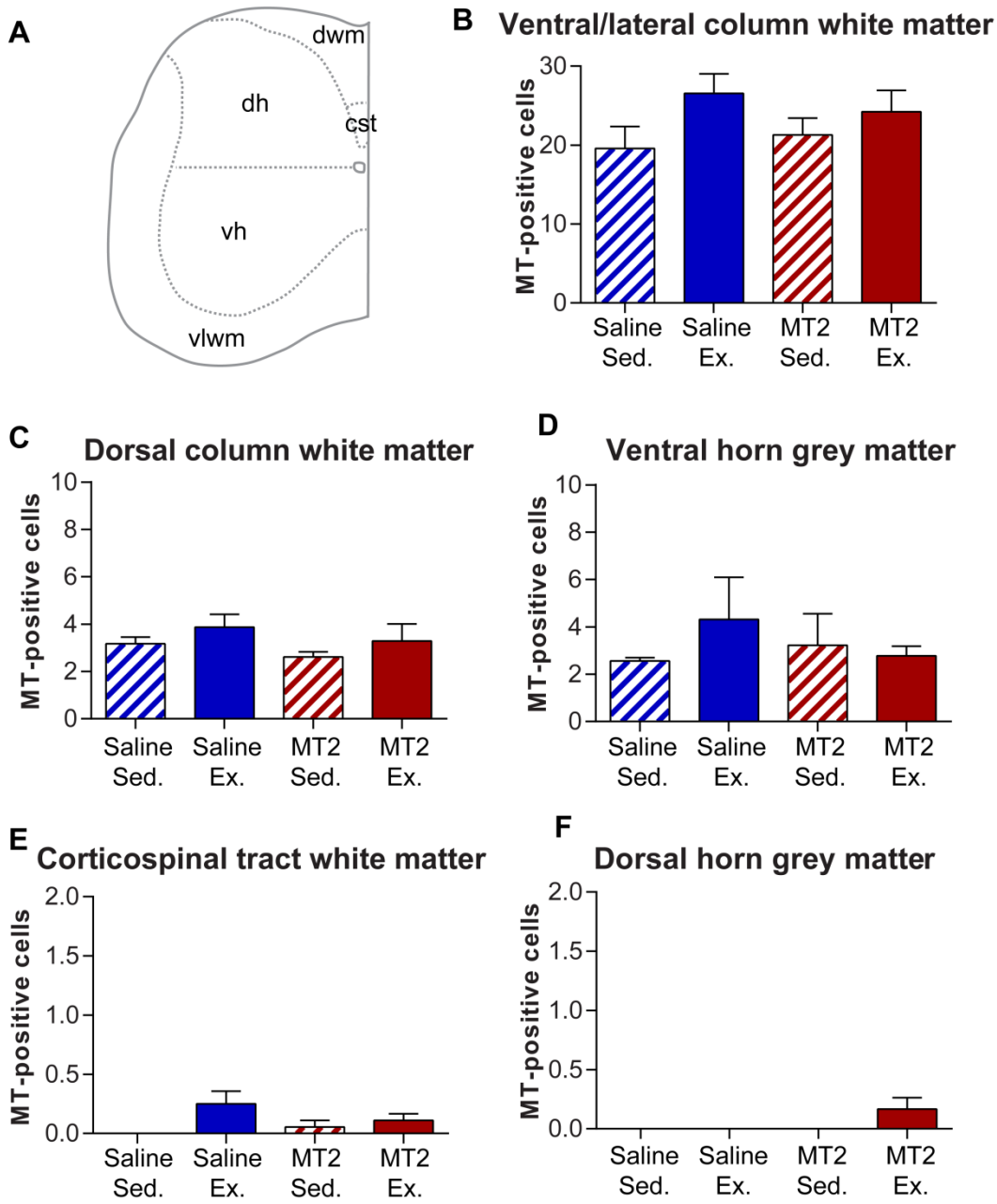

Figure 4.10 MT-1/2 immunostaining in MT2-treated and exercised SOD1 mice

MT-1/2-positive ('MT-positive') cells in different regions of the spinal cord (line drawing, A) were counted. The number of MT-1/2-positive cells in the white matter increased slightly with exercise but not with MT2 treatment (B,C). In the grey matter, exercise appeared to increase the number of MT-1/2-positive cells in saline-treated mice only (D). Few MT-1/2-positive cells were seen in the corticospinal tract or in the dorsal horn (E,F). dwm, dorsal column white matter; cst, corticospinal tract; dh, dorsal horn; vh, ventral horn; vlwm, ventral and lateral white matter; Ex., exercise; Sed., sedentary. Error bars represent standard error of the mean.

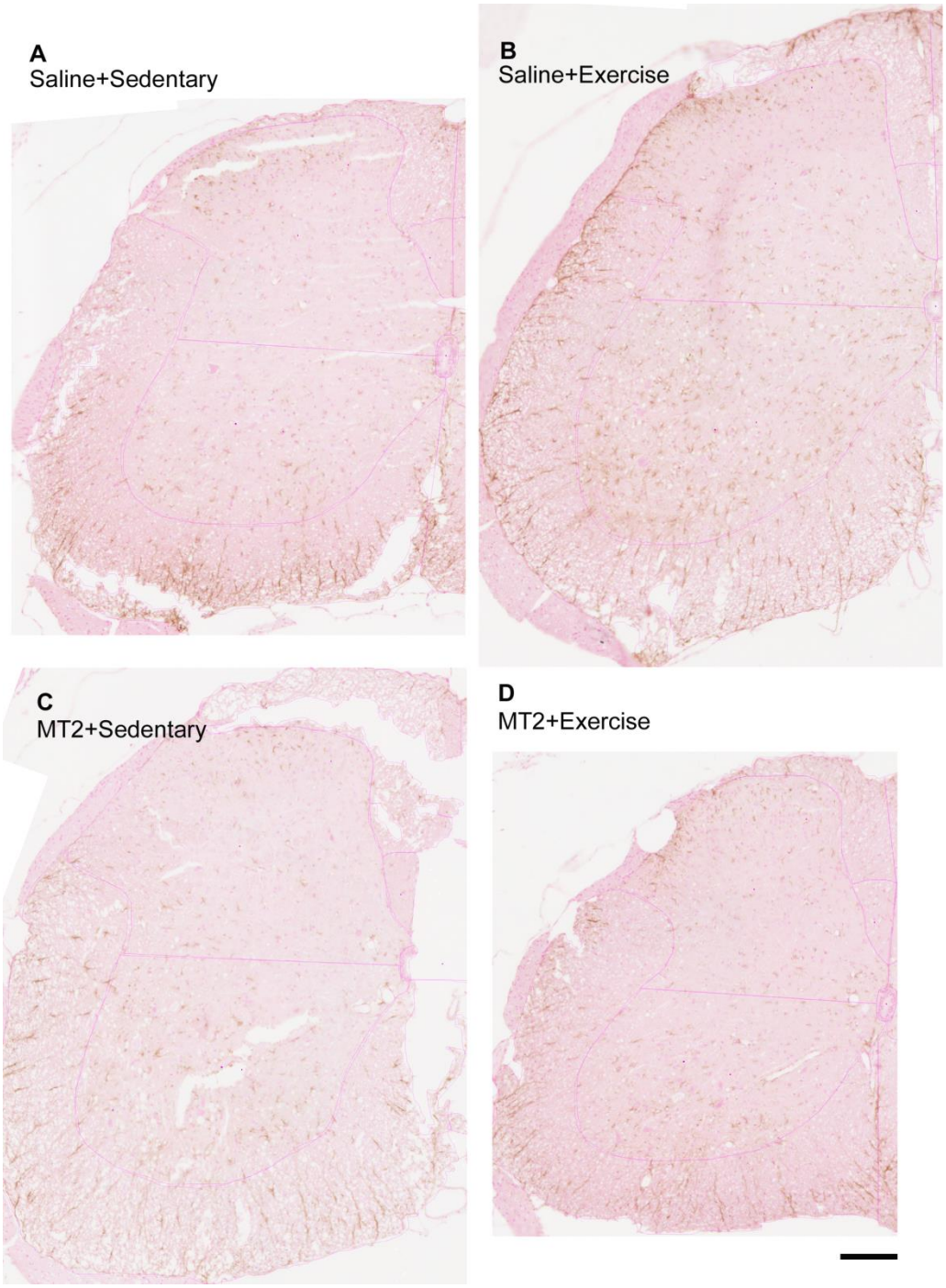

Figure 4.11 Representative images of GFAP immunoreactivity in the spinal cord of MT2-treated and exercised SOD1 mice.

Representative images of GFAP immunostaining with DAB chromogen are shown here for Saline+Sedentary (A), Saline+Exercise (B), MT2+Sedentary (C) and MT2+Exercise (D) treatment groups of SOD1 mice. Quantitation was performed and is presented in Figure 4.12. Scale bar is 150µm in A-D. Magenta lines denote regions in which GFAP-positive immunoreactivity was quantitated (see Figure 4.12F).

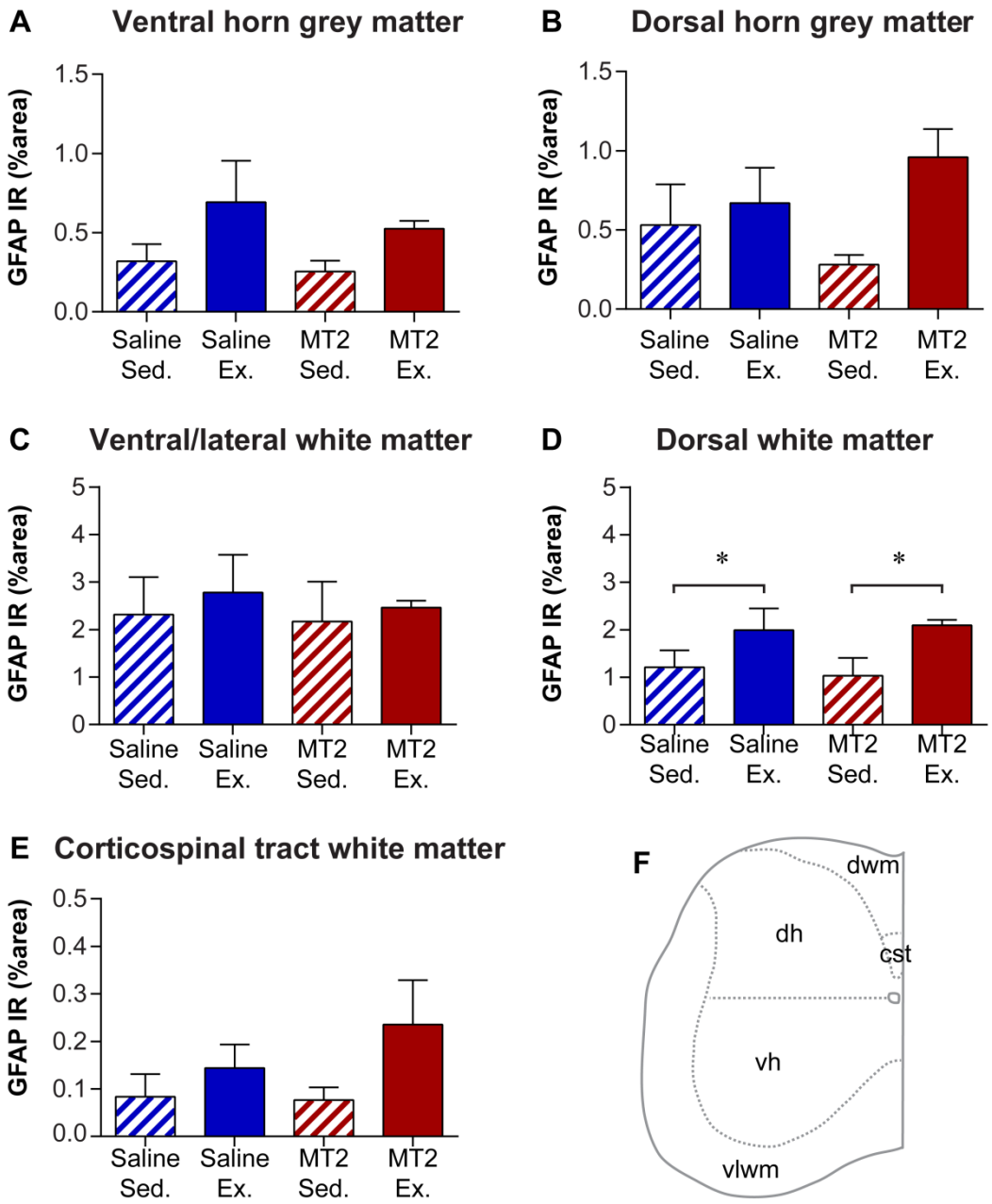

Figure 4.12 GFAP immunoreactivity in MT2-treated and exercised SOD1 mice

The astrocyte marker, GFAP, was detected by immunolabelling, and the amount of GFAP immunoreactivity (GFAP IR) was quantified using ImageJ and expressed as a percentage area of each spinal cord region (line drawing, F) displaying positive immunoreactivity. The percentage area displaying GFAP IR appeared to increase slightly with exercise in the ventral horn (A) and dorsal horn (B) grey matter, and in the dorsal (D) and corticospinal tract (E) white matter; no differences were seen in the ventral and lateral white matter with exercise (C). *$p<0.05$. dwm, dorsal column white matter; cst, corticospinal tract; dh, dorsal horn; vh, ventral horn; vlwm, ventral and lateral white matter; Ex., exercise; Sed., sedentary. Error bars represent standard error of the mean.

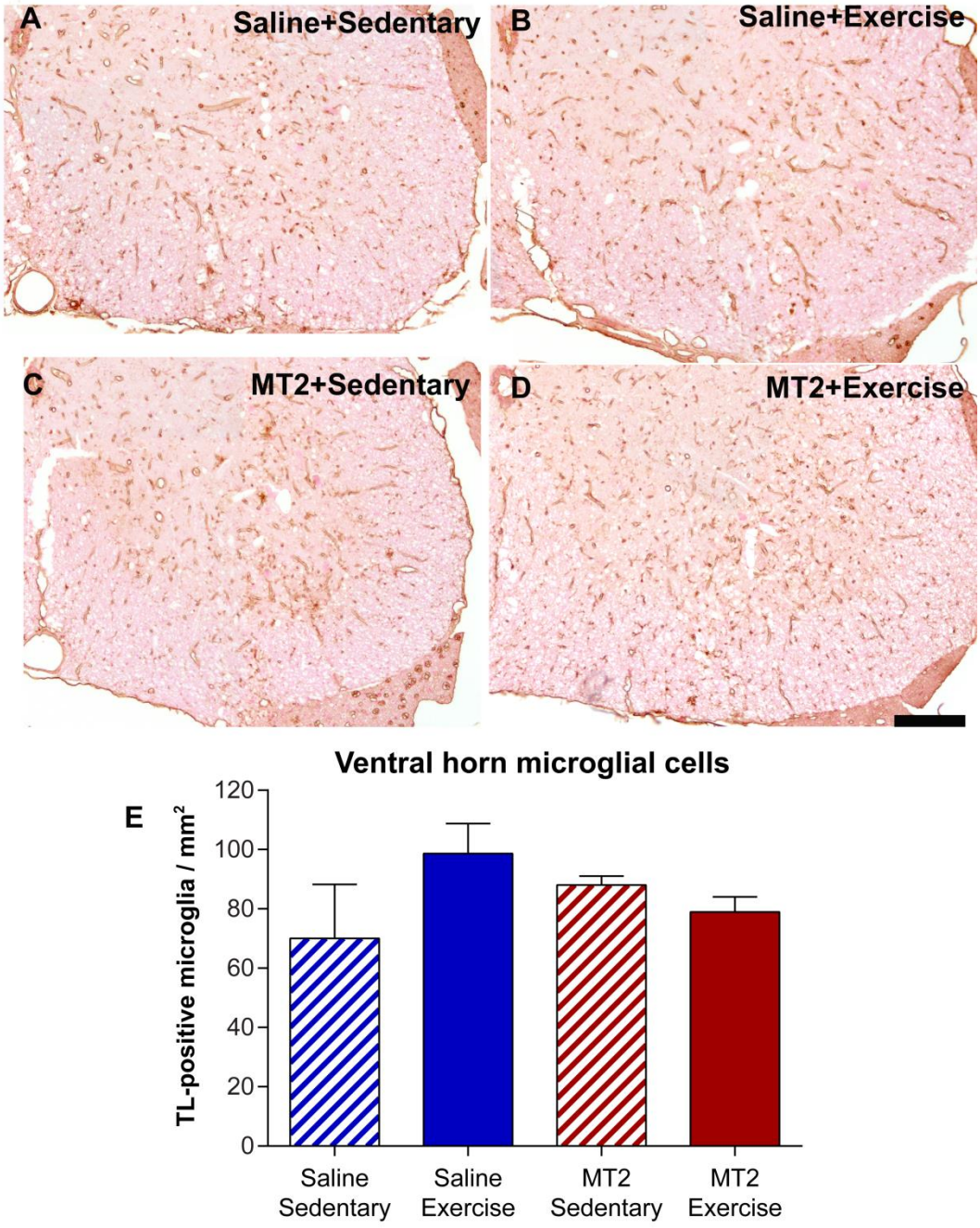

Figure 4.13 Tomato lectin labelling in MT2-treated and exercised SOD1 mice

Representative images of tomato lectin staining, labelling both blood vessels and microglia, are shown for the lumbar spinal cord of SOD1 mice in all four treatment groups (A-D). The number of microglial cells in the ventral horn was not significantly different between treatment groups at 17 weeks of age (E). However, the number of microglia did appear to increase slightly in response to exercise in saline-treated mice only. Error bars represent standard error of the mean. Scale bar is 150µm in A-D.

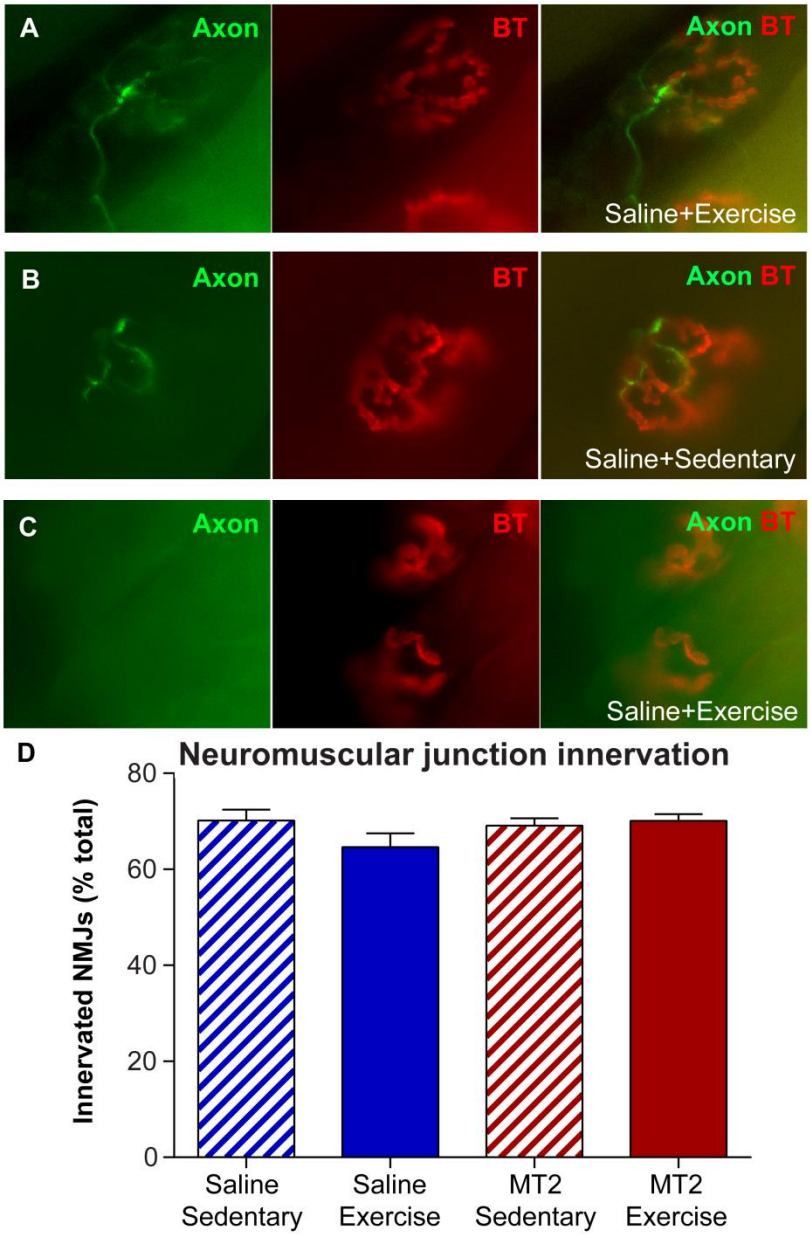

Figure 4.14 Neuromuscular junction innervation in MT2-treated and exercised SOD1 mice

Innervation was examined as colocalisation between α-bungarotoxin ("BT") and a cocktail of neuronal antibodies (synaptophysin, SMI32, SMI312, and tau, "Axon"). Examples of co-localisation between the axonal markers and α-bungarotoxin are given in panels A-C. Neuromuscular junctions either showed full or partial innervation via colocalisation between the two markers (A,B) or showed no colocalisation (C). Neither MT2 treatment nor exercise were able to significantly prevent denervation at the neuromuscular junction (NMJ) by 17 weeks of age (D). Error bars represent standard error of the mean.

4.4 Discussion

In this study, pre-symptomatic treatment with metallothionein-2A (MT2) and/or treadmill exercise were examined as potential therapies for delaying disease onset, ameliorating functional decline and increasing survival time in SOD1 mice. Pre-symptomatic MT2 treatment delayed disease onset as measured by the timing of peak body weight, and showed positive but non-significant effects on survival time (Figure 4.3, Figure 4.4). In contrast, pre-symptomatic treadmill exercise did not alter disease onset or survival time. Neither treatment substantially ameliorated disease progression as measured by stride pattern and wire hang duration (Figure 4.6, Figure 4.7). The mechanism of action for the MT2-mediated delay in disease onset and increase in survival remains as yet unknown, with no overt differences in motor neuron numbers, glial activation, or neuromuscular junction innervation as measured in this study (Figure 4.8, Figure 4.12, Figure 4.13, Figure 4.14). Potential mechanisms by which MT2 could maintain motor units, and strategies to maximise the protective effect of MT2 in future studies, are discussed below.

4.4.1 Metallothionein-2 as a potential therapeutic for ALS

The results of the current study show a delayed disease onset for MT2-treated mice, and a slight increase in survival time. These results are consistent with genetic studies showing that ablation of MT-1/2 leads to an accelerated disease progression and reduced survival in SOD1 mice (Nagano *et al.* 2001; Puttaparthi *et al.* 2002), while global over-expression of MT1 protein delayed the onset of disease symptoms and increased survival time in SOD1 mice (Tokuda *et al.* 2013). MT-1/2 has multiple putative functions as an antioxidant, a response to metal dyshomeostasis, and as a neuroprotectant following neuronal injury (West *et al.* 2008).

An advantageous feature of MT2 protein as a therapeutic for ALS is its multiple actions, which could counter multiple possible pathogenic processes in ALS. Conversely, this same feature makes it difficult to elucidate the exact mechanism of action by which MT2 may confer therapeutic benefits in SOD1 mice. As MT-1/2 can be internalised into cortical neurons (Chung *et al.* 2008b), the known intracellular and extracellular neuroprotective roles of MT-1/2, and how these properties may confer a protective role in ALS, will be discussed in the following sections.

4.4.1.1 Possible intracellular neuroprotective functions of MT2 in neurons

4.4.1.1.1 The antioxidant role of MT2

Oxidative stress appears to be central to ALS pathology (Barber & Shaw 2010). MT-1/2 shows potent antioxidant activity, and is able to release its metal ions in order to bind and sequester reactive oxygen species such as superoxide and hydroxyl radicals (Thornalley & Vasak 1985; Abel & de Ruiter 1989). MT-1/2 is also able to bind NO and peroxynitrite *in vitro*, but as this interaction is suppressed by physiological levels of reduced glutathione, it is as yet unclear whether MT-1/2 can sequester harmful NO and peroxynitrite species *in vivo* (Khatai *et al.* 2004). An MT2-mediated reduction of oxidative stress in the pre-symptomatic phase of SOD1 mice may delay the accumulation of oxidatively-damaged proteins and mRNA, preventing the development of downstream disease-related pathologies such as protein aggregation. The putative role of MT2 in scavenging NO and peroxynitrite would be very interesting to examine in more detail in ALS, due to the observed induction of iNOS in SOD1 spinal cord microglia with disease progression (see Chapter 2), and the reports of protein tyrosine nitration in ALS (Sasaki *et al.* 2000).

4.4.1.1.2 The role of MT2 in metal homeostasis

MT2 is a metal-binding protein, with each MT2 molecule capable of binding up to 7 divalent metal ions or up to 12 monovalent metal ions, through thiol linkages on cysteine residues (Hamer 1986) (Figure 4.1). Sporadic ALS has been associated with exposure to heavy metals in epidemiological studies (Trojsi *et al.* 2013), while laboratory studies have showed higher levels of heavy metals in the spinal cord motor neurons of ALS patients than non-ALS controls (Pamphlett & Kum Jew 2013). Elevated levels of copper, zinc, magnesium, iron, cadmium, lead, aluminium, manganese, vanadium and uranium have been identified in the CSF and serum of ALS patients in various studies (Hozumi *et al.* 2011; Roos *et al.* 2013), suggesting that environmental exposures to metals, or dyshomeostasis of physiological metals such as zinc and copper, may contribute to the development of ALS.

Elevated levels of redox-active metals, such as copper, are particularly damaging in the nervous system via the aberrant production of reactive oxygen species (Scheiber *et al.* 2014). The presence of elevated copper levels may also apply to familial ALS, with SOD1 mice showing a shift towards copper accumulation in the spinal cord by

alteration of copper-trafficking pathways (Tokuda *et al.* 2009). One potential neuroprotective role of MT2 may be to sequester free copper ions and prevent metal-mediated production of ROS; a previous study has shown a similar MT isoform, MT-3, is able to exchange its bound zinc ions for copper ions, silencing the redox-active copper ions (Meloni *et al.* 2007). Indeed, over-expression of MT1 in SOD1 mice normalises elevated levels of copper in the SOD1 spinal cord (Tokuda *et al.* 2013).

An alternative, more speculative, action for MT2 may be ensuring correct metallation of mutant SOD1 protein. The metallation status of SOD1 modulates its neurotoxic properties (Banci *et al.* 2008), with mutant SOD1 proteins and zinc-deficient wild-type SOD1 protein showing similar propensity for aggregation and activation of ER stress responses (Rakhit *et al.* 2002; Homma *et al.* 2013). Zinc-loaded MT-1/2 is thought to be involved in the supply of zinc ions for zinc-binding proteins such as the MTF-1 transcription factor (Zhang *et al.* 2003); if MT2 were able to facilitate the constitution of nascent mutant SOD1 with zinc, the aggregation of mutant SOD1 may be attenuated (Lelie *et al.* 2011).

Thus, the metal-binding abilities of MT2 may mediate its beneficial effects in SOD1 mice (Tokuda *et al.* 2013). This result would be in line with other copper-modulating compounds also having shown beneficial effects in the SOD1 mouse model of ALS (Soon *et al.* 2011; Parker *et al.* 2012).

4.4.1.1.3 Internalisation via low-density lipoprotein receptor related proteins

In order for MT2 to elicit intracellular effects, MT2 must be internalised into motor neurons. MT-1/2 is known to be internalised by transmembrane low-density lipoprotein receptor-related proteins (LRP1 and LRP2) by endocytosis in both kidney tubule cells (Erfurt *et al.* 2003; Klassen *et al.* 2004) and cultured cortical neurons (Chung *et al.* 2008b). Preliminary data indicates that motor neurons in the mouse spinal cord express LRP2 (Nicholas Blackburn, unpublished observations). LRP1- and LRP2-mediated endocytosis is thought to be mostly clathrin-dependent, leading to lysosomal degradation of endosome contents (Harasaki *et al.* 2005; Buchackert *et al.* 2012). The metals bound to endosomal MT2 may become liberated upon the fusion with lysosomes, due to the drop in pH; these free metals may enter the cytosol (Hao *et al.* 2007) and may stimulate the synthesis of new MT-1/2 molecules (Richards *et al.* 1984), with the overall effect of raising cellular MT-1/2 levels.

More speculatively, LRP1 can be recruited for caveolae-mediated endocytosis in adipocytes and hepatocytes (Zhang *et al.* 2004; Kanai *et al.* 2014); if these mechanisms are also present in motor neurons, it may be possible that an LRP1-MT2 complex could be internalised via non-classical endocytosis involving caveolae or lipid rafts (Hao *et al.* 2007), potentially avoiding the lysosomal degradation pathway (Kiss & Botos 2009). Regardless of whether MT2 enters the cell intact, or releases its metals upon lysosomal degradation to stimulate *de novo* MT-1/2 synthesis, the intracellular level of MT-1/2 is likely to be increased upon LRP-mediated internalisation of MT2.

4.4.1.2 Possible extracellular neuroprotective action of MT2 on neurons

MT-1/2 is known to act extracellularly on neuronal cell bodies to induce neurite outgrowth through interaction with LRP1 and LRP2 (Fitzgerald *et al.* 2007; Chung *et al.* 2008b). The cytoplasmic portion of LRP1 protein contains signal transduction motifs, and is potentially involved in both endocytosis and intracellular signalling (Boucher & Gotthardt 2004). Thus, the interaction between MT2 and LRPs may induce neuroprotection via the activation of downstream signalling pathways, in addition to the intracellular roles for LRP-internalised MT2 discussed above.

In cerebellar granule neurons, MT-1/2-LRP interactions activate pro-survival and pro-outgrowth PI3K/Akt and MAPK/ERK pathways (Dudek *et al.* 1997; Chang & Karin 2001), activate the pro-survival transcription factor CREB (Walton & Dragunow 2000), and dephosphorylate the pro-apoptotic factor Jun (Ham *et al.* 2000). Hence, LRP-mediated activation of pro-survival and pro-outgrowth pathways upon MT2 binding may represent a possible pathway for maintaining neuronal function in ALS.

4.4.1.3 A role for MT2 at the neuromuscular junction?

The combined intraneuronal and extracellular actions of MT-1/2 provide a putative mechanism by which motor neurons are protected, and disease onset is delayed, by MT2 treatment in SOD1 mice. However, no differences in the number of Nissl-stained motor neurons were seen between MT2-treated and control SOD1 mice at 17 weeks of age (Figure 4.8), indicating that the actions of MT2 did not prevent death of motor neuron cell bodies, or indicating that little data about neuronal health can be gleaned from the Nissl stain alone. Markers of neuronal apoptotic status, such as the presence of cleaved caspases, should also be examined in MT2-treated and exercised SOD1 mice, in order to give more detail about the potential mechanism of action of MT2.

Given no obvious protection of motor neuron cell bodies, it is possible that MT2 affected the motor unit at the neuromuscular junction (NMJ). The stimulation of LRPs by MT-1/2 induces neurite outgrowth in cultured neurons, and reactive sprouting in injured neurons (Chung *et al.* 2003; Fitzgerald *et al.* 2007). Motor neurons in ALS demonstrate compensatory plasticity at the NMJ, with re-innervation of denervated NMJs by neighbouring motor units in order to maintain function (Stalberg *et al.* 1975; Gurney *et al.* 1994). Any MT2-mediated increase in sprouting at the distal motor axon might enhance compensatory re-innervation, maintaining muscular connections and delaying the loss of body weight caused by denervation and muscle atrophy.

The current study showed no difference in the percentage of innervated neuromuscular junctions between treatment groups (Figure 4.14), which would argue against increased re-innervation by MT2 treatment. However, this study only looked at the percentage of NMJs showing any neuronal innervation; a more detailed assessment of the degree of colocalisation between pre- and post-synaptic NMJ components in individual NMJs may help to detect differences between treatment groups. Intriguingly, another member of the LRP family, LRP4, is involved in neuromuscular junction formation and maintenance through agrin and Musk signalling (Kim *et al.* 2008; Zhang *et al.* 2008); one could speculate that MT2, if found to be a ligand of LRP4, might play a direct role in neuromuscular junction dynamics at the muscle.

4.4.1.4 A role for MT2 in regulating glial phenotype?

Activation of astrocytes and microglia is a pathological feature of ALS (see Chapter 1 and Chapter 2). MT-1/2 may play a role in modulating astrocytic activation in cell culture and in response to focal brain injury (Chung *et al.* 2003; Leung *et al.* 2010). MT-1/2 may also modulate microglial activation and attenuate development of a neurotoxic microglial phenotype (Potter *et al.* 2007; Chung *et al.* 2009), and affect the phenotype of circulating monocytes (Pankhurst *et al.* 2011). Over-expression of MT1 in SOD1 mice has been reported to ameliorate astrocytic pathology (Tokuda *et al.* 2013). While there were no differences between astroglial and microglial numbers measured in MT2-treated and control SOD1 mice at the conclusion of treatment in the current study (Figure 4.12, Figure 4.13), markers of M1 and M2 microglial phenotypes were not examined in MT2-treated mice, and might provide clues as to the action of MT2 in SOD1 mice.

4.4.1.5 Timing and delivery of MT

In this study, pre-symptomatic MT2 treatment delayed disease onset and slightly increased survival time. However, the magnitude of the MT2-induced changes was small: disease onset was delayed by approximately 4%, while survival time was increased by approximately 3%. The small effect of MT2 may be due to the timing of treatment in this study, or due to insufficient delivery of MT2 to the CNS. Had MT2 treatment been maintained until disease endpoint, rather than stopping after 16 weeks of age, the effects of MT2 treatment on survival time may have been more pronounced. In particular, it was recently reported that the over-expression of MT1 in SOD1 mice was particularly effective in extending the duration of the later phase of disease; measured between the loss of 10% from peak body weight and disease endpoint (Tokuda *et al.* 2013). Therefore, continued MT2 injections during the symptomatic stage of disease may have resulted in significant improvements in SOD1 survival.

Alternatively, intramuscular injection may not efficiently deliver MT2 to the CNS. MT2 rapidly enters the circulation after intramuscular injection, but does not readily enter the CNS when the BBB is intact, and is cleared through the renal system (Lewis *et al.* 2012b). SOD1 mice show evidence of compromised BBB integrity in both pre-symptomatic and symptomatic stages of disease (Garbuzova-Davis *et al.* 2007; Zhong *et al.* 2008), potentially facilitating the CNS entry of systemically-administered therapeutics such as MT2. The number of MT-1/2-positive cells in the spinal cord was not significantly greater after MT2 administration (Figure 4.10); however, the diffuse immunoreactivity thought to be extracellular MT-1/2 was not quantified in this study, and future work will determine whether MT2 administration increases extracellular MT-1/2 levels. The beneficial survival effects seen by Tokuda (2013) upon MT1 over-expression in SOD1 mice, where spinal cord MT1 levels were consistently elevated, were not seen to the same extent in the current study; exogenous MT2 injection may provide only transient elevations in spinal cord MT2 levels.

Given that the number of MT-1/2-positive cells was not drastically increased following intramuscular MT2 treatment in this study, yet some positive effects on survival and disease onset were seen, the non-CNS activity of MT2 may need further exploration. As disease onset and survival parameters are both linked to body weight, it could be suggested that MT2 has some effect on body weight which is independent of CNS motor neuron counts or muscular innervation and mass. However, this is unlikely to be

the case, as Figure 4.4 shows that MT2-treated mice had virtually identical body weights compared with saline-treated mice between 6 and 14 weeks of age, during the treatment window in which MT2 was administered – this argues against a generalised body weight increase caused by MT2. Rather, after 14 weeks of age, MT2-treated mice retained their body weight slightly longer than saline-treated mice, delaying the muscle mass loss caused by disease processes (Figure 4.4). MT-1/2 expression is known to protect cardiac muscle after ischaemia/reperfusion injury (Wang *et al.* 2006); we may speculate that the injected MT2 in this study did have some direct protection on the skeletal muscles in the SOD1 hindlimb, but whether the protective mechanisms in cardiac muscle are also present in skeletal muscle are unknown.

To avoid the issue of insufficient MT2 delivery to the CNS, it may be possible to use small peptides based on the sequence of human MT2 as therapeutics for ALS. These peptides, termed 'Emtins', show effects on the outgrowth of cortical neurons similar to those seen with MT-1/2, and have the added advantage of being BBB-permeable (Ambjorn *et al.* 2008; Asmussen *et al.* 2009a; Sonn *et al.* 2010). The use of Emtin peptides in SOD1 mice will be explored in Chapter 5.

4.4.2 Exercise as a potential therapy for ALS

The role of exercise in ALS is controversial – on one hand, high levels of physical activity are correlated with the development of ALS in epidemiological studies (Beghi *et al.* 2010; Huisman *et al.* 2013), and on the other hand there are numerous case studies and small trials showing that exercise therapy may help to ameliorate disease progression to a small extent in ALS patients (Bohannon 1983; Johnson 1988; Dal Bello-Haas *et al.* 2007; Sanjak *et al.* 2010). In the current study, pre-symptomatic treadmill exercise had no significant impact on disease onset and survival time in female SOD1 mice, showing neither beneficial nor detrimental effects. However, exercised mice did show slightly increased stride length compared to sedentary mice at a few select time points in disease progression (Figure 4.6). Although this increase in stride length is not clear evidence of a protective effect, this suggests that moderate treadmill exercise is, at least, not detrimental to SOD1 mice.

4.4.2.1 Previous exercise studies in ALS mice

Previous studies of exercise in SOD1 mice have shown varying outcomes, depending on the type of exercise, the intensity of the exercise, mouse gender, and whether or not the effects of environmental enrichment were controlled for. Generally, moderate-intensity treadmill exercise has shown marginal to moderate beneficial effects on survival time, disease onset, and functional parameters when started pre-symptomatically in SOD1 mice (Kirkinezos *et al.* 2003; Veldink *et al.* 2003; Liebetanz *et al.* 2004; Sorrells *et al.* 2009; Carreras *et al.* 2010).

Wheel-running exercise and swimming exercise have also shown beneficial effects for survival of SOD1 mice (Kaspar *et al.* 2005; Deforges *et al.* 2009; Sorrells *et al.* 2009), with wheel-running mice showing increased survival even when exercise was started around the onset of disease symptoms (Kaspar *et al.* 2005). In contrast, high-intensity or forced exercise has shown detrimental effects on survival in SOD1 mice (Mahoney *et al.* 2004). The exercise intensity in the present study was designated as 'moderate' – similar to that used in two previous studies which showed beneficially effects of exercise in SOD1 mice (Kirkinezos *et al.* 2003; Carreras *et al.* 2010). However, mindful that forced running had a detrimental effect on SOD1 mouse survival (Mahoney *et al.* 2004), mice in the current study were encouraged but not forced to keep running on the treadmill – thus, the exercise intensity may not have been high enough to elicit protective effects.

Environmental enrichment may also contribute to the apparent effects of exercise seen in previous studies – SOD1 mice exposed to a novel exercise environment, without undergoing exercise, showed longer survival times than mice not exposed to the novel environment (Sorrells *et al.* 2009; Gerber *et al.* 2012). In a treadmill exercise study which controlled for environmental enrichment by placing mouse on a stationary treadmill, no effect of exercise was seen on survival of SOD1 mice (Deforges *et al.* 2009). The current study also controlled for effects of environmental enrichment by placing mice on a stationary treadmill, and saw no significant effects of exercise on survival times. Thus environmental enrichment may play some role in determining survival time, although the biochemical mechanisms behind these effects remain to be elucidated.

Gender and background strain, and interactions between the two, are known to affect SOD1 mouse survival time (Heiman-Patterson *et al.* 2005). Most previous studies on exercise in SOD1 mice involved mice with expression of the SOD1 transgene on a hybrid B6SJL genetic background, and most studies looked at the effects of exercise in male mice alone, with a few looking at a mix of male and female mice. Previous studies involving both female and male SOD1 mice have shown differing responses to exercise between the genders: three studies indicate male SOD1 mice respond more strongly to exercise than their female counterparts, regardless of whether exercise has a beneficial effect (Kirkinezos *et al.* 2003; Kaspar *et al.* 2005) or a detrimental effect (Mahoney *et al.* 2004). In contrast, another study showed exercise had a beneficial effect on survival in female but not male SOD1 mice (Veldink *et al.* 2003). To the best of my knowledge, the current study is the first to examine the effect of exercise in female SOD1 mice on a congenic B6 genetic background. As male mice were not tested in the present study, there may be an unknown effect of gender, or an interaction between gender and genetic background, which results in female SOD1 mice on a congenic B6 background being unresponsive to exercise treatment.

To further examine the effects of exercise in female SOD1 mice on a congenic B6 background, adaptations of the skeletal muscle to exercise should be examined in detail. As mentioned previously, the percentage innervation of neuromuscular junctions in the muscle was not significantly different between treatment groups (Figure 4.14). However, one of the beneficial effects of swimming exercise in SOD1 mice is the conversion of muscle fibre types from fast-twitch fibres to slow-twitch fibres (Deforges *et al.* 2009); slow-twitch fibres are more resistant to denervation and atrophy in SOD1-mediated ALS than fast-twitch fibres (Hegedus *et al.* 2008). Analysis of the muscle fibre type profile of exercised and non-exercised female SOD1 mice might help to determine whether moderate-intensity treadmill exercise does induce a protective conversion of muscle fibre types in SOD1 muscle.

4.4.2.2 Exercise and MT-1/2 induction

Part of the original rationale for examining exercise was the apparent upregulation of MT-1/2 in response to exercise in wild-type mouse spinal cord (Hashimoto *et al.* 2009). In the present study, the number of spinal cord MT-1/2-positive cells appeared slightly higher in the ventral/lateral and dorsal white matter compared to sedentary controls, but these changes were not significant and were not present in the ventral horn (Figure

4.10). While the quantitative level of MT-1/2 expression was not directly tested in this study (for example, with western blotting or RT-PCR), Hashimoto and colleagues (2009) saw a widespread increase in both the total spinal cord MT-1/2 levels and in the number of cells displaying strong MT-1/2 immunoreactivity following a two week treadmill exercise program in WT mice (Hashimoto *et al.* 2009). Although it cannot be definitively stated that exercise failed to increase MT-1/2 levels in the current study due to the lack of direct testing by western blot, the fact that the number of MT-1/2-positive cells did not drastically increase with exercise hints that exercise at the intensity used in the current study may not be sufficient to increase the production of MT-1/2 in the spinal cord above that seen with increased duration of disease (Chapter 2, Figure 2.7).

The lack of MT-1/2 upregulation with exercise in the current study may correlate with the minimal effects of exercise on survival time; however, MT-1/2 is unlikely to be the sole factor responsible for any exercise-mediated increase in SOD1 survival. Several other factors, indcluding muscle fibre type switching (Deforges *et al.* 2009), or the production of BDNF and IGF1 (Kaspar *et al.* 2005; Carreras *et al.* 2010) are likely responsible for the exercise-mediated increase in survival time seen in previous studies (McCrate & Kaspar 2008).

Interestingly, a possible interaction might exist between MT2 and exercise which does not involve upregulation of MT-1/2 in the spinal cord. The age at disease onset, as calculated from linear mixed modelling, was later in exercised MT2-treated mice than in sedentary MT2-treated mice, but was not affected by exercise in saline-treated mice (Figure 4.4D). Exercise has been reported to enhance LRP2 expression at the choroid plexus, to transport circulating IGF1 into the brain (Carro *et al.* 2005). As LRP2 is also a receptor for MT2 protein (Klassen *et al.* 2004), exercise may also facilitate the entry of MT2 into the central nervous system. As mentioned previously, examination of the spinal cord diffuse MT-1/2 immunolabelling, thought to represent extracellular MT-1/2, may determine whether exercise facilitates spinal cord entry of circulating MT2.

4.4.2.3 Exercise in ALS patients

The majority of studies in SOD1 mouse models of ALS show slight beneficial effects of moderate-intensity exercise. These correspond well with several small studies showing slight delays in disease progression in ALS patients treated with exercise-based therapies, with few adverse effects (Drory *et al.* 2001; Dal Bello-Haas *et al.* 2007; Lui

& Byl 2009; Sanjak *et al.* 2010). Exercise and physical therapy have been implicated as an important component of multidisciplinary care for ALS patients, in order to strengthen remaining muscles, maintain range of motion, and help combat stiffness and cramping in affected muscles (de Almeida *et al.* 2012; Skalsky & McDonald 2012; Arbesman & Sheard 2014).

The potential beneficial effects of exercise in ALS patients are in contrast to epidemiological studies implicating high levels of physical activity as a risk factor for ALS (Beghi *et al.* 2010; Lehman *et al.* 2012; Huisman *et al.* 2013). However, the absence of a dose-response effect for increasing levels of exercise somewhat attenuates direct causality between physical activity and ALS (Huisman *et al.* 2013). An alternate theory proposes that the genetic profiles which naturally confer some higher level of body fitness may also predispose to ALS (Chio & Mora 2012; Mattsson *et al.* 2012). Thus, rather than physical activity directly causing ALS, it may be that those with a genetic risk profile conferring susceptibility to ALS are also more likely to engage in exercise-based leisure-time activities, or lean towards careers involving physical exertion such as professional sports (Lehman *et al.* 2012) or military service (Weisskopf *et al.* 2005).

4.4.3 Summary and conclusions

In summary, this proof-of-concept study reports that pre-symptomatic MT2 treatment resulted in a slight delay in disease onset and tended to increase survival time in female SOD1 mice, while exercise failed to show significant effects on disease onset or survival. No consistent synergistic effects were observed between MT2 treatment and exercise in SOD1 mice.

The current study showed no detrimental effects of moderate-intensity treadmill exercise on SOD1 mice, and is consistent with the concept that physical exercise is not causative of ALS; rather, as-yet-unknown genetic factors may predispose to both a lifestyle involving high levels of physical activity, and the development of ALS. In this context, low-intensity to moderate-intensity exercise may be beneficial for ALS patients by providing a minor neuroprotective effect, and for maintaining strength and range of motion around affected muscle groups. However, caution should be used to avoid strenuous exercise which could potentially accelerate disease progression.

While MT2 has a solid theoretical basis for attenuating multiple pathological pathways present in ALS, the small magnitude of the effects may be due to the timing and delivery method of MT2 administration. Administration of MT2 directly to the central nervous system through intracerebroventricular injection or intrathecal pump, or via viral delivery, to deliver a consistent amount of MT2, may produce more pronounced effects on SOD1 mouse survival. Additionally, treatment beginning after the onset of disease symptoms is needed to confirm the survival-extending properties of MT2 and evaluate the use of MT2 as a potential therapeutic molecule for human ALS. To this end, the effects of a peptide analogue of MT2 will be discussed in Chapter 5.

Chapter 5

Emtin peptides as therapeutic molecules in SOD1 mice – a pilot study

5.1 Background

5.1.1 Emtin peptides

Metallothionein-2 (MT2) provides a promising therapeutic candidate for extending survival when administered pre-symptomatically to SOD1 mice, as discussed in the previous chapter. However, MT2 does not readily access the CNS when injected either intraperitoneally or intramuscularly (Lewis *et al.* 2012b). Emtin peptides, synthetic derivatives of MT2, are able to cross the BBB and have similar *in vitro* effects to MT2 protein (Ambjorn *et al.* 2008; Asmussen *et al.* 2009a; Sonn *et al.* 2010). Thus, Emtin peptides may present a therapeutic alternative to MT2 protein.

5.1.1.1 Emtin structure

Each of the Emtin peptide monomers consists of 14 amino acids, with the sequence derived from the human MT2A protein (Swiss Protein Database P02795). Four Emtin peptides have been synthesised (Schafer-N, Copenhagen, Denmark) to date: EmtinBn, based on the MT2 β-domain N-terminal sequence; EmtinB, based on the MT2 β-domain C-terminal sequence; EmtinAn, based on the MT2 α-domain N-terminal sequence; and EmtinAc, based on the MT2 α-domain C-terminal sequence (Table 5.1) (Ambjorn *et al.* 2008; Asmussen *et al.* 2009a). Some of the cysteine residues in the parent MT2 protein sequence have been replaced with serine residues in the corresponding Emtin peptide, as indicated in Table 5.1, to prevent cysteine/disulphide-mediated crosslinking of Emtin peptides in solution (Asmussen *et al.* 2009a).

Table 5.1 Amino acid sequences of human MT2A protein and Emtin peptides

	Human MT2A sequence	Monomeric Emtin sequence
EmtinAc*	45-AQGCICKGASDKCS	AQG**S**ICKGASDK**S**S
EmtinAn	30-KKSCCSCCPVGCAK	KKS**S**CSC**S**PVG**S**AK
EmtinB*	15-CAGSCKCKECKCTS	**S**AGSCKCKE**S**K**S**TS
EmtinBn	1-MDPNCSCAAGDSCT	MDPNCSCAAGDS**S**T

*EmtinAc and EmtinB were tested in the present study. The portion of human MT2A isoform protein sequence (Swiss Protein Database P02795) on which each Emtin peptide sequence was based is provided for comparison; replacement of cysteine residues in the MT2A sequence with serine residues in the Emtin sequence is denoted by bold, underlined text.

Emtin peptides can be synthesised either as monomers, dimers (two identical monomers coupled to a lysine residue) or tetramers (four identical monomers coupled to a lysine backbone) (Figure 5.1). The probable structure of Emtin tetramers, as predicted by PROFASI protein folding simulation, appeared to be unstructured (Ambjorn *et al.* 2008). The currently-published literature relates solely to tetrameric Emtin peptides; hereafter, the generic term 'Emtin' relates to tetrameric Emtin peptides unless otherwise specified.

5.1.1.2 Properties of Emtin peptides

Due to the replacement of cysteine residues with serine residues, the Emtin peptides may be less able to bind metals and sequester reactive oxygen species than the MT2 protein from which their sequence is derived (Ambjorn *et al.* 2008). Despite these differences, the Emtins exhibit similar neuroprotective properties to the MT2 protein. All four Emtin peptides prevent cultured cerebellar granule neurons (CGNs) from undergoing apoptosis in response to potassium withdrawal from the medium (Ambjorn *et al.* 2008; Asmussen *et al.* 2009a). EmtinB also protected cultured hippocampal neurons from kainic acid excitotoxicity *in vitro*, and attenuated seizure severity and hippocampal neuron death induced by kainic acid treatment of mice (Sonn *et al.* 2010). In addition, EmtinAc, EmtinAn, and EmtinB were able to induce neurite outgrowth in cultured CGNs (Ambjorn *et al.* 2008; Asmussen *et al.* 2009a). These data show that Emtin peptides, like MT-1/2, can increase survival of neurons exposed to toxic insults and can also promote neurite outgrowth.

Extracellular MT-1/2 exerts its growth-promoting and survival effects via the LRP proteins low-density lipoprotein receptor-related proteins (LRP1 and LRP2) (Fitzgerald *et al.* 2007; Chung *et al.* 2008b). The outgrowth and survival effects of EmtinAc, EmtinBn, and EmtinB, but not of EmtinAc, were blocked by receptor-associated protein (RAP), a chaperone and competitive inhibitor of LRPs, and EmtinB binding to both LRP1 and LRP2 has been demonstrated *in vitro* (Ambjorn *et al.* 2008; Asmussen *et al.* 2009a). The binding of EmtinB, EmtinAc, and EmtinAn to LRPs induces the downstream activation of MAPK, Akt, and CREB (Ambjorn *et al.* 2008; Asmussen *et al.* 2009a); these are the same neuroprotective pathways activated by MT2-LRP interactions, indicating common neuroprotective mechanisms between MT2 and Emtins (Asmussen *et al.* 2009b).

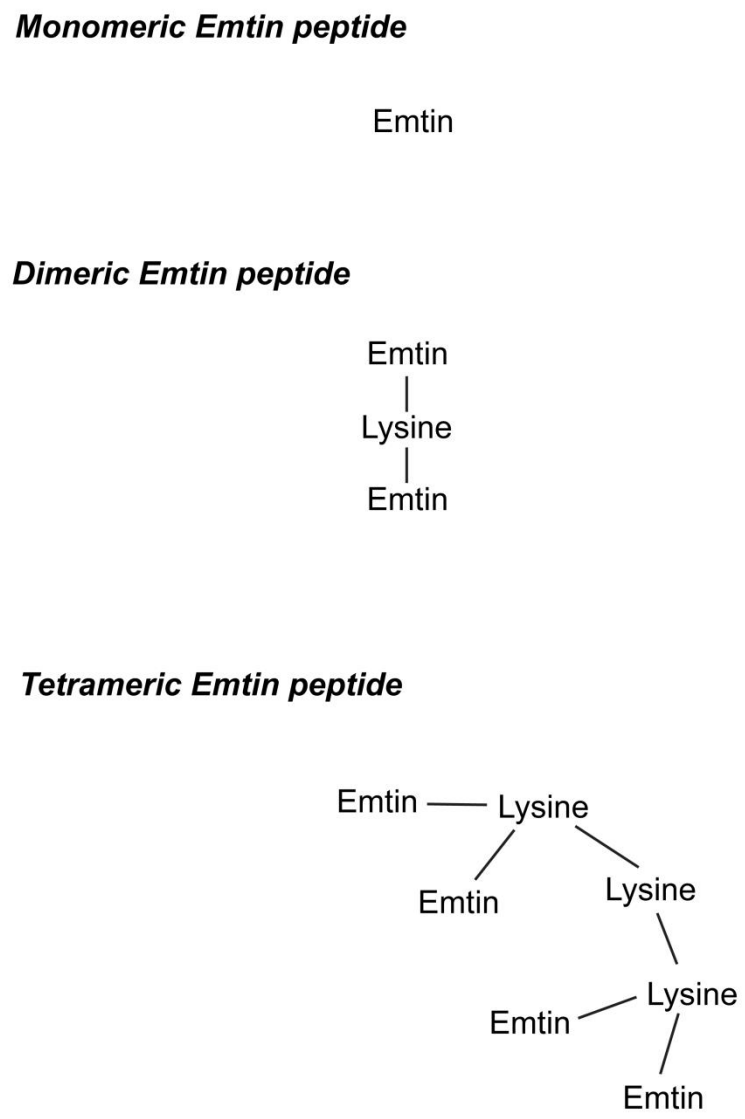

Figure 5.1 Structure of monomeric, dimeric and tetrameric Emtin peptides

A schematic diagram of the structure of monomeric, dimeric, and tetrameric emtin peptides is given. Monomeric Emtin peptides consist of a single peptide chain, here labelled 'Emtin', with the amino acid sequence of EmtinAc, EmtinAn, EmtinB, or EmtinBn as shown in Table 5.1. Dimeric Emtin peptides consist of two identical monomeric Emtin peptides joined to a single lysine. Tetrameric Emtin peptides consist of four identical monomeric Emtin peptides joined to a three-lysine backbone, or can be thought of as two dimeric Emtin peptides joined together via a third lysine. Tetrameric EmtinAc and tetrameric EmtinB were used in the current study. This diagram is based on the molecular structure of dendrimeric peptides reported by Pankratova and colleagues (Pankratova *et al.* 2010).

5.1.2 Aims and hypothesis

The ability of EmtinB to penetrate the CNS after subcutaneous injection (Sonn *et al.* 2010), makes Emtin peptides suitable as CNS-targeted therapeutic molecules. Given that the Emtin peptides display similar neuroprotective properties to MT2, and act through the same receptors, the Emtin peptides may also exert protective effects in a mouse model of ALS. The aim of this study was to examine survival in Emtin-treated and control SOD1 mice, to determine whether Emtin administration after disease onset could increase survival time in SOD1 mice.

Hypothesis: Administration of EmtinAc or EmtinB from the age of symptom onset until disease endpoint will increase survival time in female SOD1 mice.

In this pilot study, a small cohort of female SOD1 mice were divided into three treatment groups, receiving either EmtinAc, EmtinB, or vehicle control injections from 95 days of age until disease endpoint. Survival time and functional outcomes were measured as the primary outcomes of this pilot study. Additionally, a preliminary screen of post-injection Emtin distribution was carried out.

5.2 Methods

All procedures and protocols involving animals were approved by the University of Tasmania's Animal Ethics Committee (ethics permit numbers A10995 and A11958). SOD1 mice were genotyped and maintained as described in Chapter 2.

5.2.1 Pilot study for survival in the SOD1 mice with tetrameric Emtin

5.2.1.1 Administration of emtins

Tetrameric Emtin peptides (EmtinAc or EmtinB) were dissolved in filter-sterilised MilliQ water at 4mg/mL for injection. Eighteen female SOD1 mice were split into three treatment groups (n=6/group): one group received EmtinAc; one group received EmtinB; and one group received vehicle (MilliQ water) alone. Treatment with Emtin or vehicle commenced at approximately 95 days of age (Table 5.2), with treatment continuing until the mice reached disease endpoint. The dosage was 10µg Emtin per gram body weight three times weekly, giving a total dosage of 30mg/kg/week (approx. 600µg/20g mouse/week); injections of 4mg/mL Emtin solution were given subcutaneously via insulin syringes with 31-gauge needles, with control mice receiving the equivalent volume of filter-sterilised MilliQ water. No differences in copy number (ΔCT), age at start of treatment, or starting body weight, were observed between treatment groups (Table 5.2).

Table 5.2. Cohort characteristics at start of treatment

Treatment	n	Copy number (ΔCT)	Age (days)	Starting Weight (g)
Control	6	5.29 ± 0.11	94.8 ± 0.2	19.5 ± 0.3
EmtinAc	6	5.29 ± 0.07	94.7 ± 0.7	19.3 ± 0.4
EmtinB	6	5.27 ± 0.03	96.0 ± 0.7	19.5 ± 0.5

No significant difference in cohort parameters at the start of treatment (copy number, age at start).

5.2.1.2 Outcome measures and statistical analyses

Body weight and neurological score were recorded at least twice weekly, and more frequently towards disease endpoint. Survival time was assessed as the loss of 20% from peak body weight, and was analysed using Kaplan-Meier survival curves and Cox

proportional hazards regression. Stride pattern (see Figure 2.11A-D) was recorded weekly until mice could no longer provide a measureable pattern. Body weight and stride pattern were also examined in age-matched non-transgenic (WT) littermates receiving subcutaneous injections of vehicle only (n=6).

Body weight and stride pattern were averaged per week per animal and analysed by ANOVA and Tukey's post-hoc test with adjustments for inequality of variance (Welch ANOVA omnibus test with Tamhane's post-hoc test) or non-normality (Kruskal Wallis non-parametric test with Bonferroni-corrected Mann Whitney U as a post-hoc test) as appropriate. Additionally, body weight was analysed using the linear mixed modelling method outlined in Chapter 2.

During the course of the experiment, three mice received one dosage of the incorrect drug (e.g. EmtinAc instead of EmtinB). Data for these three mice (two in the EmtinAc-treatment group and one in the vehicle-treatment group) recorded after the age of incorrect treatment were not used for statistical analyses of stride length or body weight, and were censored for survival analysis.

5.2.1.3 Nissl Stain for motor neuron number at endpoint:

Upon reaching disease endpoint, mice were transcardially perfused with PBS and 4% PFA as described in Chapter 2 – briefly, the lumbar spinal cord (T12-L1 vertebrae) was removed, decalcified, embedded in paraffin and sectioned at 5µm. As some mice were censored prior to disease endpoint (see above), and some mice could not be perfused upon disease endpoint due to time constraints, spinal cords were collected from five vehicle-treated SOD1 mice, three EmtinAc-treated SOD1 mice, and five EmtinB-treated mice.

Nissl staining was performed as per Chapter 4, with slight modifications – briefly, sections were immersed in Cresyl violet solution for 30 minutes, passed through 70%, 95% and 100% ethanol, cleared in xylene and coverslipped with DPX mounting medium. Images were captured on a light microscope with attached camera (Leica). The number of α-motor neurons remaining in the lumbar spinal cord was counted in three 5µm sections from the lumbar spinal cord of each animal; these were averaged to give one measurement per mouse to avoid pseudoreplication.

5.2.2 Distribution of injected biotinylated dimeric EmtinB

To determine whether the Emtin peptides were acting upon the central nervous system, the presence or absence of dimeric EmtinB (d-EmtinB) in serum and cortical brain parenchyma was examined after subcutaneous injection.

5.2.2.1 Preparation of biotinylated d-EmtinB

d-EmtinB peptide was biotinylated using the ImmunoProbe biotinylation kit (Sigma-Aldrich) as per the manufacturer's instructions (performed by Ms Emma Eaton) and reconstituted at 2.5mg/mL in sterile PBS.

5.2.2.2 d-EmtinB administration and sample collection

Biotinylated d-EmtinB was administered at 10mg/kg body weight to two SOD1 and two WT mice at 14 weeks of age; one SOD1 and two WT mice received an equivalent volume of vehicle alone. All subcutaneous injections were performed using an insulin syringe with 31-gauge needle, under light isoflurane anaesthesia.

At 1 hour post-injection, a urine sample was able to be collected from 2 of 7 mice (two SOD1 mice: one d-EmtinB-injected, and one PBS-injected); all mice were then deeply anaesthetised with sodium pentobarbitone (100mg/kg, i.p.). When all reflexes were absent, the thoracic cavity was opened for transcardiac perfusion with PBS alone. Prior to insertion of the perfusion line, approximately 100uL whole blood was withdrawn from the left ventricle via an insulin syringe and 22-gauge needle under gentle pressure so as not to collapse the chamber walls; the collected blood was transferred to a microcentrifuge tube (Axygen Maxymum Recovery, Corning Life Science, MA, USA) and left to clot at room temperature. The mouse was then perfused with PBS until the liver paled and the foot-pads became white. The spinal cord and the cerebral cortices were dissected out and snap-frozen in liquid nitrogen, then stored at -80°C. The serum sample was prepared by removal of clotted proteins by centrifugation at 16060*g* for 10 minutes at 4°C in a benchtop microcentrifuge (Heraeus Biofuge Pico), and the supernatant (serum) was stored at -20°C until analysis.

5.2.2.3 Sample prepration and western blotting

Tissue lysates were prepared by homogenisation using an Ultra-Turrax rotor-stator homogenisation device (IKA Werke GmbH & Co, BW, Germany). Cortex and spinal cord tissues were immersed in 1mL ice-cold tissue lysis buffer (50mM Tris-HCl,

150mM NaCl, 1% v/v Igepal CA630, 0.5% w/v sodium deoxycholate, 1mM EDTA, 0.1% w/v sodium dodecyl sulphate [all Sigma-Aldrich], pH 7.4, with 1 protease inhibitor tablet added to each 10mL lysis buffer [cOmplete Mini, EDTA-free, Roche Applied Science, IN, USA]) and homogenised with 3 x 10 second pulses using the Ultra-Turrax at setting 4, each separated by 30-60 seconds on ice, then centrifuged at 16060*g* for 10min in a benchtop microcentrifuge. The supernatant, containing cytosolic proteins, was retained for analysis and stored at -20°C.

A BCA assay for total protein concentration (Pierce BCA Protein Assay Kit, Thermo Scientific, IL, USA) was performed according to the manufacturer's instructions, to ensure equal amounts of total protein were loaded for each sample. Following the BCA assay, cortical tissue homogenate samples were made up to 21µL with MilliQ water and were combined with 9µL reducing sample buffer (0.45M Tris-HCl pH 6.8, 3.5% w/v SDS, 18% v/v glycerol, 0.02% w/v bromophenol blue, 18% v/v β-mercaptoethanol [all Sigma-Aldrich]). One microliter of each urine sample was added to 20µL MilliQ water and combined with 9µL reducing sample buffer. To avoid possible coagulation of high-concentration serum proteins, serum samples were mixed 1:1 with reducing sample buffer; all samples were heated to 60°C for 5 minutes and then to 90°C for 5 minutes to solubilise proteins.

Western blotting was performed using the NuPAGE X-Cell system (Life Technologies); the protein samples and 5µL SeeBlue Plus2 protein ladder (Life Technologies) were loaded onto pre-cast NuPAGE 10% bis-tris acrylamide gels, and subjected to gel electrophoresis at 150V for 45 minutes in 1X NuPAGE MES running buffer with 500µL NuPAGE antioxidant added to the upper chamber. The proteins were then transferred to nitrocellulose membrane (Thermo Scientific) at 30V for 45 minutes in transfer buffer (25mM Trizma base [Sigma-Aldrich], 190mM glycine [Sigma-Aldrich], 20% v/v methanol [Merck Millipore]). The membrane was blocked with 5% non-fat milk powder in PBS-T for 1 hour with shaking at room temperature, washed, and incubated with HRP-conjugated streptavidin (1:2000) for 1 hour. Biotinylated d-EmtinB was visualised with SuperSignal West Dura chemiluminescent substrate (Thermo Scientific) using a Chemi-Smart 5000 imaging system (Vilber Lourmat, IDF, France).

5.3 Results

5.3.1 Treatment of SOD1 mice with Emtin

5.3.1.1 Emtin treatment slightly delays disease endpoint

All SOD1 mice reached endpoint between 152 and 177 days of age. Kaplan-Meier analysis revealed a slight right-shift in the survival curves of EmtinAc- and EmtinB-treated mice, indicating delayed endpoint ages compared with vehicle-treated mice (Figure 5.2A), although these curves were not significantly different (p=0.105, Log Rank test in Kaplan-Meier analysis). On average, mice receiving either EmtinAc or EmtinB reached endpoint approximately 5% later than mice receiving vehicle alone (EmtinAc 170.5±2.8 days, EmtinB 169.3±2.7 days, control 161.2±2.9 days; Figure 5.2B). Similarly, EmtinAc- and EmtinB-treated mice displayed a longer median survival time compared with vehicle-treated mice (EmtinAc 168.0±4.5 days, EmtinB 169.0±3.7 days, control 162.0±8.0 days, data not shown). However, these differences in mean and median survival times were not significantly different between treatment groups.

CPH regression revealed that the hazard ratio for reaching disease endpoint was reduced for mice receiving either EmtinAc treatment or EmtinB treatment compared with vehicle controls, indicating an increased survival time for Emtin-treated mice (Table 5.3). These hazard ratios (HR) approached, but did not reach, statistical significance ($HR_{EmtinAc}$=0.226, 95% CI 0.044-1.155, p=0.074; HR_{EmtinB}=0.253, 95% CI 0.055-1.164, p=0.078).

In order to examine whether any other factors were affecting survival in this cohort, the age at start of treatment, weight at start of treatment, and copy number were analysed with CPH analysis; none of these covariates had a significant effect on survival time (Table 5.3). Accordingly, the association of Emtin treatment with reduced odds ratio of reaching endpoint persisted when the model was adjusted for age at the start of treatment, weight at the start of treatment and copy number (Table 5.3).

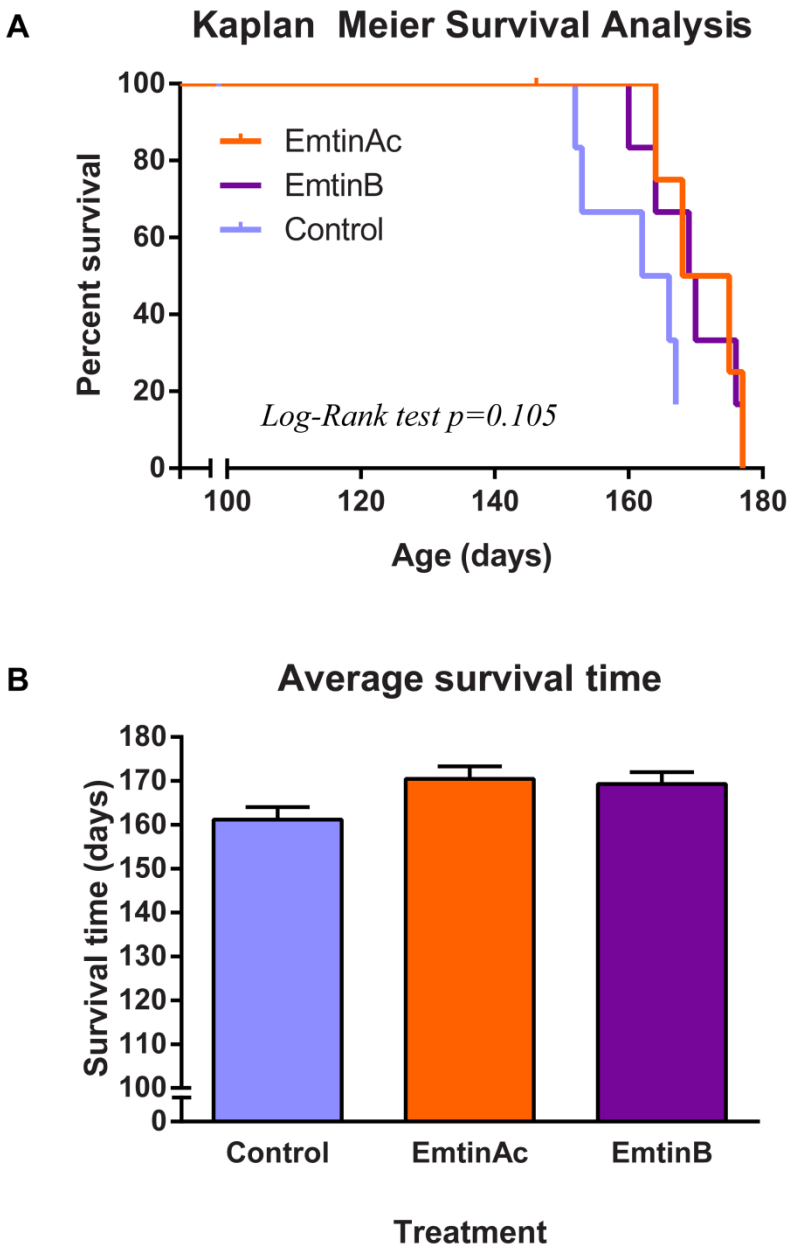

Figure 5.2 Survival in Emtin-treated and control SOD1 mice

Treatment with EmtinAc or EmtinB from symptom onset shifted Kaplan-Meier survival curves to the right (A). The average survival times for EmtinAc-treated or EmtinB-treated mice were slightly longer than vehicle-treated control mice (B). Vertical dashes represent censored data. Error bars represent standard error of the mean.

Table 5.3 Cox proportional hazards regression for reaching disease endpoint

Factor	HR (95% CI)	p-value
Univariable analysis		
Emtin treatment[1]		0.152
EmtinAc[2]	0.226 (0.044-1.155)	0.074
EmtinB[2]	0.253 (0.055-1.164)	0.078
Age at start	0.951 (0.617-1.464)	0.818
Copy number	0.352 (0.005-27.118)	0.637
Weight at start	1.442 (0.776-2.681)	0.247
Multivariable analysis[3]		
Emtin treatment[1]		0.126
EmtinAc[2]	0.193 (0.035-1.059)	0.058
EmtinB[2]	0.237 (0.048-1.165)	0.076

[1]Multi-level categorical variable, overall p-value given; [2]Subgroups of categorical variable 'Emtin'.
[3]Adjusted for age at start of treatment, weight at start of treatment, and copy number.

5.3.1.2 Body weight

Body weight was measured at least twice per week throughout the experiment. As previously mentioned, starting body weight did not differ between Emtin-treated and vehicle-treated mice (Table 5.2). Maximum body weight, weekly averages, and body weight trajectory over time are discussed below.

5.3.1.2.1 Maximum body weight

The average maximum body weight attained by these mice was not different between treatment groups, although vehicle-treated mice showed a slightly higher maximum body weight compared with Emtin-treated mice (EmtinAc 20.0±0.3g, EmtinB 20.6±0.7, vehicle 21.0±0.4g, ANOVA omnibus p=0.37). The age at which maximum body weight was reached was not different between treatment groups (EmtinAc 116.2±6.3 days, EmtinB 122.5±6.8 days, vehicle 124.7±5.4 days, ANOVA omnibus p=0.61). As treatment was only started at 95 days of age (approximately 14 weeks of age), large changes in disease onset as measured by the age of maximum body weight were not expected between treatment groups.

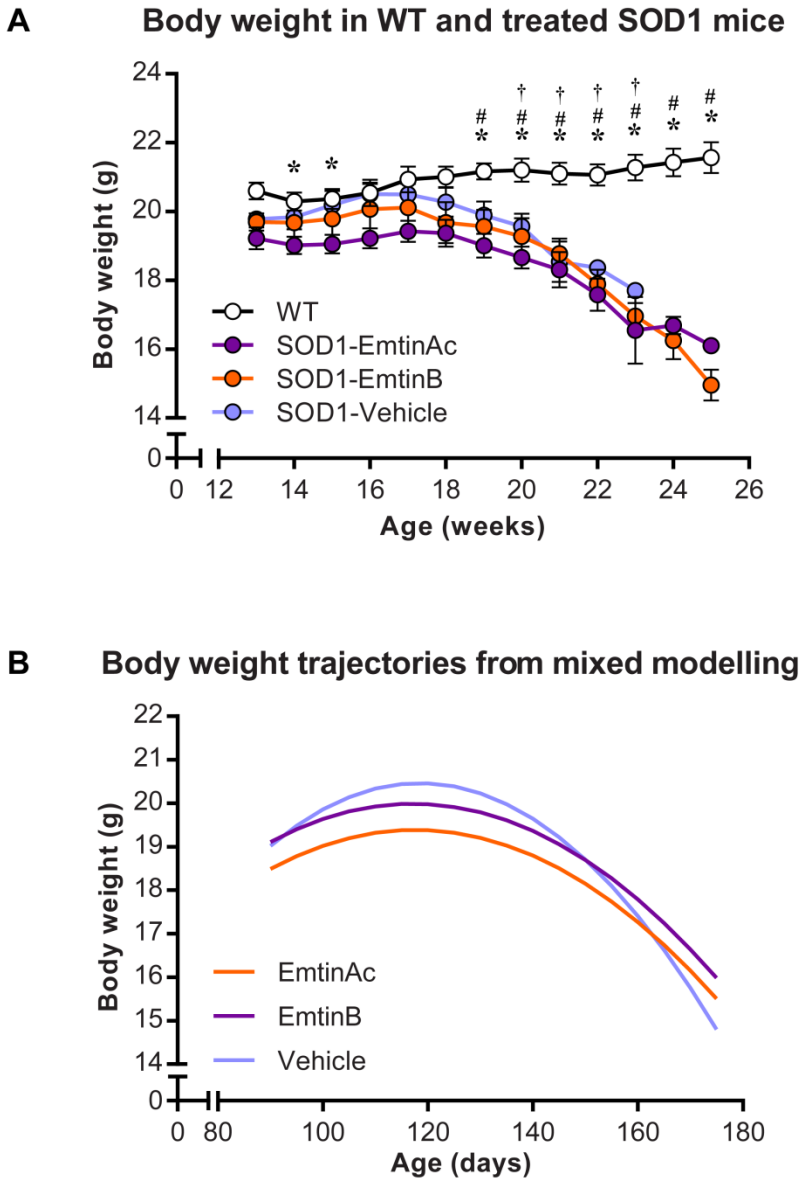

Figure 5.3 Body weight averages and body weight mixed model trajectories in Emtin-treated and control SOD1 mice

Weekly body weight averages (A) were not significantly different between Emtin-treated and control SOD1 mice. EmtinB and control SOD1 mice showed lower body weights than WT mice from 19 weeks of age, whereas all SOD1 mice showed lower body weights than WT mice from 20 weeks of age onwards (A). Body weight trajectories (B) for each treatment group of SOD1 mice were plotted from linear mixed modelling parameters (Table 5.4), showing a wider, flatter trajectory curve for Emtin-treated SOD1 mice compared to control SOD1 mice. *p<0.05 EmtinAc vs WT, #p<0.05 EmtinB vs. WT, †p<0.05 vehicle vs. WT. Error bars represent standard error of the mean.

5.3.1.2.2 Average body weight per week

Average body weight increased over time in WT mice, while the body weight of SOD1 mice peaked at approximately 17 weeks of age regardless of treatment, and declined thereafter (Figure 5.3). Average body weight was not different between SOD1 treatment groups at any of the time points measured ($p>0.05$) (Figure 5.3). However, EmtinAc-treated mice appeared to have the lowest body weights of any group from 14-17 weeks of age (14wks: EmtinAc 19.0±0.3g vs. WT 20.3±0.3g, Tamhane p=0.032; 15wks: EmtinAc 19.1±0.3g vs. WT 20.4±0.3g, Tamhane p=0.047) (Figure 5.3A). At 19 weeks of age, EmtinAc-treated and EmtinB-treated SOD1 mice showed lower body weights than WT mice (WT 21.2±0.3g; WT vs. EmtinAc 19.0±0.4g, Tukey p=0.003; WT vs. EmtinB 19.6±0.5g, Tukey p=0.034); while from 20 weeks onwards, all groups of SOD1 mice showed lower body weights than WT mice (Figure 5.3A).

5.3.1.2.3 Linear mixed modelling of body weight

Body weight trajectories of Emtin-treated and control SOD1 mice were examined by linear mixed modelling. In the absence of pre-symptomatic body weight measures, a quadratic curve was fitted, as a cubic curve could not be reliably modelled. The model included the intercept, Age and Age^2 as fixed factors, and a random intercept and slope as random factors (for full model specification, see Supplementary Data 4). The linear mixed model gives a set of parameters for the equation $\boldsymbol{Body\ weight = \beta_0 + \beta_1 * Age + \beta_2 * Age^2}$, where each $\boldsymbol{\beta}$ coefficient has a unique value for the control, EmtinAc-treated, and EmtinB-treated groups (listed in Table 5.4). The body weight trajectory parameters differed significantly between Emtin-treated mice and control mice (Supplementary Data 4). When graphed, the body weight curves showed a wider, flatter body weight trajectory for Emtin-treated mice than control mice (Figure 5.3), possibly indicating that Emtin-treated mice lose body weight at a slower rate than control mice.

Table 5.4 Parameter estimates from linear mixed model of body weight trajectory

Fixed effects parameter[1]	**Vehicle**	**EmtinAc**	**EmtinB**
Intercept (β_0)	-4.449	3.095	3.585
Age (β_1)	4.20×10^{-1}	2.77×10^{-1}	2.80×10^{-1}
Age^2 (β_2)	-1.80×10^{-3}	-1.20×10^{-3}	-1.22×10^{-3}

[1]Parameter estimates for the equation $\boldsymbol{Body\ weight = \beta_0 + \beta_1 * Age + \beta_2 * Age^2}$, where ***Age*** = age in days

5.3.1.2.4 Percentage body weights

As the three treatment groups of SOD1 mice showed no significant differences in average weekly body weights (Figure 5.3A), the percentage body weights were examined. Percentage body weights were not significantly different between Emtin-treated and vehicle-treated SOD1 mice, although vehicle-treated mice showed the lowest percentage body weight at 21 weeks of age of any group (Figure 5.4A).

As the disease endpoint, measured as reaching 80% of peak body weight, was slightly delayed in Emtin-treated SOD1 mice (Figure 5.2), the age at which SOD1 mice reached 95%, 90%, and 85% of their maximum body weight was also examined (Figure 5.4B). Although Kaplan-Meier analysis revealed no significant differences between treatment groups, survival curves showed that vehicle-treated mice reached 85% of their maximum body weight slightly earlier than Emtin-treated mice (Figure 5.4B). The mean age at which Emtin-treated mice reached 90% and 85% of maximum body weight was slightly later than those of vehicle-treated mice; the same was true for the median age of reaching 95%, 90%, and 85% of maximum body weight (Table 5.5), however these changes were not statistically significant.

Table 5.5 Average and median ages at which 95, 90, and 85% of maximum body weight were reached

	Treatment	95% BW	90% BW	85% BW
Mean age (days)	Vehicle	140.8 ± 2.7	151.3 ± 2.0	158.2 ± 2.6
	EmtinAc	140.8 ± 1.2	156.5 ± 1.6	164.3 ± 0.9
	EmtinB	142.2 ± 3.7	156.0 ± 2.6	165.2 ± 3.2
Median age (days)	Vehicle	136.0 ± 2.0	149.0 ± 2.0	156.0 ± 5.5
	EmtinAc	140.0 ± 1.8	155.0 ± 2.5	164.0 ± 1.5
	EmtinB	140.0 ± 6.7	153.0 ± 3.1	164.0 ± 1.2

Thus, both linear mixed modelling of Emtin-treated and control SOD1 mouse body weight trajectories, and analysis of the age at which 95%, 90%, and 85% of maximum body weight were reached, suggested that Emtin-treated mice may retain body weight slightly longer than control mice. These differences did not reach statistical significance, which may be due to the small cohort size used in this study.

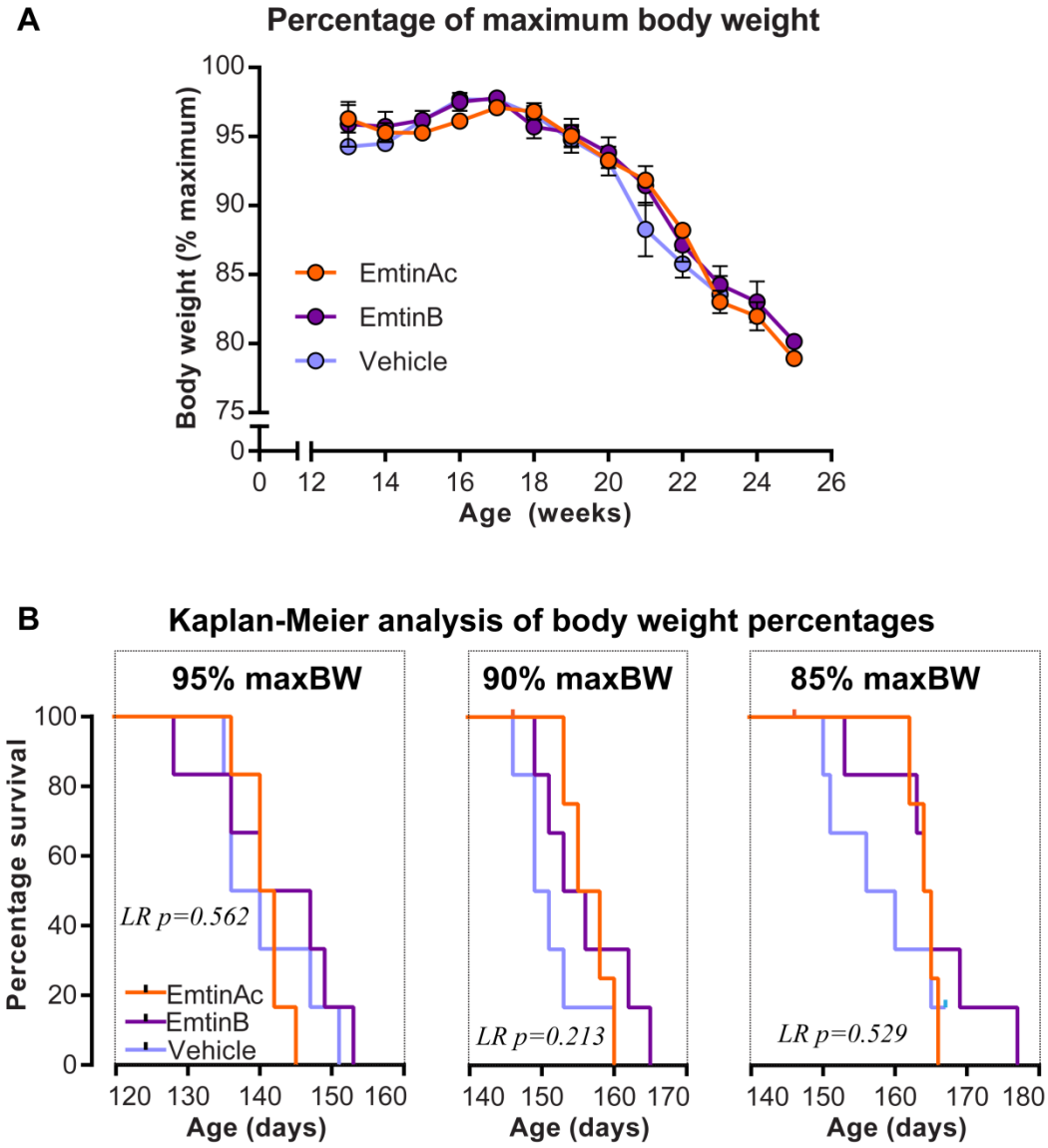

Figure 5.4 Percentage body weights in Emtin-treated and control SOD1 mice

Vehicle-treated (control) SOD1 mice showed the lowest percentage body weight at 21 weeks of age, although there were no significant differences in percentage body weight weekly averages (A). Kaplan-Meier analysis was carried out on the age at which mice reached 95% (B, left-hand panel), 90% (B, middle panel), and 85% (B, right-hand panel) of their maximum body weight. There appeared to be a slight tendency for vehicle-treated mice to reach 90% and 85% of their maximum body weight slightly earlier than EmtinAc-treated or EmtinB-treated mice (B). maxBW, maximum body weight; LR, Log-Rank test in Kaplan-Meier analysis. Error bars represent standard error of the mean.

5.3.1.3 Stride Test

Stride length and uniformity were measured weekly. As expected, the stride length and uniformity of WT mice did not change substantially over time, whereas SOD1 mice showed decreasing stride length and increasing uniformity with age (Figure 5.5). The stride length and uniformity of SOD1 mice did not differ by treatment group at the start of treatment (Table 5.6).

5.3.1.3.1 Stride length

Average stride length did not differ between Emtin-treated and control SOD1 mice throughout the experiment (Figure 5.5A). Compared to WT mice, control SOD1 mice were the first to show a significantly lower stride length, at 17 weeks of age (control 6.0±0.1cm vs. WT 7.0±0.4cm, Tukey p=0.023). Control and EmtinB-treated SOD1 mice had shorter stride lengths than WT mice at 18 weeks of age (WT 6.8±0.2cm: vs. control 5.5±0.3cm, Tukey p=0.002; vs. EmtinB 5.8±0.2cm, Tukey p=0.017), and all SOD1 mice showed a shorter stride length than WT mice thereafter (Figure 5.5A), although this was not significant for any group at 19 weeks of age due to larger variances at this time point (ANOVA omnibus p=0.103). The maximum stride length attained by SOD1 mice was not different between treatment groups, although EmtinAc-treated mice attained their maximum stride length later than control mice (Tukey p=0.043, Table 5.6); these results suggest that EmtinAc, but not EmtinB, was able to delay the onset of functional deficits as measured by maintenance of stride length to a greater age than control SOD1 mice.

Table 5.6 Starting and maximal stride pattern measurements

Treatment	n	Starting stride length (cm)	Maximum stride length (cm)	Age at maximum stride length (days)	Starting uniformity (cm)
Vehicle	6	6.0 ± 0.2	6.8 ± 0.2	114.7 ± 2.4	0.2 ± 0.1
EmtinAc	6	6.1 ± 0.2	6.6 ± 0.2	126.2 ± 3.9*	0.3 ± 0.1
EmtinB	6	6.0 ± 0.3	6.7 ± 0.2	116.7 ± 2.6	0.3 ± 0.1

*Significantly different from vehicle, Tukey p=0.043.

To examine the loss of stride length from the recorded maximum, the percentage of maximum stride length attained over time was calculated. WT mice show a slight decrease in percentage stride length over time, from an average of 93±3% of maximum at 15 weeks of age to 77±4% of maximum at 24 weeks of age (Figure 5.5B). SOD1 mice showed a far more substantial decrease in percentage stride length, from approximately 95% of maximum at 15 weeks of age down to just above 30% of maximum at 24 weeks of age (Figure 5.5B).

There were no significant differences between SOD1 treatment groups throughout the time course; however, at 20 weeks of age, only control SOD1 mice showed a significantly lower percentage stride length than WT mice (WT 88±3% vs. control 67±6%, Tukey p=0.044) (Figure 5.5B). At 21 weeks of age, both control mice and EmtinB-treated mice displayed a lower percentage stride length than WT mice (WT 86±5%; vs. control 51±5%, Tukey p=0.002; vs. EmtinB 53±7%, Tukey p=0.003) (Figure 5.5B). By 22 weeks of age, the percentage of maximum stride length was lower than WT for all SOD1 treatment groups (WT 82±5%; vs. control 47±5%, Tukey p<0.001; vs. EmtinA 50±5%, Tukey p=0.002; vs. EmtinB 43±5%, Tukey p<0.001) (Figure 5.5B). Treatment with EmtinAc, but not EmtinB, appeared to slightly delay the loss of stride length as a percentage of maximum.

5.3.1.3.2 Uniformity

Uniformity measurements at the start of treatment did not differ between SOD1 treatment groups (Table 5.6). Average uniformity measurement was not significantly different between SOD1 treatment groups over time (Figure 5.5C). At 18 weeks of age, only vehicle-treated SOD1 mice showed a larger uniformity measurement than WT mice (WT 0.3±0.1cm vs. vehicle 0.7±0.1cm, Tukey p=0.017). At all successive time points, all SOD1 mice showed a larger uniformity measurement than WT mice (Figure 5.5C). As a larger uniformity measurement indicates increasing dysfunction and inability to move the hind limbs in a forward motion, the slightly earlier increase in the control mice may indicate that treatment with EmtinAc or EmtinB resulted in initially slightly better maintenance of hindlimb function than control SOD1 mice. However, as disease progressed, neither EmtinAc nor EmtinB treatment was able to significantly delay the increase in uniformity measure.

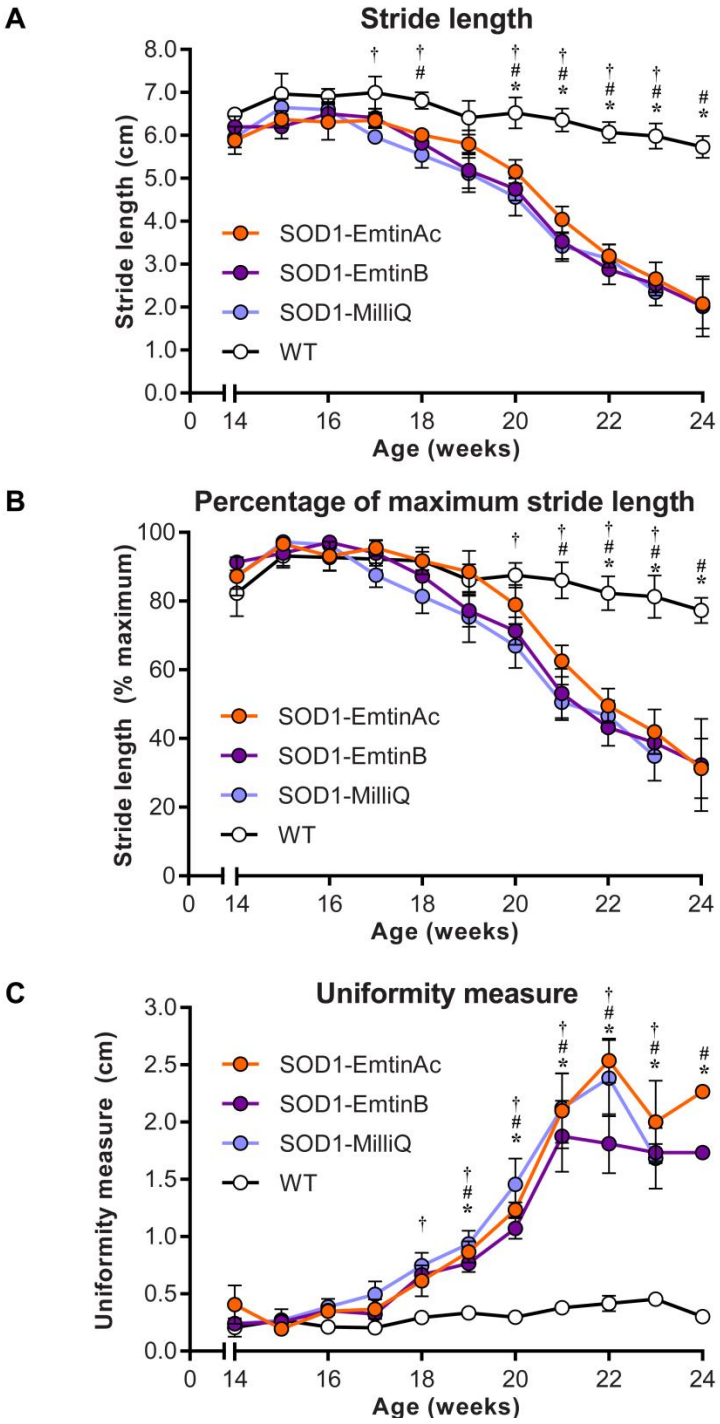

Figure 5.5 Stride pattern measurements in Emtin-treated and control SOD1 mice

Stride length (A), percentage of maximum stride length (B), and uniformity (C) were not significantly different between EmtinAc-treated, EmtinB-treated, and control SOD1 mice over time. SOD1 treatment groups varied at the age which they diverged from WT mice in stride length (A; control at 17 weeks of age, EmtinB at 18 weeks of age, EmtinAc at 20 weeks of age), percentage stride length (B; control at 20 weeks of age, EmtinB at 21 weeks of age, EmtinAc at 22 weeks of age), and uniformity measure (C; control at 18 weeks of age, EmtinAc and EmtinB at 19 weeks of age). *$p<0.05$ EmtinAc vs WT, #$p<0.05$ EmtinB vs WT, †$p<0.05$ vehicle vs WT mice. Error bars represent standard error of the mean.

5.3.1.4 Neurological Score

Neurological scoring (NS) was conducted according to the guidelines laid out in Chapter 2 (Table 2.3). As SOD1 mice were already displaying early disease symptoms upon arrival at the facility, the age of onset (NS=1) could not be determined. Additionally, most SOD1 mice reached disease endpoint (80% of maximum body weight) before reaching hindlimb paralysis (NS=3), so the age at paralysis could not be determined.

To examine disease progression in Emtin-treated and vehicle-treated SOD1 mice, the age at which SOD1 mice reached NS=2 (foot-dragging, Table 2.3) was analysed using Kaplan-Meier analysis. Survival curves for NS=2 showed a slight right-shift for EmtinB-treated mice compared to vehicle-treated mice (Figure 5.6A), indicating that EmtinB-treated mice show profound gait abnormalities at a slightly later age than vehicle-treated mice.

Accordingly, the average age at reaching NS=2 was slightly higher for EmtinAc-treated mice (164.7±3.7 days) and EmtinB-treated mice (168.0±5.9 days) than for vehicle-treated mice (158.0±5.3 days), although these differences were statistically significant (ANOVA omnibus p=0.407).

5.3.2 Endpoint Motor Neuron Numbers

At endpoint (20% loss from peak body weight), spinal cord samples were taken from SOD1 mice to count the number of motor neurons remaining in the ventral horn. There were no significant differences between treatment groups, although EmtinAc-treated mice showed the lowest number of motor neurons remaining (Figure 5.7).

To account for any variation in size of the ventral horn between sections, the number of motor neurons within a single field of view within the ventral horn was also counted, and showed the same pattern as shown in Figure 5.7 (data not shown).

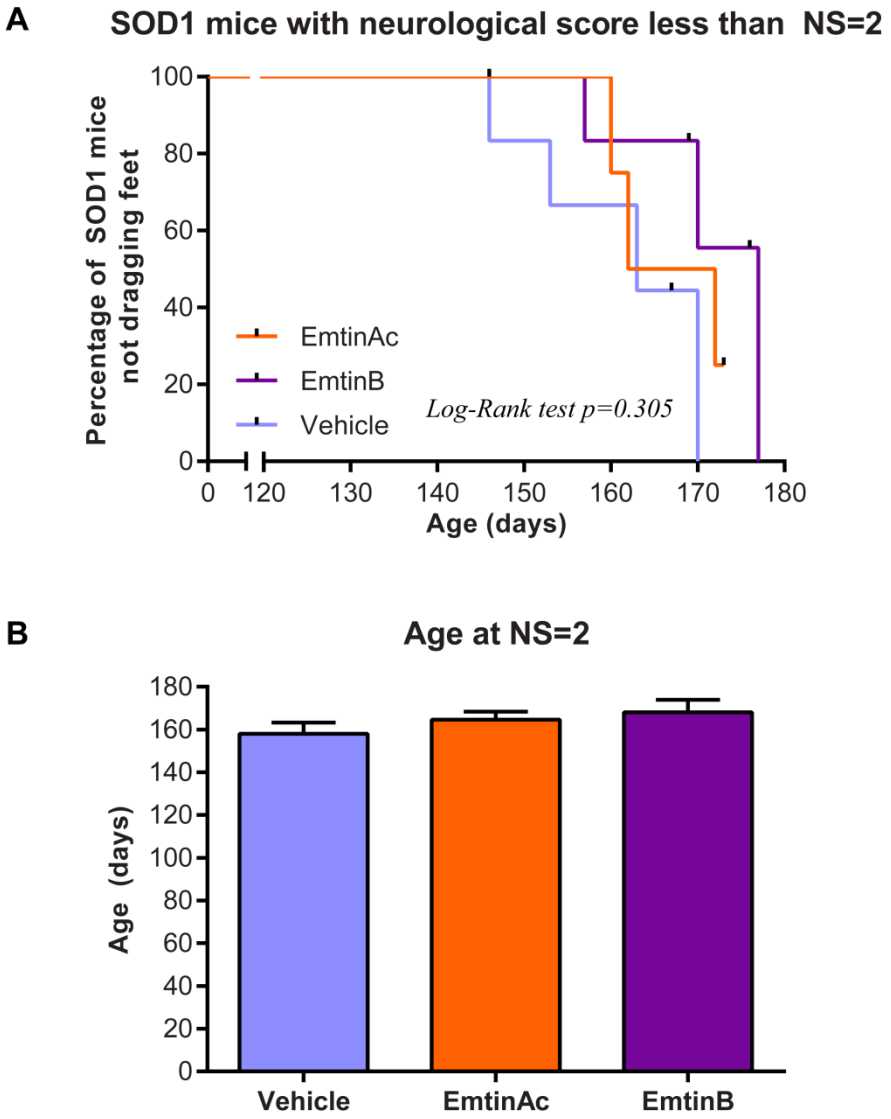

Figure 5.6 Age at which Emtin-treated and control SOD1 mice reach neurological score NS=2

Figure 5.6 Age at which Emtin-treated and control SOD1 mice reach neurological score NS=2. Using Kaplan-Meier survival curves to measure time-to-event data for SOD1 mice reaching NS=2 (Toes curl under at least twice during walking of 12 inches, or any part of foot is dragging along cage bottom/table, Table 2.3), the survival curve for EmtinB-treated mice is lightly right-shifted compared to the survival curve for vehicle-treated mice (A). EmtinAc-treated and EmtinB-treated mice reached NS=2 at a slightly higher average age than vehicle-treated mice (B). Vertical dashes represent censored data. Error bars represent standard error of the mean.

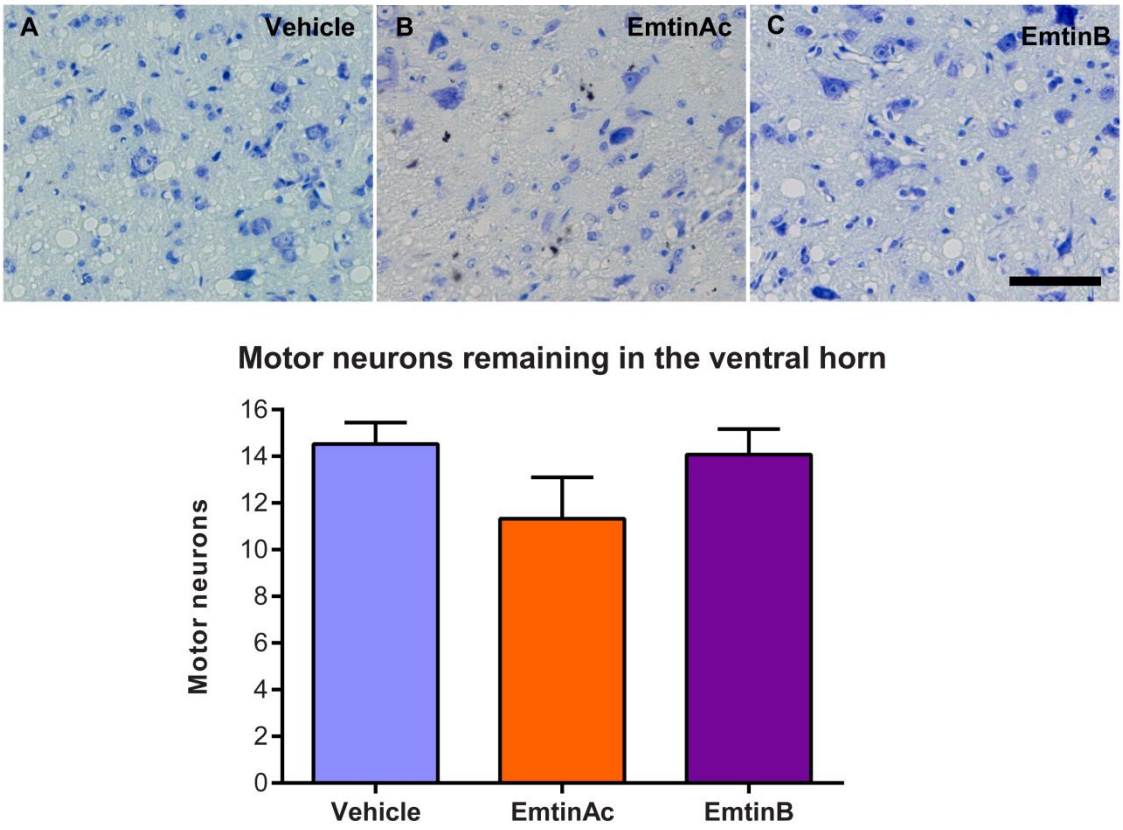

Figure 5.7 Motor neurons in the ventral horn at endpoint

The number of motor neurons remaining in the ventral horn of Emtin-treated and vehicle-treated mice was examined. Panels A-C show Nissl-stained motor neurons remaining in the ventral horn at disease endpoint in vehicle-treated (A), EmtinAc-treated (B) and EmtinB-treated (C) SOD1 mice. Quantitation of remaining motor neurons (D) showed that EmtinAc-treated mice had fewer motor neurons remaining than vehicle-treated and EmtinB-treated SOD1 mice at endpoint, however this was not significantly different between groups. Error bars represent standard error of the mean. Scale bar 40µm for A-C.

5.3.3 Distribution of biotinylated d-EmtinB

Biotinylated dimeric EmtinB (d-EmtinB) was injected subcutaneously into SOD1 and WT mice to examine its distribution in the serum and in the brain. Western blotting to detect biotinylated d-EmtinB, using HRP-conjugated streptavidin, showed the presence of d-EmtinB in the serum of both WT and SOD1 mice within an hour of injection (Figure 5.8A). Mice injected with a vehicle control (PBS) showed no such bands (Figure 5.8A). In the brain, no clear d-EmtinB signal could be seen at 1 hour after injection (Figure 5.8B), although the multiple non-specific bands observed in the brain homogenates may prevent detection of d-EmtinB. Only two urine samples were able to be collected; both were from SOD1 mice, one injected with biotinylated d-EmtinB and one injected with vehicle alone. A strong signal was observed in the urine of the d-EmtinB-injected SOD1 mouse (Figure 5.8B), and was absent from the vehicle-injected mouse (Figure 5.8A), indicating that at least some of the injected d-EmtinB may be cleared through the kidneys within one hour of subcutaneous injection.

Biotinylated d-EmtinB, with an apparent molecular weight of approximately 4kDa (Figure 5.8A, B, arrow) also appears at approximately 6-8kDa (Figure 5.8A, B, arrowhead) and in serum samples, at approximately 20kDa (Figure 5.8A, asterisk). These higher molecular weight bands suggest that biotinylated d-EmtinB could form oligomeric species in solution or *in vivo*, or may form a complex with other proteins.

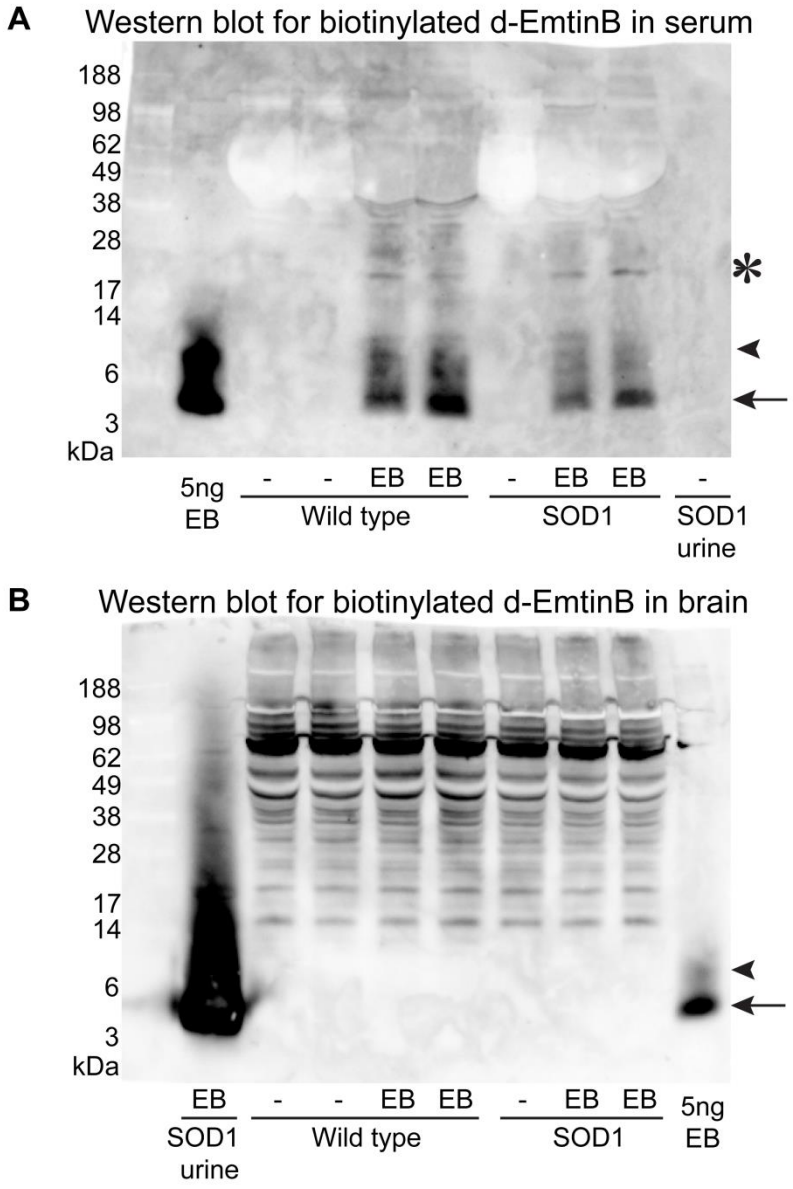

Figure 5.8 Distribution of biotinylated d-EmtinB in serum and brain samples

Western blot assayed the presence of biotinylated EmtinB dimer (d-EmtinB) in serum (A) and brain homogenate (B) of wild type or SOD1 mice at one hour after subcutaneous injection of d-EmtinB injection (EB) or vehicle (-). A positive control (5ng biotinylated d-EmtinB, 5ng EB) was run on each gel (A,B), and resolved at an apparent molecular weight of approximately 4kDa (arrow, A, B), also showing a band around 6-8kDa (arrowhead, A, B). d-EmtinB was present in serum at one hour after injection in either WT or SOD1 mice (4kDa, arrow; 6-8kDa, arrowhead; ~20kDa, asterisk; A). d-EmtinB was not detected in the brain at one hour after injection in WT or SOD1 mice (B); however, multiple non-specific signals seen in all brain samples (B) may reduce the chance of identifying changes between d-EmtinB-injected and vehicle-injected mice. One SOD1 mouse injected with d-EmtinB showed a strong positive signal in the urine at 1 hour after injection (SOD1 urine, B), compared to no signal in urine from a vehicle-injected SOD1 mouse (SOD1 urine, A).

5.4 Discussion

5.4.1 Summary of effects of Emtin peptides

Emtin peptides are tetrameric peptides based on the sequence of human metallothionein protein (Figure 5.1). In this study, EmtinAc or EmtinB peptides were administered to a small pilot cohort of female SOD1 mice, from 95 days of age until disease endpoint. Emtin treatment may delay the loss of body weight in SOD1 mice, as measured by survival time, body weight mixed modelling, and analysis of percentage body weights (Figure 5.2, Figure 5.3, Figure 5.4). EmtinAc treatment may delay the loss of stride length (Figure 5.5), while EmtinB appears to delay the onset of more severe neurological score rating (Figure 5.6). These effects indicate that administration of Emtin peptides may be able to increase survival time and maintain hindlimb function in a small cohort of SOD1 mice, despite treatment only starting around disease onset.

5.4.2 Mechanism of action of Emtin peptides

The delayed loss of body weight and maintenance of hindlimb function in Emtin-treated SOD1 mice may indicate that Emtin peptides play a role in maintaining neuromuscular connections and preventing muscular atrophy. Previous studies on the actions of Emtin peptides in cell culture may provide some insight into possible mechanisms for neuroprotection in the current study. In cerebellar granule neuron cultures, both EmtinAc and EmtinB are able to promote neurite outgrowth and prevent apoptosis in response to potassium withdrawal stress, via interaction with LRPs and activation of the MAPK and PI3K/Akt intracellular signalling pathways (Dudek *et al.* 1997; Chang & Karin 2001; Ambjorn *et al.* 2008; Asmussen *et al.* 2009a). In the current study, Emtin peptides may activate these same pathways in motor neurons in order to elicit motor neuron protection against cell death processes, or promote regenerative sprouting at the muscle. The number of motor neurons remaining at disease endpoint was not different between Emtin-treated and vehicle-treated mice (Figure 5.7); however, it is difficult to directly compare the number of motor neurons due to the different ages (endpoints) at which the spinal cord samples were obtained. Future examination of the neuromuscular junction architecture may determine whether increased sprouting or innervation at the muscle is responsible for the slight Emtin-mediated delay in disease endpoint (Figure 5.2) and maintenance of muscle function (Figure 5.5).

5.4.3 Comparison of mechanism of action of Emtin and MT2

In Chapter 4, pre-symptomatic treatment with MT2 was able to significantly delay disease onset and slightly delay disease endpoint, while in this chapter, treatment with Emtin from symptom onset onwards showed a trend for increasing survival time. The Emtin peptides are MT2 derivatives, and neuroprotective mechanisms of action utilising LRP receptors are shared between both MT-1/2 protein and Emtin peptides in cell culture (Ambjorn *et al.* 2008; Asmussen *et al.* 2009a). However, the replacement of cysteine residues in MT2 for serine residues in Emtin peptides (Table 5.1), performed to prevent intra- and inter-peptide cysteine linkages forming, may limit the metal-binding and antioxidant ability of Emtin peptides (Asmussen *et al.* 2009a). The MT-1/2 protein binds metal ions via its cysteine residues (Ruttkay-Nedecky *et al.* 2013), so although there is no published literature on the metal-binding capacity of Emtin peptides, it is likely that Emtins peptides will show reduced metal-binding ability due to the replacement of cysteine residues with serine residues. MT-1/2 also uses its cysteine residues for its antioxidant capacity (Ruttkay-Nedecky *et al.* 2013), so it is likely that Emtin peptides will display little ability to sequester reactive oxygen species. It is therefore likely that the protective effects of Emtin peptides seen in the current study are due to the interaction between Emtin peptides and their LRP receptors (Asmussen *et al.* 2009a), whereas the protective effects of MT2 administration seen in Chapter 4 may be either due to interaction between MT2 and LRP receptors, or due to the metal-binding and antioxidant capacities of the MT2 protein.

5.4.4 Delivery of EmtinB to the central nervous system

After a single subcutaneous injection of biotinylated d-EmtinB, d-EmtinB was observed in the serum and urine but was not found in brain homogenate (Figure 5.8). These data may indicate that biotinylated d-EmtinB peptides do not enter the brain tissue of the central nervous system at one hour post-injection. A previous study showed the presence of biotinylated EmtinB in the cerebrospinal fluid at one hour after injection (Sonn et al. 2010). The differing results between the current study and that of Sonn and colleagues (2010) may be due to the peptide administered, the dosage, and differences in sampling the central nervous system, as discussed below.

Instead of administering EmtinB tetramer peptide at 20mg/kg (Sonn *et al.* 2010), dimeric EmtinB peptide at 10mg/kg was administered in the current study. It is possible that the dose of 10mg/kg is too low to be detectable in brain homogenate at one hour after injection, or that the kinetics of dimeric and tetrameric EmtinB delivery to the CNS are slightly different and thus entry to the CNS was not seen at the one hour timepoint in the current study.

It is also possible that biotinylated d-EmtinB, with 2-3 molecules of biotin attached on spacer arms away from the peptide, may show altered steric interactions with mechanisms which may normally mediate the delivery of EmtinB across the blood-brain barrier. Sonn (2010) used EmtinB containing a single biotinylated site, causing minimal alterations from the kinetics of non-biotinylated EmtinB. It is likely that LRPs at the choroid plexus (Carro *et al.* 2005) allow transport of EmtinB from the blood into the CSF (Sonn *et al.* 2010). Another option for differing results between the current study and the Sonn (2010) study is that dimeric EmtinB peptides may show a weaker interaction with LRPs than tetrameric EmtinB peptides, and therefore may not be transported as efficiently into the CNS.

Additionally, Sonn and colleagues (2010) studied the presence of EmtinB in CSF, whereas the current study examined whole brain homogenates for the presence of EmtinB. As the contribution of CSF to protein levels in whole brain homogenate may be minimal, due to loss of CSF during perfusion and dissection, the absence of detectable levels of biotinylated d-EmtinB in brain homogenates do not directly rule out its presence in the CSF in the present study. As the neuroprotective actions of EmtinB can be triggered by extracellular interactions between EmtinB and its LRP receptors (Ambjorn *et al.* 2008), extracellular or CSF EmtinB may still elicit protective effects despite not being internalised into neurons.

The presence of EmtinB in the urine at one hour after injection indicates that dimeric EmtinB is readily cleared from the circulation through the kidneys in the present study. The presence of EmtinB in the urine matches that of MT2, which is also present in the kidney and urine after i.p. injection (Lewis *et al.* 2012b). Future studies examining administration of either EmtinB or MT2 must determine how much of the active molecule is lost through the kidneys in order to determine strategies for successful CNS penetration.

Multiple d-EmtinB bands, possibly representing oligomeric or aggregated forms of the injected peptide, were observed in the serum at one hour after injection. Care must be taken in future studies to avoid the formation of high molecular weight aggregates of Emtin peptides in solution, for two reasons: first, these aggregates may not properly interact with LRP receptors and may not activate the correct intracellular pathways; second, delivery of aggregated peptides to the CNS may place undue stress on motor neurons in SOD1 mice which are already under stress due to aggregated proteins (Watanabe *et al.* 2001).

5.4.5 Summary and conclusions

In summary, Emtin peptides administered from symptom onset onwards appear to show increased survival times, and slight retention of hindlimb function, in a small cohort of female SOD1 mice. The effects of Emtin peptides approach statistical significance, despite the small numbers (n=6 for each group) involved in this pilot study, and despite the treatment only being started around the point of disease onset. Emtin peptides appear to be a promising candidate for further development as a therapeutic for human ALS. Future work should involve a larger cohort of SOD1 mice in accordance with consensus guidelines for pre-clinical SOD1 trials, and should also involve analysis of motor neuron protection and neuromuscular junction innervation in a subset of SOD1 mice, to determine the mechanism of action of Emtin peptides.

Chapter 6

Concluding remarks and future work

6.1 The need for novel ALS therapeutics

Amyotrophic lateral sclerosis is a neurodegenerative disease of the motor system, with a complex aetiology potentially involving many cellular pathways, with oxidative stress, neuroinflammation, RNA metabolism, and protein degradation dysfunction featuring most prominently amongst possible aetiologies. The search for an effective therapeutic molecule for preventing motor neuron degeneration has so far not been successful, with the only approved drug treatment for ALS, Riluzole, only extending lifespan by a matter of months (Bensimon *et al.* 1994).

The work contained within this thesis uses a mouse model of ALS to explore a link between microglial activation and oxidative stress via nitric oxide metabolism, and to trial the ability of three therapeutic compounds to extend lifespan in the mouse model. Here, the results of each chapter will be reviewed in the context of attempting to understand the disease mechanisms contributing to disease in the mouse model of ALS.

6.2 Microglial activation in ALS

Microglial activation has been implicated in the progression of ALS, with SOD1 mice showing pre-symptomatic and post-symptom-onset microglial activation, and ALS patients showing microglial activation in post-mortem spinal cord (Hall *et al.* 1998b; Alexianu *et al.* 2001; Henkel *et al.* 2004). In Chapter 2, the temporal relationships between microglial activation, development of neuronal pathology, and functional decline in SOD1 mice were examined. Consistent with previous studies, it was shown that microglial activation coincided with disease onset, but preceded the development of overt functional deficits, indicating that microglial activation may accelerate disease progression.

While previous studies have indicated a swing towards M1 neurotoxic microglia as disease progresses(Liao *et al.* 2012), examination of arginine-metabolising enzymes and putative M1/M2 markers in the current study, Arg1 and iNOS, indicated that both pro-inflammatory and anti-inflammatory phenotypes of microglia are present in the lumbar spinal cord of symptomatic SOD1 mice. These data may represent ongoing conflict between neuroinflammatory states – M2 neuroprotective microglia may attempt to dampen inflammation to prevent further neuronal damage, while M1 neurotoxic microglia may induce motor neuron damage, in part through increased expression of iNOS and increased NO synthesis (Zhao *et al.* 2004). Slight changes in the inflammatory environment of the lumbar and cervical spinal cords, characterised by a slightly more M2-like environment in the cervical region, may account for the relative sparing of the cervical region compared to the lumbar region (Beers *et al.* 2011b).

Therapeutics aimed at inhibiting neuroinflammation have been trialled with positive results in SOD1 mice, yet showed no effect, or had detrimental effects, when translated into human ALS clinical trials (Bowerman *et al.* 2013). The data from clinical trials reinforce the dual role of microglia in neurodegenerative disease, with ongoing neuroprotective functions in addition to neurotoxic functions; inhibiting microglial activation may deplete any neuroprotection provided to motor neurons by microglia with an M2-like phenotype. The ongoing expression of Arg1, as described in SOD1 microglia in Chapter 2 of this thesis, correlates with ongoing neuroprotective functions of activated microglia in ALS. Additionally, the importance of microglial activation in ALS is underlined by a recent study implicating a mutation in the triggering receptor

expressed by myeloid cells 2 (TREM2) protein, involved in microglial phagocytosis of cellular debris, as a risk factor for sporadic ALS (Neumann & Takahashi 2007; Cady *et al.* 2014). It is therefore critical that more research into microglial activation in neuroinflammation is carried out, in order to determine how best to eliminate neurotoxic microglial function while retaining neuroprotective function. Future work should aim to identify mediators of the molecular switch between neuroprotective and neurotoxic microglial phenotypes, and examine the bidirectional signalling between activated microglia and motor neurons. Further elucidation of microglial-mediated disease mechanisms in ALS may identify novel targets for therapeutic intervention.

6.3 Antioxidant treatments for ALS

Oxidative stress is intricately linked to ALS, either as a potential primary cause of disease or as an effector of other upstream pathogenic mechanisms (see convergent pathology, section 1.3.9).

Two of the potential ALS therapeutics used in this thesis, Gemals and MT2, are thought to act at least in part via antioxidant mechanisms. In Chapter 4, pre-symptomatic treatment with MT2 protein resulted in a slight delay in disease onset as measured by peak body weight, and tended to increase survival time. In Chapter 3, treatment with Gemals from after symptom onset until disease endpoint did not show a significant effect on survival time in a large cohort of SOD1 mice. However, it must be noted that several confounding factors in the Gemals trial, such as the development and treatment of irritation and skin lesions, may have prevented a protective effect of the Gemals compound from being detected.

Setting aside confounding factors in the Gemals trial, the results from the Gemals trial and the MT2 trial suggest that oxidative stress-directed treatments may only be effective at slowing disease processes during the pre-symptomatic stage of disease. Indeed, the only other study examining the effect of Gemals in ALS rodent models showed an increase in survival time when Gemals was administered during the pre-symptomatic stage of disease (Nicaise *et al.* 2008).

If treating oxidative stress in the pre-symptomatic stage is able to delay disease, but treatment of oxidative stress after symptom onset has little effect, it is possible that oxidative stress is a key mechanistic event in ALS pathogenesis, but may cause a cascade of downstream pathological mechanisms, such as mitochondrial dysfunction or protein aggregation, which cannot be reversed by removing the initial oxidative insult. To effectively treat such a situation, antioxidant compounds which slow the development of pathology would need to be used in conjunction with drugs which may provide neuronal protection or promote the degradation of damaged mitochondria and aggregated proteins, preventing the formation of downstream products and facilitating the removal of altered cellular components.

In SOD1 mice, drugs with an antioxidant mechanism of action show the most promising effects for treatment after disease onset (Benatar 2007). However, a Cochrane review of

antioxidant therapies in ALS patients showed that antioxidants have little beneficial effect on survival (Orrell *et al.* 2007). More recently, an open trial of Gemals in a small group of ALS patients did indicate positive preliminary results of this compound in patients (Geffard *et al.* 2010). The Geffard (2010) study could indicate that Gemals exerts a protective effect due to its multiple putative mechanisms of action, rather than purely due to its antioxidant function (Geffard *et al.* 2010). If future work on Gemals is to take place in SOD1 mice, care should be taken to isolate the component/s causing irritation, to prevent the development of skin lesions and prevent the need for confounding analgesic treatment in further trials. Like Gemals, MT2 has multiple putative mechanisms by which it could induce protection of motor neurons, rather than a purely antioxidant mechanism.

Oxidative stress is known to be present in sporadic and familial ALS cases (Ferrante *et al.* 1997), yet the treatments used in thesis that were based around the amelioration of oxidative stress did not show robust beneficial effects. Based on the common presence of oxidative stress in sporadic and familial disease (Ferrante *et al.* 1997), I would therefore have expected that, had the treatments shown robust effects in SOD1 mice, these treatments would have been translatable into potential therapies for human ALS patients. However, as these treatments showed no substantial effects in SOD1 mice, it is unclear whether these oxidation-targeted therapeutics in their current form would hold any benefit for ALS patients. More research into the mechanisms of oxidative stress-mediated damage in motor neurons should be performed in order to determine whether oxidative stress is a primary factor causing neuronal degeneration, or purely a downstream byproduct of another degenerative process. It is possible that the pathology seen in SOD1 mice, including oxidative stress, is limited to animals and patients with SOD1-linked disease. Indeed, only SOD1-linked familial ALS cases show SOD1 protein aggregation in spinal cord motor neurons; SOD1 aggregates are not found in non-SOD1-linked familial ALS, and only rarely seen in sporadic ALS cases (Bosco *et al.* 2010; Ravits *et al.* 2013).

The targeting of other common pathologies in ALS, such as the presence of TDP43 in sporadic and virtually all non-SOD1 familial ALS cases, may provide more benefit in developing broad-spectrum therapeutics for ALS patients regardless of genetic or sporadic aetiology.

6.4 MT2 and its derivatives as putative ALS therapeutics

The multipurpose neuroprotective protein metallothionein-1/2 (MT-1/2), and its derivatives, have been discussed in Chapters 2, 4, and 5. The amount of MT-1/2 in the spinal cord of SOD1 mice increases with disease progression, with the increased MT-1/2 production mainly mediated by astrocytes. Pre-symptomatic treatment with MT2 injections, but not with an exercise regime, delayed disease onset as measured by maximum body weight, and tended to increase survival times in SOD1 mice. A small pilot study of the MT2 derivative peptides, Emtins, showed a tendency for Emtin treatment to increase survival time even when administered after the onset of disease symptoms. Thus, it appears that MT-1/2 plays a neuroprotective role, and MT2 or its derivatives may be suitable for further development as therapeutic compounds for human ALS.

However, the mechanism of action for MT2 and Emtin peptides remains to be elucidated. MT2 is known to have several neuroprotective functions, with putative intracellular roles in ameliorating oxidative stress, correcting metal dyshomeostasis, and preventing apoptosis. As an extracellular ligand of the LRP receptors, MT-1/2 induces intracellular pathways involved in neurite outgrowth and neuronal survival, such as the PI3K/Akt pathway. In comparison, Emtin peptides are also known to induce neuronal survival and outgrowth via LRP receptors, but are not metallated. Thus, in principle Emtin peptides have less metal-binding capacity than MT-1/2, indicating that the trend of Emtins to increase survival time in SOD1 mice is likely more to do with LRP binding rather than any antioxidant or metal-homeostatic capacity of Emtin peptides.

The current lack of biomarkers for ALS in the pre-symptomatic phase means that treatments should ideally be effective from after the onset of disease symptoms. Emtin peptides, tested in a small cohort of SOD1 mice, showed some improvement in survival time when administered after the onset of disease symptoms, and therefore could represent a potential therapeutic for human ALS. Future work on the Emtin peptides should first employ a large pre-clinical study in SOD1 mice and rats, to ensure that the effects seen in this small pilot study can be replicated in a larger cohort, and to establish dose-dependent effects on survival. Cell culture work, eliciting the effects and mechanisms of action of Emtins on cultured motor neurons, could help to further evaluate these peptides as potential therapeutic molecules for human ALS.

6.5 The SOD1 model of ALS

The SOD1 mouse model of ALS is the most commonly-used animal model for human ALS. While the SOD1 model has undoubtedly been useful in describing mechanisms of motor neuron degeneration, its relevance to human sporadic ALS has been questioned. Although human ALS and rodent SOD1-mediated ALS show clinical and pathological similarities, SOD1-mutation-mediated ALS accounts for only 2-3% of human ALS cases, and the exact mechanisms of neuronal degeneration in SOD1 mice and human ALS patients may differ (Martin *et al.* 2007). It is therefore important to consider whether results obtained from pre-clinical trials in the SOD1 mouse can be effectively translated to sporadic ALS. Differences between human sporadic ALS and rodent SOD1-mediated ALS may account for the robust effects of several ALS therapeutic molecules when tested in SOD1 mice, but the failure of these same compounds when introduced into clinical trials (Benatar 2007).

A final common pathway between SOD1-mediated ALS, non-SOD1 FALS, and sporadic ALS has not been definitively identified, although as discussed in Chapter 1, oxidative stress may form one such convergence point. The more recent discoveries of RNA processing, protein degradation dysfunction, and hexanucleotide repeats in C9orf72 may provide more mechanistic insight into the disease processes of ALS. In particular, elucidating the mechanism of action of TDP43-mediated ALS will prove valuable for the future study of sporadic ALS and FTD.

6.6 Thesis summary

Chapter 1 identifies oxidative stress and neuroinflammation as key pathologies in the aetiology of ALS, with oxidative stress in particular acting as a convergence point between several putative ALS causes either as a primary insult or as a consequence of upstream pathology.

Chapter 2 has identified that the increase in microglial cells in the SOD1 spinal cord ventral horn is largely associated with an increase in microglia expressing the M2-type marker Arg1, although a smaller concomitant increase in microglia expressing the M1-type marker, iNOS, was also observed. These changes indicate duelling pro- and anti-inflammatory processes occurring in the spinal cord of SOD1 mice. An increase in MT-1/2 levels, thought to be a neuroprotective response to degenerating motor neurons, was also observed over time.

Chapter 3 trialled the antioxidant compound Gemals as a treatment in post-symptomatic SOD1 mice, yet found no significant effects on survival time. However, confounding factors in this study may limit its interpretation in terms of the effectiveness of Gemals treatment.

Chapter 4 trialled the neuroprotective protein MT2, and treadmill exercise, as pre-symptomatic treatments in SOD1 mice, with an increase in survival time observed for MT2-treated SOD1 mice but not exercise-treated SOD1 mice.

Chapter 5 explored a pilot study of the MT2 derivatives, Emtin peptides, administered after symptom onset in SOD1 mice. Emtin peptides showed a small increase in survival time, although this effect was not significant in this small cohort. However, Emtin peptides may represent a promising candidate for further development into a therapeutic molecule for increasing neuronal survival in ALS.

Therapeutics targeting multiple aspects of pathology in ALS are required in order to maintain surviving motor neurons and limit functional decline in ALS. Similarly, it is clear that more research into the basic mechanisms of ALS, and methods for early detection of ALS, are required in order to effectively treat this devastating neurodegenerative disease.

Reference List

References

Abel, J & de Ruiter, N 1989, 'Inhibition of hydroxyl-radical-generated DNA degradation by metallothionein', *Toxicology Letters*, vol. 47, no. 2, pp. 191-196.

Acevedo-Arozena, A, Kalmar, B, Essa, S, et al. 2011, 'A comprehensive assessment of the SOD1G93A low-copy transgenic mouse, which models human amyotrophic lateral sclerosis', *Disease Models & Mechanisms*, vol. 4, no. 5, pp. 686-700.

Ahsan, MK, Lekli, I, Ray, D, et al. 2009, 'Redox regulation of cell survival by the thioredoxin superfamily: an implication of redox gene therapy in the heart', *Antioxidants and Redox Signaling*, vol. 11, no. 11, pp. 2741-2758.

Ahtoniemi, T, Jaronen, M, Keksa-Goldsteine, V, et al. 2008, 'Mutant SOD1 from spinal cord of G93A rats is destabilized and binds to inner mitochondrial membrane', *Neurobiology of Disease*, vol. 32, no. 3, pp. 479-485.

Al-Chalabi, A, Andersen, PM, Nilsson, P, et al. 1999, 'Deletions of the heavy neurofilament subunit tail in amyotrophic lateral sclerosis', *Human Molecular Genetics*, vol. 8, no. 2, pp. 157-164.

Al-Chalabi, A, Jones, A, Troakes, C, et al. 2012, 'The genetics and neuropathology of amyotrophic lateral sclerosis', *Acta Neuropathologica*, vol. 124, no. 3, pp. 339-352.

Al-Chalabi, A, Powell, JF & Leigh, PN 1995, 'Neurofilaments, free radicals, excitotoxins, and amyotrophic lateral sclerosis', *Muscle & Nerve*, vol. 18, no. 5, pp. 540-545.

Al-Saif, A, Al-Mohanna, F & Bohlega, S 2011, 'A mutation in sigma-1 receptor causes juvenile amyotrophic lateral sclerosis', *Annals of Neurology*, vol. 70, no. 6, pp. 913-919.

Alexander, GM, Erwin, KL, Byers, N, et al. 2004, 'Effect of transgene copy number on survival in the G93A SOD1 transgenic mouse model of ALS', *Brain Research. Molecular Brain Research*, vol. 130, no. 1-2, pp. 7-15.

Alexianu, ME, Kozovska, M & Appel, SH 2001, 'Immune reactivity in a mouse model of familial ALS correlates with disease progression', *Neurology*, vol. 57, no. 7, pp. 1282-1289.

Almer, G, Vukosavic, S, Romero, N, et al. 1999, 'Inducible nitric oxide synthase up-regulation in a transgenic mouse model of familial amyotrophic lateral sclerosis', *Journal of Neurochemistry*, vol. 72, no. 6, pp. 2415-2425.

Ambjorn, M, Asmussen, JW, Lindstam, M, et al. 2008, 'Metallothionein and a peptide modeled after metallothionein, EmtinB, induce neuronal differentiation and survival through binding to receptors of the low-density lipoprotein receptor family', *Journal of Neurochemistry*, vol. 104, no. 1, pp. 21-37.

Andrew, PJ & Mayer, B 1999, 'Enzymatic function of nitric oxide synthases', *Cardiovascular Research*, vol. 43, no. 3, pp. 521-531.

Andrus, PK, Fleck, TJ, Gurney, ME, et al. 1998, 'Protein oxidative damage in a transgenic mouse model of familial amyotrophic lateral sclerosis', *Journal of Neurochemistry*, vol. 71, no. 5, pp. 2041-2048.

Anneser, JM, Cookson, MR, Ince, PG, et al. 2001, 'Glial cells of the spinal cord and subcortical white matter up-regulate neuronal nitric oxide synthase in sporadic amyotrophic lateral sclerosis', *Experimental Neurology*, vol. 171, no. 2, pp. 418-421.

Aparicio-Erriu, IM & Prehn, JH 2012, 'Molecular Mechanisms in Amyotrophic Lateral Sclerosis: The Role of Angiogenin, a Secreted RNase', *Frontiers in Neuroscience*, vol. 6, p. 167.

Appel, SH, Beers, D, Siklos, L, et al. 2001, 'Calcium: the Darth Vader of ALS', *Amyotrophic Lateral Sclerosis and Other Motor Neuron Disorders*, vol. 2 Suppl 1, pp. S47-54.

Appel, SH, Smith, RG, Engelhardt, JI, et al. 1993, 'Evidence for autoimmunity in amyotrophic lateral sclerosis', *Journal of the Neurological Sciences*, vol. 118, no. 2, pp. 169-174.

Appel, SH, Zhao, W, Beers, DR, et al. 2011, 'The microglial-motoneuron dialogue in ALS', *Acta Myologica*, vol. 30, no. 1, pp. 4-8.

Arbesman, M & Sheard, K 2014, 'Systematic review of the effectiveness of occupational therapy-related interventions for people with amyotrophic lateral sclerosis', *The American Journal of Occupational Therapy*, vol. 68, no. 1, pp. 20-26.

Aschner, M 1996, 'The functional significance of brain metallothioneins', *FASEB Journal*, vol. 10, no. 10, pp. 1129-1136.

Ash, DE 2004, 'Structure and function of arginases', *Journal of Nutrition*, vol. 134, no. 10 Suppl, pp. 2760S-2764S; discussion 2765S-2767S.

Asmussen, JW, Ambjorn, M, Bock, E, et al. 2009a, 'Peptides modeled after the alpha-domain of metallothionein induce neurite outgrowth and promote survival of cerebellar granule neurons', *European Journal of Cell Biology*, vol. 88, no. 8, pp. 433-443.

Asmussen, JW, Von Sperling, ML & Penkowa, M 2009b, 'Intraneuronal signaling pathways of metallothionein', *Journal of Neuroscience Research*, vol. 87, no. 13, pp. 2926-2936.
Atkin, JD, Farg, MA, Soo, KY, et al. 2013, 'Mutant SOD1 inhibits ER-Golgi transport in amyotrophic lateral sclerosis', *Journal of Neurochemistry*.
Atkin, JD, Farg, MA, Walker, AK, et al. 2008, 'Endoplasmic reticulum stress and induction of the unfolded protein response in human sporadic amyotrophic lateral sclerosis', *Neurobiology of Disease*, vol. 30, no. 3, pp. 400-407.
Audet, JN, Gowing, G, Paradis, R, et al. 2012, 'Ablation of proliferating cells in the CNS exacerbates motor neuron disease caused by mutant superoxide dismutase', *PLoS ONE*, vol. 7, no. 4, p. e34932.
Bae, JS, Simon, NG, Menon, P, et al. 2013, 'The puzzling case of hyperexcitability in amyotrophic lateral sclerosis', *Journal of Clinical Neurology*, vol. 9, no. 2, pp. 65-74.
Bame, M, Pentiak, PA, Needleman, R, et al. 2012, 'Effect of sex on lifespan, disease progression, and the response to methionine sulfoximine in the SOD1 G93A mouse model for ALS', *Gender Medicine*, vol. 9, no. 6, pp. 524-535.
Banci, L, Bertini, I, Boca, M, et al. 2008, 'SOD1 and amyotrophic lateral sclerosis: mutations and oligomerization', *PLoS ONE*, vol. 3, no. 2, p. e1677.
Banerjee, BD, Seth, V & Ahmed, RS 2001, 'Pesticide-induced oxidative stress: perspectives and trends', *Reviews on Environmental Health*, vol. 16, no. 1, pp. 1-40.
Banerjee, R, Mosley, RL, Reynolds, AD, et al. 2008, 'Adaptive immune neuroprotection in G93A-SOD1 amyotrophic lateral sclerosis mice', *PLoS ONE*, vol. 3, no. 7, p. e2740.
Barbeito, LH, Pehar, M, Cassina, P, et al. 2004, 'A role for astrocytes in motor neuron loss in amyotrophic lateral sclerosis', *Brain Research. Brain Research Reviews*, vol. 47, no. 1-3, pp. 263-274.
Barber, SC & Shaw, PJ 2010, 'Oxidative stress in ALS: key role in motor neuron injury and therapeutic target', *Free Radical Biology and Medicine*, vol. 48, no. 5, pp. 629-641.
Basso, M, Pozzi, S, Tortarolo, M, et al. 2013, 'Mutant copper-zinc superoxide dismutase (SOD1) induces protein secretion pathway alterations and exosome release in astrocytes: implications for disease spreading and motor neuron pathology in amyotrophic lateral sclerosis', *The Journal of biological chemistry*, vol. 288, no. 22, pp. 15699-15711.
Beal, MF, Ferrante, RJ, Browne, SE, et al. 1997, 'Increased 3-nitrotyrosine in both sporadic and familial amyotrophic lateral sclerosis', *Annals of Neurology*, vol. 42, no. 4, pp. 644-654.
Beaulieu, JM, Jacomy, H & Julien, JP 2000, 'Formation of intermediate filament protein aggregates with disparate effects in two transgenic mouse models lacking the neurofilament light subunit', *The Journal of Neuroscience*, vol. 20, no. 14, pp. 5321-5328.
Beckman, JS, Carson, M, Smith, CD, et al. 1993, 'ALS, SOD and peroxynitrite', *Nature*, vol. 364, no. 6438, p. 584.
Beers, DR, Henkel, JS, Xiao, Q, et al. 2006, 'Wild-type microglia extend survival in PU.1 knockout mice with familial amyotrophic lateral sclerosis', *Proceedings of the National Academy of Sciences of the United States of America*, vol. 103, no. 43, pp. 16021-16026.
Beers, DR, Henkel, JS, Zhao, W, et al. 2008, 'CD4+ T cells support glial neuroprotection, slow disease progression, and modify glial morphology in an animal model of inherited ALS', *Proceedings of the National Academy of Sciences of the United States of America*, vol. 105, no. 40, pp. 15558-15563.
Beers, DR, Henkel, JS, Zhao, W, et al. 2011a, 'Endogenous regulatory T lymphocytes ameliorate amyotrophic lateral sclerosis in mice and correlate with disease progression in patients with amyotrophic lateral sclerosis', *Brain*, vol. 134, no. Pt 5, pp. 1293-1314.
Beers, DR, Zhao, W, Liao, B, et al. 2011b, 'Neuroinflammation modulates distinct regional and temporal clinical responses in ALS mice', *Brain, Behavior, and Immunity*, vol. 25, no. 5, pp. 1025-1035.
Beghi, E, Logroscino, G, Chio, A, et al. 2010, 'Amyotrophic lateral sclerosis, physical exercise, trauma and sports: results of a population-based pilot case-control study', *Amyotrophic Lateral Sclerosis*, vol. 11, no. 3, pp. 289-292.
Beltran, B, Quintero, M, Garcia-Zaragoza, E, et al. 2002, 'Inhibition of mitochondrial respiration by endogenous nitric oxide: a critical step in Fas signaling', *Proceedings of the National Academy of Sciences of the United States of America*, vol. 99, no. 13, pp. 8892-8897.
Belzil, VV, Daoud, H, Camu, W, et al. 2013, 'Genetic analysis of SIGMAR1 as a cause of familial ALS with dementia', *European Journal of Human Genetics*, vol. 21, no. 2, pp. 237-239.
Benatar, M 2007, 'Lost in translation: treatment trials in the SOD1 mouse and in human ALS', *Neurobiology of Disease*, vol. 26, no. 1, pp. 1-13.
Bendotti, C, Tortarolo, M, Suchak, SK, et al. 2001, 'Transgenic SOD1 G93A mice develop reduced GLT-1 in spinal cord without alterations in cerebrospinal fluid glutamate levels', *Journal of Neurochemistry*, vol. 79, no. 4, pp. 737-746.

Benkler, C, Ben-Zur, T, Barhum, Y, et al. 2013, 'Altered astrocytic response to activation in SOD1(G93A) mice and its implications on amyotrophic lateral sclerosis pathogenesis', *Glia*, vol. 61, no. 3, pp. 312-326.

Bennett, CL, Chen, Y, Vignali, M, et al. 2013, 'Protein interaction analysis of senataxin and the ALS4 L389S mutant yields insights into senataxin post-translational modification and uncovers mutant-specific binding with a brain cytoplasmic RNA-encoded peptide', *PLoS ONE*, vol. 8, no. 11, p. e78837.

Bensimon, G, Lacomblez, L & Meininger, V 1994, 'A controlled trial of riluzole in amyotrophic lateral sclerosis. ALS/Riluzole Study Group', *New England Journal of Medicine*, vol. 330, no. 9, pp. 585-591.

Bentmann, E, Haass, C & Dormann, D 2013, 'Stress granules in neurodegeneration--lessons learnt from TAR DNA binding protein of 43 kDa and fused in sarcoma', *FEBS Journal*, vol. 280, no. 18, pp. 4348-4370.

Berg, JM, Tymoczko, JL & Stryer, L 2002, 'Regulation of cellular respiration', in *Biochemistry*, 5th edn, W. H. Freeman, New York.

Bilak, M, Wu, L, Wang, Q, et al. 2004, 'PGE2 receptors rescue motor neurons in a model of amyotrophic lateral sclerosis', *Annals of Neurology*, vol. 56, no. 2, pp. 240-248.

Binet, S & Meininger, V 1988, 'Modifications of microtubule proteins in ALS nerve precede detectable histologic and ultrastructural changes', *Neurology*, vol. 38, no. 10, pp. 1596-1600.

Blaauwgeers, HG, Anwar Chand, M, van den Berg, FM, et al. 1996, 'Expression of different metallothionein messenger ribonucleic acids in motor cortex, spinal cord and liver from patients with amyotrophic lateral sclerosis', *Journal of the Neurological Sciences*, vol. 142, no. 1-2, pp. 39-44.

Blindauer, CA & Leszczyszyn, OI 2010, 'Metallothioneins: unparalleled diversity in structures and functions for metal ion homeostasis and more', *Natural Product Reports*, vol. 27, no. 5, pp. 720-741.

Blokhuis, AM, Groen, EJ, Koppers, M, et al. 2013, 'Protein aggregation in amyotrophic lateral sclerosis', *Acta Neuropathologica*, vol. 125, no. 6, pp. 777-794.

Bogdanov, M, Brown, RH, Matson, W, et al. 2000, 'Increased oxidative damage to DNA in ALS patients', *Free Radical Biology and Medicine*, vol. 29, no. 7, pp. 652-658.

Bohannon, RW 1983, 'Results of resistance exercise on a patient with amyotrophic lateral sclerosis. A case report', *Physical Therapy*, vol. 63, no. 6, pp. 965-968.

Boillee, S, Yamanaka, K, Lobsiger, CS, et al. 2006, 'Onset and progression in inherited ALS determined by motor neurons and microglia', *Science*, vol. 312, no. 5778, pp. 1389-1392.

Bonaparte, KL, Hudson, CA, Wu, C, et al. 2006, 'Inverse regulation of inducible nitric oxide synthase (iNOS) and arginase I by the protein tyrosine phosphatase SHP-1 in CNS glia', *Glia*, vol. 53, no. 8, pp. 827-835.

Borchelt, DR, Guarnieri, M, Wong, PC, et al. 1995, 'Superoxide dismutase 1 subunits with mutations linked to familial amyotrophic lateral sclerosis do not affect wild-type subunit function', *The Journal of biological chemistry*, vol. 270, no. 7, pp. 3234-3238.

Borchelt, DR, Lee, MK, Slunt, HS, et al. 1994, 'Superoxide dismutase 1 with mutations linked to familial amyotrophic lateral sclerosis possesses significant activity', *Proceedings of the National Academy of Sciences of the United States of America*, vol. 91, no. 17, pp. 8292-8296.

Borthwick, GM, Johnson, MA, Ince, PG, et al. 1999, 'Mitochondrial enzyme activity in amyotrophic lateral sclerosis: implications for the role of mitochondria in neuronal cell death', *Annals of Neurology*, vol. 46, no. 5, pp. 787-790.

Bosco, DA, Morfini, G, Karabacak, NM, et al. 2010, 'Wild-type and mutant SOD1 share an aberrant conformation and a common pathogenic pathway in ALS', *Nature Neuroscience*, vol. 13, no. 11, pp. 1396-1403.

Boucher, P & Gotthardt, M 2004, 'LRP and PDGF signaling: a pathway to atherosclerosis', *Trends in Cardiovascular Medicine*, vol. 14, no. 2, pp. 55-60.

Bowerman, M, Vincent, T, Scamps, F, et al. 2013, 'Neuroimmunity dynamics and the development of therapeutic strategies for amyotrophic lateral sclerosis', *Frontiers in Cellular Neuroscience*, vol. 7, p. 214.

Bowling, AC, Barkowski, EE, McKenna-Yasek, D, et al. 1995, 'Superoxide dismutase concentration and activity in familial amyotrophic lateral sclerosis', *Journal of Neurochemistry*, vol. 64, no. 5, pp. 2366-2369.

Bowling, AC, Schulz, JB, Brown, RH, Jr., et al. 1993, 'Superoxide dismutase activity, oxidative damage, and mitochondrial energy metabolism in familial and sporadic amyotrophic lateral sclerosis', *Journal of Neurochemistry*, vol. 61, no. 6, pp. 2322-2325.

Breuer, AC & Atkinson, MB 1988a, 'Calcium dependent modulation of fast axonal transport', *Cell Calcium*, vol. 9, no. 5-6, pp. 293-301.

—— 1988b, 'Fast axonal transport alterations in amyotrophic lateral sclerosis (ALS) and in parathyroid hormone (PTH)-treated axons', *Cell Motility and the Cytoskeleton*, vol. 10, no. 1-2, pp. 321-330.

Breuer, AC, Lynn, MP, Atkinson, MB, et al. 1987, 'Fast axonal transport in amyotrophic lateral sclerosis: an intra-axonal organelle traffic analysis', *Neurology*, vol. 37, no. 5, pp. 738-748.

Brooks, BR 1994, 'El Escorial World Federation of Neurology criteria for the diagnosis of amyotrophic lateral sclerosis. Subcommittee on Motor Neuron Diseases/Amyotrophic Lateral Sclerosis of the World Federation of Neurology Research Group on Neuromuscular Diseases and the El Escorial "Clinical limits of amyotrophic lateral sclerosis" workshop contributors', *Journal of the Neurological Sciences*, vol. 124 Suppl, pp. 96-107.

Brooks, BR, Miller, RG, Swash, M, et al. 2000, 'El Escorial revisited: revised criteria for the diagnosis of amyotrophic lateral sclerosis', *Amyotrophic Lateral Sclerosis and Other Motor Neuron Disorders*, vol. 1, no. 5, pp. 293-299.

Browne, SE, Bowling, AC, Baik, MJ, et al. 1998, 'Metabolic dysfunction in familial, but not sporadic, amyotrophic lateral sclerosis', *Journal of Neurochemistry*, vol. 71, no. 1, pp. 281-287.

Bruijn, LI, Beal, MF, Becher, MW, et al. 1997a, 'Elevated free nitrotyrosine levels, but not protein-bound nitrotyrosine or hydroxyl radicals, throughout amyotrophic lateral sclerosis (ALS)-like disease implicate tyrosine nitration as an aberrant in vivo property of one familial ALS-linked superoxide dismutase 1 mutant', *Proceedings of the National Academy of Sciences of the United States of America*, vol. 94, no. 14, pp. 7606-7611.

Bruijn, LI, Becher, MW, Lee, MK, et al. 1997b, 'ALS-linked SOD1 mutant G85R mediates damage to astrocytes and promotes rapidly progressive disease with SOD1-containing inclusions', *Neuron*, vol. 18, no. 2, pp. 327-338.

Bruijn, LI, Houseweart, MK, Kato, S, et al. 1998, 'Aggregation and motor neuron toxicity of an ALS-linked SOD1 mutant independent from wild-type SOD1', *Science*, vol. 281, no. 5384, pp. 1851-1854.

Buchackert, Y, Rummel, S, Vohwinkel, CU, et al. 2012, 'Megalin mediates transepithelial albumin clearance from the alveolar space of intact rabbit lungs', *The Journal of physiology*, vol. 590, no. Pt 20, pp. 5167-5181.

Buratti, E, Brindisi, A, Giombi, M, et al. 2005, 'TDP-43 binds heterogeneous nuclear ribonucleoprotein A/B through its C-terminal tail: an important region for the inhibition of cystic fibrosis transmembrane conductance regulator exon 9 splicing', *The Journal of biological chemistry*, vol. 280, no. 45, pp. 37572-37584.

Buratti, E, De Conti, L, Stuani, C, et al. 2010, 'Nuclear factor TDP-43 can affect selected microRNA levels', *FEBS Journal*, vol. 277, no. 10, pp. 2268-2281.

Cady, J, Koval, ED, Benitez, BA, et al. 2014, 'TREM2 variant p.R47H as a risk factor for sporadic amyotrophic lateral sclerosis', *JAMA Neurology*, vol. 71, no. 4, pp. 449-453.

Campagne, MV, Thibodeaux, H, van Bruggen, N, et al. 2000, 'Increased binding activity at an antioxidant-responsive element in the metallothionein-1 promoter and rapid induction of metallothionein-1 and -2 in response to cerebral ischemia and reperfusion', *The Journal of Neuroscience*, vol. 20, no. 14, pp. 5200-5207.

Carreras, I, Yuruker, S, Aytan, N, et al. 2010, 'Moderate exercise delays the motor performance decline in a transgenic model of ALS', *Brain Research*, vol. 1313, pp. 192-201.

Carro, E, Spuch, C, Trejo, JL, et al. 2005, 'Choroid plexus megalin is involved in neuroprotection by serum insulin-like growth factor I', *The Journal of Neuroscience*, vol. 25, no. 47, pp. 10884-10893.

Cassina, P, Peluffo, H, Pehar, M, et al. 2002, 'Peroxynitrite triggers a phenotypic transformation in spinal cord astrocytes that induces motor neuron apoptosis', *Journal of Neuroscience Research*, vol. 67, no. 1, pp. 21-29.

Cereda, C, Baiocchi, C, Bongioanni, P, et al. 2008, 'TNF and sTNFR1/2 plasma levels in ALS patients', *Journal of Neuroimmunology*, vol. 194, no. 1-2, pp. 123-131.

Chang, L & Karin, M 2001, 'Mammalian MAP kinase signalling cascades', *Nature*, vol. 410, no. 6824, pp. 37-40.

Chang, Y, Kong, Q, Shan, X, et al. 2008, 'Messenger RNA oxidation occurs early in disease pathogenesis and promotes motor neuron degeneration in ALS', *PLoS ONE*, vol. 3, no. 8, p. e2849.

Cheah, BC, Vucic, S, Krishnan, AV, et al. 2010, 'Riluzole, neuroprotection and amyotrophic lateral sclerosis', *Current Medicinal Chemistry*, vol. 17, no. 18, pp. 1942-1199.

Chen, HJ, Anagnostou, G, Chai, A, et al. 2010, 'Characterization of the properties of a novel mutation in VAPB in familial amyotrophic lateral sclerosis', *The Journal of biological chemistry*, vol. 285, no. 51, pp. 40266-40281.

Chen, S, Zhang, X, Song, L, et al. 2012, 'Autophagy dysregulation in amyotrophic lateral sclerosis', *Brain Pathology*, vol. 22, no. 1, pp. 110-116.

Chen, YZ, Bennett, CL, Huynh, HM, et al. 2004, 'DNA/RNA helicase gene mutations in a form of juvenile amyotrophic lateral sclerosis (ALS4)', *American Journal of Human Genetics*, vol. 74, no. 6, pp. 1128-1135.

Chernyak, BV 1997, 'Redox regulation of the mitochondrial permeability transition pore', *Bioscience Reports*, vol. 17, no. 3, pp. 293-302.
Chevalier-Larsen, E & Holzbaur, EL 2006, 'Axonal transport and neurodegenerative disease', *Biochimica et Biophysica Acta*, vol. 1762, no. 11-12, pp. 1094-1108.
Chio, A, Logroscino, G, Hardiman, O, et al. 2009, 'Prognostic factors in ALS: A critical review', *Amyotrophic Lateral Sclerosis*, vol. 10, no. 5-6, pp. 310-323.
Chio, A & Mora, G 2012, 'Physical fitness and amyotrophic lateral sclerosis: dangerous liaisons or common genetic pathways?', *Journal of Neurology, Neurosurgery and Psychiatry*, vol. 83, no. 4, p. 389.
Chiu, AS, Gehringer, MM, Welch, JH, et al. 2011, 'Does alpha-amino-beta-methylaminopropionic acid (BMAA) play a role in neurodegeneration?', *International Journal of Environmental Research and Public Health*, vol. 8, no. 9, pp. 3728-3746.
Chiu, IM, Chen, A, Zheng, Y, et al. 2008, 'T lymphocytes potentiate endogenous neuroprotective inflammation in a mouse model of ALS', *Proceedings of the National Academy of Sciences of the United States of America*, vol. 105, no. 46, pp. 17913-17918.
Chou, SM, Wang, HS & Komai, K 1996, 'Colocalization of NOS and SOD1 in neurofilament accumulation within motor neurons of amyotrophic lateral sclerosis: an immunohistochemical study', *Journal of Chemical Neuroanatomy*, vol. 10, no. 3-4, pp. 249-258.
Chow, CY, Landers, JE, Bergren, SK, et al. 2009, 'Deleterious variants of FIG4, a phosphoinositide phosphatase, in patients with ALS', *American Journal of Human Genetics*, vol. 84, no. 1, pp. 85-88.
Chung, RS, Adlard, PA, Dittmann, J, et al. 2004, 'Neuron-glia communication: metallothionein expression is specifically up-regulated by astrocytes in response to neuronal injury', *Journal of Neurochemistry*, vol. 88, no. 2, pp. 454-461.
Chung, RS, Hidalgo, J & West, AK 2008a, 'New insight into the molecular pathways of metallothionein-mediated neuroprotection and regeneration', *Journal of Neurochemistry*, vol. 104, no. 1, pp. 14-20.
Chung, RS, Leung, YK, Butler, CW, et al. 2009, 'Metallothionein treatment attenuates microglial activation and expression of neurotoxic quinolinic acid following traumatic brain injury', *Neurotoxicity research*, vol. 15, no. 4, pp. 381-389.
Chung, RS, Penkowa, M, Dittmann, J, et al. 2008b, 'Redefining the role of metallothionein within the injured brain: extracellular metallothioneins play an important role in the astrocyte-neuron response to injury', *The Journal of biological chemistry*, vol. 283, no. 22, pp. 15349-15358.
Chung, RS, Vickers, JC, Chuah, MI, et al. 2003, 'Metallothionein-IIA promotes initial neurite elongation and postinjury reactive neurite growth and facilitates healing after focal cortical brain injury', *The Journal of Neuroscience*, vol. 23, no. 8, pp. 3336-3342.
Collard, JF, Cote, F & Julien, JP 1995, 'Defective axonal transport in a transgenic mouse model of amyotrophic lateral sclerosis', *Nature*, vol. 375, no. 6526, pp. 61-64.
Colton, CA 2009, 'Heterogeneity of microglial activation in the innate immune response in the brain', *Journal of Neuroimmune Pharmacology*, vol. 4, no. 4, pp. 399-418.
Consilvio, C, Vincent, AM & Feldman, EL 2004, 'Neuroinflammation, COX-2, and ALS--a dual role?', *Experimental Neurology*, vol. 187, no. 1, pp. 1-10.
Cooke, MS, Evans, MD, Dizdaroglu, M, et al. 2003, 'Oxidative DNA damage: mechanisms, mutation, and disease', *FASEB Journal*, vol. 17, no. 10, pp. 1195-1214.
Cookson, MR, Menzies, FM, Manning, P, et al. 2002, 'Cu/Zn superoxide dismutase (SOD1) mutations associated with familial amyotrophic lateral sclerosis (ALS) affect cellular free radical release in the presence of oxidative stress', *Amyotrophic Lateral Sclerosis and Other Motor Neuron Disorders*, vol. 3, no. 2, pp. 75-85.
Cote, F, Collard, JF & Julien, JP 1993, 'Progressive neuronopathy in transgenic mice expressing the human neurofilament heavy gene: a mouse model of amyotrophic lateral sclerosis', *Cell*, vol. 73, no. 1, pp. 35-46.
Cousins, RJ & Leinart, AS 1988, 'Tissue-specific regulation of zinc metabolism and metallothionein genes by interleukin 1', *FASEB Journal*, vol. 2, no. 13, pp. 2884-2890.
Cox, PA, Richer, R, Metcalf, JS, et al. 2009, 'Cyanobacteria and BMAA exposure from desert dust: a possible link to sporadic ALS among Gulf War veterans', *Amyotrophic Lateral Sclerosis*, vol. 10 Suppl 2, pp. 109-117.
Cozzolino, M & Carri, MT 2012, 'Mitochondrial dysfunction in ALS', *Progress in Neurobiology*, vol. 97, no. 2, pp. 54-66.
Crow, JP, Sampson, JB, Zhuang, Y, et al. 1997, 'Decreased zinc affinity of amyotrophic lateral sclerosis-associated superoxide dismutase mutants leads to enhanced catalysis of tyrosine nitration by peroxynitrite', *Journal of Neurochemistry*, vol. 69, no. 5, pp. 1936-1944.

Crugnola, V, Lamperti, C, Lucchini, V, et al. 2010, 'Mitochondrial respiratory chain dysfunction in muscle from patients with amyotrophic lateral sclerosis', *Archives of Neurology*, vol. 67, no. 7, pp. 849-854.

Dal Bello-Haas, V, Florence, JM, Kloos, AD, et al. 2007, 'A randomized controlled trial of resistance exercise in individuals with ALS', *Neurology*, vol. 68, no. 23, pp. 2003-2007.

Dal Bello-Haas, V, Florence, JM & Krivickas, LS 2008, 'Therapeutic exercise for people with amyotrophic lateral sclerosis or motor neuron disease', *The Cochrane database of systematic reviews*, no. 2, p. CD005229.

Das, A & Plotkin, SS 2013, 'Mechanical probes of SOD1 predict systematic trends in metal and dimer affinity of ALS-associated mutants', *Journal of Molecular Biology*, vol. 425, no. 5, pp. 850-874.

Das, K, Nag, C & Ghosh, M 2012, 'Familial, environmental, and occupational risk factors in development of amyotrophic lateral sclerosis', *North American Journal of Medical Sciences*, vol. 4, no. 8, pp. 350-355.

de Almeida, JP, Silvestre, R, Pinto, AC, et al. 2012, 'Exercise and amyotrophic lateral sclerosis', *Neurological Sciences*, vol. 33, no. 1, pp. 9-15.

de Carvalho, M, Dengler, R, Eisen, A, et al. 2008, 'Electrodiagnostic criteria for diagnosis of ALS', *Clinical Neurophysiology*, vol. 119, no. 3, pp. 497-503.

De Vos, K, Severin, F, Van Herreweghe, F, et al. 2000, 'Tumor necrosis factor induces hyperphosphorylation of kinesin light chain and inhibits kinesin-mediated transport of mitochondria', *The Journal of cell biology*, vol. 149, no. 6, pp. 1207-1214.

De Vos, KJ, Morotz, GM, Stoica, R, et al. 2012, 'VAPB interacts with the mitochondrial protein PTPIP51 to regulate calcium homeostasis', *Human Molecular Genetics*, vol. 21, no. 6, pp. 1299-1311.

Deforges, S, Branchu, J, Biondi, O, et al. 2009, 'Motoneuron survival is promoted by specific exercise in a mouse model of amyotrophic lateral sclerosis', *The Journal of physiology*, vol. 587, no. Pt 14, pp. 3561-3572.

DeJesus-Hernandez, M, Mackenzie, IR, Boeve, BF, et al. 2011, 'Expanded GGGGCC hexanucleotide repeat in noncoding region of C9ORF72 causes chromosome 9p-linked FTD and ALS', *Neuron*, vol. 72, no. 2, pp. 245-256.

Deng, HX, Chen, W, Hong, ST, et al. 2011, 'Mutations in UBQLN2 cause dominant X-linked juvenile and adult-onset ALS and ALS/dementia', *Nature*, vol. 477, no. 7363, pp. 211-215.

Deng, HX, Hentati, A, Tainer, JA, et al. 1993, 'Amyotrophic lateral sclerosis and structural defects in Cu,Zn superoxide dismutase', *Science*, vol. 261, no. 5124, pp. 1047-1051.

Deng, HX, Shi, Y, Furukawa, Y, et al. 2006, 'Conversion to the amyotrophic lateral sclerosis phenotype is associated with intermolecular linked insoluble aggregates of SOD1 in mitochondria', *Proceedings of the National Academy of Sciences of the United States of America*, vol. 103, no. 18, pp. 7142-7147.

Derave, W, Van Den Bosch, L, Lemmens, G, et al. 2003, 'Skeletal muscle properties in a transgenic mouse model for amyotrophic lateral sclerosis: effects of creatine treatment', *Neurobiology of Disease*, vol. 13, no. 3, pp. 264-272.

Dewil, M, Van Den Bosch, L & Robberecht, W 2007, 'Microglia in amyotrophic lateral sclerosis', *Acta Neurologica Belgica*, vol. 107, no. 3, pp. 63-70.

Dhaliwal, GK & Grewal, RP 2000, 'Mitochondrial DNA deletion mutation levels are elevated in ALS brains', *Neuroreport*, vol. 11, no. 11, pp. 2507-2509.

Dodson, M, Darley-Usmar, V & Zhang, J 2013, 'Cellular metabolic and autophagic pathways: traffic control by redox signaling', *Free Radical Biology and Medicine*, vol. 63, pp. 207-221.

Doroudchi, MM, Minotti, S, Figlewicz, DA, et al. 2001, 'Nitrotyrosination contributes minimally to toxicity of mutant SOD1 associated with ALS', *Neuroreport*, vol. 12, no. 6, pp. 1239-1243.

Drachman, DB, Frank, K, Dykes-Hoberg, M, et al. 2002, 'Cyclooxygenase 2 inhibition protects motor neurons and prolongs survival in a transgenic mouse model of ALS', *Annals of Neurology*, vol. 52, no. 6, pp. 771-778.

Drechsel, DA, Estevez, AG, Barbeito, L, et al. 2012, 'Nitric oxide-mediated oxidative damage and the progressive demise of motor neurons in ALS', *Neurotoxicity research*, vol. 22, no. 4, pp. 251-264.

Drory, VE, Goltsman, E, Reznik, JG, et al. 2001, 'The value of muscle exercise in patients with amyotrophic lateral sclerosis', *Journal of the Neurological Sciences*, vol. 191, no. 1-2, pp. 133-137.

Duan, W, Li, X, Shi, J, et al. 2010, 'Mutant TAR DNA-binding protein-43 induces oxidative injury in motor neuron-like cell', *Neuroscience*, vol. 169, no. 4, pp. 1621-1629.

Dudek, H, Datta, SR, Franke, TF, et al. 1997, 'Regulation of neuronal survival by the serine-threonine protein kinase Akt', *Science*, vol. 275, no. 5300, pp. 661-665.

Dupuis, L, Gonzalez de Aguilar, JL, Echaniz-Laguna, A, et al. 2009, 'Muscle mitochondrial uncoupling dismantles neuromuscular junction and triggers distal degeneration of motor neurons', *PLoS ONE*, vol. 4, no. 4, p. e5390.

Dupuis, L, Oudart, H, Rene, F, et al. 2004, 'Evidence for defective energy homeostasis in amyotrophic lateral sclerosis: benefit of a high-energy diet in a transgenic mouse model', *Proceedings of the National Academy of Sciences of the United States of America*, vol. 101, no. 30, pp. 11159-11164.

Dykens, JA 1994, 'Isolated cerebral and cerebellar mitochondria produce free radicals when exposed to elevated CA2+ and Na+: implications for neurodegeneration', *Journal of Neurochemistry*, vol. 63, no. 2, pp. 584-591.

Ebadi, M, Brown-Borg, H, El Refaey, H, et al. 2005, 'Metallothionein-mediated neuroprotection in genetically engineered mouse models of Parkinson's disease', *Brain Research. Molecular Brain Research*, vol. 134, no. 1, pp. 67-75.

Echaniz-Laguna, A, Zoll, J, Ponsot, E, et al. 2006, 'Muscular mitochondrial function in amyotrophic lateral sclerosis is progressively altered as the disease develops: a temporal study in man', *Experimental Neurology*, vol. 198, no. 1, pp. 25-30.

Echaniz-Laguna, A, Zoll, J, Ribera, F, et al. 2002, 'Mitochondrial respiratory chain function in skeletal muscle of ALS patients', *Annals of Neurology*, vol. 52, no. 5, pp. 623-627.

Elden, AC, Kim, HJ, Hart, MP, et al. 2010, 'Ataxin-2 intermediate-length polyglutamine expansions are associated with increased risk for ALS', *Nature*, vol. 466, no. 7310, pp. 1069-1075.

Engelhardt, G, Bogel, R, Schnitzler, C, et al. 1996, 'Meloxicam: influence on arachidonic acid metabolism. Part II. In vivo findings', *Biochemical Pharmacology*, vol. 51, no. 1, pp. 29-38.

Ercal, N, Gurer-Orhan, H & Aykin-Burns, N 2001, 'Toxic metals and oxidative stress part I: mechanisms involved in metal-induced oxidative damage', *Current Topics in Medicinal Chemistry*, vol. 1, no. 6, pp. 529-539.

Erfurt, C, Roussa, E & Thevenod, F 2003, 'Apoptosis by Cd2+ or CdMT in proximal tubule cells: different uptake routes and permissive role of endo/lysosomal CdMT uptake', *American Journal of Physiology: Cell Physiology*, vol. 285, no. 6, pp. C1367-1376.

Esmaeili, MA, Panahi, M, Yadav, S, et al. 2013, 'Premature death of TDP-43 (A315T) transgenic mice due to gastrointestinal complications prior to development of full neurological symptoms of amyotrophic lateral sclerosis', *International Journal of Experimental Pathology*, vol. 94, no. 1, pp. 56-64.

Estevez, AG, Crow, JP, Sampson, JB, et al. 1999, 'Induction of nitric oxide-dependent apoptosis in motor neurons by zinc-deficient superoxide dismutase', *Science*, vol. 286, no. 5449, pp. 2498-2500.

Evans, MC, Couch, Y, Sibson, N, et al. 2013, 'Inflammation and neurovascular changes in amyotrophic lateral sclerosis', *Molecular and Cellular Neurosciences*, vol. 53, pp. 34-41.

Ezzi, SA, Urushitani, M & Julien, JP 2007, 'Wild-type superoxide dismutase acquires binding and toxic properties of ALS-linked mutant forms through oxidation', *Journal of Neurochemistry*, vol. 102, no. 1, pp. 170-178.

Fallini, C, Bassell, GJ & Rossoll, W 2012, 'The ALS disease protein TDP-43 is actively transported in motor neuron axons and regulates axon outgrowth', *Human Molecular Genetics*, vol. 21, no. 16, pp. 3703-3718.

Farah, CA, Nguyen, MD, Julien, JP, et al. 2003, 'Altered levels and distribution of microtubule-associated proteins before disease onset in a mouse model of amyotrophic lateral sclerosis', *Journal of Neurochemistry*, vol. 84, no. 1, pp. 77-86.

Fasana, E, Fossati, M, Ruggiano, A, et al. 2010, 'A VAPB mutant linked to amyotrophic lateral sclerosis generates a novel form of organized smooth endoplasmic reticulum', *FASEB Journal*, vol. 24, no. 5, pp. 1419-1430.

Fecto, F & Siddique, T 2011, 'Making connections: pathology and genetics link amyotrophic lateral sclerosis with frontotemporal lobe dementia', *Journal of Molecular Neuroscience*, vol. 45, no. 3, pp. 663-675.

Fecto, F, Yan, J, Vemula, SP, et al. 2011, 'SQSTM1 mutations in familial and sporadic amyotrophic lateral sclerosis', *Archives of Neurology*, vol. 68, no. 11, pp. 1440-1446.

Ferguson, CJ, Lenk, GM & Meisler, MH 2009, 'Defective autophagy in neurons and astrocytes from mice deficient in PI(3,5)P2', *Human Molecular Genetics*, vol. 18, no. 24, pp. 4868-4878.

Ferraiuolo, L, Kirby, J, Grierson, AJ, et al. 2011, 'Molecular pathways of motor neuron injury in amyotrophic lateral sclerosis', *Nature Reviews: Neurology*, vol. 7, no. 11, pp. 616-630.

Ferrante, RJ, Browne, SE, Shinobu, LA, et al. 1997, 'Evidence of increased oxidative damage in both sporadic and familial amyotrophic lateral sclerosis', *Journal of Neurochemistry*, vol. 69, no. 5, pp. 2064-2074.

Ferri, A, Cozzolino, M, Crosio, C, et al. 2006, 'Familial ALS-superoxide dismutases associate with mitochondria and shift their redox potentials', *Proceedings of the National Academy of Sciences of the United States of America*, vol. 103, no. 37, pp. 13860-13865.

Ferri, A, Nencini, M, Casciati, A, et al. 2004, 'Cell death in amyotrophic lateral sclerosis: interplay between neuronal and glial cells', *FASEB Journal*, vol. 18, no. 11, pp. 1261-1263.

Fidler, JA, Treleaven, CM, Frakes, A, et al. 2011, 'Disease progression in a mouse model of amyotrophic lateral sclerosis: the influence of chronic stress and corticosterone', *FASEB Journal*, vol. 25, no. 12, pp. 4369-4377.

Figlewicz, DA, Krizus, A, Martinoli, MG, et al. 1994, 'Variants of the heavy neurofilament subunit are associated with the development of amyotrophic lateral sclerosis', *Human Molecular Genetics*, vol. 3, no. 10, pp. 1757-1761.

Fischer, U, Englbrecht, C & Chari, A 2011, 'Biogenesis of spliceosomal small nuclear ribonucleoproteins', *Wiley Interdisciplinary Reviews RNA*, vol. 2, no. 5, pp. 718-731.

Fitch, MT & Silver, J 2008, 'CNS injury, glial scars, and inflammation: Inhibitory extracellular matrices and regeneration failure', *Experimental Neurology*, vol. 209, no. 2, pp. 294-301.

Fitzgerald, M, Nairn, P, Bartlett, CA, et al. 2007, 'Metallothionein-IIA promotes neurite growth via the megalin receptor', *Experimental Brain Research*, vol. 183, no. 2, pp. 171-180.

Frey, D, Schneider, C, Xu, L, et al. 2000, 'Early and selective loss of neuromuscular synapse subtypes with low sprouting competence in motoneuron diseases', *The Journal of Neuroscience*, vol. 20, no. 7, pp. 2534-2542.

Furukawa, Y, Fu, R, Deng, HX, et al. 2006, 'Disulfide cross-linked protein represents a significant fraction of ALS-associated Cu, Zn-superoxide dismutase aggregates in spinal cords of model mice', *Proceedings of the National Academy of Sciences of the United States of America*, vol. 103, no. 18, pp. 7148-7153.

Furukawa, Y & O'Halloran, TV 2005, 'Amyotrophic lateral sclerosis mutations have the greatest destabilizing effect on the apo- and reduced form of SOD1, leading to unfolding and oxidative aggregation', *The Journal of biological chemistry*, vol. 280, no. 17, pp. 17266-17274.

Garbuzova-Davis, S, Haller, E, Saporta, S, et al. 2007, 'Ultrastructure of blood-brain barrier and blood-spinal cord barrier in SOD1 mice modeling ALS', *Brain Research*, vol. 1157, pp. 126-137.

Geffard, M, de Bisschop, L, Duleu, S, et al. 2010, 'Endotherapia', *Anti-Inflammatory and Anti-Allergy Agents in Medicinal Chemistry*, vol. 9, no. 3, pp. 197-211.

Georgoulopoulou, E, Fini, N, Vinceti, M, et al. 2013, 'The impact of clinical factors, riluzole and therapeutic interventions on ALS survival: a population based study in Modena, Italy', *Amyotrophic Lateral Sclerosis and Frontotemporal Degeneration*, vol. 14, no. 5-6, pp. 338-345.

Gerber, YN, Sabourin, JC, Hugnot, JP, et al. 2012, 'Unlike physical exercise, modified environment increases the lifespan of SOD1G93A mice however both conditions induce cellular changes', *PLoS ONE*, vol. 7, no. 9, p. e45503.

Gibson, SB & Bromberg, MB 2012, 'Amyotrophic lateral sclerosis: drug therapy from the bench to the bedside', *Seminars in Neurology*, vol. 32, no. 3, pp. 173-178.

Gkogkas, C, Middleton, S, Kremer, AM, et al. 2008, 'VAPB interacts with and modulates the activity of ATF6', *Human Molecular Genetics*, vol. 17, no. 11, pp. 1517-1526.

Gobert, AP, Daulouede, S, Lepoivre, M, et al. 2000, 'L-Arginine availability modulates local nitric oxide production and parasite killing in experimental trypanosomiasis', *Infection and Immunity*, vol. 68, no. 8, pp. 4653-4657.

Gonatas, NK, Stieber, A, Mourelatos, Z, et al. 1992, 'Fragmentation of the Golgi apparatus of motor neurons in amyotrophic lateral sclerosis', *American Journal of Pathology*, vol. 140, no. 3, pp. 731-737.

Gong, YH & Elliott, JL 2000, 'Metallothionein expression is altered in a transgenic murine model of familial amyotrophic lateral sclerosis', *Experimental Neurology*, vol. 162, no. 1, pp. 27-36.

Gong, YH, Parsadanian, AS, Andreeva, A, et al. 2000, 'Restricted expression of G86R Cu/Zn superoxide dismutase in astrocytes results in astrocytosis but does not cause motoneuron degeneration', *The Journal of Neuroscience*, vol. 20, no. 2, pp. 660-665.

Gonzalez de Aguilar, JL, Niederhauser-Wiederkehr, C, Halter, B, et al. 2008, 'Gene profiling of skeletal muscle in an amyotrophic lateral sclerosis mouse model', *Physiological Genomics*, vol. 32, no. 2, pp. 207-218.

Good, M & Vasak, M 1986, 'Iron(II)-substituted metallothionein: evidence for the existence of iron-thiolate clusters', *Biochemistry*, vol. 25, no. 26, pp. 8353-8356.

Gordon, PH & Meininger, V 2011, 'How can we improve clinical trials in amyotrophic lateral sclerosis?', *Nature Reviews: Neurology*, vol. 7, no. 11, pp. 650-654.

Gowing, G, Lalancette-Hebert, M, Audet, JN, et al. 2009, 'Macrophage colony stimulating factor (M-CSF) exacerbates ALS disease in a mouse model through altered responses of microglia expressing mutant superoxide dismutase', *Experimental Neurology*, vol. 220, no. 2, pp. 267-275.

Gowing, G, Philips, T, Van Wijmeersch, B, et al. 2008, 'Ablation of proliferating microglia does not affect motor neuron degeneration in amyotrophic lateral sclerosis caused by mutant superoxide dismutase', *The Journal of Neuroscience*, vol. 28, no. 41, pp. 10234-10244.

Graber, DJ, Hickey, WF & Harris, BT 2010, 'Progressive changes in microglia and macrophages in spinal cord and peripheral nerve in the transgenic rat model of amyotrophic lateral sclerosis', *Journal of neuroinflammation*, vol. 7, p. 8.

Greenway, MJ, Alexander, MD, Ennis, S, et al. 2004, 'A novel candidate region for ALS on chromosome 14q11.2', *Neurology*, vol. 63, no. 10, pp. 1936-1938.

Gregory, R, Mills, K & Donaghy, M 1993, 'Progressive sensory nerve dysfunction in amyotrophic lateral sclerosis: a prospective clinical and neurophysiological study', *Journal of Neurology*, vol. 240, no. 5, pp. 309-314.

Gros-Louis, F, Lariviere, R, Gowing, G, et al. 2004, 'A frameshift deletion in peripherin gene associated with amyotrophic lateral sclerosis', *The Journal of biological chemistry*, vol. 279, no. 44, pp. 45951-45956.

Gurney, ME, Pu, H, Chiu, AY, et al. 1994, 'Motor neuron degeneration in mice that express a human Cu,Zn superoxide dismutase mutation', *Science*, vol. 264, no. 5166, pp. 1772-1775.

Ha, Y, Dun, Y, Thangaraju, M, et al. 2011, 'Sigma receptor 1 modulates endoplasmic reticulum stress in retinal neurons', *Investigative Ophthalmology and Visual Science*, vol. 52, no. 1, pp. 527-540.

Hafezparast, M, Klocke, R, Ruhrberg, C, et al. 2003, 'Mutations in dynein link motor neuron degeneration to defects in retrograde transport', *Science*, vol. 300, no. 5620, pp. 808-812.

Haidet-Phillips, AM, Hester, ME, Miranda, CJ, et al. 2011, 'Astrocytes from familial and sporadic ALS patients are toxic to motor neurons', *Nature Biotechnology*, vol. 29, no. 9, pp. 824-828.

Hall, ED, Andrus, PK, Oostveen, JA, et al. 1998a, 'Relationship of oxygen radical-induced lipid peroxidative damage to disease onset and progression in a transgenic model of familial ALS', *Journal of Neuroscience Research*, vol. 53, no. 1, pp. 66-77.

Hall, ED, Oostveen, JA & Gurney, ME 1998b, 'Relationship of microglial and astrocytic activation to disease onset and progression in a transgenic model of familial ALS', *Glia*, vol. 23, no. 3, pp. 249-256.

Ham, J, Eilers, A, Whitfield, J, et al. 2000, 'c-Jun and the transcriptional control of neuronal apoptosis', *Biochemical Pharmacology*, vol. 60, no. 8, pp. 1015-1021.

Hamer, DH 1986, 'Metallothionein', *Annual Review of Biochemistry*, vol. 55, pp. 913-951.

Han, SM, El Oussini, H, Scekic-Zahirovic, J, et al. 2013, 'VAPB/ALS8 MSP ligands regulate striated muscle energy metabolism critical for adult survival in caenorhabditis elegans', *PLoS Genetics*, vol. 9, no. 9, p. e1003738.

Hao, Q, Hong, SH & Maret, W 2007, 'Lipid raft-dependent endocytosis of metallothionein in HepG2 cells', *Journal of Cellular Physiology*, vol. 210, no. 2, pp. 428-435.

Harasaki, K, Lubben, NB, Harbour, M, et al. 2005, 'Sorting of major cargo glycoproteins into clathrin-coated vesicles', *Traffic*, vol. 6, no. 11, pp. 1014-1026.

Hashimoto, K, Hayashi, Y, Inuzuka, T, et al. 2009, 'Exercise induces metallothioneins in mouse spinal cord', *Neuroscience*, vol. 163, no. 1, pp. 244-251.

Hayward, LJ, Rodriguez, JA, Kim, JW, et al. 2002, 'Decreased metallation and activity in subsets of mutant superoxide dismutases associated with familial amyotrophic lateral sclerosis', *The Journal of biological chemistry*, vol. 277, no. 18, pp. 15923-15931.

Hegedus, J, Putman, CT, Tyreman, N, et al. 2008, 'Preferential motor unit loss in the SOD1 G93A transgenic mouse model of amyotrophic lateral sclerosis', *The Journal of physiology*, vol. 586, no. 14, pp. 3337-3351.

Heiman-Patterson, TD, Deitch, JS, Blankenhorn, EP, et al. 2005, 'Background and gender effects on survival in the TgN(SOD1-G93A)1Gur mouse model of ALS', *Journal of the Neurological Sciences*, vol. 236, no. 1-2, pp. 1-7.

Henkel, JS, Beers, DR, Zhao, W, et al. 2009, 'Microglia in ALS: the good, the bad, and the resting', *Journal of Neuroimmune Pharmacology*, vol. 4, no. 4, pp. 389-398.

Henkel, JS, Engelhardt, JI, Siklos, L, et al. 2004, 'Presence of dendritic cells, MCP-1, and activated microglia/macrophages in amyotrophic lateral sclerosis spinal cord tissue', *Annals of Neurology*, vol. 55, no. 2, pp. 221-235.

Hensley, K, Abdel-Moaty, H, Hunter, J, et al. 2006, 'Primary glia expressing the G93A-SOD1 mutation present a neuroinflammatory phenotype and provide a cellular system for studies of glial inflammation', *Journal of neuroinflammation*, vol. 3, p. 2.

Herbert, RP, Harris, J, Chong, KP, et al. 2012, 'Cytokines and olfactory bulb microglia in response to bacterial challenge in the compromised primary olfactory pathway', *Journal of neuroinflammation*, vol. 9, p. 109.

Herdewyn, S, Cirillo, C, Van Den Bosch, L, et al. 2014, 'Prevention of intestinal obstruction reveals progressive neurodegeneration in mutant TDP-43 (A315T) mice', *Molecular neurodegeneration*, vol. 9, p. 24.

Hilario, MO, Terreri, MT & Len, CA 2006, 'Nonsteroidal anti-inflammatory drugs: cyclooxygenase 2 inhibitors', *Jornal de Pediatria*, vol. 82, no. 5 Suppl, pp. S206-212.

Hirling, H 2009, 'Endosomal trafficking of AMPA-type glutamate receptors', *Neuroscience*, vol. 158, no. 1, pp. 36-44.

Hirokawa, N 1998, 'Kinesin and dynein superfamily proteins and the mechanism of organelle transport', *Science*, vol. 279, no. 5350, pp. 519-526.

Hoffman, PN, Griffin, JW & Price, DL 1984, 'Control of axonal caliber by neurofilament transport', *The Journal of cell biology*, vol. 99, no. 2, pp. 705-714.

Holscher, C 1997, 'Nitric oxide, the enigmatic neuronal messenger: its role in synaptic plasticity', *Trends in Neurosciences*, vol. 20, no. 7, pp. 298-303.

Homma, K, Fujisawa, T, Tsuburaya, N, et al. 2013, 'SOD1 as a molecular switch for initiating the homeostatic ER stress response under zinc deficiency', *Molecular Cell*, vol. 52, no. 1, pp. 75-86.

Houi, K, Kobayashi, T, Kato, S, et al. 2002, 'Increased plasma TGF-beta1 in patients with amyotrophic lateral sclerosis', *Acta Neurologica Scandinavica*, vol. 106, no. 5, pp. 299-301.

Howland, DS, Liu, J, She, Y, et al. 2002, 'Focal loss of the glutamate transporter EAAT2 in a transgenic rat model of SOD1 mutant-mediated amyotrophic lateral sclerosis (ALS)', *Proceedings of the National Academy of Sciences of the United States of America*, vol. 99, no. 3, pp. 1604-1609.

Hozumi, I, Hasegawa, T, Honda, A, et al. 2011, 'Patterns of levels of biological metals in CSF differ among neurodegenerative diseases', *Journal of the Neurological Sciences*, vol. 303, no. 1-2, pp. 95-99.

Hozumi, I, Yamada, M, Uchida, Y, et al. 2008, 'The expression of metallothioneins is diminished in the spinal cords of patients with sporadic ALS', *Amyotrophic Lateral Sclerosis*, vol. 9, no. 5, pp. 294-298.

Huisman, MH, Seelen, M, de Jong, SW, et al. 2013, 'Lifetime physical activity and the risk of amyotrophic lateral sclerosis', *Journal of Neurology, Neurosurgery and Psychiatry*, vol. 84, no. 9, pp. 976-981.

Iadecola, C, Pelligrino, DA, Moskowitz, MA, et al. 1994, 'Nitric oxide synthase inhibition and cerebrovascular regulation', *Journal of Cerebral Blood Flow and Metabolism*, vol. 14, no. 2, pp. 175-192.

Igaz, LM, Kwong, LK, Chen-Plotkin, A, et al. 2009, 'Expression of TDP-43 C-terminal Fragments in Vitro Recapitulates Pathological Features of TDP-43 Proteinopathies', *The Journal of biological chemistry*, vol. 284, no. 13, pp. 8516-8524.

Igaz, LM, Kwong, LK, Lee, EB, et al. 2011, 'Dysregulation of the ALS-associated gene TDP-43 leads to neuronal death and degeneration in mice', *The Journal of clinical investigation*, vol. 121, no. 2, pp. 726-738.

Ikenaka, K, Kawai, K, Katsuno, M, et al. 2013, 'dnc-1/dynactin 1 knockdown disrupts transport of autophagosomes and induces motor neuron degeneration', *PLoS ONE*, vol. 8, no. 2, p. e54511.

Ilieva, EV, Ayala, V, Jove, M, et al. 2007, 'Oxidative and endoplasmic reticulum stress interplay in sporadic amyotrophic lateral sclerosis', *Brain*, vol. 130, no. Pt 12, pp. 3111-3123.

Ilzecka, J, Stelmasiak, Z & Dobosz, B 2002, 'Transforming growth factor-Beta 1 (tgf-Beta 1) in patients with amyotrophic lateral sclerosis', *Cytokine*, vol. 20, no. 5, pp. 239-243.

Imai, Y, Ibata, I, Ito, D, et al. 1996, 'A novel gene iba1 in the major histocompatibility complex class III region encoding an EF hand protein expressed in a monocytic lineage', *Biochemical and Biophysical Research Communications*, vol. 224, no. 3, pp. 855-862.

Imbert, G, Saudou, F, Yvert, G, et al. 1996, 'Cloning of the gene for spinocerebellar ataxia 2 reveals a locus with high sensitivity to expanded CAG/glutamine repeats', *Nature Genetics*, vol. 14, no. 3, pp. 285-291.

Ischiropoulos, H, Zhu, L, Chen, J, et al. 1992, 'Peroxynitrite-mediated tyrosine nitration catalyzed by superoxide dismutase', *Archives of Biochemistry and Biophysics*, vol. 298, no. 2, pp. 431-437.

Jiang, YM, Yamamoto, M, Kobayashi, Y, et al. 2005, 'Gene expression profile of spinal motor neurons in sporadic amyotrophic lateral sclerosis', *Annals of Neurology*, vol. 57, no. 2, pp. 236-251.

Johnson, BS, Snead, D, Lee, JJ, et al. 2009, 'TDP-43 is intrinsically aggregation-prone, and amyotrophic lateral sclerosis-linked mutations accelerate aggregation and increase toxicity', *The Journal of biological chemistry*, vol. 284, no. 30, pp. 20329-20339.

Johnson, CR 1988, 'Aquatic therapy for an ALS patient', *The American Journal of Occupational Therapy*, vol. 42, no. 2, pp. 115-120.

Johnson, JA, Johnson, DA, Kraft, AD, et al. 2008, 'The Nrf2-ARE pathway: an indicator and modulator of oxidative stress in neurodegeneration', *Annals of the New York Academy of Sciences*, vol. 1147, pp. 61-69.

Johnson, JO, Mandrioli, J, Benatar, M, et al. 2010, 'Exome sequencing reveals VCP mutations as a cause of familial ALS', *Neuron*, vol. 68, no. 5, pp. 857-864.
Johnston, JA, Dalton, MJ, Gurney, ME, et al. 2000, 'Formation of high molecular weight complexes of mutant Cu, Zn-superoxide dismutase in a mouse model for familial amyotrophic lateral sclerosis', *Proceedings of the National Academy of Sciences of the United States of America*, vol. 97, no. 23, pp. 12571-12576.
Joshi, G & Johnson, JA 2012, 'The Nrf2-ARE pathway: a valuable therapeutic target for the treatment of neurodegenerative diseases', *Recent Patents on CNS Drug Discovery*, vol. 7, no. 3, pp. 218-229.
Ju, JS, Fuentealba, RA, Miller, SE, et al. 2009, 'Valosin-containing protein (VCP) is required for autophagy and is disrupted in VCP disease', *The Journal of cell biology*, vol. 187, no. 6, pp. 875-888.
Jung, C, Higgins, CM & Xu, Z 2002, 'Mitochondrial electron transport chain complex dysfunction in a transgenic mouse model for amyotrophic lateral sclerosis', *Journal of Neurochemistry*, vol. 83, no. 3, pp. 535-545.
Jung, T & Grune, T 2013, 'The proteasome and the degradation of oxidized proteins: Part I-structure of proteasomes', *Redox Biology*, vol. 1, no. 1, pp. 178-182.
Kabashi, E, Valdmanis, PN, Dion, P, et al. 2008, 'TARDBP mutations in individuals with sporadic and familial amyotrophic lateral sclerosis', *Nature Genetics*, vol. 40, no. 5, pp. 572-574.
Kagi, JH & Valee, BL 1960, 'Metallothionein: a cadmium- and zinc-containing protein from equine renal cortex', *The Journal of biological chemistry*, vol. 235, pp. 3460-3465.
Kaji, R, Izumi, Y, Adachi, Y, et al. 2012, 'ALS-parkinsonism-dementia complex of Kii and other related diseases in Japan', *Parkinsonism & Related Disorders*, vol. 18 Suppl 1, pp. S190-191.
Kamo, H, Haebara, H, Akiguchi, I, et al. 1987, 'A distinctive distribution of reactive astroglia in the precentral cortex in amyotrophic lateral sclerosis', *Acta Neuropathologica*, vol. 74, no. 1, pp. 33-38.
Kanai, Y, Dohmae, N & Hirokawa, N 2004, 'Kinesin transports RNA: isolation and characterization of an RNA-transporting granule', *Neuron*, vol. 43, no. 4, pp. 513-525.
Kanai, Y, Wang, D & Hirokawa, N 2014, 'KIF13B enhances the endocytosis of LRP1 by recruiting LRP1 to caveolae', *The Journal of cell biology*, vol. 204, no. 3, pp. 395-408.
Kanekura, K, Nishimoto, I, Aiso, S, et al. 2006, 'Characterization of amyotrophic lateral sclerosis-linked P56S mutation of vesicle-associated membrane protein-associated protein B (VAPB/ALS8)', *The Journal of biological chemistry*, vol. 281, no. 40, pp. 30223-30233.
Karbowski, M & Neutzner, A 2012, 'Neurodegeneration as a consequence of failed mitochondrial maintenance', *Acta Neuropathologica*, vol. 123, no. 2, pp. 157-171.
Kaspar, BK, Frost, LM, Christian, L, et al. 2005, 'Synergy of insulin-like growth factor-1 and exercise in amyotrophic lateral sclerosis', *Annals of Neurology*, vol. 57, no. 5, pp. 649-655.
Kawahara, Y, Ito, K, Sun, H, et al. 2004, 'Glutamate receptors: RNA editing and death of motor neurons', *Nature*, vol. 427, no. 6977, p. 801.
Kawahara, Y, Kwak, S, Sun, H, et al. 2003, 'Human spinal motoneurons express low relative abundance of GluR2 mRNA: an implication for excitotoxicity in ALS', *Journal of Neurochemistry*, vol. 85, no. 3, pp. 680-689.
Kawamata, T, Akiyama, H, Yamada, T, et al. 1992, 'Immunologic reactions in amyotrophic lateral sclerosis brain and spinal cord tissue', *American Journal of Pathology*, vol. 140, no. 3, pp. 691-707.
Kawamura, Y, Dyck, PJ, Shimono, M, et al. 1981, 'Morphometric comparison of the vulnerability of peripheral motor and sensory neurons in amyotrophic lateral sclerosis', *Journal of Neuropathology & Experimental Neurology*, vol. 40, no. 6, pp. 667-675.
Kedersha, NL, Gupta, M, Li, W, et al. 1999, 'RNA-binding proteins TIA-1 and TIAR link the phosphorylation of eIF-2 alpha to the assembly of mammalian stress granules', *The Journal of cell biology*, vol. 147, no. 7, pp. 1431-1442.
Khatai, L, Goessler, W, Lorencova, H, et al. 2004, 'Modulation of nitric oxide-mediated metal release from metallothionein by the redox state of glutathione in vitro', *European Journal of Biochemistry*, vol. 271, no. 12, pp. 2408-2416.
Kiaei, M, Kipiani, K, Petri, S, et al. 2005, 'Integrative role of cPLA with COX-2 and the effect of non-steriodal anti-inflammatory drugs in a transgenic mouse model of amyotrophic lateral sclerosis', *Journal of Neurochemistry*, vol. 93, no. 2, pp. 403-411.
Kiernan, MC, Vucic, S, Cheah, BC, et al. 2011, 'Amyotrophic lateral sclerosis', *The Lancet*, vol. 377, no. 9769, pp. 942-955.
Kim, N, Stiegler, AL, Cameron, TO, et al. 2008, 'Lrp4 is a receptor for Agrin and forms a complex with MuSK', *Cell*, vol. 135, no. 2, pp. 334-342.
Kim, WK, Liu, X, Sandner, J, et al. 2009, 'Study of 962 patients indicates progressive muscular atrophy is a form of ALS', *Neurology*, vol. 73, no. 20, pp. 1686-1692.

King, AE, Dickson, TC, Blizzard, CA, et al. 2011, 'Neuron-glia interactions underlie ALS-like axonal cytoskeletal pathology', *Neurobiology of Aging*, vol. 32, no. 3, pp. 459-469.
Kirkinezos, IG, Hernandez, D, Bradley, WG, et al. 2003, 'Regular exercise is beneficial to a mouse model of amyotrophic lateral sclerosis', *Annals of Neurology*, vol. 53, no. 6, pp. 804-807.
Kiss, AL & Botos, E 2009, 'Endocytosis via caveolae: alternative pathway with distinct cellular compartments to avoid lysosomal degradation?', *Journal of Cellular and Molecular Medicine*, vol. 13, no. 7, pp. 1228-1237.
Kitamura, F, Fujimaki, N, Okita, W, et al. 2011, 'Structural instability and Cu-dependent pro-oxidant activity acquired by the apo form of mutant SOD1 associated with amyotrophic lateral sclerosis', *Biochemistry*, vol. 50, no. 20, pp. 4242-4250.
Klassen, RB, Crenshaw, K, Kozyraki, R, et al. 2004, 'Megalin mediates renal uptake of heavy metal metallothionein complexes', *American Journal of Physiology: Renal Physiology*, vol. 287, no. 3, pp. F393-403.
Klivenyi, P, Kiaei, M, Gardian, G, et al. 2004, 'Additive neuroprotective effects of creatine and cyclooxygenase 2 inhibitors in a transgenic mouse model of amyotrophic lateral sclerosis', *Journal of Neurochemistry*, vol. 88, no. 3, pp. 576-582.
Knippenberg, S, Thau, N, Dengler, R, et al. 2010, 'Significance of behavioural tests in a transgenic mouse model of amyotrophic lateral sclerosis (ALS)', *Behavioural Brain Research*, vol. 213, no. 1, pp. 82-87.
Kohler, LB, Berezin, V, Bock, E, et al. 2003, 'The role of metallothionein II in neuronal differentiation and survival', *Brain Research*, vol. 992, no. 1, pp. 128-136.
Kong, J & Xu, Z 1998, 'Massive mitochondrial degeneration in motor neurons triggers the onset of amyotrophic lateral sclerosis in mice expressing a mutant SOD1', *The Journal of Neuroscience*, vol. 18, no. 9, pp. 3241-3250.
Kraft, AD & Harry, GJ 2011, 'Features of microglia and neuroinflammation relevant to environmental exposure and neurotoxicity', *International Journal of Environmental Research and Public Health*, vol. 8, no. 7, pp. 2980-3018.
Krasnianski, A, Deschauer, M, Neudecker, S, et al. 2005, 'Mitochondrial changes in skeletal muscle in amyotrophic lateral sclerosis and other neurogenic atrophies', *Brain*, vol. 128, no. Pt 8, pp. 1870-1876.
Kuntz, Ct, Kinoshita, Y, Beal, MF, et al. 2000, 'Absence of p53: no effect in a transgenic mouse model of familial amyotrophic lateral sclerosis', *Experimental Neurology*, vol. 165, no. 1, pp. 184-190.
Kushner, PD, Stephenson, DT & Wright, S 1991, 'Reactive astrogliosis is widespread in the subcortical white matter of amyotrophic lateral sclerosis brain', *Journal of Neuropathology & Experimental Neurology*, vol. 50, no. 3, pp. 263-277.
Kuzma-Kozakiewicz, M, Chudy, A, Gajewska, B, et al. 2013a, 'Kinesin expression in the central nervous system of humans and transgenic hSOD1G93A mice with amyotrophic lateral sclerosis', *Neurodegenerative diseases*, vol. 12, no. 2, pp. 71-80.
Kuzma-Kozakiewicz, M, Chudy, A, Kazmierczak, B, et al. 2013b, 'Dynactin Deficiency in the CNS of Humans with Sporadic ALS and Mice with Genetically Determined Motor Neuron Degeneration', *Neurochemical Research*.
Kwak, S & Kawahara, Y 2005, 'Deficient RNA editing of GluR2 and neuronal death in amyotropic lateral sclerosis', *Journal of Molecular Medicine*, vol. 83, no. 2, pp. 110-120.
Kwiatkowski, TJ, Jr., Bosco, DA, Leclerc, AL, et al. 2009, 'Mutations in the FUS/TLS gene on chromosome 16 cause familial amyotrophic lateral sclerosis', *Science*, vol. 323, no. 5918, pp. 1205-1208.
Lafon-Cazal, M, Pietri, S, Culcasi, M, et al. 1993, 'NMDA-dependent superoxide production and neurotoxicity', *Nature*, vol. 364, no. 6437, pp. 535-537.
Lagier-Tourenne, C & Cleveland, DW 2009, 'Rethinking ALS: the FUS about TDP-43', *Cell*, vol. 136, no. 6, pp. 1001-1004.
Lagier-Tourenne, C, Polymenidou, M, Hutt, KR, et al. 2012, 'Divergent roles of ALS-linked proteins FUS/TLS and TDP-43 intersect in processing long pre-mRNAs', *Nature Neuroscience*, vol. 15, no. 11, pp. 1488-1497.
Laird, FM, Farah, MH, Ackerley, S, et al. 2008, 'Motor neuron disease occurring in a mutant dynactin mouse model is characterized by defects in vesicular trafficking', *The Journal of Neuroscience*, vol. 28, no. 9, pp. 1997-2005.
Lamanauskas, N & Nistri, A 2008, 'Riluzole blocks persistent Na+ and Ca2+ currents and modulates release of glutamate via presynaptic NMDA receptors on neonatal rat hypoglossal motoneurons in vitro', *European Journal of Neuroscience*, vol. 27, no. 10, pp. 2501-2514.
Lariviere, RC & Julien, JP 2004, 'Functions of intermediate filaments in neuronal development and disease', *Journal of Neurobiology*, vol. 58, no. 1, pp. 131-148.

Leclerc, N, Ribera, F, Zoll, J, et al. 2001, 'Selective changes in mitochondria respiratory properties in oxidative or glycolytic muscle fibers isolated from G93AhumanSOD1 transgenic mice', *Neuromuscular Disorders*, vol. 11, no. 8, pp. 722-727.

Lee, J, Ryu, H & Kowall, NW 2009, 'Differential regulation of neuronal and inducible nitric oxide synthase (NOS) in the spinal cord of mutant SOD1 (G93A) ALS mice', *Biochemical and Biophysical Research Communications*, vol. 387, no. 1, pp. 202-206.

Lee, JC, Seong, J, Kim, SH, et al. 2012, 'Replacement of microglial cells using Clodronate liposome and bone marrow transplantation in the central nervous system of SOD1(G93A) transgenic mice as an in vivo model of amyotrophic lateral sclerosis', *Biochemical and Biophysical Research Communications*, vol. 418, no. 2, pp. 359-365.

Lee, JY, Sohn, KH, Rhee, SH, et al. 2001, 'Saturated fatty acids, but not unsaturated fatty acids, induce the expression of cyclooxygenase-2 mediated through Toll-like receptor 4', *The Journal of biological chemistry*, vol. 276, no. 20, pp. 16683-16689.

Lee, M, McGeer, E & McGeer, PL 2013a, 'Neurotoxins released from interferon-gamma-stimulated human astrocytes', *Neuroscience*, vol. 229, pp. 164-175.

Lee, MK, Marszalek, JR & Cleveland, DW 1994, 'A mutant neurofilament subunit causes massive, selective motor neuron death: implications for the pathogenesis of human motor neuron disease', *Neuron*, vol. 13, no. 4, pp. 975-988.

Lee, YB, Chen, HJ, Peres, JN, et al. 2013b, 'Hexanucleotide repeats in ALS/FTD form length-dependent RNA foci, sequester RNA binding proteins, and are neurotoxic', *Cell Reports*, vol. 5, no. 5, pp. 1178-1186.

Lefebvre, S, Burglen, L, Reboullet, S, et al. 1995, 'Identification and characterization of a spinal muscular atrophy-determining gene', *Cell*, vol. 80, no. 1, pp. 155-165.

Lehman, EJ, Hein, MJ, Baron, SL, et al. 2012, 'Neurodegenerative causes of death among retired National Football League players', *Neurology*, vol. 79, no. 19, pp. 1970-1974.

Lelie, HL, Liba, A, Bourassa, MW, et al. 2011, 'Copper and zinc metallation status of copper-zinc superoxide dismutase from amyotrophic lateral sclerosis transgenic mice', *The Journal of biological chemistry*, vol. 286, no. 4, pp. 2795-2806.

Leung, CL, He, CZ, Kaufmann, P, et al. 2004, 'A pathogenic peripherin gene mutation in a patient with amyotrophic lateral sclerosis', *Brain Pathology*, vol. 14, no. 3, pp. 290-296.

Leung, YK, Pankhurst, M, Dunlop, SA, et al. 2010, 'Metallothionein induces a regenerative reactive astrocyte phenotype via JAK/STAT and RhoA signalling pathways', *Experimental Neurology*, vol. 221, no. 1, pp. 98-106.

Levine, TP, Daniels, RD, Gatta, AT, et al. 2013, 'The product of C9orf72, a gene strongly implicated in neurodegeneration, is structurally related to DENN Rab-GEFs', *Bioinformatics*, vol. 29, no. 4, pp. 499-503.

Lewis, CA, Manning, J, Rossi, F, et al. 2012a, 'The Neuroinflammatory Response in ALS: The Roles of Microglia and T Cells', *Neurology research international*, vol. 2012, p. 803701.

Lewis, KE, Chung, RS, West, AK, et al. 2012b, 'Distribution of exogenous metallothionein following intraperitoneal and intramuscular injection of metallothionein-deficient mice', *Histology and Histopathology*, vol. 27, no. 11, pp. 1459-1470.

Lewis, KE, Rasmussen, AL, Bennett, W, et al. 2014, 'Microglia and motor neurons during disease progression in the SOD1G93A mouse model of amyotrophic lateral sclerosis: changes in arginase1 and inducible nitric oxide synthase', *Journal of neuroinflammation*, vol. 11, p. 55.

Liao, B, Zhao, W, Beers, DR, et al. 2012, 'Transformation from a neuroprotective to a neurotoxic microglial phenotype in a mouse model of ALS', *Experimental Neurology*, vol. 237, no. 1, pp. 147-152.

Liebetanz, D, Hagemann, K, von Lewinski, F, et al. 2004, 'Extensive exercise is not harmful in amyotrophic lateral sclerosis', *European Journal of Neuroscience*, vol. 20, no. 11, pp. 3115-3120.

Ligon, LA, LaMonte, BH, Wallace, KE, et al. 2005, 'Mutant superoxide dismutase disrupts cytoplasmic dynein in motor neurons', *Neuroreport*, vol. 16, no. 6, pp. 533-536.

Lill, CM, Abel, O, Bertram, L, et al. 2011, 'Keeping up with genetic discoveries in amyotrophic lateral sclerosis: the ALSoD and ALSGene databases', *Amyotrophic lateral sclerosis : official publication of the World Federation of Neurology Research Group on Motor Neuron Diseases*, vol. 12, no. 4, pp. 238-249.

Lin, CL, Bristol, LA, Jin, L, et al. 1998, 'Aberrant RNA processing in a neurodegenerative disease: the cause for absent EAAT2, a glutamate transporter, in amyotrophic lateral sclerosis', *Neuron*, vol. 20, no. 3, pp. 589-602.

Ling, SC, Polymenidou, M & Cleveland, DW 2013, 'Converging mechanisms in ALS and FTD: disrupted RNA and protein homeostasis', *Neuron*, vol. 79, no. 3, pp. 416-438.

Liu, J, Lillo, C, Jonsson, PA, et al. 2004, 'Toxicity of familial ALS-linked SOD1 mutants from selective recruitment to spinal mitochondria', *Neuron*, vol. 43, no. 1, pp. 5-17.
Logroscino, G, Traynor, BJ, Hardiman, O, et al. 2010, 'Incidence of amyotrophic lateral sclerosis in Europe', *Journal of Neurology, Neurosurgery and Psychiatry*, vol. 81, no. 4, pp. 385-390.
Lomen-Hoerth, C, Murphy, J, Langmore, S, et al. 2003, 'Are amyotrophic lateral sclerosis patients cognitively normal?', *Neurology*, vol. 60, no. 7, pp. 1094-1097.
Lowe, J, Aldridge, F, Lennox, G, et al. 1989, 'Inclusion bodies in motor cortex and brainstem of patients with motor neurone disease are detected by immunocytochemical localisation of ubiquitin', *Neuroscience Letters*, vol. 105, no. 1-2, pp. 7-13.
Ludolph, AC, Brettschneider, J & Weishaupt, JH 2012, 'Amyotrophic lateral sclerosis', *Current Opinion in Neurology*, vol. 25, no. 5, pp. 530-535.
Lui, AJ & Byl, NN 2009, 'A systematic review of the effect of moderate intensity exercise on function and disease progression in amyotrophic lateral sclerosis', *Journal of Neurologic Physical Therapy*, vol. 33, no. 2, pp. 68-87.
Lyons, TJ, Liu, H, Goto, JJ, et al. 1996, 'Mutations in copper-zinc superoxide dismutase that cause amyotrophic lateral sclerosis alter the zinc binding site and the redox behavior of the protein', *Proceedings of the National Academy of Sciences of the United States of America*, vol. 93, no. 22, pp. 12240-12244.
Magrane, J, Cortez, C, Gan, WB, et al. 2013, 'Abnormal mitochondrial transport and morphology are common pathological denominators in SOD1 and TDP43 ALS mouse models', *Human Molecular Genetics*.
Mahoney, DJ, Rodriguez, C, Devries, M, et al. 2004, 'Effects of high-intensity endurance exercise training in the G93A mouse model of amyotrophic lateral sclerosis', *Muscle & Nerve*, vol. 29, no. 5, pp. 656-662.
Mangas, A, Covenas, R, Bodet, D, et al. 2006, 'Evaluation of the effects of a new drug on brain leukocyte infiltration in an experimental model of autoimmune encephalomyelitis', *Letters in Drug Design & Discovery*, vol. 3, no. 3, pp. 138-148.
Mangas, A, Covenas, R, Bodet, D, et al. 2008, 'Evaluation of the effects of a new drug candidate (GEMSP) in a chronic EAE model', *International Journal of Biological Sciences*, vol. 4, no. 3, pp. 150-160.
Manso, Y, Adlard, PA, Carrasco, J, et al. 2011, 'Metallothionein and brain inflammation', *Journal of Biological Inorganic Chemistry*, vol. 16, no. 7, pp. 1103-1113.
Martin, D, Thompson, MA & Nadler, JV 1993, 'The neuroprotective agent riluzole inhibits release of glutamate and aspartate from slices of hippocampal area CA1', *European Journal of Pharmacology*, vol. 250, no. 3, pp. 473-476.
Martin, LJ 2010, 'The mitochondrial permeability transition pore: a molecular target for amyotrophic lateral sclerosis therapy', *Biochimica et Biophysica Acta*, vol. 1802, no. 1, pp. 186-197.
Martin, LJ, Liu, Z, Chen, K, et al. 2007, 'Motor neuron degeneration in amyotrophic lateral sclerosis mutant superoxide dismutase-1 transgenic mice: mechanisms of mitochondriopathy and cell death', *Journal of Comparative Neurology*, vol. 500, no. 1, pp. 20-46.
Maruyama, H, Morino, H, Ito, H, et al. 2010, 'Mutations of optineurin in amyotrophic lateral sclerosis', *Nature*, vol. 465, no. 7295, pp. 223-226.
Mates, JM, Perez-Gomez, C & Nunez de Castro, I 1999, 'Antioxidant enzymes and human diseases', *Clinical Biochemistry*, vol. 32, no. 8, pp. 595-603.
Mattiazzi, M, D'Aurelio, M, Gajewski, CD, et al. 2002, 'Mutated human SOD1 causes dysfunction of oxidative phosphorylation in mitochondria of transgenic mice', *The Journal of biological chemistry*, vol. 277, no. 33, pp. 29626-29633.
Mattsson, P, Lonnstedt, I, Nygren, I, et al. 2012, 'Physical fitness, but not muscle strength, is a risk factor for death in amyotrophic lateral sclerosis at an early age', *Journal of Neurology, Neurosurgery and Psychiatry*, vol. 83, no. 4, pp. 390-394.
Mayadev, AS, Weiss, MD, Distad, BJ, et al. 2008, 'The amyotrophic lateral sclerosis center: a model of multidisciplinary management', *Physical Medicine and Rehabilitation Clinics of North America*, vol. 19, no. 3, pp. 619-631, xi.
McCrate, ME & Kaspar, BK 2008, 'Physical activity and neuroprotection in amyotrophic lateral sclerosis', *Neuromolecular Medicine*, vol. 10, no. 2, pp. 108-117.
McGeer, PL & McGeer, EG 2002, 'Inflammatory processes in amyotrophic lateral sclerosis', *Muscle & Nerve*, vol. 26, no. 4, pp. 459-470.
McGeer, PL & Steele, JC 2011, 'The ALS/PDC syndrome of Guam: potential biomarkers for an enigmatic disorder', *Progress in Neurobiology*, vol. 95, no. 4, pp. 663-669.

McLean, JR & Robertson, J 2011, 'Isoform-specific expression and ratio changes accompany oxidant-induced peripherin aggregation in a neuroblastoma cell line', *Brain Research*, vol. 1422, pp. 57-65.
Meloni, G, Faller, P & Vasak, M 2007, 'Redox silencing of copper in metal-linked neurodegenerative disorders: reaction of Zn7metallothionein-3 with Cu2+ ions', *The Journal of biological chemistry*, vol. 282, no. 22, pp. 16068-16078.
Meyer, K, Ferraiuolo, L, Miranda, CJ, et al. 2014, 'Direct conversion of patient fibroblasts demonstrates non-cell autonomous toxicity of astrocytes to motor neurons in familial and sporadic ALS', *Proceedings of the National Academy of Sciences of the United States of America*, vol. 111, no. 2, pp. 829-832.
Michalska, AE & Choo, KH 1993, 'Targeting and germ-line transmission of a null mutation at the metallothionein I and II loci in mouse', *Proceedings of the National Academy of Sciences of the United States of America*, vol. 90, no. 17, pp. 8088-8092.
Migheli, A, Pezzulo, T, Attanasio, A, et al. 1993, 'Peripherin immunoreactive structures in amyotrophic lateral sclerosis', *Laboratory Investigation*, vol. 68, no. 2, pp. 185-191.
Miller, RG, Jackson, CE, Kasarskis, EJ, et al. 2009, 'Practice parameter update: the care of the patient with amyotrophic lateral sclerosis: multidisciplinary care, symptom management, and cognitive/behavioral impairment (an evidence-based review): report of the Quality Standards Subcommittee of the American Academy of Neurology', *Neurology*, vol. 73, no. 15, pp. 1227-1233.
Mitchell, J, Paul, P, Chen, HJ, et al. 2010, 'Familial amyotrophic lateral sclerosis is associated with a mutation in D-amino acid oxidase', *Proceedings of the National Academy of Sciences of the United States of America*, vol. 107, no. 16, pp. 7556-7561.
Mitne-Neto, M, Ramos, CR, Pimenta, DC, et al. 2007, 'A mutation in human VAP-B--MSP domain, present in ALS patients, affects the interaction with other cellular proteins', *Protein Expression and Purification*, vol. 55, no. 1, pp. 139-146.
Morahan, JM, Yu, B, Trent, RJ, et al. 2007, 'Genetic susceptibility to environmental toxicants in ALS', *American Journal of Medical Genetics B Neuropsychiatric Genetics*, vol. 144B, no. 7, pp. 885-890.
Moreira, MC, Klur, S, Watanabe, M, et al. 2004, 'Senataxin, the ortholog of a yeast RNA helicase, is mutant in ataxia-ocular apraxia 2', *Nature Genetics*, vol. 36, no. 3, pp. 225-227.
Mori, K, Weng, SM, Arzberger, T, et al. 2013, 'The C9orf72 GGGGCC repeat is translated into aggregating dipeptide-repeat proteins in FTLD/ALS', *Science*, vol. 339, no. 6125, pp. 1335-1338.
Morotz, GM, De Vos, KJ, Vagnoni, A, et al. 2012, 'Amyotrophic lateral sclerosis-associated mutant VAPBP56S perturbs calcium homeostasis to disrupt axonal transport of mitochondria', *Human Molecular Genetics*, vol. 21, no. 9, pp. 1979-1988.
Munch, C, Sedlmeier, R, Meyer, T, et al. 2004, 'Point mutations of the p150 subunit of dynactin (DCTN1) gene in ALS', *Neurology*, vol. 63, no. 4, pp. 724-726.
Murakami, T, Nagano, I, Hayashi, T, et al. 2001, 'Impaired retrograde axonal transport of adenovirus-mediated E. coli LacZ gene in the mice carrying mutant SOD1 gene', *Neuroscience Letters*, vol. 308, no. 3, pp. 149-152.
Murnane, RJ & Willett, JB 2011, *Methods matter : improving causal inference in educational and social science research*, Oxford University Press, Oxford ; New York.
Murphy, S 2000, 'Production of nitric oxide by glial cells: regulation and potential roles in the CNS', *Glia*, vol. 29, no. 1, pp. 1-13.
N'Diaye, EN, Kajihara, KK, Hsieh, I, et al. 2009, 'PLIC proteins or ubiquilins regulate autophagy-dependent cell survival during nutrient starvation', *EMBO Reports*, vol. 10, no. 2, pp. 173-179.
Nagai, M, Aoki, M, Miyoshi, I, et al. 2001, 'Rats expressing human cytosolic copper-zinc superoxide dismutase transgenes with amyotrophic lateral sclerosis: associated mutations develop motor neuron disease', *The Journal of Neuroscience*, vol. 21, no. 23, pp. 9246-9254.
Nagai, M, Re, DB, Nagata, T, et al. 2007, 'Astrocytes expressing ALS-linked mutated SOD1 release factors selectively toxic to motor neurons', *Nature Neuroscience*, vol. 10, no. 5, pp. 615-622.
Nagano, S, Satoh, M, Sumi, H, et al. 2001, 'Reduction of metallothioneins promotes the disease expression of familial amyotrophic lateral sclerosis mice in a dose-dependent manner', *European Journal of Neuroscience*, vol. 13, no. 7, pp. 1363-1370.
Nagley, P, Higgins, GC, Atkin, JD, et al. 2010, 'Multifaceted deaths orchestrated by mitochondria in neurones', *Biochimica et Biophysica Acta*, vol. 1802, no. 1, pp. 167-185.
Nandedkar, SD, Barkhaus, PE & Stalberg, EV 2010, 'Motor unit number index (MUNIX): principle, method, and findings in healthy subjects and in patients with motor neuron disease', *Muscle & Nerve*, vol. 42, no. 5, pp. 798-807.
Neumann, H & Takahashi, K 2007, 'Essential role of the microglial triggering receptor expressed on myeloid cells-2 (TREM2) for central nervous tissue immune homeostasis', *Journal of Neuroimmunology*, vol. 184, no. 1-2, pp. 92-99.

Neumann, M, Sampathu, DM, Kwong, LK, et al. 2006, 'Ubiquitinated TDP-43 in frontotemporal lobar degeneration and amyotrophic lateral sclerosis', *Science*, vol. 314, no. 5796, pp. 130-133.
Ngu, TT & Stillman, MJ 2006, 'Arsenic binding to human metallothionein', *Journal of the American Chemical Society*, vol. 128, no. 38, pp. 12473-12483.
Nicaise, C, Coupier, J, Dabadie, MP, et al. 2008, 'Gemals, a new drug candidate, extends lifespan and improves electromyographic parameters in a rat model of amyotrophic lateral sclerosis', *Amyotrophic Lateral Sclerosis*, vol. 9, no. 2, pp. 85-90.
Nicolson, G 2008, 'Chronic bacterial and viral infections in neurodegenerative and neurobehavioural diseases', *Laboratory Medicine*, vol. 39, no. 5, pp. 291-299.
Nishimura, AL, Mitne-Neto, M, Silva, HC, et al. 2004, 'A mutation in the vesicle-trafficking protein VAPB causes late-onset spinal muscular atrophy and amyotrophic lateral sclerosis', *American Journal of Human Genetics*, vol. 75, no. 5, pp. 822-831.
Ohtsuji, M, Katsuoka, F, Kobayashi, A, et al. 2008, 'Nrf1 and Nrf2 play distinct roles in activation of antioxidant response element-dependent genes', *The Journal of biological chemistry*, vol. 283, no. 48, pp. 33554-33562.
Okamoto, K, Fujita, Y & Mizuno, Y 2010, 'Pathology of protein synthesis and degradation systems in ALS', *Neuropathology*, vol. 30, no. 2, pp. 189-193.
Okuno, T, Nakatsuji, Y, Kumanogoh, A, et al. 2004, 'Induction of cyclooxygenase-2 in reactive glial cells by the CD40 pathway: relevance to amyotrophic lateral sclerosis', *Journal of Neurochemistry*, vol. 91, no. 2, pp. 404-412.
Orrell, RW, Lane, RJ & Ross, M 2007, 'Antioxidant treatment for amyotrophic lateral sclerosis / motor neuron disease', *The Cochrane database of systematic reviews*, no. 1, p. CD002829.
Ostrakhovitch, EA, Olsson, PE, Jiang, S, et al. 2006, 'Interaction of metallothionein with tumor suppressor p53 protein', *FEBS Letters*, vol. 580, no. 5, pp. 1235-1238.
Oteiza, PI, Uchitel, OD, Carrasquedo, F, et al. 1997, 'Evaluation of antioxidants, protein, and lipid oxidation products in blood from sporadic amyotrophic lateral sclerosis patients', *Neurochemical Research*, vol. 22, no. 4, pp. 535-539.
Palacios-Callender, M, Quintero, M, Hollis, VS, et al. 2004, 'Endogenous NO regulates superoxide production at low oxygen concentrations by modifying the redox state of cytochrome c oxidase', *Proceedings of the National Academy of Sciences of the United States of America*, vol. 101, no. 20, pp. 7630-7635.
Palmiter, RD, Findley, SD, Whitmore, TE, et al. 1992, 'MT-III, a brain-specific member of the metallothionein gene family', *Proceedings of the National Academy of Sciences of the United States of America*, vol. 89, no. 14, pp. 6333-6337.
Pamphlett, R & Kum Jew, S 2013, 'Heavy metals in locus ceruleus and motor neurons in motor neuron disease', *Acta neuropathologica communications*, vol. 1, no. 1, p. 81.
Pan, L, Yoshii, Y, Otomo, A, et al. 2012, 'Different human copper-zinc superoxide dismutase mutants, SOD1G93A and SOD1H46R, exert distinct harmful effects on gross phenotype in mice', *PLoS ONE*, vol. 7, no. 3, p. e33409.
Pankhurst, MW, Bennett, W, Kirkcaldie, MT, et al. 2011, 'Increased circulating leukocyte numbers and altered macrophage phenotype correlate with the altered immune response to brain injury in metallothionein (MT)-I/II null mutant mice', *Journal of neuroinflammation*, vol. 8, p. 172.
Pankiv, S, Clausen, TH, Lamark, T, et al. 2007, 'p62/SQSTM1 binds directly to Atg8/LC3 to facilitate degradation of ubiquitinated protein aggregates by autophagy', *The Journal of biological chemistry*, vol. 282, no. 33, pp. 24131-24145.
Pankratova, S, Kiryushko, D, Sonn, K, et al. 2010, 'Neuroprotective properties of a novel, non-haematopoietic agonist of the erythropoietin receptor', *Brain*, vol. 133, no. Pt 8, pp. 2281-2294.
Panov, A, Kubalik, N, Zinchenko, N, et al. 2011, 'Respiration and ROS production in brain and spinal cord mitochondria of transgenic rats with mutant G93a Cu/Zn-superoxide dismutase gene', *Neurobiology of Disease*, vol. 44, no. 1, pp. 53-62.
Pantelidou, M, Zographos, SE, Lederer, CW, et al. 2007, 'Differential expression of molecular motors in the motor cortex of sporadic ALS', *Neurobiology of Disease*, vol. 26, no. 3, pp. 577-589.
Papadeas, ST, Kraig, SE, O'Banion, C, et al. 2011, 'Astrocytes carrying the superoxide dismutase 1 (SOD1G93A) mutation induce wild-type motor neuron degeneration in vivo', *Proceedings of the National Academy of Sciences of the United States of America*, vol. 108, no. 43, pp. 17803-17808.
Papapetropoulos, S 2007, 'Is there a role for naturally occurring cyanobacterial toxins in neurodegeneration? The beta-N-methylamino-L-alanine (BMAA) paradigm', *Neurochemistry International*, vol. 50, no. 7-8, pp. 998-1003.

Papiani, G, Ruggiano, A, Fossati, M, et al. 2012, 'Restructured endoplasmic reticulum generated by mutant amyotrophic lateral sclerosis-linked VAPB is cleared by the proteasome', *Journal of Cell Science*, vol. 125, no. Pt 15, pp. 3601-3611.
Parker, SJ, Meyerowitz, J, James, JL, et al. 2012, 'Inhibition of TDP-43 accumulation by bis(thiosemicarbazonato)-copper complexes', *PLoS ONE*, vol. 7, no. 8, p. e42277.
Parkinson, N, Ince, PG, Smith, MO, et al. 2006, 'ALS phenotypes with mutations in CHMP2B (charged multivesicular body protein 2B)', *Neurology*, vol. 67, no. 6, pp. 1074-1077.
Pehar, M, Cassina, P, Vargas, MR, et al. 2004, 'Astrocytic production of nerve growth factor in motor neuron apoptosis: implications for amyotrophic lateral sclerosis', *Journal of Neurochemistry*, vol. 89, no. 2, pp. 464-473.
Pehar, M, Vargas, MR, Robinson, KM, et al. 2007, 'Mitochondrial superoxide production and nuclear factor erythroid 2-related factor 2 activation in p75 neurotrophin receptor-induced motor neuron apoptosis', *The Journal of Neuroscience*, vol. 27, no. 29, pp. 7777-7785.
Pelicano, H, Feng, L, Zhou, Y, et al. 2003, 'Inhibition of mitochondrial respiration: a novel strategy to enhance drug-induced apoptosis in human leukemia cells by a reactive oxygen species-mediated mechanism', *The Journal of biological chemistry*, vol. 278, no. 39, pp. 37832-37839.
Perrot, R, Lonchampt, P, Peterson, AC, et al. 2007, 'Axonal neurofilaments control multiple fiber properties but do not influence structure or spacing of nodes of Ranvier', *The Journal of Neuroscience*, vol. 27, no. 36, pp. 9573-9584.
Phul, RK, Shaw, PJ, Ince, PG, et al. 2000, 'Expression of nitric oxide synthase isoforms in spinal cord in amyotrophic lateral sclerosis', *Amyotrophic Lateral Sclerosis and Other Motor Neuron Disorders*, vol. 1, no. 4, pp. 259-267.
Plaitakis, A, Constantakakis, E & Smith, J 1988, 'The neuroexcitotoxic amino acids glutamate and aspartate are altered in the spinal cord and brain in amyotrophic lateral sclerosis', *Annals of Neurology*, vol. 24, no. 3, pp. 446-449.
Poderoso, JJ, Carreras, MC, Lisdero, C, et al. 1996, 'Nitric oxide inhibits electron transfer and increases superoxide radical production in rat heart mitochondria and submitochondrial particles', *Archives of Biochemistry and Biophysics*, vol. 328, no. 1, pp. 85-92.
Pollari, E, Savchenko, E, Jaronen, M, et al. 2011, 'Granulocyte colony stimulating factor attenuates inflammation in a mouse model of amyotrophic lateral sclerosis', *Journal of neuroinflammation*, vol. 8, p. 74.
Polymenidou, M, Lagier-Tourenne, C, Hutt, KR, et al. 2011, 'Long pre-mRNA depletion and RNA missplicing contribute to neuronal vulnerability from loss of TDP-43', *Nature Neuroscience*, vol. 14, no. 4, pp. 459-468.
Pompl, PN, Ho, L, Bianchi, M, et al. 2003, 'A therapeutic role for cyclooxygenase-2 inhibitors in a transgenic mouse model of amyotrophic lateral sclerosis', *FASEB Journal*, vol. 17, no. 6, pp. 725-727.
Potter, EG, Cheng, Y, Knight, JB, et al. 2007, 'Basic science; metallothionein I and II attenuate the thalamic microglial response following traumatic axotomy in the immature brain', *Journal of Neurotrauma*, vol. 24, no. 1, pp. 28-42.
Prell, T, Lautenschlager, J & Grosskreutz, J 2013, 'Calcium-dependent protein folding in amyotrophic lateral sclerosis', *Cell Calcium*, vol. 54, no. 2, pp. 132-143.
Puls, I, Jonnakuty, C, LaMonte, BH, et al. 2003, 'Mutant dynactin in motor neuron disease', *Nature Genetics*, vol. 33, no. 4, pp. 455-456.
Pulst, SM, Nechiporuk, A, Nechiporuk, T, et al. 1996, 'Moderate expansion of a normally biallelic trinucleotide repeat in spinocerebellar ataxia type 2', *Nature Genetics*, vol. 14, no. 3, pp. 269-276.
Puttaparthi, K, Gitomer, WL, Krishnan, U, et al. 2002, 'Disease progression in a transgenic model of familial amyotrophic lateral sclerosis is dependent on both neuronal and non-neuronal zinc binding proteins', *The Journal of Neuroscience*, vol. 22, no. 20, pp. 8790-8796.
Quaife, CJ, Findley, SD, Erickson, JC, et al. 1994, 'Induction of a new metallothionein isoform (MT-IV) occurs during differentiation of stratified squamous epithelia', *Biochemistry*, vol. 33, no. 23, pp. 7250-7259.
Raasi, S & Wolf, DH 2007, 'Ubiquitin receptors and ERAD: a network of pathways to the proteasome', *Seminars in Cell and Developmental Biology*, vol. 18, no. 6, pp. 780-791.
Rabin, SJ, Kim, JM, Baughn, M, et al. 2010, 'Sporadic ALS has compartment-specific aberrant exon splicing and altered cell-matrix adhesion biology', *Human Molecular Genetics*, vol. 19, no. 2, pp. 313-328.
Rabizadeh, S, Gralla, EB, Borchelt, DR, et al. 1995, 'Mutations associated with amyotrophic lateral sclerosis convert superoxide dismutase from an antiapoptotic gene to a proapoptotic gene: studies in yeast and neural cells', *Proceedings of the National Academy of Sciences of the United States of America*, vol. 92, no. 7, pp. 3024-3028.

Radi, R 2013, 'Protein tyrosine nitration: biochemical mechanisms and structural basis of functional effects', *Accounts of Chemical Research*, vol. 46, no. 2, pp. 550-559.
Rakhit, R, Cunningham, P, Furtos-Matei, A, et al. 2002, 'Oxidation-induced misfolding and aggregation of superoxide dismutase and its implications for amyotrophic lateral sclerosis', *The Journal of biological chemistry*, vol. 277, no. 49, pp. 47551-47556.
Ravits, J, Appel, S, Baloh, RH, et al. 2013, 'Deciphering amyotrophic lateral sclerosis: what phenotype, neuropathology and genetics are telling us about pathogenesis', *Amyotrophic Lateral Sclerosis and Frontotemporal Degeneration*, vol. 14 Suppl 1, pp. 5-18.
Reaume, AG, Elliott, JL, Hoffman, EK, et al. 1996, 'Motor neurons in Cu/Zn superoxide dismutase-deficient mice develop normally but exhibit enhanced cell death after axonal injury', *Nature Genetics*, vol. 13, no. 1, pp. 43-47.
Renton, AE, Chio, A & Traynor, BJ 2014, 'State of play in amyotrophic lateral sclerosis genetics', *Nature Neuroscience*, vol. 17, no. 1, pp. 17-23.
Reynolds, MR, Berry, RW & Binder, LI 2007, 'Nitration in neurodegeneration: deciphering the "Hows" "nYs"', *Biochemistry*, vol. 46, no. 25, pp. 7325-7336.
Richards, RI, Heguy, A & Karin, M 1984, 'Structural and functional analysis of the human metallothionein-IA gene: differential induction by metal ions and glucocorticoids', *Cell*, vol. 37, no. 1, pp. 263-272.
Ringbom, T, Huss, U, Stenholm, A, et al. 2001, 'Cox-2 inhibitory effects of naturally occurring and modified fatty acids', *Journal of Natural Products*, vol. 64, no. 6, pp. 745-749.
Roberts, K, Zeineddine, R, Corcoran, L, et al. 2013, 'Extracellular aggregated Cu/Zn superoxide dismutase activates microglia to give a cytotoxic phenotype', *Glia*, vol. 61, no. 3, pp. 409-419.
Robertson, J, Beaulieu, JM, Doroudchi, MM, et al. 2001, 'Apoptotic death of neurons exhibiting peripherin aggregates is mediated by the proinflammatory cytokine tumor necrosis factor-alpha', *The Journal of cell biology*, vol. 155, no. 2, pp. 217-226.
Roos, PM, Vesterberg, O & Nordberg, M 2006, 'Metals in motor neuron diseases', *Experimental Biology and Medicine*, vol. 231, no. 9, pp. 1481-1487.
Roos, PM, Vesterberg, O, Syversen, T, et al. 2013, 'Metal concentrations in cerebrospinal fluid and blood plasma from patients with amyotrophic lateral sclerosis', *Biological Trace Element Research*, vol. 151, no. 2, pp. 159-170.
Rosen, DR, Siddique, T, Patterson, D, et al. 1993, 'Mutations in Cu/Zn superoxide dismutase gene are associated with familial amyotrophic lateral sclerosis', *Nature*, vol. 362, no. 6415, pp. 59-62.
Ross, MA, Miller, RG, Berchert, L, et al. 1998, 'Toward earlier diagnosis of amyotrophic lateral sclerosis: revised criteria. rhCNTF ALS Study Group', *Neurology*, vol. 50, no. 3, pp. 768-772.
Rothstein, JD, Tsai, G, Kuncl, RW, et al. 1990, 'Abnormal excitatory amino acid metabolism in amyotrophic lateral sclerosis', *Annals of Neurology*, vol. 28, no. 1, pp. 18-25.
Rothstein, JD, Van Kammen, M, Levey, AI, et al. 1995, 'Selective loss of glial glutamate transporter GLT-1 in amyotrophic lateral sclerosis', *Annals of Neurology*, vol. 38, no. 1, pp. 73-84.
Rulten, SL, Rotheray, A, Green, RL, et al. 2013, 'PARP-1 dependent recruitment of the amyotrophic lateral sclerosis-associated protein FUS/TLS to sites of oxidative DNA damage', *Nucleic Acids Research*.
Rusten, TE & Simonsen, A 2008, 'ESCRT functions in autophagy and associated disease', *Cell Cycle*, vol. 7, no. 9, pp. 1166-1172.
Ruttkay-Nedecky, B, Nejdl, L, Gumulec, J, et al. 2013, 'The role of metallothionein in oxidative stress', *International journal of molecular sciences*, vol. 14, no. 3, pp. 6044-6066.
Saeed, M, Siddique, N, Hung, WY, et al. 2006, 'Paraoxonase cluster polymorphisms are associated with sporadic ALS', *Neurology*, vol. 67, no. 5, pp. 771-776.
Sahlender, DA, Roberts, RC, Arden, SD, et al. 2005, 'Optineurin links myosin VI to the Golgi complex and is involved in Golgi organization and exocytosis', *The Journal of cell biology*, vol. 169, no. 2, pp. 285-295.
Sanagi, T, Yuasa, S, Nakamura, Y, et al. 2010, 'Appearance of phagocytic microglia adjacent to motoneurons in spinal cord tissue from a presymptomatic transgenic rat model of amyotrophic lateral sclerosis', *Journal of Neuroscience Research*, vol. 88, no. 12, pp. 2736-2746.
Sanjak, M, Bravver, E, Bockenek, WL, et al. 2010, 'Supported treadmill ambulation for amyotrophic lateral sclerosis: a pilot study', *Archives of Physical Medicine and Rehabilitation*, vol. 91, no. 12, pp. 1920-1929.
Sanpei, K, Takano, H, Igarashi, S, et al. 1996, 'Identification of the spinocerebellar ataxia type 2 gene using a direct identification of repeat expansion and cloning technique, DIRECT', *Nature Genetics*, vol. 14, no. 3, pp. 277-284.

Sargsyan, SA, Blackburn, DJ, Barber, SC, et al. 2011, 'A comparison of in vitro properties of resting SOD1 transgenic microglia reveals evidence of reduced neuroprotective function', *BMC Neuroscience*, vol. 12, p. 91.
Sarlette, A, Krampfl, K, Grothe, C, et al. 2008, 'Nuclear erythroid 2-related factor 2-antioxidative response element signaling pathway in motor cortex and spinal cord in amyotrophic lateral sclerosis', *Journal of Neuropathology & Experimental Neurology*, vol. 67, no. 11, pp. 1055-1062.
Sasabe, J, Chiba, T, Yamada, M, et al. 2007, 'D-serine is a key determinant of glutamate toxicity in amyotrophic lateral sclerosis', *EMBO Journal*, vol. 26, no. 18, pp. 4149-4159.
Sasaki, S & Iwata, M 1996, 'Impairment of fast axonal transport in the proximal axons of anterior horn neurons in amyotrophic lateral sclerosis', *Neurology*, vol. 47, no. 2, pp. 535-540.
Sasaki, S, Shibata, N, Komori, T, et al. 2000, 'iNOS and nitrotyrosine immunoreactivity in amyotrophic lateral sclerosis', *Neuroscience Letters*, vol. 291, no. 1, pp. 44-48.
Scheiber, IF, Mercer, JF & Dringen, R 2014, 'Metabolism and functions of copper in brain', *Progress in Neurobiology*.
Schiffer, D, Cordera, S, Cavalla, P, et al. 1996, 'Reactive astrogliosis of the spinal cord in amyotrophic lateral sclerosis', *Journal of the Neurological Sciences*, vol. 139 Suppl, pp. 27-33.
Schorle, H, Holtschke, T, Hunig, T, et al. 1991, 'Development and function of T cells in mice rendered interleukin-2 deficient by gene targeting', *Nature*, vol. 352, no. 6336, pp. 621-624.
Schroder, M 2008, 'Endoplasmic reticulum stress responses', *Cellular and Molecular Life Sciences*, vol. 65, no. 6, pp. 862-894.
Schymick, JC, Talbot, K & Traynor, BJ 2007, 'Genetics of sporadic amyotrophic lateral sclerosis', *Human Molecular Genetics*, vol. 16 Spec No. 2, pp. R233-242.
Scott, S, Kranz, JE, Cole, J, et al. 2008, 'Design, power, and interpretation of studies in the standard murine model of ALS', *Amyotrophic Lateral Sclerosis*, vol. 9, no. 1, pp. 4-15.
Seibenhener, ML, Babu, JR, Geetha, T, et al. 2004, 'Sequestosome 1/p62 is a polyubiquitin chain binding protein involved in ubiquitin proteasome degradation', *Molecular and Cellular Biology*, vol. 24, no. 18, pp. 8055-8068.
Sekizawa, T, Openshaw, H, Ohbo, K, et al. 1998, 'Cerebrospinal fluid interleukin 6 in amyotrophic lateral sclerosis: immunological parameter and comparison with inflammatory and non-inflammatory central nervous system diseases', *Journal of the Neurological Sciences*, vol. 154, no. 2, pp. 194-199.
Shaw, PJ, Ince, PG, Falkous, G, et al. 1995, 'Oxidative damage to protein in sporadic motor neuron disease spinal cord', *Annals of Neurology*, vol. 38, no. 4, pp. 691-695.
Shibata, N, Nagai, R, Uchida, K, et al. 2001, 'Morphological evidence for lipid peroxidation and protein glycoxidation in spinal cords from sporadic amyotrophic lateral sclerosis patients', *Brain Research*, vol. 917, no. 1, pp. 97-104.
Shih, DM, Gu, L, Xia, YR, et al. 1998, 'Mice lacking serum paraoxonase are susceptible to organophosphate toxicity and atherosclerosis', *Nature*, vol. 394, no. 6690, pp. 284-287.
Siddique, T & Ajroud-Driss, S 2011, 'Familial amyotrophic lateral sclerosis, a historical perspective', *Acta Myologica*, vol. 30, no. 2, pp. 117-120.
Siklos, L, Engelhardt, J, Harati, Y, et al. 1996, 'Ultrastructural evidence for altered calcium in motor nerve terminals in amyotropic lateral sclerosis', *Annals of Neurology*, vol. 39, no. 2, pp. 203-216.
Sillevis Smitt, PA, Mulder, TP, Verspaget, HW, et al. 1994, 'Metallothionein in amyotrophic lateral sclerosis', *Biological Signals*, vol. 3, no. 4, pp. 193-197.
Simmons, Z 2005, 'Management strategies for patients with amyotrophic lateral sclerosis from diagnosis through death', *The Neurologist*, vol. 11, no. 5, pp. 257-270.
Skalsky, AJ & McDonald, CM 2012, 'Prevention and management of limb contractures in neuromuscular diseases', *Physical Medicine and Rehabilitation Clinics of North America*, vol. 23, no. 3, pp. 675-687.
Skehel, PA, Fabian-Fine, R & Kandel, ER 2000, 'Mouse VAP33 is associated with the endoplasmic reticulum and microtubules', *Proceedings of the National Academy of Sciences of the United States of America*, vol. 97, no. 3, pp. 1101-1106.
Skourti-Stathaki, K, Proudfoot, NJ & Gromak, N 2011, 'Human senataxin resolves RNA/DNA hybrids formed at transcriptional pause sites to promote Xrn2-dependent termination', *Molecular Cell*, vol. 42, no. 6, pp. 794-805.
Slowik, A, Tomik, B, Wolkow, PP, et al. 2006, 'Paraoxonase gene polymorphisms and sporadic ALS', *Neurology*, vol. 67, no. 5, pp. 766-770.
Smith, RG, Henry, YK, Mattson, MP, et al. 1998, 'Presence of 4-hydroxynonenal in cerebrospinal fluid of patients with sporadic amyotrophic lateral sclerosis', *Annals of Neurology*, vol. 44, no. 4, pp. 696-699.
Solomon, JA, Tarnopolsky, MA & Hamadeh, MJ 2011, 'One universal common endpoint in mouse models of amyotrophic lateral sclerosis', *PLoS ONE*, vol. 6, no. 6, p. e20582.

Sonn, K, Pankratova, S, Korshunova, I, et al. 2010, 'A metallothionein mimetic peptide protects neurons against kainic acid-induced excitotoxicity', *Journal of Neuroscience Research*, vol. 88, no. 5, pp. 1074-1082.

Soo, KY, Farg, M & Atkin, JD 2011, 'Molecular motor proteins and amyotrophic lateral sclerosis', *International journal of molecular sciences*, vol. 12, no. 12, pp. 9057-9082.

Soon, CP, Donnelly, PS, Turner, BJ, et al. 2011, 'Diacetylbis(N(4)-methylthiosemicarbazonato) copper(II) (CuII(atsm)) protects against peroxynitrite-induced nitrosative damage and prolongs survival in amyotrophic lateral sclerosis mouse model', *The Journal of biological chemistry*, vol. 286, no. 51, pp. 44035-44044.

Sorrells, AD, Corcoran-Gomez, K, Eckert, KA, et al. 2009, 'Effects of environmental enrichment on the amyotrophic lateral sclerosis mouse model', *Laboratory Animals*, vol. 43, no. 2, pp. 182-190.

Spataro, R, Bono, V, Marchese, S, et al. 2012, 'Tracheostomy mechanical ventilation in patients with amyotrophic lateral sclerosis: clinical features and survival analysis', *Journal of the Neurological Sciences*, vol. 323, no. 1-2, pp. 66-70.

Spataro, R, Ficano, L, Piccoli, F, et al. 2011, 'Percutaneous endoscopic gastrostomy in amyotrophic lateral sclerosis: effect on survival', *Journal of the Neurological Sciences*, vol. 304, no. 1-2, pp. 44-48.

Sreedharan, J, Blair, IP, Tripathi, VB, et al. 2008, 'TDP-43 mutations in familial and sporadic amyotrophic lateral sclerosis', *Science*, vol. 319, no. 5870, pp. 1668-1672.

Stalberg, E, Schwartz, MS & Trontelj, JV 1975, 'Single fibre electromyography in various processes affecting the anterior horn cell', *Journal of the Neurological Sciences*, vol. 24, no. 4, pp. 403-415.

Straube-West, K, Loomis, PA, Opal, P, et al. 1996, 'Alterations in neural intermediate filament organization: functional implications and the induction of pathological changes related to motor neuron disease', *Journal of Cell Science*, vol. 109 (Pt 9), pp. 2319-2329.

Strong, MJ, Volkening, K, Hammond, R, et al. 2007, 'TDP43 is a human low molecular weight neurofilament (hNFL) mRNA-binding protein', *Molecular and Cellular Neurosciences*, vol. 35, no. 2, pp. 320-327.

Sunico, CR, Dominguez, G, Garcia-Verdugo, JM, et al. 2011, 'Reduction in the motoneuron inhibitory/excitatory synaptic ratio in an early-symptomatic mouse model of amyotrophic lateral sclerosis', *Brain Pathology*, vol. 21, no. 1, pp. 1-15.

Suraweera, A, Lim, Y, Woods, R, et al. 2009, 'Functional role for senataxin, defective in ataxia oculomotor apraxia type 2, in transcriptional regulation', *Human Molecular Genetics*, vol. 18, no. 18, pp. 3384-3396.

Suzuki, H, Kanekura, K, Levine, TP, et al. 2009, 'ALS-linked P56S-VAPB, an aggregated loss-of-function mutant of VAPB, predisposes motor neurons to ER stress-related death by inducing aggregation of co-expressed wild-type VAPB', *Journal of Neurochemistry*, vol. 108, no. 4, pp. 973-985.

Suzuki, K & Koizumi, S 2000, 'Individual metal responsive elements of the human metallothionein-IIA gene independently mediate responses to various heavy metal signals', *Industrial Health*, vol. 38, no. 1, pp. 87-90.

Szaro, BG & Strong, MJ 2010, 'Post-transcriptional control of neurofilaments: New roles in development, regeneration and neurodegenerative disease', *Trends in Neurosciences*, vol. 33, no. 1, pp. 27-37.

Tada, S, Okuno, T, Yasui, T, et al. 2011, 'Deleterious effects of lymphocytes at the early stage of neurodegeneration in an animal model of amyotrophic lateral sclerosis', *Journal of neuroinflammation*, vol. 8, no. 1, p. 19.

Takeuchi, H, Mizuno, T, Zhang, G, et al. 2005, 'Neuritic beading induced by activated microglia is an early feature of neuronal dysfunction toward neuronal death by inhibition of mitochondrial respiration and axonal transport', *The Journal of biological chemistry*, vol. 280, no. 11, pp. 10444-10454.

Talman, P, Forbes, A & Mathers, S 2009, 'Clinical phenotypes and natural progression for motor neuron disease: analysis from an Australian database', *Amyotrophic Lateral Sclerosis*, vol. 10, no. 2, pp. 79-84.

Tarabal, O, Caldero, J, Casas, C, et al. 2005, 'Protein retention in the endoplasmic reticulum, blockade of programmed cell death and autophagy selectively occur in spinal cord motoneurons after glutamate receptor-mediated injury', *Molecular and Cellular Neurosciences*, vol. 29, no. 2, pp. 283-298.

Tateno, M, Kato, S, Sakurai, T, et al. 2009, 'Mutant SOD1 impairs axonal transport of choline acetyltransferase and acetylcholine release by sequestering KAP3', *Human Molecular Genetics*, vol. 18, no. 5, pp. 942-955.

Teuling, E, Ahmed, S, Haasdijk, E, et al. 2007, 'Motor neuron disease-associated mutant vesicle-associated membrane protein-associated protein (VAP) B recruits wild-type VAPs into endoplasmic reticulum-derived tubular aggregates', *The Journal of Neuroscience*, vol. 27, no. 36, pp. 9801-9815.

Thonhoff, JR, Gao, J, Dunn, TJ, et al. 2012, 'Mutant SOD1 microglia-generated nitroxidative stress promotes toxicity to human fetal neural stem cell-derived motor neurons through direct damage and noxious interactions with astrocytes', *American Journal of Stem Cells*, vol. 1, no. 1, pp. 2-21.

Thornalley, PJ & Vasak, M 1985, 'Possible role for metallothionein in protection against radiation-induced oxidative stress. Kinetics and mechanism of its reaction with superoxide and hydroxyl radicals', *Biochimica et Biophysica Acta*, vol. 827, no. 1, pp. 36-44.

Ticozzi, N, Vance, C, Leclerc, AL, et al. 2011, 'Mutational analysis reveals the FUS homolog TAF15 as a candidate gene for familial amyotrophic lateral sclerosis', *American Journal of Medical Genetics B Neuropsychiatric Genetics*, vol. 156B, no. 3, pp. 285-290.

Tokuda, E, Okawa, E & Ono, S 2009, 'Dysregulation of intracellular copper trafficking pathway in a mouse model of mutant copper/zinc superoxide dismutase-linked familial amyotrophic lateral sclerosis', *Journal of Neurochemistry*, vol. 111, no. 1, pp. 181-191.

Tokuda, E, Okawa, E, Watanabe, S, et al. 2013, 'Overexpression of metallothionein-I, a copper-regulating protein, attenuates intracellular copper dyshomeostasis and extends lifespan in a mouse model of amyotrophic lateral sclerosis caused by mutant superoxide dismutase-1', *Human Molecular Genetics*.

Tokuda, E, Ono, S, Ishige, K, et al. 2007, 'Metallothionein proteins expression, copper and zinc concentrations, and lipid peroxidation level in a rodent model for amyotrophic lateral sclerosis', *Toxicology*, vol. 229, no. 1-2, pp. 33-41.

Tollervey, JR, Curk, T, Rogelj, B, et al. 2011, 'Characterizing the RNA targets and position-dependent splicing regulation by TDP-43', *Nature Neuroscience*, vol. 14, no. 4, pp. 452-458.

Topp, JD, Gray, NW, Gerard, RD, et al. 2004, 'Alsin is a Rab5 and Rac1 guanine nucleotide exchange factor', *The Journal of biological chemistry*, vol. 279, no. 23, pp. 24612-24623.

Tran, D, Chalhoub, A, Schooley, A, et al. 2012, 'A mutation in VAPB that causes amyotrophic lateral sclerosis also causes a nuclear envelope defect', *Journal of Cell Science*, vol. 125, no. Pt 12, pp. 2831-2836.

Traynor, BJ, Codd, MB, Corr, B, et al. 2000, 'Amyotrophic lateral sclerosis mimic syndromes: a population-based study', *Archives of Neurology*, vol. 57, no. 1, pp. 109-113.

Trendelenburg, G, Prass, K, Priller, J, et al. 2002, 'Serial analysis of gene expression identifies metallothionein-II as major neuroprotective gene in mouse focal cerebral ischemia', *The Journal of Neuroscience*, vol. 22, no. 14, pp. 5879-5888.

Trojsi, F, Monsurro, MR & Tedeschi, G 2013, 'Exposure to environmental toxicants and pathogenesis of amyotrophic lateral sclerosis: state of the art and research perspectives', *International journal of molecular sciences*, vol. 14, no. 8, pp. 15286-15311.

Trotti, D, Rolfs, A, Danbolt, NC, et al. 1999, 'SOD1 mutants linked to amyotrophic lateral sclerosis selectively inactivate a glial glutamate transporter', *Nature Neuroscience*, vol. 2, no. 5, pp. 427-433.

Tsuda, H, Han, SM, Yang, Y, et al. 2008, 'The amyotrophic lateral sclerosis 8 protein VAPB is cleaved, secreted, and acts as a ligand for Eph receptors', *Cell*, vol. 133, no. 6, pp. 963-977.

Tumbarello, DA, Kendrick-Jones, J & Buss, F 2013, 'Myosin VI and its cargo adaptors - linking endocytosis and autophagy', *Journal of Cell Science*, vol. 126, no. Pt 12, pp. 2561-2570.

Turner, MR & Kiernan, MC 2012, 'Does interneuronal dysfunction contribute to neurodegeneration in amyotrophic lateral sclerosis?', *Amyotrophic Lateral Sclerosis*, vol. 13, no. 3, pp. 245-250.

Turrens, JF 2003, 'Mitochondrial formation of reactive oxygen species', *The Journal of physiology*, vol. 552, no. Pt 2, pp. 335-344.

Urushitani, M, Sik, A, Sakurai, T, et al. 2006, 'Chromogranin-mediated secretion of mutant superoxide dismutase proteins linked to amyotrophic lateral sclerosis', *Nature Neuroscience*, vol. 9, no. 1, pp. 108-118.

Usarek, E, Kuzma-Kozakiewicz, M, Schwalenstocker, B, et al. 2006, 'Tau isoforms expression in transgenic mouse model of amyotrophic lateral sclerosis', *Neurochemical Research*, vol. 31, no. 5, pp. 597-602.

Van Den Bosch, L, Vandenberghe, W, Klaassen, H, et al. 2000, 'Ca(2+)-permeable AMPA receptors and selective vulnerability of motor neurons', *Journal of the Neurological Sciences*, vol. 180, no. 1-2, pp. 29-34.

van Lookeren Campagne, M, Thibodeaux, H, van Bruggen, N, et al. 1999, 'Evidence for a protective role of metallothionein-1 in focal cerebral ischemia', *Proceedings of the National Academy of Sciences of the United States of America*, vol. 96, no. 22, pp. 12870-12875.

Vance, C, Rogelj, B, Hortobagyi, T, et al. 2009, 'Mutations in FUS, an RNA processing protein, cause familial amyotrophic lateral sclerosis type 6', *Science*, vol. 323, no. 5918, pp. 1208-1211.

Vande Velde, C, Miller, TM, Cashman, NR, et al. 2008, 'Selective association of misfolded ALS-linked mutant SOD1 with the cytoplasmic face of mitochondria', *Proceedings of the National Academy of Sciences of the United States of America*, vol. 105, no. 10, pp. 4022-4027.

Vargas, MR & Johnson, JA 2010, 'Astrogliosis in amyotrophic lateral sclerosis: role and therapeutic potential of astrocytes', *Neurotherapeutics*, vol. 7, no. 4, pp. 471-481.

Veldink, JH, Bar, PR, Joosten, EA, et al. 2003, 'Sexual differences in onset of disease and response to exercise in a transgenic model of ALS', *Neuromuscular Disorders*, vol. 13, no. 9, pp. 737-743.
Vinsant, S, Mansfield, C, Jimenez-Moreno, R, et al. 2013, 'Characterization of early pathogenesis in the SOD1(G93A) mouse model of ALS: part II, results and discussion', *Brain and Behavior*, vol. 3, no. 4, pp. 431-457.
Visser, J, van den Berg-Vos, RM, Franssen, H, et al. 2007, 'Disease course and prognostic factors of progressive muscular atrophy', *Archives of Neurology*, vol. 64, no. 4, pp. 522-528.
Walker, AK, Soo, KY, Sundaramoorthy, V, et al. 2013, 'ALS-associated TDP-43 induces endoplasmic reticulum stress, which drives cytoplasmic TDP-43 accumulation and stress granule formation', *PLoS ONE*, vol. 8, no. 11, p. e81170.
Walker, HK 1990, 'Deep Tendon Reflexes', in HKWWDHJW Hurst (ed.), *Clinical Methods: The History, Physical, and Laboratory Examinations*, 3 edn, Butterworths, Boston.
Walton, MR & Dragunow, I 2000, 'Is CREB a key to neuronal survival?', *Trends in Neurosciences*, vol. 23, no. 2, pp. 48-53.
Wang, IF, Wu, LS, Chang, HY, et al. 2008, 'TDP-43, the signature protein of FTLD-U, is a neuronal activity-responsive factor', *Journal of Neurochemistry*, vol. 105, no. 3, pp. 797-806.
Wang, J, Song, Y, Elsherif, L, et al. 2006, 'Cardiac metallothionein induction plays the major role in the prevention of diabetic cardiomyopathy by zinc supplementation', *Circulation*, vol. 113, no. 4, pp. 544-554.
Wang, J, Xu, G, Gonzales, V, et al. 2002, 'Fibrillar inclusions and motor neuron degeneration in transgenic mice expressing superoxide dismutase 1 with a disrupted copper-binding site', *Neurobiology of Disease*, vol. 10, no. 2, pp. 128-138.
Wang, L, Gutmann, DH & Roos, RP 2011a, 'Astrocyte loss of mutant SOD1 delays ALS disease onset and progression in G85R transgenic mice', *Human Molecular Genetics*, vol. 20, no. 2, pp. 286-293.
Wang, R, Yang, B & Zhang, D 2011b, 'Activation of interferon signaling pathways in spinal cord astrocytes from an ALS mouse model', *Glia*, vol. 59, no. 6, pp. 946-958.
Wang, WY, Pan, L, Su, SC, et al. 2013, 'Interaction of FUS and HDAC1 regulates DNA damage response and repair in neurons', *Nature Neuroscience*, vol. 16, no. 10, pp. 1383-1391.
Watanabe, M, Dykes-Hoberg, M, Culotta, VC, et al. 2001, 'Histological evidence of protein aggregation in mutant SOD1 transgenic mice and in amyotrophic lateral sclerosis neural tissues', *Neurobiology of Disease*, vol. 8, no. 6, pp. 933-941.
Waterman-Storer, CM, Karki, S & Holzbaur, EL 1995, 'The p150Glued component of the dynactin complex binds to both microtubules and the actin-related protein centractin (Arp-1)', *Proceedings of the National Academy of Sciences of the United States of America*, vol. 92, no. 5, pp. 1634-1638.
Waterman-Storer, CM, Karki, SB, Kuznetsov, SA, et al. 1997, 'The interaction between cytoplasmic dynein and dynactin is required for fast axonal transport', *Proceedings of the National Academy of Sciences of the United States of America*, vol. 94, no. 22, pp. 12180-12185.
Wegorzewska, I, Bell, S, Cairns, NJ, et al. 2009, 'TDP-43 mutant transgenic mice develop features of ALS and frontotemporal lobar degeneration', *Proceedings of the National Academy of Sciences of the United States of America*, vol. 106, no. 44, pp. 18809-18814.
Weisskopf, MG, O'Reilly, EJ, McCullough, ML, et al. 2005, 'Prospective study of military service and mortality from ALS', *Neurology*, vol. 64, no. 1, pp. 32-37.
West, AK, Hidalgo, J, Eddins, D, et al. 2008, 'Metallothionein in the central nervous system: Roles in protection, regeneration and cognition', *Neurotoxicology*, vol. 29, no. 3, pp. 489-503.
Weydt, P, Hong, SY, Kliot, M, et al. 2003, 'Assessing disease onset and progression in the SOD1 mouse model of ALS', *Neuroreport*, vol. 14, no. 7, pp. 1051-1054.
Wiedemann, FR, Manfredi, G, Mawrin, C, et al. 2002, 'Mitochondrial DNA and respiratory chain function in spinal cords of ALS patients', *Journal of Neurochemistry*, vol. 80, no. 4, pp. 616-625.
Wiedemann, FR, Winkler, K, Kuznetsov, AV, et al. 1998, 'Impairment of mitochondrial function in skeletal muscle of patients with amyotrophic lateral sclerosis', *Journal of the Neurological Sciences*, vol. 156, no. 1, pp. 65-72.
Wijesekera, LC, Mathers, S, Talman, P, et al. 2009, 'Natural history and clinical features of the flail arm and flail leg ALS variants', *Neurology*, vol. 72, no. 12, pp. 1087-1094.
Winton, MJ, Igaz, LM, Wong, MM, et al. 2008, 'Disturbance of nuclear and cytoplasmic TAR DNA-binding protein (TDP-43) induces disease-like redistribution, sequestration, and aggregate formation', *The Journal of biological chemistry*, vol. 283, no. 19, pp. 13302-13309.
Witgert, M, Salamone, AR, Strutt, AM, et al. 2010, 'Frontal-lobe mediated behavioral dysfunction in amyotrophic lateral sclerosis', *European Journal of Neurology*, vol. 17, no. 1, pp. 103-110.

Wong, PC, Pardo, CA, Borchelt, DR, et al. 1995, 'An adverse property of a familial ALS-linked SOD1 mutation causes motor neuron disease characterized by vacuolar degeneration of mitochondria', *Neuron*, vol. 14, no. 6, pp. 1105-1116.
Wooley, CM, Sher, RB, Kale, A, et al. 2005, 'Gait analysis detects early changes in transgenic SOD1(G93A) mice', *Muscle & Nerve*, vol. 32, no. 1, pp. 43-50.
Wu, CH, Fallini, C, Ticozzi, N, et al. 2012, 'Mutations in the profilin 1 gene cause familial amyotrophic lateral sclerosis', *Nature*, vol. 488, no. 7412, pp. 499-503.
Xiao, S, Tjostheim, S, Sanelli, T, et al. 2008, 'An aggregate-inducing peripherin isoform generated through intron retention is upregulated in amyotrophic lateral sclerosis and associated with disease pathology', *The Journal of Neuroscience*, vol. 28, no. 8, pp. 1833-1840.
Xu, C, Bailly-Maitre, B & Reed, JC 2005, 'Endoplasmic reticulum stress: cell life and death decisions', *Journal of Clinical Investigation*, vol. 115, no. 10, pp. 2656-2664.
Xu, YF, Prudencio, M, Hubbard, JM, et al. 2013, 'The pathological phenotypes of human TDP-43 transgenic mouse models are independent of downregulation of mouse Tdp-43', *PLoS ONE*, vol. 8, no. 7, p. e69864.
Yamanaka, K, Boillee, S, Roberts, EA, et al. 2008, 'Mutant SOD1 in cell types other than motor neurons and oligodendrocytes accelerates onset of disease in ALS mice', *Proceedings of the National Academy of Sciences of the United States of America*, vol. 105, no. 21, pp. 7594-7599.
Yang, FC, Lin, YH, Chen, WH, et al. 2013, 'Interaction between salt-inducible kinase 2 (SIK2) and p97/valosin-containing protein (VCP) regulates endoplasmic reticulum (ER)-associated protein degradation in mammalian cells', *The Journal of biological chemistry*, vol. 288, no. 47, pp. 33861-33872.
Yang, WW, Sidman, RL, Taksir, TV, et al. 2011, 'Relationship between neuropathology and disease progression in the SOD1(G93A) ALS mouse', *Experimental Neurology*, vol. 227, no. 2, pp. 287-295.
Yang, Y, Hentati, A, Deng, HX, et al. 2001, 'The gene encoding alsin, a protein with three guanine-nucleotide exchange factor domains, is mutated in a form of recessive amyotrophic lateral sclerosis', *Nature Genetics*, vol. 29, no. 2, pp. 160-165.
Yasojima, K, Tourtellotte, WW, McGeer, EG, et al. 2001, 'Marked increase in cyclooxygenase-2 in ALS spinal cord: implications for therapy', *Neurology*, vol. 57, no. 6, pp. 952-956.
Yiangou, Y, Facer, P, Durrenberger, P, et al. 2006, 'COX-2, CB2 and P2X7-immunoreactivities are increased in activated microglial cells/macrophages of multiple sclerosis and amyotrophic lateral sclerosis spinal cord', *BMC Neurology*, vol. 6, p. 12.
Yoshihara, T, Ishigaki, S, Yamamoto, M, et al. 2002, 'Differential expression of inflammation- and apoptosis-related genes in spinal cords of a mutant SOD1 transgenic mouse model of familial amyotrophic lateral sclerosis', *Journal of Neurochemistry*, vol. 80, no. 1, pp. 158-167.
Yuce, O & West, SC 2013, 'Senataxin, defective in the neurodegenerative disorder ataxia with oculomotor apraxia 2, lies at the interface of transcription and the DNA damage response', *Molecular and Cellular Biology*, vol. 33, no. 2, pp. 406-417.
Zhang, B, Georgiev, O, Hagmann, M, et al. 2003, 'Activity of metal-responsive transcription factor 1 by toxic heavy metals and H2O2 in vitro is modulated by metallothionein', *Molecular and Cellular Biology*, vol. 23, no. 23, pp. 8471-8485.
Zhang, B, Luo, S, Wang, Q, et al. 2008, 'LRP4 serves as a coreceptor of agrin', *Neuron*, vol. 60, no. 2, pp. 285-297.
Zhang, B, Tu, P, Abtahian, F, et al. 1997, 'Neurofilaments and orthograde transport are reduced in ventral root axons of transgenic mice that express human SOD1 with a G93A mutation', *The Journal of cell biology*, vol. 139, no. 5, pp. 1307-1315.
Zhang, F, Strom, AL, Fukada, K, et al. 2007, 'Interaction between familial amyotrophic lateral sclerosis (ALS)-linked SOD1 mutants and the dynein complex', *The Journal of biological chemistry*, vol. 282, no. 22, pp. 16691-16699.
Zhang, H, Links, PH, Ngsee, JK, et al. 2004, 'Localization of low density lipoprotein receptor-related protein 1 to caveolae in 3T3-L1 adipocytes in response to insulin treatment', *The Journal of biological chemistry*, vol. 279, no. 3, pp. 2221-2230.
Zhao, W, Xie, W, Le, W, et al. 2004, 'Activated microglia initiate motor neuron injury by a nitric oxide and glutamate-mediated mechanism', *Journal of Neuropathology & Experimental Neurology*, vol. 63, no. 9, pp. 964-977.
Zhao, W, Xie, W, Xiao, Q, et al. 2006, 'Protective effects of an anti-inflammatory cytokine, interleukin-4, on motoneuron toxicity induced by activated microglia', *Journal of Neurochemistry*, vol. 99, no. 4, pp. 1176-1187.
Zhong, Z, Deane, R, Ali, Z, et al. 2008, 'ALS-causing SOD1 mutants generate vascular changes prior to motor neuron degeneration', *Nature Neuroscience*, vol. 11, no. 4, pp. 420-422.

Zu, T, Gibbens, B, Doty, NS, et al. 2011, 'Non-ATG-initiated translation directed by microsatellite expansions', *Proceedings of the National Academy of Sciences of the United States of America*, vol. 108, no. 1, pp. 260-265.

Supplementary Data

Supplementary Data 1: General notes on model fitting

Linear mixed models were fitted in SPSS Statistics 20 (IBM), using the following conditions for likelihood estimation:

Maximum iterations = 100
Maximum step-halvings = 10
Log-likelihood convergence = Absolute (0)
Parameter convergence = Absolute (0.000001)
Hessian convergence = Absolute (0)
Maximum scoring steps = 1
Singularity tolerance = 0.000000000001
Type III sum of squares was used for fixed effects
Variance/covariance matrix (G) structure = unstructured

When fitting each model, maximum likelihood (ML) estimation was used to check the improved fit of fixed effects, by comparing log likelihoods (as -2LL, in smaller-is-better format) with a chi squared test (χ^2) with degrees of freedom (df) equal to the number of parameters differing between models.

Restricted maximum likelihood (REML) estimation was used to check the improved fit of random effects, by comparing restricted log likelihoods (-2RLL) as above.

Both ML and REML log likelihoods (-2LL and -2RLL, respectively) are reported for the relevant models; however, it should be noted that the model specifications (fixed effects and covariance parameter estimates) are reported as obtained from ML estimation rather than REML estimation.

Supplementary Data 2: Fitting a linear mixed model to SOD1 and WT body weight trajectories

Fixed effects of the final model (Model 6, below) are summarised in Chapter 2, Table 2.4 and Figure 2.10.

Factors: **Age** = Age in days, continuous covariate; **Genotype** = dummy-coded binary variable, where 0 = WT and 1 = SOD1; interaction parameters between eg. Genotype*Age are therefore only applicable to SOD1 mice.

Model 1: Linear trajectory, no random effects

$\boldsymbol{Body\ weight_{ij} = \beta_0 + \beta_1 * Age + \varepsilon_{ij}}$ ($\boldsymbol{\varepsilon_{ij}}$ = errors for subject i at age j, $\boldsymbol{\varepsilon_{ij}} \sim$ iid $N(0,\sigma^2)$)

Factors: Fixed factors: Intercept, Age
Random factors: (none)

Estimates of fixed effects:

Parameter	Estimate (β)	95% CI, lower	95% CI, upper	Sig (p-value)
Intercept (β_0)	17.964030	17.624058	18.304002	<0.001
Age (β_1)	0.020006	0.017121	0.022890	<0.001

Estimates of covariance parameters:

Parameter	Estimate	Std. Error
Residual	2.944904	0.119976

Model fit (fixed effects): -2LL = 4721.134

Model 2: Quadratic trajectory, no random effects

$\boldsymbol{Body\ weight_{ij} = \beta_0 + \beta_1 * Age + \beta_2 * Age^2 + \varepsilon_{ij}}$

Factors: Fixed factors: Intercept, Age, Age^2
Random factors: (none)

Estimates of fixed effects:

Parameter	Estimate (β)	95% CI, lower	95% CI, upper	Sig (p-value)
Intercept (β_0)	14.681763	13.720716	15.642811	<0.001
Age (β_1)	0.083179	0.065600	0.100759	<0.001
Age^2 (β_2)	-0.00277	-0.000354	-0.000201	<0.001

Estimates of covariance parameters:

Parameter	Estimate	Std. Error
Residual	2.825273	0.115102

Model fit (fixed effects): -2LL = 4671.161
Difference from Model 1 = χ^2(4721.134 - 4671.161, df=1), p<0.001

The quadratic model (Model 2) fits the data significantly better than the linear model (Model 1).

Model 3: Cubic trajectory, no random effects

$$\textit{Body weight}_{ij} = \beta_0 + \beta_1 * \textit{Age} + \beta_2 * \textit{Age}^2 + \beta_3 * \textit{Age}^3 + \varepsilon_{ij}$$

Factors: Fixed factors: Intercept, Age, Age^2, Age^3
Random factors: (none)

Estimates of fixed effects:

Parameter	Estimate (β)	95% CI, lower	95% CI, upper	Sig (p-value)
Intercept (β_0)	3.759549	1.183858	6.335241	0.004
Age (β_1)	0.413304	0.338744	0.487863	<0.001
Age^2 (β_2)	-0.003348	-0.004028	-0.002669	<0.001
Age^3 (β_3)	0.000009	0.000007	0.000011	<0.001

Estimates of covariance parameters:

Parameter	Estimate	Std. Error
Residual	2.650180	0.107968

Model fit (fixed effects): -2LL = 4595.068
Difference from Model 2 = χ^2(4671.161 – 4595.068, df=1), p<0.001

The cubic model (Model 3) fits the data significantly better than the quadratic model (Model 2).

Model fit (random effects): -2RLL = 4653.988

Model 4: Cubic trajectory, random intercept

$$\textit{Body weight}_{ij} = \beta_0 + \beta_1 * \textit{Age} + \beta_2 * \textit{Age}^2 + \beta_3 * \textit{Age}^3 + \varepsilon_{ij} + u_i$$

$\boldsymbol{\varepsilon_{ij}}$ = within-subject variance = errors for subject i at age j, $\boldsymbol{\varepsilon_{ij}} \sim N(0,\sigma^2)$
$\mathbf{u_i}$ = between-subject variance = variance around intercept for subject i, $u_i \sim N(0, \sigma_0^2)$

Factors: Fixed factors: Intercept, Age, Age^2, Age^3
Random factors: Intercept

Estimates of fixed effects:

Parameter	Estimate (β)	95% CI, lower	95% CI, upper	Sig (p-value)
Intercept (β_0)	6.738034	5.229137	8.246931	<0.001
Age (β_1)	0.337954	0.297155	0.378752	<0.001
Age^2 (β_2)	-0.002716	-0.003089	-0.002343	<0.001
Age^3 (β_3)	0.000007	0.000006	0.000008	<0.001

Estimates of covariance parameters:

Parameter	Estimate	Std. Error
Residual	0.771785	0.031843
Intercept (subject=ID)	2.232236	0.582854

Model fit (fixed effects): -2LL (log likelihood) = 3249.436
Model fit (random effects): -2RLL (log likelihood) = 3309.259
Difference from Model 3 = χ^2(4653.988 – 3309.259, df=1), p<0.001

Unique starting body weights for each mouse (random intercept, Model 4) account for a significant portion of the overall variance in the cubic model, giving a significantly better model fit than when no randomeffects are included (Model 3).

Model 5: Cubic trajectory, random intercept and slope

$$\textbf{Body weight}_{ij} = \beta_0 + \beta_1 * Age + \beta_2 * Age^2 + \beta_3 * Age^3 + \varepsilon_{ij} + u_{0i} + u_{1i} * Age$$

$\boldsymbol{\varepsilon_{ij}}$ = within-subject variance = errors for subject i at age j, $\boldsymbol{\varepsilon_{ij}} \sim N(0,\sigma^2)$
$\mathbf{u_{0i}}$ = between-subject variance = variance around intercept for subject i
$\mathbf{u_{1i}}$ = between-subject variance = variance around slope for subject i

$$u_i = \begin{bmatrix} u_{0i} \\ u_{1i} \end{bmatrix} \sim N(0, G) \quad G = \begin{bmatrix} \sigma^2_{u0} & \sigma_{u0,u1} \\ \sigma_{u0,u1} & \sigma^2_{u1} \end{bmatrix}$$

n.b. G, a 2x2 matrix for two random effects (intercept and slope), is unstructured

Factors: Fixed factors: Intercept, Age, Age^2, Age^3
Random factors: Intercept, slope

Estimates of fixed effects:

Parameter	Estimate (β)	95% CI, lower	95% CI, upper	Sig (p-value)
Intercept (β_0)	11.010998	9.664808	12.357188	<0.001
Age (β_1)	0.217180	0.184939	0.249421	<0.001
Age^2 (β_2)	-0.001570	-0.001852	-0.001289	<0.001
Age^3 (β_3)	0.000004	0.000003	0.000004	<0.001

Estimates of covariance parameters: (G)

Parameter		Estimate	Std. Error
Residual		0.368620	0.015413
Intercept + Age	Var.(Intercept); σ^2_{u0}	4.385741	1.216009
(subject=ID)	Covar.(Intercept, slope); $\sigma_{u0,u1}$	-0.039050	0.012020
	Var.(slope); σ^2_{u1}	0.000531	0.000143

Var., variance; Covar., covariance; corresponding to the random effects variance/covariance matrix, G.

Model fit (fixed effects): -2LL (log likelihood) = 2484.105
Model fit (random effects): -2RLL (log likelihood) = 2541.979
Difference from Model 4 = χ^2(3309.259 – 2541.979, df=2), p<0.001
Including both unique starting body weights and unique rates of change over time for individual mice (random intercept and slope, Model 5) accounts for a significant portion of the overall variance in the cubic model, giving a significantly better model fit than when random intercept is included as the only random effect (Model 4).

Model 6: Cubic trajectory, random intercept and slope, with genotype
(final model; a summary of fixed effects parameters is presented in Chapter 2)

$$\textit{Body weight}_{ij} = \beta_0 + \beta_1 * Age + \beta_2 * Age^2 + \beta_3 * Age^3 + \beta_4 * Genotype + \beta_5 * Genotype * Age + \beta_6 * Genotype * Age^2 + \beta_7 * Genotype * Age^3 + \varepsilon_{ij} + u_{0i} + u_{1i} * Age$$

$\boldsymbol{\varepsilon_{ij}}$ = within-subject variance = errors for subject i at age j, $\boldsymbol{\varepsilon_{ij}} \sim N(0,\sigma^2)$
$\mathbf{u_{0i}}$ = between-subject variance = variance around intercept for subject i
$\mathbf{u_{1i}}$ = between-subject variance = variance around slope for subject i

$$u_i = \begin{bmatrix} u_{0i} \\ u_{1i} \end{bmatrix} \sim N(0, G) \quad G = \begin{bmatrix} \sigma^2_{u0} & \sigma_{u0,u1} \\ \sigma_{u0,u1} & \sigma^2_{u1} \end{bmatrix}$$

n.b. G, a 2x2 matrix for two random effects (intercept and slope), is unstructured

Factors: Fixed factors: Intercept, Age, Age^2, Age^3, Genotype, Age*Genotype, Age^2*Genotype, Age^3*Genotype
Random factors: Intercept, slope

Estimates of fixed effects:

Parameter	Estimate (β)	95% CI, lower	95% CI, upper	p-value
Intercept (β_0)	14.504774	12.957579	16.051968	<0.001
Age (β_1)	0.128064	0.093210	0.162919	<0.001
Age^2 (β_2)	-0.000853	-0.001157	-0.000549	<0.001
Age^3 (β_3)	0.000002	0.000001	0.000003	<0.001
Genotype (β_4)	0.182480	-1.973811	2.338771	0.868
Genotype*Age (β_5)	-0.066064	-0.117532	-0.014596	0.012
Genotype*Age^2 (β_6)	0.001096	0.000626	0.001565	<0.001
Genotype*Age^3 (β_7)	-0.000005	-0.000007	-0.000004	<0.001

Estimates of covariance parameters: (G)

Parameter		Estimate	Std. Error
Residual		0.219971	0.009216
Intercept + Age	Var.(Intercept); σ^2_{u0}	2.771801	0.770205
(subject=ID)	Covar.(Intercept, slope); $\sigma_{u0,u1}$	-0.011721	0.004209
	Var.(slope); σ^2_{u1}	0.000104	0.000031

Var., variance; Covar., covariance; corresponding to the random effects variance/covariance matrix, G.

Model fit: (fixed effects): -2LL (log likelihood) = 1843.907
Difference from model 1 = χ^2(2484.105 – 1843.907, df=4), p<0.001
Including genotype in the model (Model 6) significantly improved the model fit to the data compared to the cubic model excluding genotype as a factor (Model 5).
Model fit (random effects): -2RLL (log likelihood) = 1958.998

Supplementary Data 3: Fitting a mixed model to body weight trajectories of MT2-treated and exercised SOD1 mice

Fixed effects of the final model (Model 3, below) are summarised in Chapter 4, Table 4.3 and Figure 4.4.

Factors:
Age = Age in days, continuous covariate, censored at 42 days (6 weeks of age, start of treatment).
Exercise = dummy-coded binary variable, where exercised SOD1 mice = 1 and sedentary SOD1 mice = 0.
Drug = dummy-coded binary variable, where MT2-treated SOD1 mice = 1 and vehicle-treated SOD1 = 0.
The process of model fitting was carried out as described in Supplementary Data 2. For brevity, a summary of model fit to determine model shape is provided below.

Summary of model fitting:

Model trajectory	Random effects	-2LL (ML)	-2RLL (REML)	Fit improvement
Linear	-	6551.276		-
Quadratic	-	6060.683		Fixed effects: p<0.001 vs. linear model
Cubic	-	6000.729	6064.434	Fixed effects: p<0.001 vs. quadratic model
Cubic	Intercept		3121.209	Random effects: p<0.001 from cubic model with no random effects
Cubic ***(Model 1)***	Intercept, slope		2818.106	Random effects: p<0.001 from model with random intercept alone

Model 1: Cubic trajectory, random intercept and slope

$$\textit{Body weight} = \beta_0 + \beta_1 * Age + \beta_2 * Age^2 + \beta_3 * Age^3 + \varepsilon_{ij} + u_{0i} + u_{1i} * Age$$

(see Supplementary Data 2 for error term notation)

Factors: Fixed factors: Intercept, Age, Age^2, Age^3
Random factors: Intercept, slope

Estimates of fixed effects:

Parameter	Estimate (β)	95% CI, lower	95% CI, upper	Sig (p-value)
Intercept (β_0)	17.576294	17.262493	17.890096	<0.001
Age (β_1)	0.007678	0.000911	0.014446	0.026
Age^2 (β_2)	0.000705	0.000592	0.000819	<0.001
Age^3 (β_3)	-0.000006	-0.000007	-0.000006	<0.001

Estimates of covariance parameters:

Parameter	Estimate	Std. Error

Residual		0.204463	0.006897
Intercept + Age	Var.(Intercept)	1.273455	0.241583
(subject=ID)	Covar.(Intercept, slope)	-0.002332	0.001178
	Var.(slope)	0.000048	0.000011

Var., variance; Covar., covariance; corresponding to the random effects variance/covariance matrix.

Model fit (fixed effects): -2LL (log likelihood) = 2754.600

Model 2: Cubic trajectory, random intercept and slope, with Exercise parameters

$$\textit{Body weight} = \beta_0 + \beta_1 * Age + \beta_2 * Age^2 + \beta_3 * Age^3 + \beta_4 * Exercise + \beta_5 * Exercise * Age + \beta_6 * Exercise * Age^2 + \beta_7 * Exercise * Age^3 + \varepsilon_{ij} + u_{0i} + u_{1i} * Age$$

Factors: Fixed factors: Intercept, Age, Age^2, Age^3, Exercise, Exercise*Age, Exercise*Age^2, Exercise*Age^3
Random factors: Intercept, slope

Estimates of fixed effects:

Parameter	Estimate (β)	95% CI, lower	95% CI, upper	p-value
Intercept (β_0)	17.558523	17.122241	17.994804	<0.001
Age (β_1)	0.008845	-0.000642	0.018333	0.068
Age^2 (β_2)	0.000730	0.000569	0.000890	<0.001
Age^3 (β_3)	-0.000007	-0.000008	-0.000006	<0.001
Exercise (β_4)	0.048568	-0.578484	0.675621	0.878
Exercise*Age (β_5)	-0.003474	-0.016889	0.009940	0.612
Exercise*Age^2 (β_6)	-0.000025	-0.000250	0.000199	0.824
Exercise*Age^3 (β_7)	0.000001	0.000000	0.000002	0.220

Estimates of covariance parameters:

Parameter		Estimate	Std. Error
Residual		0.200393	0.006760
Intercept + Age	Var.(Intercept)	1.272323	0.241299
(subject=ID)	Covar.(Intercept, slope)	-0.002310	0.001172
	Var.(slope)	0.000048	0.000011

Var., variance; Covar., covariance; corresponding to the random effects variance/covariance matrix.

Model fit (fixed effects): -2LL (log likelihood) = 2718.779
Difference from model 1 = χ^2(2754.600 – 2718.779, df=4), p<0.001

Including Exercise as a factor in the body weight model improved the model fit, as measured by decreasing -2LL values, yet the parameter estimates for exercised mice (β4-β7) were not significantly different from those of sedentary mice. Thus, while exercise/sedentary status contributed to explaining some of the variation between treatment groups, the body weight trajectories of exercised and sedentary mice did not differ significantly.

Model 3: Cubic trajectory, random intercept and slope, with Exercise (exercise/sedentary) and Drug (MT2/vehicle) parameters

$$Body\ weight = \beta_0 + \beta_1 * Age + \beta_2 * Age^2 + \beta_3 * Age^3 + \beta_4 * Exercise + \beta_5 * Exercise * Age + \beta_6 * Exercise * Age^2 + \beta_7 * Exercise * Age^3 + \beta_8 * Drug + \beta_9 * Drug * Age + \beta_{10} * Drug * Age^2 + \beta_{11} * Drug * Age^3 + \varepsilon_{ij} + u_{0i} + u_{1i} * Age$$

Factors: Fixed factors: Intercept, Age, Age^2, Age^3, Exercise, Exercise*Age, Exercise*Age^2, Exercise*Age^3, Drug, Drug*Age, Drug*Age^2, Drug*Age^3
Random factors: Intercept, slope

Estimates of fixed effects:

Parameter	Estimate (β)	95% CI, lower	95% CI, upper	p-value
Intercept (β_0)	17.363634	16.837901	17.889367	<0.001
Age (β_1)	0.021013	0.009705	0.032322	<0.001
Age^2 (β_2)	0.000478	0.000285	0.000671	<0.001
Age^3 (β_3)	-0.000006	-0.000007	-0.000005	<0.001
Exercise (β_4)	0.023367	-0.604711	0.651446	0.941
Exercise*Age (β_5)	-0.002076	-0.015401	0.011250	0.760
Exercise*Age^2 (β_6)	-0.000049	-0.000273	0.000175	0.669
Exercise*Age^3 (β_7)	0.000001	0.000000	0.000002	0.151
Drug (β_8)	0.418199	-0.210027	1.046425	0.189
Drug*Age (β_9)	-0.025340	-0.038716	-0.011964	<0.001
Drug*Age^2 (β_{10})	0.000510	0.000285	0.000735	<0.001
Drug*Age^3 (β_{11})	-0.000003	-0.000004	-0.000001	<0.001

Estimates of covariance parameters:

Parameter		Estimate	Std. Error
Residual		0.198360	0.006693
Intercept + Age	Var.(Intercept)	1.276821	0.242147
(subject=ID)	Covar.(Intercept, slope)	-0.002386	0.001147
	Var.(slope)	0.000045	0.000010

Var., variance; Covar., covariance; corresponding to the random effects variance/covariance matrix.

Model fit (fixed effects): -2LL (log likelihood) = 2697.062
Difference from model 2 = χ^2(2718.779 – 2697.062, df=4), p<0.001

Including Drug as a factor in the body weight model improved the model fit, as measured by decreasing -2LL values. The parameter estimates for MT2-treated mice differed from those of vehicle-treated mice, indicating that the body weight trajectories of MT2-treated mice were significantly different compared to vehicle-treated mice.

Model 4: Cubic trajectory, random intercept and slope, with Exercise (exercise/sedentary), Drug (MT2/vehicle), and Exercise*Drug parameters

$$Body\ weight = \beta_0 + \beta_1*Age + \beta_2*Age^2 + \beta_3*Age^3 + \beta_4*Exercise + \beta_5*Exercise*Age + \beta_6*Exercise*Age^2 + \beta_7*Exercise*Age^3 + \beta_8*Drug + \beta_9*Drug*Age + \beta_{10}*Drug*Age^2 + \beta_{11}*Drug*Age^3 + \beta_{12}*Exercise*Drug + \beta_{13}*Drug*Age + \beta_{14}*Drug*Age^2 + \beta_{15}*Drug*Age^3 + \varepsilon_{ij} + u_{0i} + u_{1i}*Age$$

Factors: Fixed factors: Intercept, Age, Age^2, Age^3, Exercise, Exercise*Age, Exercise*Age^2, Exercise*Age^3, Drug, Drug*Age, Drug*Age^2, Drug*Age^3, Exercise*Drug, Exercise*Drug*Age, Exercise*Drug*Age^2, Exercise*Drug*Age^3
Random factors: Intercept, slope

Estimates of fixed effects:

Parameter	Estimate (β)	95% CI, lower	95% CI, upper	p-value
Intercept (β_0)	17.311491	16.714817	17.908166	<0.001
Age (β_1)	0.022860	0.009924	0.035796	0.001
Age^2 (β_2)	0.000470	0.000248	0.000693	<0.001
Age^3 (β_3)	-0.000006	-0.000007	-0.000004	<0.001
Exercise (β_4)	0.135588	-0.737744	1.008921	0.758
Exercise*Age (β_5)	-0.006105	-0.024843	0.012633	0.523
Exercise*Age^2 (β_6)	-0.000027	-0.000347	0.000293	0.867
Exercise*Age^3 (β_7)	0.000001	-0.000001	0.000002	0.316
Drug (β_8)	0.536375	-0.337797	1.410548	0.225
Drug*Age (β_9)	-0.029863	-0.048782	-0.010945	0.001
Drug*Age^2 (β_{10})	0.000541	0.000221	0.000861	0.001
Drug*Age^3 (β_{11})	-0.000003	-0.000004	-0.000001	0.001
Exercise*Drug (β_{12})	-0.243375	-1.498343	1.011594	0.700
Exercise*Drug*Age (β_{13})	0.009398	-0.017341	0.036136	0.491
Exercise*Drug*Age^2 (β_{14})	-0.000068	-0.000518	0.000382	0.767
Exercise*Drug*Age^3 (β_{15})	0.000000	-0.000002	0.000002	0.929

Estimates of covariance parameters:

Parameter		Estimate	Std. Error
Residual		0.198192	0.006687
Intercept + Age	Var.(Intercept)	1.272228	0.241323
(subject=ID)	Covar.(Intercept, slope)	-0.002334	0.001139
	Var.(slope)	0.000044	0.000010

Var., variance; Covar., covariance; corresponding to the random effects variance/covariance matrix.

Model fit (fixed effects): -2LL (log likelihood) = 2695.162
Difference from model 3 = χ^2(2697.062 – 2695.162, df=4), p=0.754

*The addition of interaction terms between Exercise*Drug did not improve the fit of the model to the data, indicating that no synergistic effects were present between exercise treatment and MT2 treatment. As a result, the final model presented in Chapter 4 was Model 3, above, containing Exercise parameters and Drug parameters, but without including an interaction term.*

Supplementary Data 4: Fitting a mixed model to body weight trajectories of Emtin-treated and control SOD1 mice

Fixed effects of the final model (Model 2, below) are summarised in Chapter 5, Table 5.4 and Figure 5.3.

Factors:
Age = Age in days, continuous covariate
Treatment = dummy-coded categorical variable;
'EmtinAc' is encoded by EmtinAc-treated SOD1 mice = 1 and control SOD1 mice = 0.
'EmtinB' is encoded by EmtinB-treated SOD1 mice = 1 and control SOD1 mice = 0.

The process of model fitting was carried out as described in Supplementary Data 2. For brevity, a summary of model fit to determine model shape is provided below.

Summary of model fitting:

Model trajectory	Random effects	-2LL (ML)	-2RLL (REML)	Fit improvement
Linear	-	1717.129		-
Quadratic	-	1584.622	1615.791	Fixed effects: p<0.001 vs. linear model
Cubic	-	1583.377		Fixed effects: p=0.264 vs. quadratic model; no improvement in fit
Quadratic	Intercept		826.631	Random effects: p<0.001 vs. quadratic model with no random effects
Quadratic (***Model 1***)	Intercept, slope	722.235	751.726	Random effects: p<0.001 vs. model with random intercept alone

Model 1: Quadratic trajectory, random intercept and slope

$$\textit{Body weight} = \beta_0 + \beta_1 * Age + \beta_2 * Age^2 + \varepsilon_{ij} + u_{0i} + u_{1i} * Age$$

(see Supplementary Data 2 for error term notation)

Factors: Fixed factors: Intercept, Age, Age^2
Random factors: Intercept, slope

Estimates of fixed effects:

Parameter	Estimate (β)	95% CI, lower	95% CI, upper	Sig (p-value)
Intercept (β_0)	1.520609	-0.189412	3.230630	0.081
Age (β_1)	0.312842	0.289456	0.336228	<0.001
Age^2 (β_2)	-0.001329	-0.001417	-0.001241	<0.001

Estimates of covariance parameters:

Parameter		Estimate	Std. Error
Residual		0.181894	0.011626
Intercept + Age	Var.(Intercept)	3.474587	1.237779

(subject=ID)	Covar.(Intercept, slope)	-0.015722	0.006300
	Var.(slope)	0.000094	0.000037

Var., variance; Covar., covariance; corresponding to the random effects variance/covariance matrix.

Model fit (fixed effects): -2LL (log likelihood) = 722.235

Model 2: Quadratic trajectory, random intercept and slope, with Treatment (EmtinAc/EmtinB) parameters

$$\textit{Body weight} = \beta_0 + \beta_1 * Age + \beta_2 * Age^2 + \beta_3 * EmtinAc + \beta_4 * EmtinAc * Age + \beta_5 * EmtinAc * Age^2 + \beta_6 * EmtinB + \beta_7 * EmtinB * Age + \beta_8 * EmtinB * Age^2 + \varepsilon_{ij} + u_{0i} + u_{1i} * Age$$

(see Supplementary Data 2 for error term notation)

Factors: Fixed factors: Intercept, Age, Age^2, EmtinAc, EmtinAc*Age, EmtinAc*Age^2, EmtinB, EmtinB*Age, EmtinB*Age^2
Random factors: Intercept, slope

Estimates of fixed effects:

Parameter	Estimate (β)	95% CI, lower	95% CI, upper	p-value
Intercept (β_0)	-4.449126	-7.501088	-1.397165	0.004
Age (β_1)	0.420456	0.376231	0.464681	<0.001
Age^2 (β_2)	-0.001774	-0.001943	-0.001604	<0.0001
EmtinAc (β_3)	7.543884	3.421179	11.666589	<0.001
EmtinAc*Age (β_4)	-0.143378	-0.202179	-0.084577	<0.001
EmtinAc*Age^2 (β_5)	0.000596	0.000372	0.000821	<0.001
EmtinB (β_6)	8.034302	3.981721	12.086882	<0.001
EmtinB*Age (β_7)	-0.140318	-0.197457	-0.083178	<0.001
EmtinB*Age^2 (β_8)	0.000578	0.000362	0.000794	<0.001

Estimates of covariance parameters:

Parameter		Estimate	Std. Error
Residual		0.168984	0.010795
Intercept + Age	Var.(Intercept)	2.730534	0.982709
(subject=ID)	Covar.(Intercept, slope)	-0.012786	0.005322
	Var.(slope)	0.000087	0.000034

Var., variance; Covar., covariance; corresponding to the random effects variance/covariance matrix.

Model fit (fixed effects): -2LL (log likelihood) = 684.849
Difference from Model 1 = χ^2(722.235 – 684.849, df=6), p<0.001

The addition of Treatment (EmtinAc, EmtinB) parameters to the model explained a significant portion of the variation as seen by decreasing -2LL values. The parameter estimates for EmtinAc-treated and EmtinB-treated SOD1 mice were significantly different from those of control SOD1 mice, indicating that treatment with Emtin peptides significantly affected body weight trajectory over time.

Appendix

Behavioural testing procedures for mouse motor phenotype

This document is not a task risk assessment, nor a standard operating procedure. All investigators attempting these procedures must have prior training in animal handling.

Stride test

One mouse at a time was removed from its home cage and placed on a transport cage lid, then scruffed with the left (or preferred) hand of the investigator. Scruffing should attempt to gather as much skin as possible in order to limit limb movement when applying paint to the paws. With the mouse scruffed, paint which had been diluted to a thin consistency with water was applied to the paws with a paintbrush – blue for hind paws and red for front paws. The mouse was then placed onto the start of the strip between the dividers, and walked along the strip of paper between the dividers towards the wire basket. Upon entering the wire basket, the mouse was retrieved by its tail, and had its paws dipped into the petri dish containing water in order to remove paint, then was transferred into a tissue-lined cage to dry the feet. The mouse was then returned to its home cage.

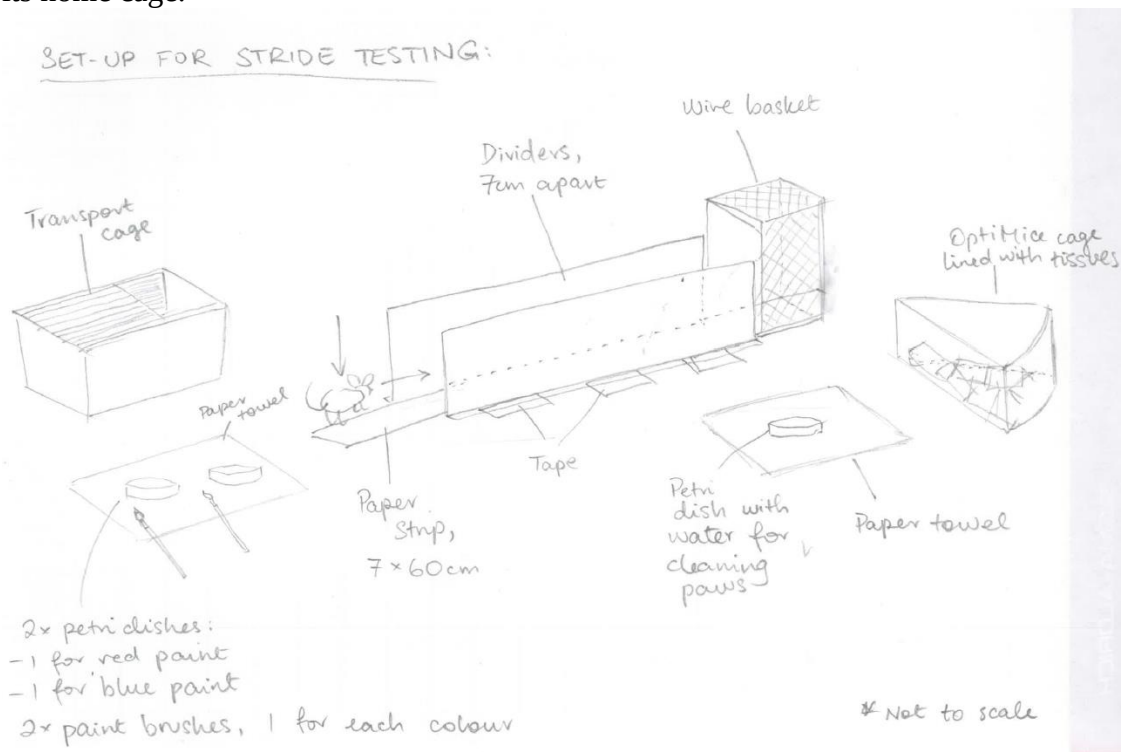

Rotarod

Coordinated motor performance was assessed using a 5-lane mouse rotarod (TSE Systems). Mice were acclimatised to the rotarod from approximately 85-90 days of age, with three once-daily sessions. Each acclimatisation session consisted of 5 minutes on the rotarod drum at a constant speed of 3rpm – while the mice were learning to stay on the rotating drum, they were partly supported to stay on the drum, and prevented from

falling off the drum, by the investigator placing their hand below the drum to as a platform and safety net. The mice were then trained to stay on the accelerating rotarod, with at least two once-daily sessions consisting of a 3rpm-16rpm acceleration over 3 minutes. In testing sessions, the speed at which mice were unable to stay on the rotating drum during an acceleration from 3rpm-16rpm over 3 minutes was recorded. As few mice achieved the maximum score of staying on the rotarod up to 16rpm, future studies using the rotarod should commence training prior to the onset of disease symptoms.

Grip strength meter

Grip strength was measured in newtons (N) with a grip strength meter (Columbus Instruments) mounted on a stand. Each mouse was scruffed, held over the grip strength meter equipped with triangular bar, and moved backwards at a constant speed, gripping the bar with its hind paws and generating a maximum force measurement. The maximum force recorded from three attempts was used for analysis.

Wire hang duration test

To perform wire hang duration testing, mice were removed from their home cage, and placed on a wire cage lid. The cage lid was then gently inverted and held approximately 20cm above a large transport cage with foam padding at the bottom (A, below). The mouse gripped onto the bars (B, below), while the cage lid was held inverted for a maximum of 60 seconds. The latency to fall, from the best of three attempts, was recorded as the wire hang duration.

As an interesting aside, it was noted that the first 3-4 weeks of testing were highly variable for both genotypes. The home cages for all mice featured a clear plastic lid rather than metal bars – the only wire structure in the home cage would be the food hopper, so these mice effectively had no prior training in gripping an inverted set of wire bars. The first few weeks of testing may have effectively only served as a training period, hence the variable measurements obtained. For future use of the wire hang duration test, it would be recommended to train mice in the wire hang duration procedure for a period of some weeks prior to recording data for analysis.